CRANFIELD UNIVERSITY

MELETIOS PAGONIS

ELECTRICAL POWER ASPECTS OF DISTRIBUTED PROPULSION SYSTEMS IN TURBO-ELECTRIC POWERED AIRCRAFT

SCHOOL OF AEROSPACE, TRANSPORT, AND MANUFACTURING

PhD THESIS
Academic Year: 2012 - 2015

Supervisor: Professor Peter Malkin
October 2015

CRANFIELD UNIVERSITY

SCHOOL OF AEROSPACE TRANSPORT AND MANUFACTURING
Power And Propulsion Division

PhD THESIS

Academic Year 2012 - 2015

MELETIOS PAGONIS

Electrical Power Aspects of Distributed Propulsion Systems in Turbo-electric Powered Aircraft

Supervisor: Professor Peter Malkin
October 2015

This thesis is submitted in partial fulfilment of the requirements for the degree of Doctor of Philosophy

ABSTRACT

The aerospace industry is currently looking at options for fulfilling the technological development targets set for the next aircraft generations. Conventional engines and aircraft architectures are now at a maturity level which makes the realisation of these targets extremely problematic. Radical solutions seem to be necessary and Electric Distributed Propulsion is the most promising concept for future aviation. Several studies showed that the viability of this novel concept depends on the implementation of a superconducting power network.

The particularities of a superconducting power network are described in this study where novel components and new design conditions of these networks are highlighted. Simulink models to estimate the weight of fully superconducting machines have been developed in this research work producing a relatively conservative prediction model compared to the NASA figures which are the only reference available in the literature. A conceptual aircraft design architecture implementing a superconducting secondary electrical power system is also proposed. Depending on the size of the aircraft, and hence the electric load demand, the proposed superconducting architecture proved to be up to three times lighter than the current more electric configurations. The selection of such a configuration will also align with the general tendency towards a superconducting network for the proposed electric distributed propulsion concept. In addition, the hybrid nature of these configurations has also been explored and the potential enhanced role of energy storage mechanisms has been further investigated leading to almost weight neutral but far more flexible aircraft solutions. For the forecast timeframe battery technology seems the only viable choice in terms of energy storage options. The anticipated weight of the Lithium sulphur technology is the most promising for the proposed architectures and for the timeframe under investigation. The whole study is based on products and technologies which are expected to be available on the 2035 timeframe. However, future radical changes in energy storage technologies may

be possible but the approach used in this study can be readily adapted to meet such changes.

Keywords:

Superconductivity, electric, power, networks, machines, energy, storage, more, electric, aircraft, battery

ACKNOWLEDGEMENTS

First of all, I would like to express my gratitude to my supervisor, Professor Peter Malkin, for his continuous guidance and support throughout these three years. His passion for looking for new insights has been inspirational and his contribution to my work has been crucial to the completion of this thesis. Furthermore, I will always be grateful to Professor Pericles Pilidis for this amazing opportunity he offered me when I most needed one. He believed in me before I even believed in myself and for that I will always be indebted to him.

Through this PhD I had also the chance to work with numerous professionals from Airbus Group Innovations (AGI) and Rolls Royce (RR) which also significantly supported my work. Working along Graham Dodds and Frederick Berg from AGI as well as with Mark Husband and John Cullen from RR has been an amazing experience which helped me develop myself as a professional engineer. In addition to them, I had also the pleasure to work and share concerns and ambitions with several fellow Cranfield University students and post graduates. Special regards to Joseph Palmer and Emanuele Pagone with whom we worked countless hours together during the DEAP project.

I cannot begin to thank enough all these amazing people I met and befriended during my Cranfield experience. Special thanks to my volleyball teammates who have been a breath of fresh air during the stressful periods of my PhD. Particularly to Giacomo, Radka, Giulio, Jakub, and Megane who have been the best teammates I could have ever wished for! Moreover, my “Spanish group” (i.e. Pedro, Ernest, Lola, Lelia, Alex, Paolo and Belen), thank you for all the fun times you offered me. I would also never forget my “Bedfordians” and especially my guardian angel Antonella for her constant support. Last but not least a special thank you to all my loyal Greek friends that-no matter the distance-remain important pieces of my life.

Finally, special thanks to my parents for their support and encouragement all these years as well as to my brother and his wonderful family for being there for me both at good and bad times.

TABLE OF CONTENTS

LIST OF FIGURES

LIST OF TABLES

LIST OF ABBREVIATIONS

Nomenclature

AC	Alternating Current
ACARE	Advisory Council for Aviation Research and Innovation in Europe
ACT	Advanced Capacitors Technology
AGI	Airbus Group Innovations
APU	Auxiliary Power Unit
ATRU	Auto Transformer Rectifier Unit
BLAC	Brushless AC machines
BLI	Boundary Layer Ingestion
BSCCO	Bismuth Strontium Calcium Copper Oxide
BWB	Blended Wing Body
CAA	Civil Aviation Authority
CAEP	Committee on Aviation Environmental Protection
CB	Circuit Breaker
CFD	Computational Fluid Dynamics
CNT	Carbon Nanotubes
CO_2	Carbon Dioxide
CVG	Constant Velocity Gearbox
DAPRA	Defence Advanced Research Projects Agency
DC	Direct Current
DEAP	Distributed Electrical Aerospace Propulsion
DoD	Depth-of-Discharge
DP	Distributed Propulsion
ECS	Environmental Control System
EDLC	Electric Double Layer Capacitor
EOR	End-Of-Runway
EPN	Electric Power Network
E.S.	Energy Storage
FAA	Federal Aviation Administration
FOD	Foreign Object Damage
FC	Fuel Cell
GE	General Electric
GT	Gas Turbine
GTA	Gas Turbine Alternator
HEDP	Hybrid Electric Distributed Propulsion
HPC	High Power Compressor
HTS	High Temperature Superconductors

HVLC	High Voltage Low Current
IDG	Integrated Drive Generator
IM	Induction Motor
IP	Intermediate Power
KERI	Korea Electro-technology Research Institute
LED	Light-Emitting Diode
LH2	Liquid Hydrogen
LIC	Lithium-Ion Capacitors
LP	Low Pressure
LTS	Low Temperature Superconductors
LVHC	Low Voltage High Current
MEA	More Electric Aircraft
MEE	More Electric Engine
MEL	Maximum engine Electric Loading
MgB2	Magnesium Diboride
NASA	National Aeronautics and Space Administration
NOx	Nitrogen Oxide
PAX	Passengers
P.E.	Power Electronics
PM	Permanent Magnet
PMAD	Power Management and Distribution
PSAM	Programmable Superconducting AC Machine Project
PVC	Polyvinyl Chloride
RMS	Root Mean Square
RPDU	Remote Power Distribution Unit
RPM	Rotations Per Minute
RR	Rolls Royce
SEA	Superconducting Electric Aircraft
SFCL	Superconducting Fault Current Limiter
SIG	Superconducting Induction Generator
SLS	Sea Level Standard
SM	Superconducting Machine
SMES	Superconducting Magnetic Energy Storage
SoC	State of Charge
SOTA	State-Of-The-Art
SPN	Superconducting Power Network
SPS	Secondary Power System
SPU	Secondary Power Unit
SR	Switched Reluctance

SUGAR	Subsonic Ultra Green Aircraft Research
TeDP	Turbo-electric Distributed Propulsion
TO	Take-off
TOC	Top-of-Climb
TRL	Technology Readiness Level
TRU	Transformer Rectifier Unit
TRV	Torque per unit of Rotor Volume
TSB	Technology Strategy Board
TSFC	Thrust Specific Fuel Consumption
UAV	Unmanned Aerial Vehicle
VF	Variable Frequency
VFSG	Variable Frequency Starter Generator
WAI	Wing Anti-Icing
WF	Wound Field
YBCO	Yttrium Barium Copper Oxide

Symbols

B	Magnetic field
H*	Irreversibility Field
H_c	Upper Critical Field
J_c	Critical Current Density
m_{cryo}	Mass of the cryo-cooler
n_{prop}	Propulsive efficiency
P_{in}	Input Power requirement
T_c	Critical Temperature
v_j	Jet velocity
v_o	Free-stream velocity
V_S	System's Voltage
I_S	System's Current
F	Frequency
i_s	Steady state alternating current
i_t	Transient direct current
U	Voltage

Z	Impedance
R	Resistance
L	Inductance
ω	Fundamental frequency
T	Time
θ	Voltage angle
i_{mm}	Maximum momentary short circuit
P_{Shaft}	Shaft Propulsion Power
n_{trans}	Electric transmission efficiency
P_{Bprop}	Engine brake power for transmission
P_{elec}	Electric consumer load
n_{alt}	Alternator efficiency
P_{Belec}	Engine brake power for consumer
P_E	Total engine brake power demand
P_{Total}	Total engine brake power installed
I_{Gsc}	Generator short circuit current
n	Number of generators/motors
P_{Gen}	Rated power of the generator
V_r	Rated Voltage
x_d"	Sub-transient reactance
$\cos\varphi$	Power factor
I_{Msc}	Motor short circuit current
P_{mot}	Rated power of the motor
V_B	Breakdown Voltage
p	Atmospheric pressure
d	Distance
F_{em}	Electromagnetic forces per unit length
μ_0	Permeability constant
P	Electromagnetic Power
T	Torque
ω_m	Rotational speed
N	Number of rotations
A	Electric loading

B	Magnetic loading
m	Number of phases
T_{ph}	Number of turns in series per phase
D	Diameter
Φ	Fundamental flux/pole
p	Number of pair poles
L_{stk}	Stack length
E	Electro-magnetic force (emf)
k_w	Winding factor
v_r	Rotor volume
L	Length
V_{ph}	Phase Voltage
I_{ph}	RMS phase current
t_c	Thickness of the environmental screen
γ	Environmental screen density
r_s	Mean stator radius
r_x	Inner screen radius
W_{screen}	Environmental screen mass
$LiCoO_2$	Lithium cobalt oxide
$LiFePO_4$	Lithium iron phosphate
NiMH	Nickel Metal Hydride
Li-ion	Lithium ion
NMC	Nickel-manganece-cobalt
Li-air	Lithium air
Li-S	Lithium sulphur

1 Introduction & Project Specifications

1.1 Introduction

The scope of this research study is to investigate, mainly in terms of weight, several system architectures of novel future aircraft designs which are characterised by their multiple propulsion power sources (“distributed propulsion”). This will include a more/all electric approach and the presence of a superconducting power network.

The concept of distributed propulsion (DP) for aerospace applications implies the separation and distribution of the propulsive system that allows improvements in “propulsive efficiencies” to enhance the overall vehicle performance. It has been shown that electric DP is the most beneficial configuration, hence the more electric approach described in this thesis. However, the feasibility of this approach depends on the weight reduction of the whole system. In order to achieve the latter a superconducting network might be necessary.

A more graphical representation of the proposed design can be seen in figure 1. In this graph a couple of Gas Turbines Alternators (GTAs) are responsible for providing the required propulsive power to a number of motor driven fans, whilst the energy storage system is also operating as a supplementary power source. This figure gives only a preliminary idea of the concept being investigated in this research work. Several variations of this approach will be described later in this thesis.

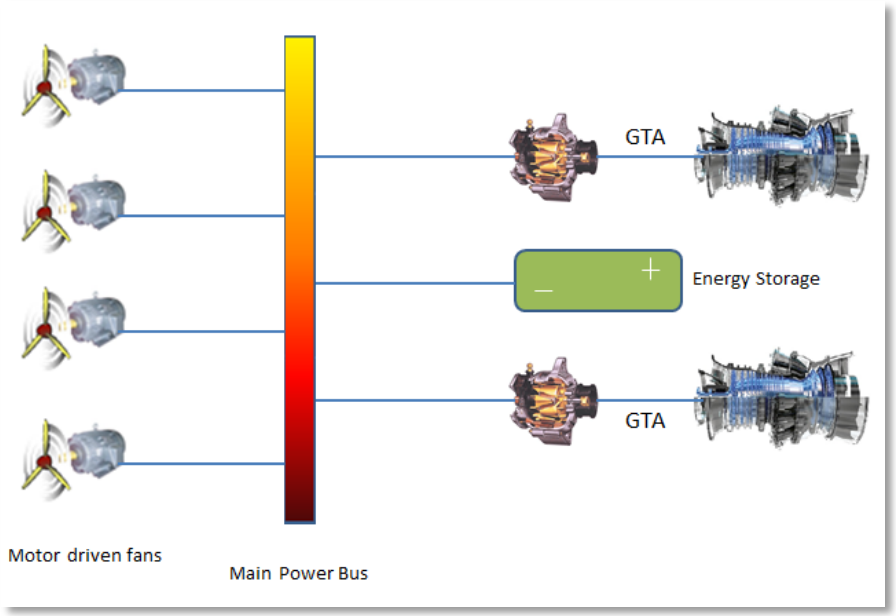

Figure 1 Electric Distributed Propulsion System

It is important to clarify the reasons behind the investigation of such a disruptive technology. The following subchapter will present the expected improvements of next aircraft generations and it will demonstrate the incapability of conventional configurations to satisfy these demands.

1.2 Future Goals and Trends in Aviation

The aerospace industry is a sector that throughout the recent past has consistently made significant improvements in regards to the performance and fuel efficiency of civil aircraft. The last 50 years or so (i.e. after the introduction of the jet engine) the majority of researchers have been focusing on the implementation of technology advances regarding the propulsion system, airframe alternatives, materials selection, aerodynamics etc. with the goal of a more efficient and safer aircraft. However, one important thing to note is that recently the rate of improvement has been significantly decreased as a result of the physical limitations that have been reached in many technologies. Figure 2 illustrates a typical technology development s-curve which includes the introduction, expansion and maturation of innovations that most industries, including aerospace, experience.

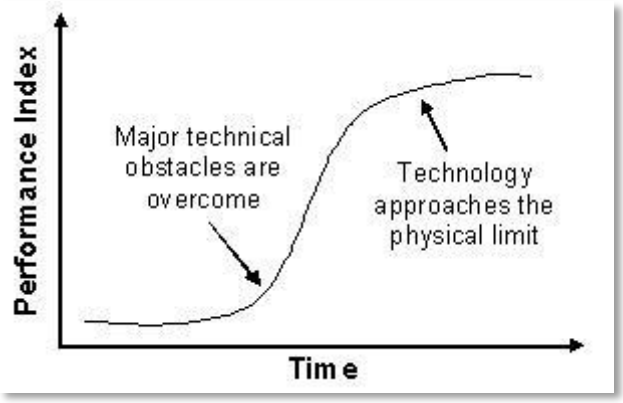

Figure 2 Technology Development S-Curve (Scocco, 2006)

Aerospace industry has been approaching the phase where any performance improvements take longer to be attained and require significantly more effort and money. Combining the latter with the testing emission targets that important institutions such as NASA (National Aeronautics and Space Administration) and ACARE (Advisory Council for Aviation Research and Innovation in Europe) have set for the future aviation underlines the importance of innovative aircraft design options that will open numerous unexplored paths for designing civil and military airplanes.

1.2.1 Technology goals for next aircraft generations

The expected continued growth in air traffic, combined with the increased demand for minimisation of environmental damage in all aspects of technology has led the aviation industry to search for ways to diminish the negative impact of future aircraft on environment. NASA released some very aggressive targets for next generation commercial airplanes (Ashcraft W. et al., 2011), concentrating on basic key aspects like noise, NOx emissions, and last but not least fuel burn (CO_2 emissions). In 2001 ACARE also set some similar targets (Graham R., Hall A. and Morales V., 2014). Both these goals have been summarised in table 1. Note that different references have been chosen in these two cases. More specifically, ACARE used as a reference a 2000 aircraft for all three categories while NASA used a 2005 state-of-the-art aircraft for the fuel burn savings, an aircraft-engine NOx emissions standard being set by the Committee on Aviation Environmental Protection (CAEP) and a cumulative sum

of lateral, flyover and approach noise certification points under the FAA stage 4 noise regulation.

Table 1 NASA and ACARE goals for next aircraft generations

Category	NASA		ACARE	
	N+2 (~2020)	N+3 (~2035)	Vision 2020	FlightPath 2050
Fuel Burn	-50%	-60%*	-50%	-75%
Noise	-42dB	-71dB	-50%	-65%
NOx Emissions	-75%	-80%*	-80%	-90%

*Note that these values have changed throughout the years and different numbers can be found in literature, however the most recent ones were chosen.

It is clear that such optimistic targets will not be achieved following the "conventional approach". For this reason all the important aerospace companies and research centres are looking for rather disruptive technologies that could significantly alter the aviation industry. These concepts will be briefly described in the next subchapter while a more detailed description of the chosen approach will be presented in Chapter 2.

1.2.2 Potential future design options for the civil aerospace industry

Several different concepts have been suggested and developed by various organisations for the next aircraft generations, some of which will be briefly described here. Naturally, the so-called Turbo-electric Distributed Propulsion concept is the approach which will be investigated in more depth in this research study as it is considered by the author as the most promising technology.

- *Open rotor concept*

One of the concepts that have attracted significant interest lately is the unducted -"open rotor"- propulsion approach. This is not a new concept at all, but it was firstly investigated in the late 1970s and early 80s triggered by the sharp increase of the fuel prices during this period. More specifically, NASA's Advanced Turboprop Project was one of the most high-profile projects of this

era claiming fuel cost benefits of almost 50% (Whitlow B. and Sievers K., 1988). However, the fuel benefits did not come without a penalty. Noise levels being achieved with this configuration were below FAA stage 3 limits, whilst the probability of foreign object damage (FOD) was also significantly increased. Note that all these results (positive and negative) were based on the state-of-the-art technology of that era and do not reflect the current situation. Since this concept was out of any agenda for almost two decades efforts to re-establish the know-how were necessary. An initial assessment of the open rotor propulsion concept capabilities as well as predicted benefits was carried out by NASA (Guynn D. et al., 2011) focusing on counter-rotating pusher approach with a rear-mounted installation (Figure 3). The first results showed Thrust Specific Fuel Consumption (TSFC) reductions of around 30% in the top-of-climb (TOC) phase and more than 45% for the Sea Level Standard (SLS) and Take-off (TO) phase. Even more optimistic results about the NOx emissions were presented, claiming a reduction of the order of 80%. On the other hand, the Thrust-to-Weight ratio of the open rotor engines was more than 15% lower than other turbofan technologies mitigating the fuel savings of this configuration. Finally, the results of the noise measurements were not so disheartening but were presented for demonstration purposes only and their reliability at this point is questionable.

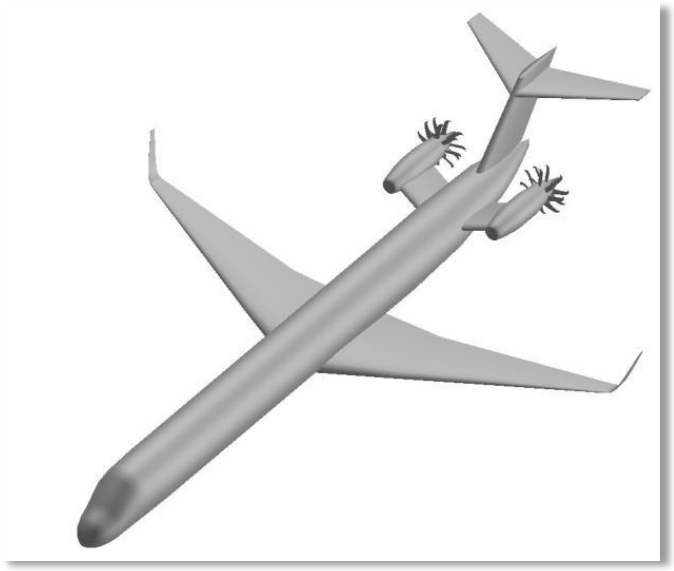

Figure 3 Advanced Single-Aisle Aircraft configuration with rear-mounted open rotor engines (Guynn D. et al., 2011)

- Boeing Subsonic Ultra Green Aircraft Research ("*SUGAR"*)

Boeing Corporation has done a lot of work aiming at fulfilling NASA's targets for future aviation and to that direction a series of aircraft designs were proposed. The "SUGAR" family (acronym for Subsonic Ultra Green Aircraft Research) consists of five different aircraft designs: SUGAR Free, Refined SUGAR, SUGAR High, SUGAR Ray, and SUGAR Volt. The latter was the one that presented results closer to the desired ones. More specifically, fuel burn savings greater than 70% and large emission reductions could be achieved. SUGAR Volt is characterised by its hybrid electric-gas turbine engines designed by General Electric (GE) and the use of batteries during take-off and landing. Boeing SUGAR team concluded that hybrid electric energy technology is the clear winner for future aviation and has the greatest potential of achieving NASA's targets (Stephenson, 2010). However, in order this concept to become feasible important improvements on battery technologies are necessary. Several modifications of SUGAR Volt design will be investigated in this project thesis (Chapter 6).

Figure 4 SUGAR Volt: Boeing's proposed design for next aircraft generations (courtesy of Boeing)

- NASA N3-X Turbo-electric Distributed Propulsion Concept (TeDP)

One of the most high profile studies that was the basis for a lot more to come is the so-called N3-X model. This configuration consists of two turboshaft engines driving two superconducting electrical generators. The primary function of these devices is to produce electrical power, rather than thrust. These two turbo-generators are mounted on the wing-tips, a location that proved to be more beneficial for such a model. The electrical power is transmitted along redundant superconducting electrical cables to an array of propulsors embedded in the entire upper trailing edge of the fuselage section of the aircraft. In the N3-X configuration there are 14 propulsors, each with a superconducting motor driven fan. The aforementioned configuration can be seen in Figure 5.

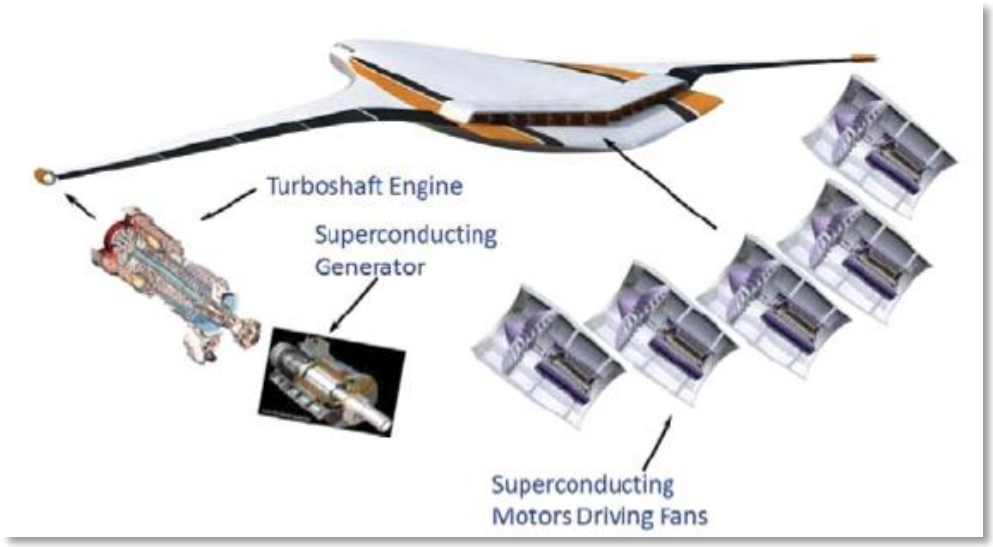

Figure 5 NASA N3-X Hybrid wing body aircraft with TeDP (Kim et al., 2013)

The initial results showed a 70-72% mission fuel burn reduction compared to a B777-200LR-like vehicle (Felder et al., 2011b). A more extended analysis of the N3-X project will follow in the next chapter (Chapter 2) where all the technologies, architectures, enablers and limitations of this concept will be described.

- Distributed Electrical Aerospace Propulsion (DEAP) Project

This is a UK government funded project with the participation of Airbus Group Innovations (AGI), Rolls Royce (RR), and Cranfield University. It is also linked with this research study where parts of it were inputs for the several phases of this project. Thus, a more detailed description of this project and its links with this study is necessary and will follow in the next subchapter (1.3).

1.3 DEAP Project

Airbus and Rolls Royce are lately exploring different paths for the propulsion system of future aircraft. In order to achieve this, they joined forces in the DEAP project also collaborating with Cranfield University. This project investigates key innovative technologies that will enable improved fuel economy and reduced emissions for future airliner designs having Distributed Propulsion (DP) and Boundary Layer Ingestion (BLI). The main objectives of the project were to

evaluate distributed propulsion concepts as well as to analyse the feasibility and potentials of a more electric approach combined with BLI. A concept plane proposed by Airbus was the baseline for any models and calculations being carried out (Figure 6).

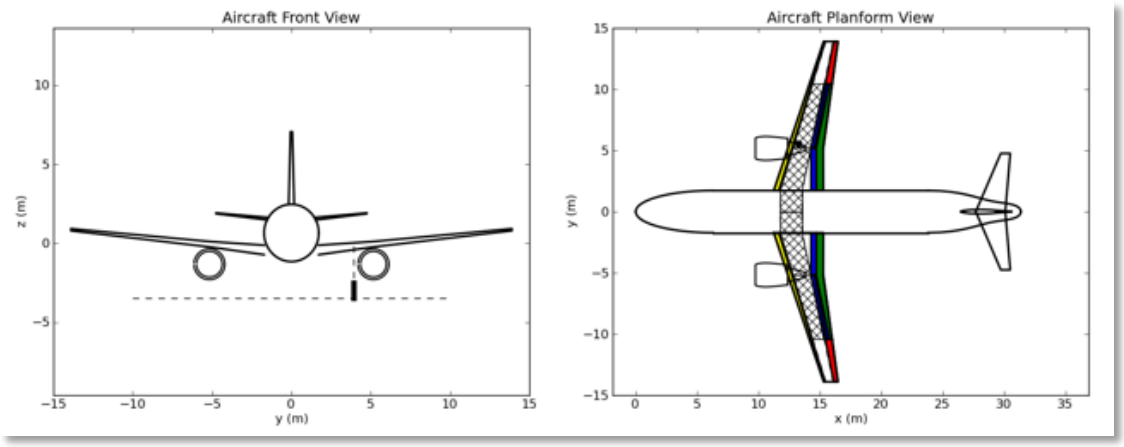

Figure 6 Front and planform view of the proposed DEAP aircraft baseline (Alderman, 2014)

The project consists of three main work packages. The first one is about the aircraft integration study and investigates a number of techniques to define the initial aircraft and to review other candidate configurations as part of exploitation case studies. The second word package-which is also related to this thesis study-had as an initial objective the development of an electrical system model to a high fidelity, the consideration of different transmission solutions and the contribution to the optimised fan design. Finally, the third package concentrated on the development and testing of the BLI fan design.

Some of this research study results were also used and verified during the DEAP project. The challenges of a possible fully superconducting network were pointed out, whilst the weight estimation of components that have not been built yet was an important input to the DEAP project. Energy storage possibilities were also investigated in this thesis report supporting the work package 2 of DEAP project. A more detailed description of the structure of this thesis will follow in the next section.

1.4 Thesis methodology and structure

The overall aim of the study is to assess the challenges, limitations and potential benefits of the TeDP concept as a future aircraft propulsion approach. Early studies have shown superconductivity to be one of the main enablers of this concept; hence primarily a focus on the design of such a network was necessary. Some of the components of this network have never been used before in airborne applications, whilst others have not even been built yet. Hence, it was important to investigate the performance of these components, the interaction between them and some crucial attributes such as their weight which became the number one priority as the research was moving forward. The novelty of the whole approach however creates numerous design possibilities for the hybrid electric aircraft under investigation. Some of these possibilities were explored during this study enhancing the attractiveness of the concept. The thesis outline could be summarised as follows:

- **A literature review** will follow in Chapter 2. This review will initially cover the DP concept comparing the possible modifications of this approach. All the previous and current studies will be presented whilst the electric hybrid approach will be emphasized. Superconductivity as a phenomenon will be presented and a brief description of the cooling options in this type of aircraft will also be described.
- **The study of Autonomous Power Networks** will be the main focus of the third Chapter. Firstly the design process of a conventional power network will be described, whilst a specific working example will also be presented. After that, the novel components of a superconducting network will be analysed and a comparison between the design process of a conventional and a superconducting network will conclude this section.
- Chapter 4 describes a **method to estimate the weight of fully superconducting machines.** Corresponding machine models will be demonstrated and used throughout this research study. Sensitivity studies in regards to the several inputs of the models will conclude this section.

- **A Superconducting Electric Aircraft** approach will be the subject of Chapter 5. In this approach a superconducting version of the More Electric Aircraft (MEA) concept will be described testing the limits and the design possibilities that such an approach could create.
- **A novel flight cycle study** will then be reviewed in Chapter 6. This chapter will focus on the numerous design options of the DEAP concept for the optimisation of the propulsion system of such an electric hybrid aircraft. The role of energy storage subsystems will also be explored. Batteries, Supercapacitors, and Superconducting Magnetic Energy Storage (SMES) will be investigated as possible energy storage options for the TeDP concept.
- The results and outcomes of the study will be discussed in Chapter 7 **(Conclusions).** A summary of the most important concluding remarks and key findings of this research study will be pointed out. Finally, **future work** will be the last section of this study. Since this project applies for the timeframe 2035+, this Chapter will reasonably be an important contribution guiding the future research studies on the fields and knowledge gaps of this innovative concept.

2 Literature Review

Before each chapter of this research study the corresponding literature review will be described. An overview of the main aspects of the novel concept under investigation will be presented in the current section of this thesis aiming on determining the optimal solution for the next aircraft generations and revealing the knowledge gaps of the proposed design.

Initially the historical evolution of the Distributed Propulsion (DP) concept will be presented and different modifications of DP configurations will be compared. The most promising of them (i.e. Turboelectric Distributed Propulsion) will be further analysed by both using a more conventional electrical power network as well as a superconducting version of it. This will lead to a quick overview of the phenomenon of superconductivity focusing on the materials and actual applications being used. Finally, a look on the possible cooling system options will conclude the first part of this study covering up all the background work that led to the implementation of this research study.

2.1 Distributed Propulsion (DP)

A first definition of the distributed propulsion term has been given in Chapter 1.1. However, DP could also more simplistically be described as any propulsion system which spreads the thrust requirements along the span of the aircraft. This could happen either by spreading the engines' exhaust or by spreading the propulsors. As a concept DP is not new at all with the first conceptual designs having started in the early twenties. More specifically, in 1924 Manzel proposed a patent for the propulsion system of airships, aircraft and like, consisted of multiple propeller units arranged in two rows (Manzel, 1924). This patent was aiming on an airship capable to ascent without a special landing field. Griffith in 1954 (Griffith, 1954) proposed a configuration with one master turbofan and several slave turbojet units distributed spanwise. The motivation behind this concept was the possibility of thrust vectoring and short take-off and landing phases. The next studies of distributed propulsion were driven by the lower weight to thrust ratio of the small gas turbines but the main breakthrough started

in the mid-70s where the fuel cost started to rise sharply and alternative propulsion options, including DP, attracted more interest. Figure 7 highlights some of the conceptual milestones in regards to the DP concept.

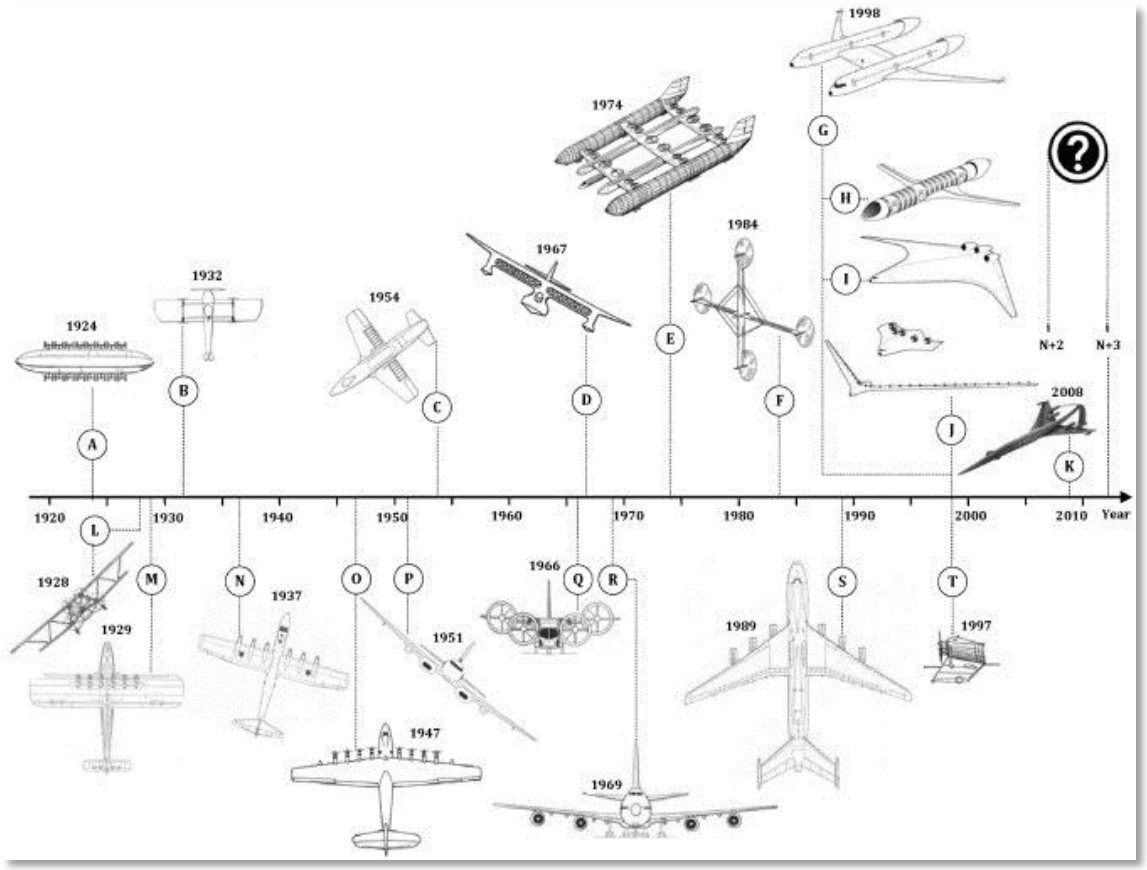

Figure 7 Distributed Propulsion Concepts Historical Overview (Gohardani, Doulgeris and Singh, 2011)

2.1.1 Small Gas Turbines (GTs) Concept

The majority of the initial DP studies were focusing on the distribution of smaller gas turbines. Although this concept presented some benefits, it has also shown some detrimental effects that were quite difficult to be overcome. In regards to the former, breaking the propulsion system into smaller units could lead to a more flexible and robust system, which can be characterised by its multi-functionality and possibly lower weight. Another benefit could be the so-called economies of scale, because by increasing the number of engines in an aircraft mass manufacturing might be necessary (Ameyogo, 2007). Moreover, by

distributing the engine weight and thrust loads a lighter wing structure could become feasible. The possibility of Boundary Layer Ingestion (BLI) is also enhanced in such a configuration, since a larger number of small engines will occupy more space in the wingspan, increasing the area available for boundary layer ingestion. BLI potential positive effect in future aircraft was one of the main areas of interest of both the DEAP project as well as for many other studies carried out in Cranfield University (Liu, 2013). Finally, noise reduction could be another advantage of the small gas turbines DP approach.

Theoretically, GT engine weight should be proportional to the cube of its dimensions. This could potentially lead in a weight benefit for the distributed configurations. However, as we scale down the engines, a number of component dimension constraints and manufacturing limitations can be observed. Due to the lack of research in small gas turbines and in new materials technology, considerable weight gains can be feasible only at the expense of severe performance degradation (Ameyogo, 2007).

The number and weight of the engines also affect the overall airframe weight. According to Torenbeek (Torenbeek, 1992) a single engine per wing already brings an approximately 3.5% reduction in wing structural weight. However, Eggenspieler (Eggenspieler, 2006) claimed that the maximum reduction in bending moment is not achieved with the maximum number of engines, but with a number of 11 engines per wing. The lack of space to optimise engine placement in the wing seems to be the main reason that further increase in the number of engines per wing does not lead to further wing box weight savings. The root moment reduction in the case of 11 engines per wing approaches 13%.

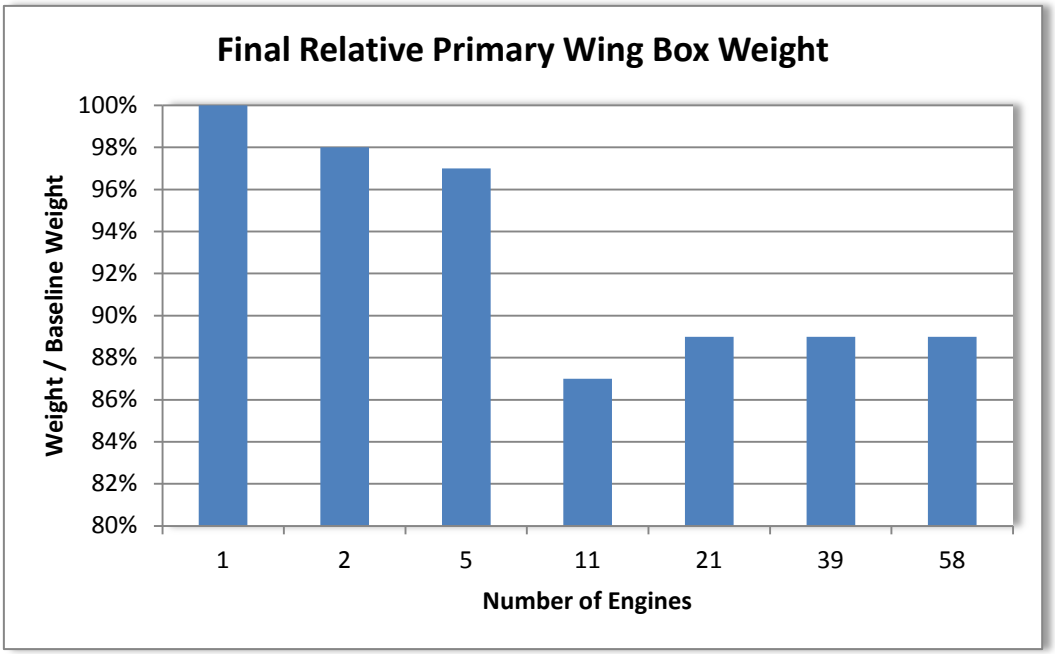

Figure 8 Wing box savings with different number of engines (Eggenspieler, 2006)

Notwithstanding the potential benefits of such a configuration, there are also many important disadvantages mainly derived from the small gas turbines themselves. Performance wise, small engines are less efficient since they suffer from manufacturing limitations that can make the cooling procedure impossible (Harada, 2003). Combustion efficiency also is degraded as combustors are scaled down. Moreover, tip losses will be relatively large for small engines, as the gap between the casing and the blade is proportionally wider, a fact that has a direct effect on compressor performance (Schaub, Vlasic and Moustapha, 1993). Additionally, below their critical value Reynolds numbers can lead to laminar flow and early separation, decreasing that way the components' efficiency.

The reliability of the engines is also an important issue for any aircraft configuration. Clearly, the more the engines the more possible is one of them to fail. However, thrust losses will be significantly less even if more than one engine fail simultaneously. On the other hand, if we place the engines close to each other, the possibility of cascading engines failure increases, since a rotor fragment could hit one of the adjacent engines. A chain reaction could therefore eliminate half of the available engines, jeopardising airframe reliability. In

addition, the large number of engines is directly connected with the number of sensors which are necessary to control the whole propulsion system. Thus, controls and instrumentation seem to be a significant barrier in the case of distributed propulsion configurations. If preventive maintenance is used, less instrumentation would be necessary, but even then the cost of instrumentation will still be high.

Another significant issue for this configuration is the location of the engines. Conventional airframes do not seem to be able to exploit the benefits of the distributed propulsion. Embedded engine configurations seem to present the best alternative. By embedding engines in the wing wave drag rise could be avoided, nacelle drag could be reduced and BLI would be enabled. The available space for the engines in the wing is the main concern in such a configuration. The engines that are now used are too large to embed them into a conventional wing. On the other hand, there is a limit of how much the size of the engine could be reduced, since the core cannot be too small. For the above reasons airframes such as the Blended Wing Body (BWB) might present a more optimal solution for DP concepts.

It becomes clear that current technology does not allow optimism in regards to the feasibility of small gas turbine distributed propulsion. Fuel consumption appears to be the most important hurdle, as well as the effect of nacelle drag which aggravates the fuel consumption issue even further. Furthermore, main disadvantages could be considered the size effects that lead to reduced overall thermal efficiency (Laskaridis et al., 2015). However, in the long term there are technologies that with improvements could make this project possible. In general, for aerodynamic reasons small gas turbine compressors have lower overall pressure ratios. The use of lighter heat exchangers with a higher effectiveness is therefore critical. The use of high temperature materials, such as ceramic matrix composites could, up to a point, eliminate the problem of manufacturing small-scale turbine blade cooling systems (Williams et al., 2008).

The most critical enabler for such a configuration will be the alternative airframes. Although BWB may not seem an ideal solution, many research

studies showed a lot of potential benefits using such an airframe in a DP configuration (Ko et al., 2003).

2.1.2 Distributed Driven Fans

Distributed driven fans are a more attractive case of distributed propulsion for many reasons. This configuration includes a core that generates power for a number of fans, transmitted via a transmission line. The distributed driven fans concept not only has most of the benefits that were previously mentioned for small gas turbine distributed propulsion, but also yields a significantly better overall efficiency of the system (Ameyogo and Singh, 2007). Clearly, this makes them more attractive from an environmental point of view. The three main components of this propulsion system are: the core, the transmission system and the fans.

Whilst high thermal efficiencies and fan propulsive efficiencies would be relatively easy to achieve by using either current or advanced technologies, the transmission of the power from the core to the fans will be a challenge and will most probably need unconventional technologies. Buquet (Buquet, 2007) carried out a research study of three different potential transmission systems for a distributed propulsion configuration: mechanical, core gas, and electrical transmission.

- *Mechanical transmission:* This type of transmission forms the smallest technological step of all the options. A free power turbine is connected to the core gas turbine and provides power to the fans through an arrangement of gearboxes and shafts. This configuration is similar to the one being used in helicopters. The biggest drawback of this method is clearly the weight which could become prohibitive as the number of fans rises. Buquet (Buquet, 2007) concluded that with current materials, the shaft weight required to transfer power to 20 fans would exceed 30,000lbs, in addition to the 20,000lbs weight of the gearboxes. This method is therefore prohibitive for a distribution system consisting of more than two fans.

- *Gas transmission:* In this case, instead of using a free power turbine the gas turbine exhaust is mounted into a plenum chamber. This chamber feeds a series of tip turbines through a manifold. These tip turbines then drive the distributed fans. Although the insulation required to transmit the core gas without excessive heat losses is relatively light, the weight of the ducts, of the supporting structure and of the tip turbines is still excessive. Moreover, the issue of ducting hot gas through the wing structure will create significant problems for an aerospace application (Kim, 2010). Furthermore, unknowns such as tip turbine size limitations and weight make this transmission method less attractive.
- *Electrical transmission:* Although this kind of transmission is the least developed, it shows the greatest potential to achieve low-weight, high efficiency energy transmission. Extensive analysis of this concept will follow in the upcoming sections.

The first advantage of the electrical transmission method is safety. Since high-energy rotating shafts or hot pressurized ducts are not involved, the system is safer. Also, if one of the fans failed it would be easier to isolate the fault without disturbing the normal function of the propulsion system. Furthermore, transmission efficiency in electric power systems is at least comparable to simple gearbox systems and significantly higher than gas transmission systems. However, perhaps the greatest benefit of electrical distribution is the flexibility that offers. If electric motors were mounted before each of the distributed fan, it will allow them to be independently driven at different rotational speeds (Figure 9). Each generator will be mechanically linked with a core engine, while the fans will be electrically connected to the generators through a kind of “electrical gearbox”. Thus, since generators can tolerate higher speeds than fans, the LP shafts of the core engines could run faster, decreasing the number of stages and the weight of the turboshaft engines. Moreover, decoupling torque and speed would lead to more control flexibility, enabling a better trade-off between design and off-design performance. Additionally, the use of electrical power transmission allows a high degree of freedom to place the generators and fan

modules to their most advantageous location. Power transmission lines do not require a particular strong and heavy supporting structure.

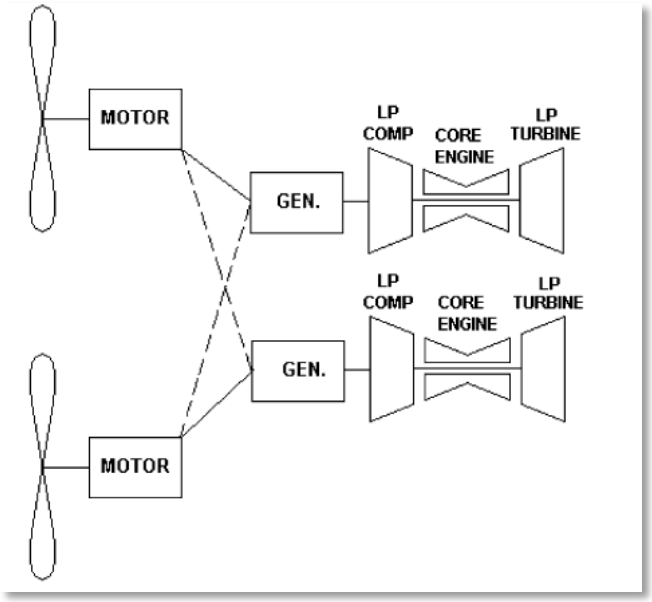

Figure 9 Electric Propulsion System (Luongo et al., 2009)

Although conventional technology does not allow optimism about the feasibility of distributed driven fans propulsion systems due to the weight penalties associated with the electrical machines, there are still ways to improve the attractiveness of the whole concept. Superconducting electrical machines and networks have been proposed by many researchers as the main enabler of the DP concept. Superconductivity could lead both to higher overall efficiencies and to lighter electric machines and components. The lighter the transmission system, the higher the optimum number of fans will be. The phenomenon of superconductivity will be described in this chapter (Chapter 2.2), whilst the benefits and constraints of a fully superconducting network will be presented in Chapter 3 and an extensive analysis of superconducting electrical machines will follow in Chapter 4. Superconducting networks require a cooling system to operate and a number of cooling methods will be presented later in this literature review study.

2.1.3 Electric Distributed Propulsion with a Conventional Electric Power Network

The first reasonable step towards the direction of hybrid electric distributed propulsion was the investigation of an aircraft implementing a conventional electric power network. The feasibility, potential benefits and possible hurdles of such a configuration could be easier explored by using electric components that are currently used in several industries and their technology is mature enough to be used in such a sensitive application as the aerospace. NASA, as part of a program called 'N+2 Distributed Propulsion Studies', developed the idea of a dual-use commercial/military transport vehicle, an aircraft with a rather conventional design, with two turbo-generators mounted in the middle of the wings and 16 propulsive fans each directly driven by an electric motor (Figure 10).

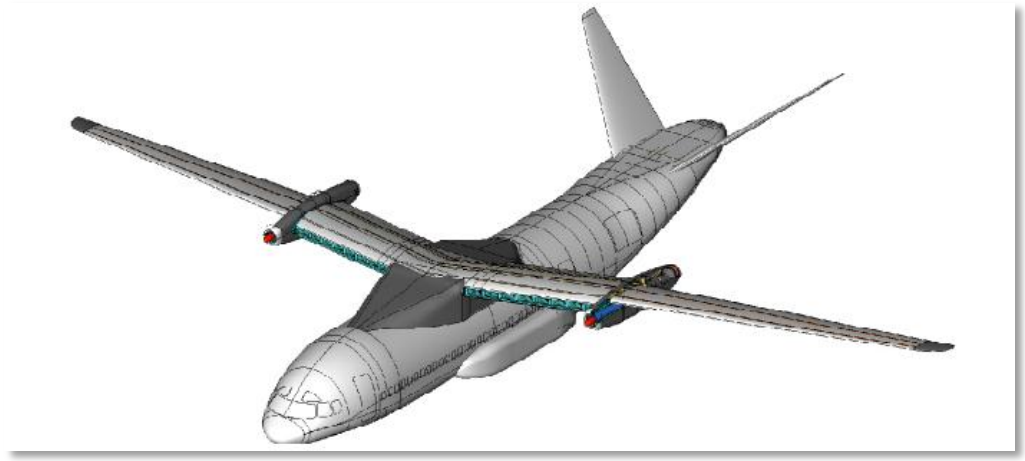

Figure 10 Dual-use commercial/military transport vehicle (Green, Schiltgen and Gibson, 2012)

In the aircraft above conventional electric machines and cables were used with an operating temperature around 450K. Green et al.(Green, Schiltgen and Gibson, 2012) created a program in Matlab aiming to analyse hybrid propulsion systems for future aircraft concepts and managed to make some useful conclusions about the feasibility of NASA's aircraft. For this study a single design point at 3000 ft. altitude and Mach number of 0.65 was chosen for all the components of the propulsion system. However, in such a configuration where

there is no mechanical decoupling between the various components different design points might prove more beneficial.

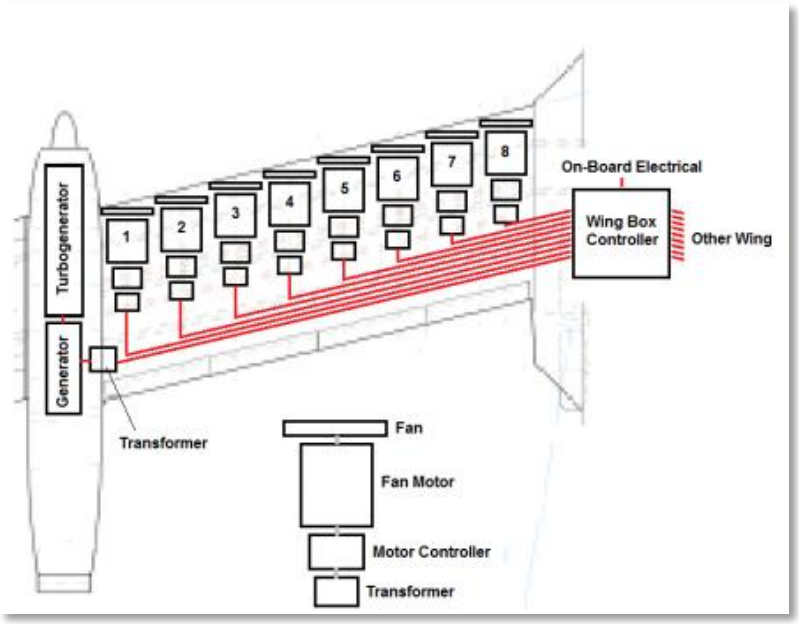

Figure 11 Hybrid electric distributed propulsion system example (Schiltgen et al., 2012)

Figure 11 demonstrates the system architecture that has been investigated during this NASA study. The turboshaft engine produces power to drive the generator, which produces the required electrical power to the whole network. This power is then transmitted through a transformer to a central wing box controller which directs this power to each motor, as well as to several other on-board systems. Another series of controllers and transformers are mounted before every motor-fan couple where the necessary thrust is being produced.

The study concluded that using conventional electric components (i.e. motors, generators, cables, and controllers) the propulsion system becomes much heavier than the state of the art conventional propulsion systems. However, benefits such as decoupled energy management, increased thermal and propulsive efficiency leading to possible reduced fuel consumption and capability of the aircraft to “fly smart”, are facts that cannot be ignored. More specifically, this aircraft design showed a potential 40% reduction in fuel burn, providing the implementation of an embedded turbo-electric distributed

propulsion system combined with cryogenic cooling (Schiltgen et al., 2011). Ways to diminish the weight penalties and to take advantage as much as possible the benefits of such a configuration need to be found. With this in mind NASA developed the N3-X model as part of the N+3 Advanced Aircraft Concepts.

2.1.4 N3-X Turbo-electric Distributed Propulsion Configuration

NASA is the organisation which has investigated in more depth the concept of DP. After several research studies the most suitable configuration of distributed propulsion seems to be the so-called N3-X configuration (Figure 12).

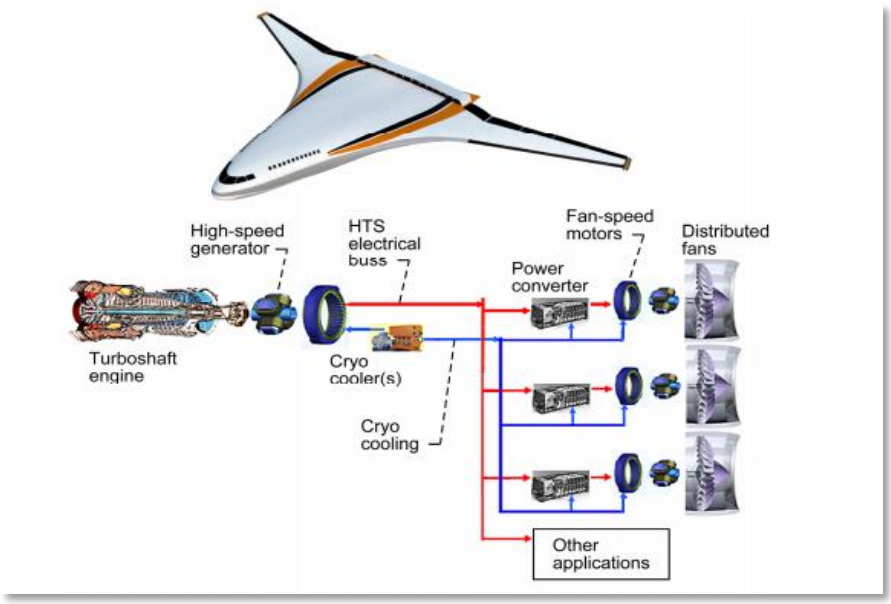

Figure 12 N3-X Hybrid Wing Body Aircraft Turbo-electric Distributed Propulsion Concept (Felder, Kim and Brown, 2009)

This configuration consists of two turboshaft engines driving two superconducting electrical generators. The primary function of these components is to produce electrical power and not thrust as in the conventional architectures. The electrical power is transmitted along redundant superconducting electrical cables to an array of propulsors embedded in the entire upper trailing edge of the fuselage section of the aircraft. In the N3-X configuration there are 14 propulsors, each consisted of a superconducting motor driven fan.

The two turbo-generators are assumed to be located on the wing-tips. Although this is not a common location for turbo-machinery in this application it offers some advantages. First of all, it minimises the risks to the aircraft and the passengers in the event of a turbine disk failure. Moreover, it allows the inlet to ingest free-stream air. As most of the energy of the gas stream is extracted by the power turbine in order to drive the generator, the exhaust velocity is low which consequently should result in low jet noise; hence one of the main goals of future aviation becomes easier to be achieved. Some bending moment relief in the normal direction is also possible due to this location (Felder, Kim and Brown, 2009). Additionally, research conducted by NASA in 1970 showed reductions in induced drag of up to 40% when a device that produces thrust is located at the wing-tip; this is due to the higher velocity thrust stream which reduces the wing-tip vortex well downstream of the wing itself. Last but not least the phenomenon of BLI will also be facilitated. The force required to decelerate the incoming air is the diffusion (or inlet drag) of the propulsion system and is proportional to the velocity of the incoming air. Thus, the propulsor inlet flow is decelerated by upper fuselage surface viscous forces and allows the propulsor system to take advantage of the wake, by reducing the inlet velocity of the propulsor and hence reducing the amount of inlet drag (Chengyuan et al., 2012). Furthermore, if the fan nozzle is not choked, the slower the inlet velocity the slower the exit velocity will be. The propulsive efficiency is given by the following equation:

$$n_{prop} = \frac{2}{1 + \frac{v_j}{v_o}} \qquad \textbf{(2-1)}$$

Where v_o is the free-stream velocity and v_j is the nozzle exit velocity. This equation is valid only if the inlet velocity equals the free-stream velocity (Pilidis, 2012). However, ingesting the boundary layer can result in significant losses. The trade-off between the benefits and drawbacks of BLI is a complicated task, but in order to enhance the potential benefits a hybrid wing body aircraft should have the following characteristics (Felder et al., 2011b):

- Inlets that ingest a large percentage of the upper surface boundary layer
- Inlets that are located near the trailing edge
- Continuous inlets and nozzles for minimizing external wetted area
- No boundary ingestion through the core engines, so that thermal efficiency will not be affected
- Minimum number of core engines, and
- High transmission efficiency.

Boundary layer ingestion is an important feature of the distributed propulsion concept. Many researchers have investigated several aspects of this phenomenon, but a lot of research is still to be done in this field. NASA (Felder et al., 2011b) examined the effect of boundary layer ingestion on turboelectric distributed propulsion systems in more detail, while Cranfield University (Doulgeris et al., 2012) investigated the dynamic response and high cycle fatigue analysis of fan blades under inlet distortion, a phenomenon linked with the boundary layer ingestion. Finally, several MSc students of Cranfield University have investigated the effect of boundary layer ingestion in areas such as ducted axial fans (Costi, 2012), noise generation (Chambon, 2012) etc. and studies concerning this subject are still under progress(Valencia and Nalianda, 2015).

2.1.5 Distributed Electrical Aerospace Propulsion European Projects

NASA is not the only organisation investigating the TeDP concept. There are also some European projects mainly leaded by Airbus which explore both the distributed propulsion and the hybrid/electric concepts for the next generation aircraft. The baseline for the current and future projects is the Airbus' E-Thrust configuration (Figure 13).

Figure 13 EADS Innovations Work E-Thrust Concept Configuration (Courtesy of Airbus)

This distributed propulsion configuration consists of a single large turbine engine producing electricity to six ducted fans which provide the required thrust. This concept presents many similarities with NASA's N3-X models. Engines are optimised in turning fuel to shaft power; fans are optimised for higher propulsive efficiency, whilst both superconductivity and BLI are also taken into consideration. More specifically, the gas turbine is embedded in the tail so that it ingests the fuselage boundary layer and the motor driven by the engine is assumed to be superconducting. Finally, advanced lithium ion batteries are used mainly as a supplementary power unit during take-off and climb, whilst they are recharged during cruise with power provided by the engine. At all times the batteries should have sufficient energy to power the aircraft in the case of the turbine failure (Warwick, 2013).

The DEAP project which was earlier described (1.3) and constitutes an important part of this thesis was basically based on the E-Thrust project. In the DEAP configuration there are two gas turbine generators producing the power that drives eight motor driven fans who produce the require thrust (Berg et al., 2015a). Both the electrical machines and the transmission system are superconducting, whilst different architectures in regards to AC and DC distribution were investigated. Figure 6 demonstrates the proposed airframe,

while Figure 14 presents an example of the basic electric architecture investigated during the DEAP project.

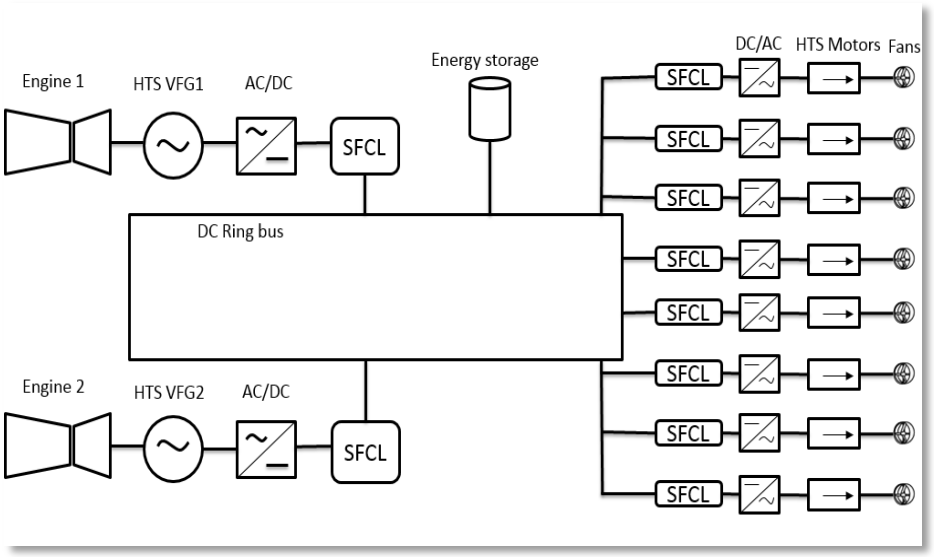

Figure 14 Basic electric architecture case in DEAP project

Boundary layer ingestion was also one of the main fields of study for the DEAP configuration. The DP propulsors were placed in the boundary layer at the rear of the fuselage. CFD studies were carried out to determine the characteristics of the BLI intake and the possible efficiency penalties on the fans derived from the fuselage BLI (Wright et al., 2015).

In the following chapters, DEAP project will often be mentioned as a reference since significant work of this research study was carried out under the Cranfield University required deliverables during this two-year TSB funded program.

2.1.6 Distributed Propulsion Summary

Although TeDP seems as a very promising design concept, there are some particular aspects of it that should be further investigated in order the proposed configuration to be successful. As it has already been mentioned, the major barrier of this design is the weight penalty of the conventional electrical machines.

Adding almost 14,000 lbs of motors, generators, power electronics and transmission equipment instead of a single shaft and gearbox may seem

impossible to result any fuel savings (Felder, Tong and Chu, 2012). But the comparison is more complicated than that. Turbo-electric powered aircraft saves weight by eliminating the gearbox, the pylons and most importantly reduces the fuel load (better efficiency) which leads to a lighter propulsive system; hence a lighter aircraft.

Superconductivity is perhaps the main enabler of manufacturing lighter machines, but there are a lot of side effects which someone needs to take into consideration. A major challenge will be the manufacturing of superconducting motors and generators with superconducting filaments of sufficiently small diameter to keep losses low in the stator. The phenomenon of superconductivity will be described in more detail in the following subchapter.

2.2 Superconductivity

Superconductivity is a phenomenon observed in certain materials that present true zero electrical resistance and expulsion of magnetic fields when cooled below a critical temperature. As a phenomenon it was discovered in 1911 by Dutch physicist Heike Kamerlingh Onnes. Mercury was the first material which Onnes discovered suddenly losing its resistivity when cooled to the temperature of liquid Helium (i.e. 4K). In the next few decades the same behaviour was observed in several metals, alloys, and compounds. However, strong interest in the field of superconductivity was mainly revived in the 80's when the first so-called High Temperature Superconducting (HTS) materials were discovered (Malkin and Pagonis, 2013). Critical temperatures of up to 110 K have been recently reached, whilst significant efforts to fully understand the capabilities and limits of these materials have been made. In addition to temperature, a superconducting material should not exceed certain limits of current density and magnetic field (Figure 15).

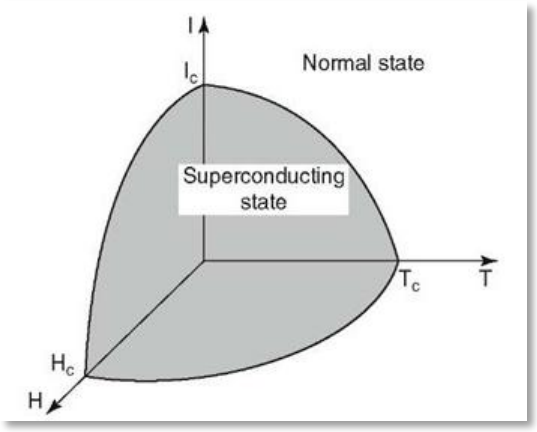

Figure 15 Critical T-H-I Diagram for a superconducting material (www.what-when-how.com, 2015)

2.2.1 Superconducting Materials

There are numerous materials presenting the superconducting properties but not all of them are appropriate for an industrial or an aerospace power application. The requirement of cooling to near liquid helium temperatures was the main limiting factor of applying the superconducting technology to any application for several decades. However, the discovery of superconducting materials at temperatures above 77K initiated a new era in the field of superconductivity. For power applications similar to the ones investigated in this research study there are three main superconducting materials which have attracted more interest; Bismuth Strontium Calcium Copper Oxide (BSCCO), Yttrium Barium Copper Oxide (YBCO), and Magnesium Diboride (MgB_2).

YBCO is the first material ever discovered to become superconducting above the boiling point of liquid nitrogen (i.e. 77K) having a critical temperature over 90K. It was discovered in 1986 by Georg Bednorz and Alex Mueller who were working in IBM Switzerland (Bellis, 2015) and it was the base of many HTS materials to come. The significant breakthrough of the discovery of YBCO is the much lower cost of the refrigerant used to cool the material below their critical temperature. YBCO has been used as the main material in the rotor of several superconducting electrical motor and generators prototypes (Chapter 4.1), as well as in electrical equipment such as Superconducting Magnetic Energy

Storage (SMES) devices (Jin et al., 2014) and Superconducting Fault Current Limiters (SFCLs) (Kim, Sim and Hyun, 2006). Both these superconducting applications will be analysed in following sections of this study. There are two primary reasons that prevent the use of these materials in several applications. Firstly, their low critical current densities compared to the competitive superconducting materials and secondly the difficulties in processing these materials into the commonly required wire form. The critical current density for an YBCO material operating at a temperature of 77K can be found around 350 A/cm^2 (Sözeri, Özkan and Ghazanfari, 2007).

BSCCO on the other hand was first discovered around 1987 by H. Maeda and his colleagues at the National Research Institute for Metals in Japan (Maeda et al., 1988). Its high critical temperature of above 105K attracted the interest of many industries the years following its discovery. The understanding of this material even today is a complicated task. However, the last decade BSCCO has been progressed to the point of being commercially available with solid mechanical properties in operational temperatures around 77K (Scanlan, Malozemoff and Larbalestier, 2004). Many superconducting electrical machines prototypes have been using BSCOO for their rotor (Chapter 4.1), whilst other electrical equipment such as HTS transformers of maximum power rating between 500 kVA and 1MVA have been using BSCOO-2223 winding cooled at 77K (McConnell, Walker and Mehta, 2000). Furthermore, BSCOO filaments have also been used in SMES devices (Shi et al., 2007).

BSCCO was also the first HTS material that was used for making practical superconducting wires. It is typically available in tape form (Figure 16) making the production of BSCOO material in wire form a challenging task. The critical current density (Jc) of BSCOO-2223 based wires has been the research focus of many companies for over 20 years steadily improving its performance over time. Long-length wires (>150m) with maximum current up to 170 A (Scanlan, Malozemoff and Larbalestier, 2004) and critical current density of 12-14 kA/cm^2 at 77 K self-field (Jin et al., 2014) are nowadays available.

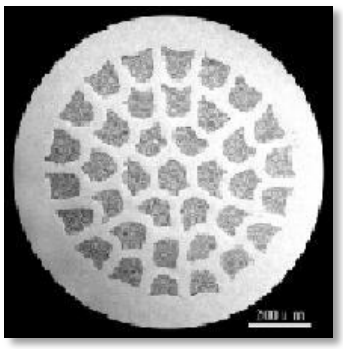

Figure 16 Micrograph showing the cross-section of an as-drawn BSCCO wire (courtesy of Applied Superconductivity Research Center)

Finally, MgB_2 is the simplest and less expensive superconducting material under investigation. It was discovered in 2001 by the group of Akimitsu (Akimitsu, 2001) and is considered as the "conventional superconductor" with the highest critical temperature (i.e. 39K). Although its critical temperature is lower than the one of the HTS materials, its simple and robust mechanical properties make it an attractive option for many applications. It is also available in fine twisted filaments and in a wire form reducing the AC losses that the other two popular superconducting materials (i.e. YBCO and BSCOO) present. For this reason it seems reasonable to believe that future fully superconducting machines will use MgB_2 as their main material for their stator (more information in Chapter 4). Furthermore, its relatively low cost and its capability of very sharp transition for the superconducting to the normal state enhance their attractiveness for protection devices such as SFCLs (Shcherbakov, 2011). Finally, recent publications about MgB_2 indicate that further developments of

this material will be available with even higher critical current densities J_c (figure below) (Li et al., 2012).

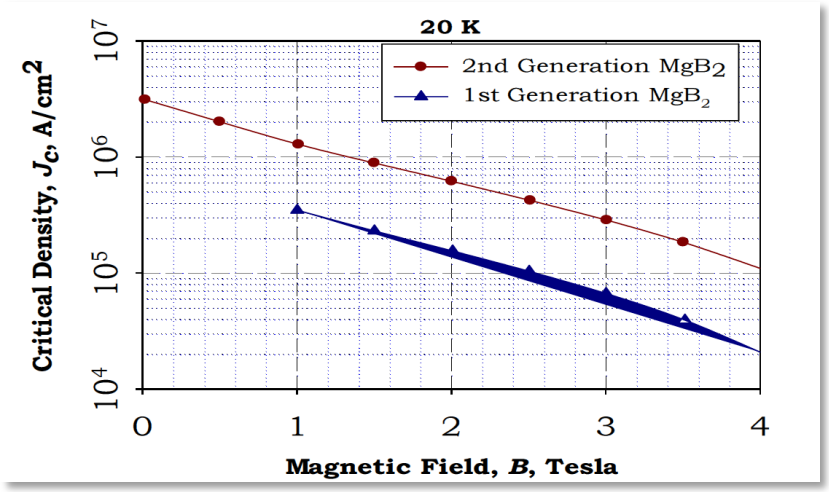

Figure 17 2nd Generation MgB_2 wires improved current density. *(Courtesy of Hyper Tech Research Columbus)*

Table 2 summarises some of the critical values of the aforementioned superconducting materials. Generally, it is really difficult to give absolute values for these parameters since they are a function of several secondary factors. In the following table the current density was based on an operational temperature of 77K for both the YBCO and BSCOO case (Scanlan, Malozemoff and Larbalestier, 2004), whilst the value for the MgB_2 case was based on an operational temperature of 20K. The last column is independent of the operational temperature and it is just an indication of the upper H_c limit in each material. Note that although BSCOO has a higher H_c limit it has a much lower irreversibility field H^* than YBCO which enhance YBCO's use in creating high field magnets (Golovashkin et al., 1991). The value of 74 T in the MgB_2 case can be reached only in thin films.

Table 2 Summary of the main characteristics of several superconducting materials

Material	Critical Temperature (K)	Upper Critical Field (T)	Critical Current Density (kA/cm^2)
YBCO	93	170	0.35
BSCOO	110	200	12-14
MgB_2	39	74	>100

Clearly, the choice of the ideal superconducting material is highly dependent on the application itself. YBCO might be the best choice for applications where really high magnetic fields are required, BSCOO is the ideal candidate in applications where the required cooling power needs to be the minimum possible, whilst MgB_2 could be the favourite option in cases where low cost and high current densities are the main priorities.

2.2.2 Superconducting Components

These materials have been used in several components of generation, transmission (i.e. power cables), distribution (i.e. transformers) and in end-use devices such as motors. In the TeDP concept a fully superconducting network is expected to be used. This network will consist of numerous superconducting components, most of which will be further analysed during this research study.

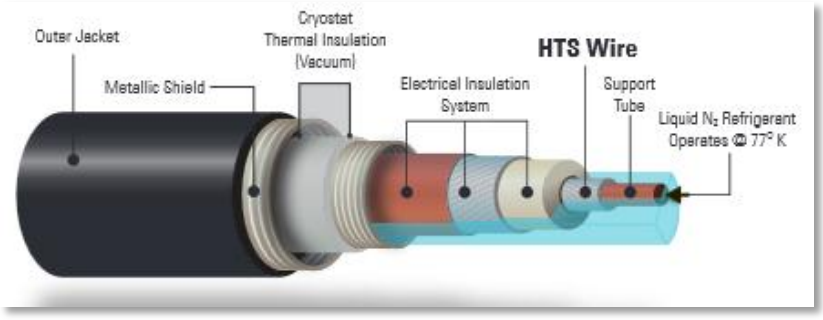

Figure 18 Typical HTS Cable structure (Courtesy of Suptech.com)

In a power application the superconductors are consisted of multifilamentary wires in which the superconducting filaments are embedded in a matrix of a normal metal, an insulation system (electrical and thermal) and possibly more layers which aim to protect the cables from magnetic flux jumps and quenching (Larbalestier et al., 2001).

Figure 18 demonstrates the structure of a typical HTS cable. Each high power application defines different parameter sets in regards to the critical limits of magnetic field, temperature, and current density of these superconducting cables. Table 3 summarises the wire performance requirements for various industrial devices, whilst an ongoing dialogue between several science communities continuously changes these requirements based on the technology improvements and evolution of superconducting materials. The three materials described in the previous section (2.2.1) are the only superconducting materials which can satisfy these requirements.

Table 3 Industry wire performance requirements for various device applications (Larbalestier et al., 2001)*****

Application	H_c **(T)**	T_c **(K)**	J_c (A/cm^2)	I_c (A)	**Wire Length (m)**
Fault current limiter	$0.1-3$	$20-77$	10^4-10^5	10^3-10^4	1000
Motor	$4-5$	$20-77$	10^5	500	1000
Generator	$4-5$	$20-50$	10^5	>1000	1000
Transmission cable	<0.2	$65-77$	10^4-10^5	100 per strand	100
Transformer	$0.1-0.5$	$65-77$	10^5	10^2-10^3	1000

*According to the reference data was supplied by R.Blaugher

Generally, the commercialisation of many HTS wires have made the use of these cables in practical applications widely possible. However, there is still

need for a better understanding of these materials which could lead to even better wire performances. The reduction of AC losses, the stability improvement, the simplification of the processing, and the improvement of the wire robustness are only some of the areas that need further development (Zhang et al., 2014).

The electrical machines (i.e. motors and generators) of a configuration similar to the TeDP are expected to be fully superconducting. The motivation behind using this type of machines is their ability to carry very high current density without any resistance, thus enabling lighter machines. Superconducting generators can increase the machine's efficiency to over 99%, while simultaneously losses can be reduced by up to 50%. These numbers are even higher for airborne generators (Barnes, Sumption and Rhoads, 2005). A full list of the state of the art superconducting machines will be presented in Chapter 4.1. The majority of these machines have only their rotor primarily made of superconducting materials, whilst they consist of a conventional copper stator. Fully superconducting machines have only been built once or twice, and little has been published on those that have. However, in order to acquire the required power densities for a TeDP configuration, both the rotor and the stator will have to be superconducting for high currents, compactness and low losses. In Chapter 4.2 a method of estimating the weight of these machines as reliably as possible, given the current state of understanding, is described.

Other equipment that is expected to be superconducting in the TeDP configurations under investigation are the whole transmission system (i.e. cables), parts of the protection equipment, switching devices and possible energy storage mechanisms. All these components will be described in detail in the following chapter (i.e. Chapter 3.3) where the several elements of fully superconducting networks will be explored.

Superconductors require cryogenic temperatures to operate and hence the cooling system constitutes an important feature in this new aircraft design. The feasibility of such a configuration highly depends on this secondary system which will add weight and complexity to the whole architecture.

2.3 Cooling system

The importance of the cooling system in these novel configurations has been highlighted in many parts of this research study. The complexity and additional weight of this system has been considered by many as the main barrier of using superconductors in power applications which are weight sensitive. Furthermore, the need for excessive cooling power was the main reason why Low Temperature Superconductors (LTS) were never broadly used.

There are two main cooling methods which have been examined as potential cooling systems for the TeDP configurations; the use of cryo-coolers or the use of liquid cryogen cooling.

2.3.1 Cryogenic Fluid with a Heat Sink

The main advantage of this method is the possibility of using the liquid coolant also as a fuel for the aircraft. This will result in an almost 100% efficient cooling system since any losses this system may have could be automatically used as a fuel for the propulsion system. In this concept the cryogen is being loaded at the airport in a quantity that will be enough for the flight duration in addition to an adequate margin for safety reasons. Before each flight the tank will have to be refilled allowing the minimum possible weight penalty for the cooling system.

In NASA studies hydrogen has been explored as a possible cryogenic fluid for their N3-X model (Gibson et al., 2010). Hydrogen can be cleanly converted into electrical energy through fuel cells or even by burning it in high speed turbo-generators without any significant emissions. The disadvantage of hydrogen is its volume; for the same fuel energy hydrogen has four times the volume of jet fuel. Notwithstanding its volume, hydrogen has a substantially high energy unit mass which results to only one third of the weight compared to a jet fuel of the same energy (Felder et al., 2011a). Hence, it can be stored in liquid form at cryogenic temperatures without adding excessive weight, providing an adequate cooling system for the proposed designs. An example of a typical LH2 powered aircraft power system configuration is shown in the next figure:

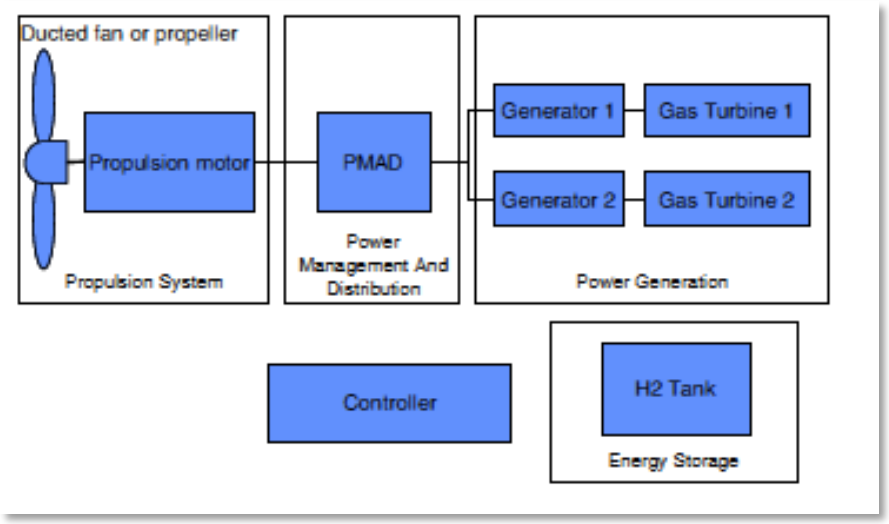

Figure 19 An example of a LH2 power system TeDP configuration (Masson et al., 2007)

In such a configuration the gas turbines run at their optimum rotational speed, maximizing their efficiency, while coupled to high speed generators. The H2 tank provides hydrogen to the propulsion motors as well as the generators, which in this case could be fully superconducting. Hydrogen has a boiling point at 20.28 K which is significantly lower than the expected operating temperature of HTS. In addition, it could potentially cool even MgB_2 superconductors. Moreover, liquid hydrogen provides an operating temperature that yields very high current densities and as a result smaller and lighter electrical components (Felder et al., 2011a).

Other liquid coolants such as nitrogen or methane could also be considered. However, their boiling points (77 and 111 K respectively) complicates their use as an exclusive mean of cooling. Methane's boiling point is too high to be used as the main coolant even for a HTS network, nonetheless its use should not be excluded in the case of a double stage cryo-cooler (presented in A.2) cooling system where it can serve as a heat sink for the cryo-coolers. On the other hand, liquid nitrogen might not be the best alternative to hydrogen mainly because the critical current density at 77K is typically too low to yield competitive superconducting machines and transmission lines in terms of weight and efficiency (Felder, Kim and Brown, 2009).

2.3.2 Cryo-coolers

A cryo-cooler, in simple terms, is a refrigerator that produces very low temperatures. In the TeDP case the required temperatures are expected to be between 20K and 65K, depending on the superconducting material that is being used. Later, in this research study the worst case scenario in terms of temperature (i.e. 20K) will be explored. Cryo-coolers pump the heat generated by losses in the superconducting machines from the highest available temperature of the device to the sink temperature where the heat is rejected. Unfortunately, by today standards, cryo-coolers are too heavy for airborne applications. A cryo-cooler specific mass less than 3 kg/KW of input power is required to keep the cryo-cooler mass into accepted limits. In general, most cryo-coolers have 3 to 5 times the desired mass (Radebaugh, 2012). The most promising type of cryo-cooler in terms of weight seems to be the reverse Brayton. In comparison to other active cooling configurations, turbo-Brayton cryo-coolers produce a continuous cycle gas flow at a high flow rate. The latter allows a constant heat transfer of high capacity from the cooling load to the heat rejection site (Guzik and Tomsik, 2011). Figure 20 presents a survey of the existing reverse Brayton cryo-coolers used in industrial applications. Note that significantly lighter machines should be expected if these components are optimised for use in an airborne application (Palmer et al., 2013).

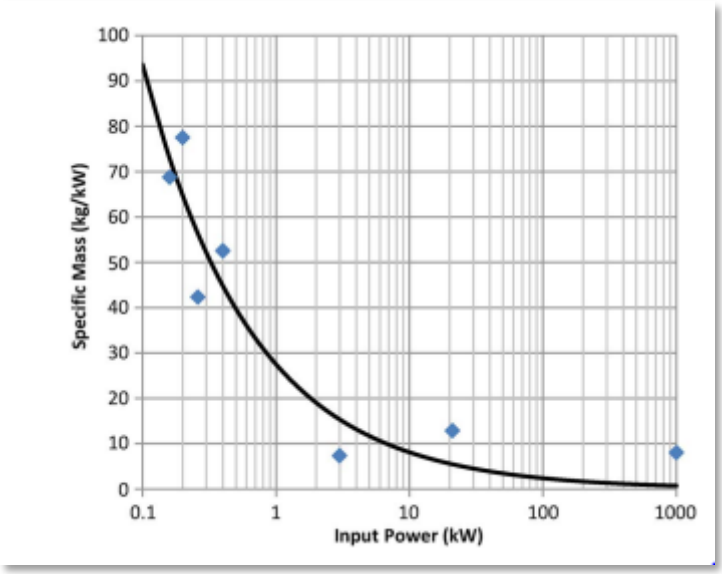

Figure 20 Reverse Brayton Cryo-cooler study (Berg et al., 2015a)

Based on the study shown in the figure above an equation that links the specific mass of the cryo-cooler (m_{cryo}) with the input power requirement (P_{in}) can be derived:

$$\mathrm{m_{cryo}} = 27.5 \exp\left(-1.225 * (\log_{10} \mathrm{P_{in}})\right) \quad \textbf{(2-2)}$$

The specific mass estimated from the equation above includes the heat exchangers, the compressors, the piping and the insulation of the cryo-cooler and is measured in kg/kW, whilst the input power requirement in kW is based on a Carnot efficiency of 0.3 (Berg et al., 2015a). . The amount of required cooling power depends on the operational temperature of the superconducting materials being used as well as the sink temperature where the heat is rejected. The bigger the difference between these two temperatures the greater the power required. That is the main reason why this power is larger for $\mathrm{MgB_2}$ than for BSCCO based devices.

The most critical components of these components have been identified; compressors, turbines, and heat exchangers must all show some level of improvement over the current level of technology if goals outlined by Luongo et

al. (Luongo et al., 2009) are to be realized. The following figure shows the past performance as well as the projected trendline of aerospace cryo-coolers until the 2050 timeframe.

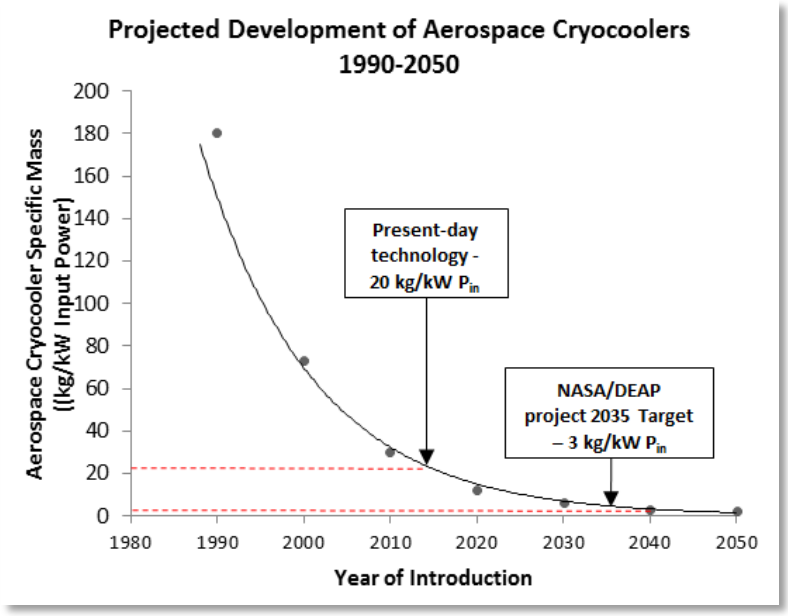

Figure 21 Projected development of cryo-coolers optimised for aerospace applications (Palmer, Pagonis and Malkin, 2015)

The optimal number of the required cryo-coolers in a TeDP configuration is yet to be decided. However, the choice of a single central cooler is already being excluded, because of the unaccepted case of a single point failure. Each turbo-generator should have one or even more cryo-coolers on its own, while a group of adjacent motors in the propulsor units could probably share one cooler. Either way, factors such as weight, safety, efficiency and cost should be taken into consideration before the cooling system is fully decided.

In the DEAP project, models that estimate the weight of single and double stage turbo-Brayton cryo-coolers were developed and used also in the present study. A more detailed analysis of these models can be found in A.2 where the chosen architecture and all the assumptions being made during the development of these models will be pointed out.

2.4 Summary

Throughout the years there have been several studies focusing on the concept of Distributed Propulsion (DP). Several versions of DP have been analysed in this chapter which have as a target to decide the most promising configuration in terms of weight and efficiency. The feasibility of small gas turbines DP, which has been popular in the first DP studies, is limited mainly due to the excessive fuel consumption associated with the small gas turbines. However, their performance could be improved in case of significant advances in heat exchangers technology. The configuration with distributed driven fans seems as a more beneficial architecture. In driven fans DP concept there are three different possible transmission systems: mechanical transmission, tip turbine driven fans, and electrical transmission. The weight of the mechanical transmission system and the lack of available space in the case of gas transmission were the main barriers for the first two versions of distributed driven fans configurations. Electrical transmission seems to be the most promising architecture in the long term.

Turbo-electric Distributed Propulsion (TeDP) appears to be the most favourable future disruptive technology. The weight of the electrical components is the main drawback of such a configuration. Hence, its feasibility as a concept depends on the availability of superconducting elements. Both NASA and European projects such as DEAP are investigating the electric DP and the potential superconducting nature of the proposed propulsion systems.

Based on the power requirements of the equipment in a DP configuration only three superconducting materials could be used in this network: BSCCO, YBCO, and MgB_2. Although the first two have higher operational temperatures, MgB_2 has some attractive characteristics (such as availability in wire form, lower cost etc.) that cannot be ignored. There is however a caveat to superconducting materials; they require cooling to cryogenic temperatures in order to perform as superconducting.

The cooling system is clearly an important secondary system of these novel configurations. The two options explored by the major Institutions at the

moment are the use of a cryogenic fluid or of mechanical cryo-coolers. Although a cryogenic fluid could also be used as a fuel in some configurations leading to an almost loss-free cooling system it is a technological step which requires significant background studies and combined with the already disruptive technology of TeDP suggested in this study might jeopardise the consolidation of electric DP as one of the most promising future concepts. Both in DEAP project and in the present research study the cryo-coolers' option has been further investigated.

3 Design of Autonomous Electrical Power Networks

One of the initial objectives of this research study was the design and the simulation of the complete superconducting power network which a Turboelectric Distributed Propulsion (TeDP) powered aircraft will implement. However, in the early stages of this study it became clear that such a model cannot be developed without extensive laboratory work. What makes the modelling of such a configuration unfeasible is the fact that fully superconducting DC networks present, at least theoretically, zero resistance making the current sharing of the superconducting transmission lines really difficult to be predicted. Conventional modelling strategies and tools are not designed to simulate zero resistance systems; hence, even the design of a steady state model for such a configuration requires additional experimental work.

In this chapter, the main design issues and characteristics of a Superconducting Power Network (SPN) will be described. In order to achieve this, firstly the design process of a conventional power network will be presented. As a first example, the design procedure of a hybrid/electric ship will be described and an actual working example will be presented. The next step will be the description of a SPN, emphasising its different design approach compared to the conventional power network designs and the novel elements that such a network include. Some of the design issues and limitations of these networks will also be pointed out, whilst an overall synopsis of benefits and constraints of FSNs will conclude this chapter.

3.1 Introduction to Electric Power Network Design

The design process of a SPN could become clearer if the design procedure of an autonomous conventional power network is firstly described. This design process is not as clear and far more complex than might have been imagined since most of the current power networks are extensions (i.e. grid power networks) or modifications of already existed power systems (i.e. automotive, marine, and aerospace industries). Clearly, setting up a general network design

process might be misleading since the requirements of each power network depend on the application it is designed for. However, a generic design methodology will be described in the following section followed by a specific working example. The ultimate goal of this section is the representation of the power network of a TeDP type of aircraft where superconductivity will be in use. A conventional power network with many similarities both in components and in power rating terms is the hybrid/electric ship. Besides, modern maritime vessels include advanced systems in many areas of interest for aircraft designers (Bollman et al., 2015). Marine electric vehicles were occupying a $2.6 billion market in 2013, a number that is expected to be more than double by 2023 (Harrop, 2013).

3.2 Conventional Design of Autonomous Electric Power Networks (EPNs)

In this section a general design process of a conventional power network will be initially described. A specific example of such a network will follow, where the several steps of the design process will be supported by equations and numerical examples. The main objective of this section is to point out the factors that drive the design of a conventional power network, so that a comparison could later be made with the superconducting version of these networks.

3.2.1 Proposed Autonomous Power Network Design Process

The following graph (Figure 22) demonstrates a design methodology of a conventional autonomous power network. The first stage in the design process of any power network is the analysis of the requirements. The power requirements of each network are typically known at the very beginning even when someone starts the design process from a blank page. Power and operational requirements need to be specified and allocated to relevant functional components. The power requirements are what basically size the whole network. These determine the basic parameters of each electric network such as the system voltage (*Vs*), the normal currents (*Is*), and the frequency (*f*). Depending on the application a different selection of basic parameters can be made even for networks of similar power requirements. Main bus bar size,

protection devices availability, required power converters, and overall system losses are some of the criteria that typically determine the basic parameters selection. More specifically, normal currents are the sizing factor for the main bus-bar of each network. The higher these currents are the heavier the bas bar will be. Furthermore, normal currents level also determine the fault currents level and hence the required rating of the switchgear. Switchgear devices have typically an interruption performance limit of around 40 kA (kilo Ampere) and ratings above this limit should be avoided (Malkin and Pagonis, 2013).

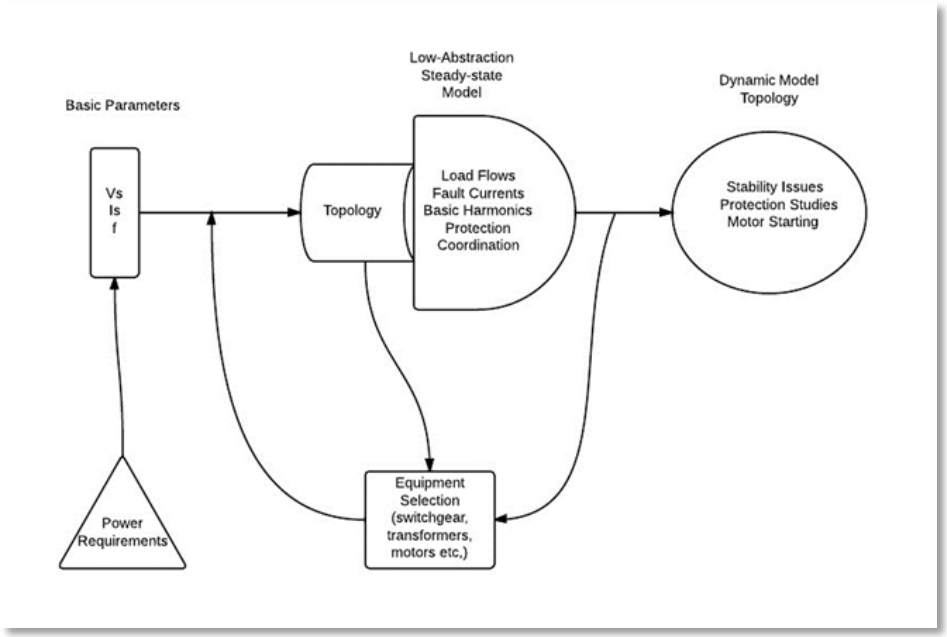

Figure 22 Design Process diagram of a conventional power network (Malkin and Pagonis, 2013)

Once these parameters are selected, an initial topology of the network will be defined. This topology will include the type and number of the main power sources (i.e. engines, generator sets, energy storage etc.), the number of switchboard sections, the converters and transformers of the system, and generally all the necessary equipment for the network. Depending on the network nature and requirements different architectures could be implemented such as bus, star, tree, ring, mesh, and/or a combination of them. The selection between AC and DC distribution is also a challenging task which requires

careful consideration in the initial stages of the design process of a power network since it dictates many of the equipment later being used.

The next stage of the design process will be an initial load analysis (i.e. steady-state low-abstraction model) of the power network which will determine the overall power system design. The load-flow study is basically a numerical analysis of the electric power flow in an interconnected system. Various power parameters of the network such as voltages, voltage angles, real and reactive power of each bus and line of the network are determined during this load flow analysis. These studies are important both for optimising the performance of existing networks but also for planning future expansion of already existed networks (Andersson, 2006). Generally the load flow problem is formulated by a set of non-linear equations.

$$\mathbf{f}(\mathbf{x}, \mathbf{u}, \mathbf{p}) = 0 \qquad \textbf{(3-1)}$$

Where **f** is a n-dimension non-linear function, **x** is a n-dimension vector of the unknown component parameters (i.e. voltage magnitudes and angles in each node), **u** is a vector with known parameters (i.e. machines' voltages), and **p** a vector including the network parameters (i.e. lines' resistance and reactances). Due to the non-linearity of the power flow analysis, this cannot be solved analytically and hence iterative solutions are commonly implemented. Newton-Raphson, Gauss-Seidel, and fast-decoupled-load-flow-method are just a few of the solution methods being used to deal with the non-linear set of equations of a network's load flow. This analysis is of utmost importance to design the different power system components (such as alternators, transformers, transmission lines etc.) in order to be able to withstand any stresses they are exposed to during their steady state operation. These stresses could be a result of fault and short-circuit currents.

These fault conditions are typically caused accidentally through insulation failure of the components, externally factors difficult to predict (such as lightning strokes), or simply by faulty operations. Short circuits are the most frequent fault

in high power applications and depending on the location could cause stability problems, mechanical and thermal stresses and interference with conductors. The system needs to be protected from such faulty conditions by isolating the faulty parts of the network as quickly as possible typically with the use of protection devices such as circuit breakers. These devices ought to be capable of withstanding the maximum anticipated short circuits. As an example the calculation of a transient short circuit in a transmission line will be described (Andersson, 2006). It is known from circuit theory that the current of a circuit is composed of a steady state alternating current (i_s) and a transient direct current (i_t):

$$\mathrm{i} = i_s + i_t \tag{3-2}$$

Where,

$$i_s = \frac{\sqrt{2}U}{|Z|}\sin(\omega t + \alpha - \theta) \tag{3-3}$$

$$i_t = \frac{\sqrt{2}U}{|Z|} sin(\theta - \alpha) e^{-(R/L)t} \tag{3-4}$$

$$Z = \sqrt{R^2 + \omega^2 L^2} \angle(\theta = \tan^{-1}\frac{\omega L}{R}) \tag{3-5}$$

Where U is the system's voltage, R the resistance, L the inductance, Z the impedance, ω the frequency, t the time that the short circuit started, and θ is the voltage angle, whilst the parameter α controls the instant on the voltage wave when the short circuit occurs. However, the selection of circuit breakers is based on another short circuit value the so-called maximum momentary short circuit current (i_{mm}) which corresponds on the first peak of the short circuit

waveform and can be as high as double the value of the symmetrical short circuit current:

$$i_{mm} \leq 2\frac{\sqrt{2}U}{|Z|} \quad \textbf{(3-6)}$$

Power quality is one of the main priorities while designing an electric power network. This can be jeopardised by the distortion in the voltage and current waveforms caused by the harmonics. The most common type of distortion is a periodic steady-state where the distorted waveform has a Fourier series with a fundamental frequency similar to the power system's frequency (Ranade and Xu, 1998). Generally, the Fourier series for a regular periodic function is given by the following equation:

$$f(t) = C_0 + \sum_{n=1}^{\infty} C_n \cos(n\omega t + \theta_n) \quad \textbf{(3-7)}$$

Where C_0 is the dc value of the function, $C_n$the peak value of the n_{th} harmonic component, θ_n is the phase angle, whilst ω is the fundamental frequency and is equal to $\omega = 2\pi f \ rad/sec$. An example of the synthesis of a waveform from harmonics can be seen in the next figure:

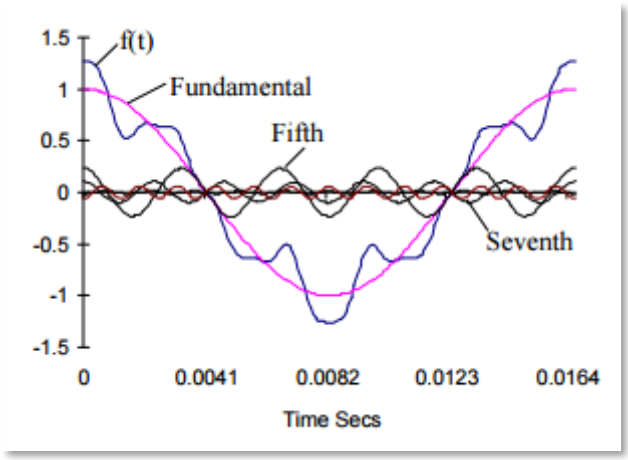

Figure 23 Synthesis of a waveform from harmonics

Generally, the propagation of each harmonic is studied separately since as it was described earlier the transmission system is typically simplified to a linear system. A small number of harmonics is typically considered in the early design stages. Harmonic studies are aiming on identifying the distortion levels in voltage and current waveforms of several points of the power network and evaluate the measures that need to be taken in order the harmonic caused problems not to affect the power quality of the whole network. The need for a harmonic study is typically indicated by the excessive measured distortion in systems which include several harmonic-producing equipment (i.e. transformers, switching devices, rotating machines etc.).

Finally, one of the main objectives of the steady-state model is the optimisation of the protection system coordination. Protective device coordination could be defined in simple words as the process of determining the optimal solution in terms of current interruption in abnormal electrical condition circumstances. Different protective zones are commonly set up in order to isolate potential faults in small regions of the network (Glover, Sarma and Overbye, 2010). However, the main objective of the coordination study is to minimise the outage of any zone as much as possible.

Once the steady-state modelling is complete the key elements of the network will then might be resized and redefined in order to optimise the network performance during normal operation. A more comprehensive dynamic model is

the next step of the design process of an autonomous power network. Figure 24 summarises some of the dynamic phenomena being investigated during this stage. C and D dynamics have already been described as parts of the steady-state analysis.

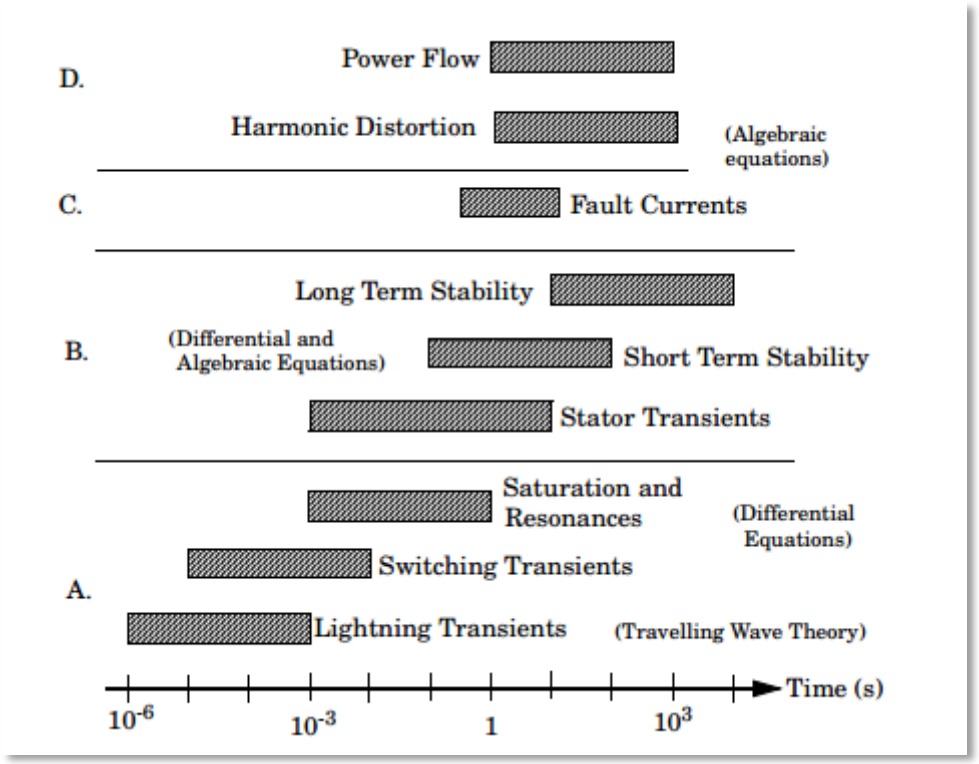

Figure 24 Dynamic phenomena with their corresponding timescales in a power network: A. Electro-magnetic transients, B. Synchronous machine transients, C. Quasi steady state, and D. Steady-state phenomena (Andersson, 2006)

Transient motor starting analysis is another example of dynamic phenomenon in an electric power network. When motors start they typically require a high inrush of current (5-7 times their normal current) for a short period of time which could lead to excessive voltage drop. This drop needs to be monitored and analysed so that its effect both on the motor itself (i.e. possibility of stall) and on other equipment to be fully understood. In most of the cases variable frequency drives are used to overcome this initial low voltage condition (AVO, 2015). Similar to motor starting transients transformers' inrush currents could also exceed the nominal current and depending on their magnitude they can affect the power quality of the network as well as they could trip protective relays.

Power transformers are typically one of the most expensive components in an electric power network and the excessive high current forces caused by these transients could affect their life expectancy (Ebner, 2007).

Stability issues are the main concern during this dynamic stage of the design process. The power system stability can be defined as the ability of an autonomous power network to regain a state of operating equilibrium after being subjected to any type of disturbance. Regaining an operating equilibrium does not necessarily mean returning to the initial steady-state condition but to a steady-state acceptable condition which will not result to protection actions causing further disturbance to the system (Andersson, 2006).

The latter stage (i.e. dynamic model topology) will again redefine the system's requirements possibly leading to different network architectures and component ratings. The design process is basically a constant feedback procedure on how well a design satisfies the system requirements. Several modifications of the initial design concept will lead to a final design that will meet the total mission effectiveness requirements.

All the aforementioned steps can be better demonstrated with a current working example of such a network. Hence, the design process of a hybrid/electric ship example will be described in the following section. The selection of this network was based on the many similarities this network share with the TeDP concept for aerospace applications.

3.2.2 Hybrid/electric ship design process example

An example of the propulsion system of an electric ship is demonstrated in Figure 25. This system typically consists of a number of prime movers which provide the required electric power both for the propulsive units and for the auxiliary loads. This electric power is transmitted to the whole power network via generators connected to the prime movers, whilst power conversion equipment, switchgear and the main bus-bars and transmission lines are located between the power sources and the propulsive units (loads) to secure the transmission of the electric power efficiently and reliably.

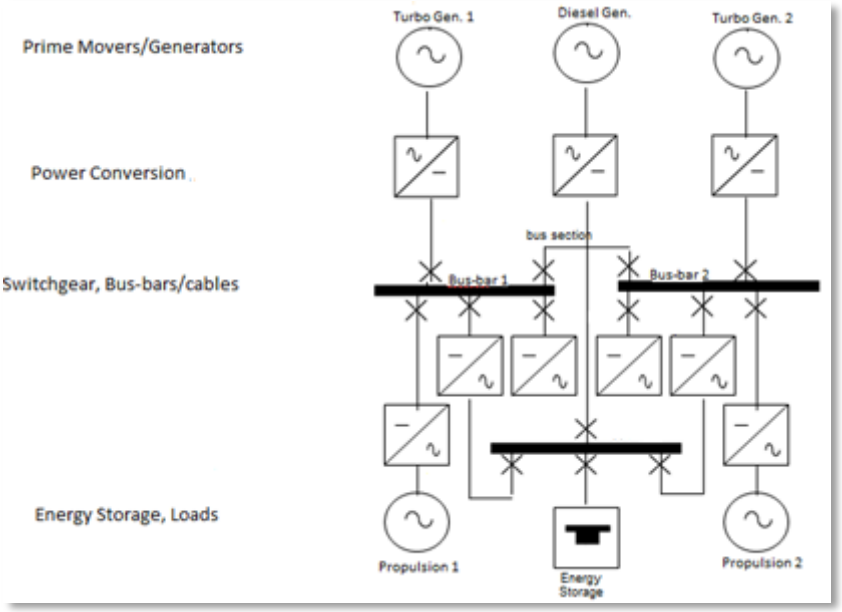

Figure 25 Electric/Hybrid Ship Propulsion System Diagram (Malkin and Pagonis, 2014)

In a hybrid ship architecture power generation modules convert fuel into electrical power. This module typically consists either of gas turbines or diesel engines (or even both), generators and possibly power electronics and control modules. The majority of ships have at least two different types of power generation sources: a main and an auxiliary one. In case that both gas turbines and diesel engines are used as parallel main prime movers, special attention is needed due to their different transient response. Diesel engines tend to react faster than gas turbines in the transients and a danger of diesel overloading can only be avoided by careful modelling and simulation (Doerry and Fireman, 2006).

Figure 26 Diesel-electric ship propulsion plant (marine.man.eu, 2015)

The image above demonstrates an example of a diesel-electric propulsion plant. From the right to the left one can see the diesel engine alternators, main switchboards, frequency converters/variable speed drives, electric propulsion motors, gearboxes, and finally the propellers. The operation mode with the highest expected electric load typically evaluates the type, rating and capability of the engines. If for example the propulsion power demand of a vessel is 8MW with a maximum consumer electric load of 2MW then the engines selection will be driven by the following equations:

$$P_{Bprop} = \frac{P_{shaft}}{n_{trans}} = \frac{8}{0.90} = 8.88\ MW \quad \textbf{(3-8)}$$

$$P_{Belec} = \frac{P_{elec}}{n_{alt}} = \frac{2}{0.95} = 2.11\ MW \quad \textbf{(3-9)}$$

$$P_B = P_{Bprop} + P_{Belec} = 10.99\ MW \quad \textbf{(3-10)}$$

After the total engine brake power demand is calculated the number and type of the diesel engines are selected based on the maintenance strategy, the mission profile, the boundary conditions and the fact that the maximum allowed loading of the engines should not exceed the 90%. Thus:

$$P_{Total} = \frac{P_B}{MEL} = \frac{10.99}{0.9} = 12.21\ MW \quad \textbf{(3-11)}$$

An even number of engines is typically chosen to ensure the symmetrical loading of the bus bars. If a number of four engines were selected in this example then a power rating of around 3.05 MW each will be required. The following table summarises the parameters and the values of this example:

Table 4 Diesel-electric propulsion plant main parameters

Parameters	Symbol	Value
Shaft Propulsion Power	P_{Shaft}	8 MW
Electric transmission efficiency	n_{trans}	90%
Engine brake power for transmission	P_{Bprop}	8.88 MW
Electric consumer load	P_{elec}	2 MW
Alternator efficiency	n_{alt}	95%
Engine brake power for consumer	P_{Belec}	2.11 MW
Total engine brake power demand	P_B	10.99 MW
Maximum engines electric loading	MEL	90%
Total engine brake power installed	P_{Total}	12.21 MW

The overall electric transmission efficiency was assumed to be 90%, whilst a relatively conservative assumption for the generator's efficiency was made (i.e. 95%).

Power generation modules in marine applications typically produce 3 phase/60 Hz power. The standard generated voltages could be either a low voltage 450VAC system or high voltage systems typically between 4.16 and 13.8kV. The choice between the two main voltage levels depends on the availability of circuit breakers of sufficient rating and the total ship power demand. In many occasions split plant operation might be chosen in order to double the total ship power generation capability limits and increase the reliability of the vessel.

The power distribution system transfers the electric power to the different network subsystems. It consists of cables, switchgear, and load monitoring and fault protection equipment. A selection between high and low voltage buses, as well as a choice between AC or DC electrical distribution system needs to be made. As it was previously mentioned circuit breakers' power rating availability and total system generation power required favour the use of an architecture choice over the others. Propulsion motor modules can also have an impact on the selection of a bus voltage. Figure 27 demonstrates the recommended bus voltage levels depending on the generation power required.

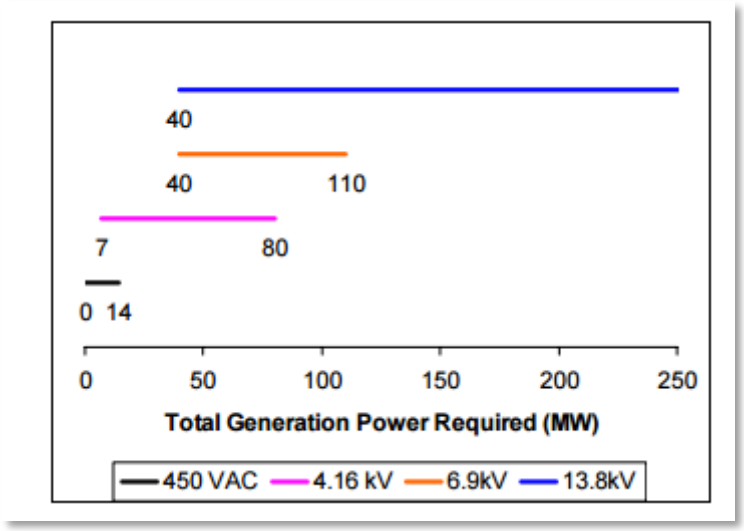

Figure 27 Bus Voltage Levels for given total required power demand (Doerry and Fireman, 2006)

The switchboard design is mainly determined by the short circuit currents and by the required capacity of the circuit breakers. In the previous example where a total engine power lower than 14 MW was estimated, the 450 VAC might be the preferable choice in regards to the system's voltage. A rough estimation of the anticipated short circuit levels of this example can be made by using the following equations:

$$I_{Gsc} = \frac{n * P_{Gen}}{\sqrt{3} * V_r * x_d" * \cos\varphi} = \frac{4 * 3050}{\sqrt{3} * 450 * 0.16 * 0.9} = 108.69\ kA \quad \textbf{(3-12)}$$

$$I_{Msc} = \frac{n * 6 * P_{mot}}{\sqrt{3} * V_r * x_d" * \cos\varphi} = \frac{2 * 6 * 6100}{\sqrt{3} * 450 * 0.16 * 0.9} = 652.19\ kA \quad \textbf{(3-13)}$$

Where:

Table 5 Diesel-electric propulsion plant switchboard parameters

Parameters	Symbol	Units
Generator short circuit current	I_{Gsc}	kA
Number of generators/motors	n	-
Rated power of the generator	P_{Gen}	kW
Rated Voltage	V_r	V
Sub-transient reactance	$x_d"$	%
Power factor	$\cos\varphi$	-
Motor short circuit current	I_{Msc}	kA
Rated power of the motor	P_{mot}	kW

In this case the circuit breaker capacity is extremely high; hence a different voltage level shall be more appropriate for both the generators and the motors. Typically, marine switchboards have short-circuit withstand strength of up to 150 kA (peak 330 kA) (Kongsberg, 2015). If for example generator voltages of 690 V were chosen instead, then the short-circuit levels will be reduced to 70.89 kA. A higher voltage level will be necessary for the motors where a 6.9 kV might be the preferred choice. This would reduce the motor short circuits to acceptable levels (i.e. around 42.5 kA). Generally, on board it is easier to deal with lower voltages. Thus, the choice of the switchboard voltage is a trade-off between short circuit and voltage controllability. In the previous equations sub-transient reactance of 0.16 was assumed for both the motors and the generators. This is a typical figure for low voltage generators, whilst a value around 0.14 should be assumed for medium voltage machines (marine.man.eu, 2015).

The power conversion equipment converts electric power from the form (i.e. voltage and frequency) of one distribution system to the form of another. It generally consists of solid state converters and transformers. The power conversion equipment associated with the generators and motors is typically considered as part of the power generation system. Several methods regarding the optimal power rating for power conversion modules are available in the literature (Amy, 2005). In any case the total electric load demand needs to be met in every instance with at least 95% probability.

Figure 28 presents a simplistic diagram with typical efficiencies of a hybrid-electric ship propulsion system including the electrical machines and the transmission system. An overall system's efficiency of 92% is estimated, a value which in aerospace applications will not be acceptable both for efficiency reasons and mainly due to the derived cooling requirements. Note that any losses derived from the generation of power where at this point neglected. A similar diagram will be presented for the superconducting case in order to highlight the improved efficiency these systems present.

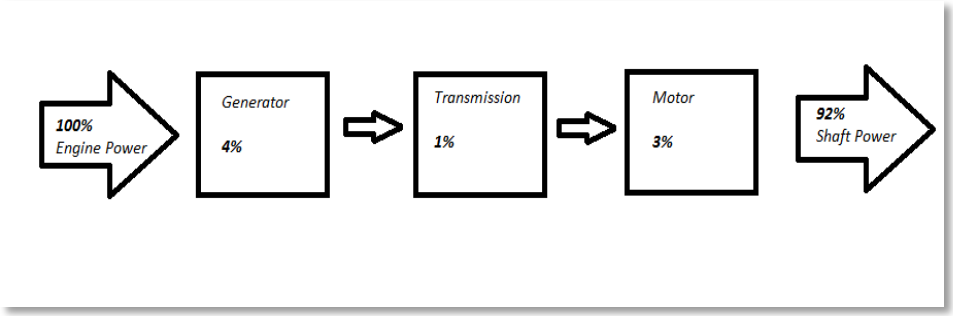

Figure 28 Typical losses diagram of a hybrid-electric ship propulsion system

Although quite similar, the design process of an aircraft presents some main differences. In an aircraft network the importance of lightweight components which occupy the minimum space possible becomes more important. Minimum weight combined with maximum efficiency is the main priority in an aerospace application; hence superconducting networks' attractiveness is enhanced. The proposed TeDP concept is characterised by its superconducting nature and

includes some elements that have never been used before in an aircraft system. Some of these elements will be described in the following section.

3.3 Superconducting Electric Power Network Elements

Some of the characteristics of the TeDP network have already been described in the literature review section of this research study. A fully superconducting network is expected to be necessary in a TeDP configuration. This network will include several elements that are quite novel, whilst some of them have not even been built yet. This section will present some of these novel superconducting components, whilst the design process of a fully superconducting network will be described in the following subchapter (i.e. 3.4). The various innovative elements are outlined in this part of the study for reasons of completeness. These elements combined with the exceptional characteristics of superconducting networks are expected to notably change the way these networks are designed.

3.3.1 Superconducting Electrical Machines

The EPN of the aircraft under investigation will consist of a number of gas turbine alternator sets and numerous motor driven fans as propellers. Both the generators and the motors of this configuration are expected to be superconducting. These machines are attractive for an aerospace application due to their significantly lower weight and volume and their extremely high efficiency. The vast majority of existing superconducting electrical machines are partially superconducting (i.e. superconductors used only in their rotor). These machines are expected to provide extra weight and efficiency benefits if both the stator and the rotor are constructed primarily by superconducting materials. Machines with efficiency around 99.97% and two to five times better power density than the conventional equivalents should be available in the 2035 timeframe (Brown, 2011). An extensive literature review of the already existing superconducting machines will be presented in the next chapter (4.1), whilst a novel method of reliably estimating the weight and volume of future fully superconducting machines will be the main objective of Chapter 4.

3.3.2 Superconducting Switches

The control and switching subsystems of these networks are expected to minimise the use of conventional mechanical switches by the use of superconducting equivalents, which will implement local temperature and magnetic control (Malkin and Pagonis, 2015a). Switching has to be available not only for fault currents, but also to normal currents, when a quick reconfiguration of the circuit is essential. These revolutionary switching devices are expected to eliminate one of the constraints on high-current DC networks which normally are difficult to switch due to the lack of current zeros. The main attractive feature of these devices is their almost zero resistance which allows them to scale-up to high operating voltages and currents without any severe weight and conduction losses penalty. This eliminates one of the major constraints in the design of conventional power networks which is the switchgear capabilities and availability. Besides, superconducting switches with fast responses have already been developed showing promising results (Solovyov and Li, 2013).

3.3.3 Superconducting Fault Current Limiters (SFCLs)

The possibly high normal currents chosen in such a configuration will lead to extremely high fault currents. The latter in a conventional network creates significant problems since circuit breakers of sufficient rating both for normal and fault operations of that extend will be difficult to become available. Instead, in superconducting devices such as Superconducting Fault Current Limiters (SFCLs) are expected to solve some of the fault currents design constraints.

Superconducting Fault Current Limiter (SFCLs) possibly attract the most interest as current limiting devices in a SPN. A Fault Current Limiter is a device that limits the prospective fault current of a network when a fault like a short circuit occurs. The most up to date current limiters are superconducting and they are divided into two categories: resistive or inductive. The idea of using superconductors to hold electric power is not something new. The current limiting behaviour of superconductors derives from their non-linear response to current, temperature and magnetic field changes. Exceeding a limit of one of

these three parameters could lead these materials to lose their superconductivity and behave as normal conductors. In a resistive FCL, which is the most common type of limiter, when a fault current occurs the superconductor quenches (i.e. loses its superconductivity) and the resistance rises sharply and quickly limiting the fault current. This superconducting device seems ideal because in the steady state has almost zero impedance whilst when a fault current occurs this impedance rises high enough to control the fault. After recovery of the fault, impedance goes back to zero, making the device “invisible” again. Thus, three are the modes of a SFCL:

- Normal mode
- Fault-limiting mode and
- Recovery period

With its relatively low cost and its capability of very sharp transition for the superconducting to the normal state, MgB_2 seems the most appropriate superconductor for this type of devices (Pei et al., 2015).

In order to get a clearer view of the performance and function of a SFCL, Matlab Simulink models and cases were developed. Figure 29 demonstrates the Simulink model of a single phase system consisted of a 700 VAC voltage source, a simple resistive load and a RMS Simulink block combined with a SFCL subsystem.

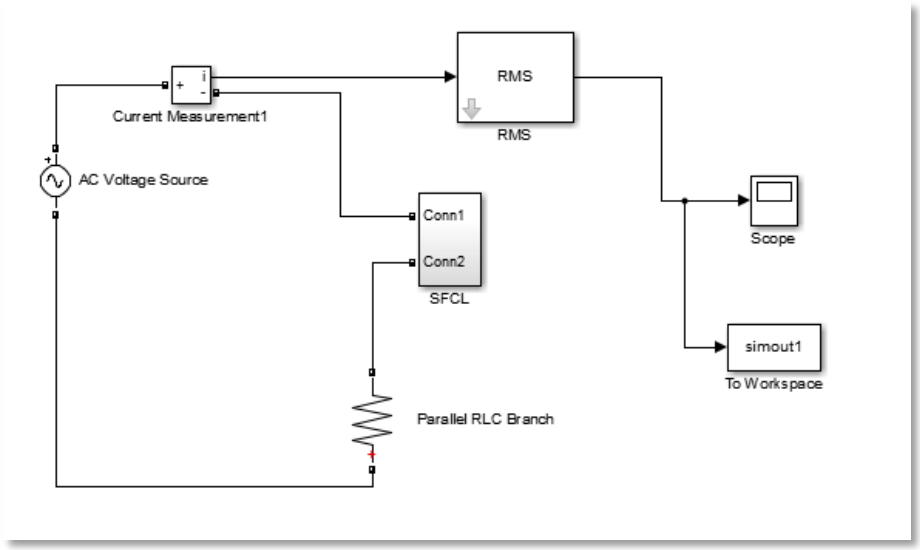

Figure 29 Simulink model of a single phase system with SFCL

The SFCL subsystem can be seen in Figure 30; the fundamental parameters which have been used as inputs in this resistive type SFCL can be found in Table 6. The response time corresponds to the time needed for the SFCL to detect and clear the fault and it is in the order of milliseconds. A triggering current is being used as a comparison with the system's nominal current. If the latter is bigger than the triggering current then the maximum impedance is being implemented to the system to control the fault currents, whereas in the reverse case a minimum impedance of 0.01 is imposed to the system.

Table 6 Fundamental parameters of a resistive SFCL

Inputs	**Units**	**Value**
Response Time	ms	2
Minimum Impedance	Ω	0.01
Maximum Impedance	Ω	25
Recovery time	ms	20
Triggering Current	A	550

The RMS value of the system's current is being used as an input to the SFCL subsystem, whilst the output is the result of the product between the produced impedance and the input current. A first order filter is also used to reduce the harmonics, whilst a controlled voltage source is used to compensate for the voltage sag derived from the induced fault currents (Biswas, Khan and Sarker, 2013).

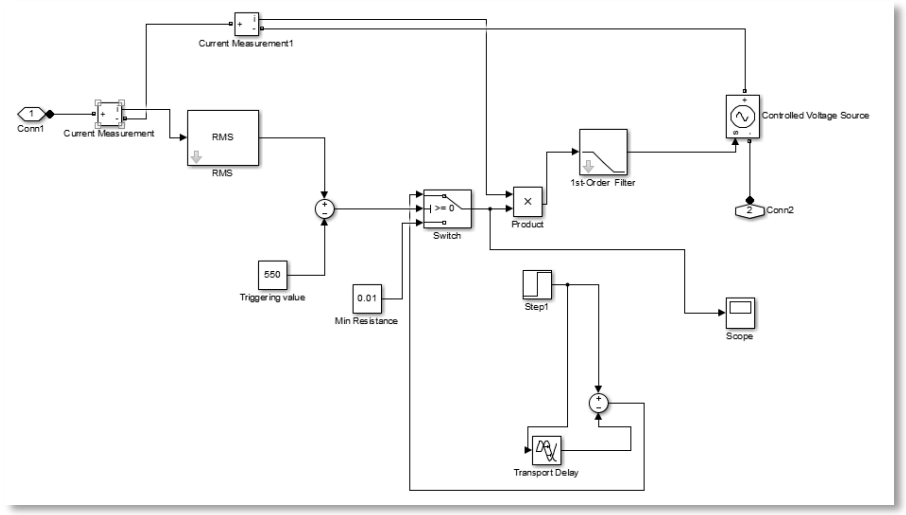

Figure 30 Simulink model of SFCL subsystem

This simple example shows the basic function of a resistive SFCL. The results of using a SFCL in a single phase system could be seen in Figure 31. The SFCL responds quickly enough to limit any currents higher than the triggering current securing the stability of the whole system.

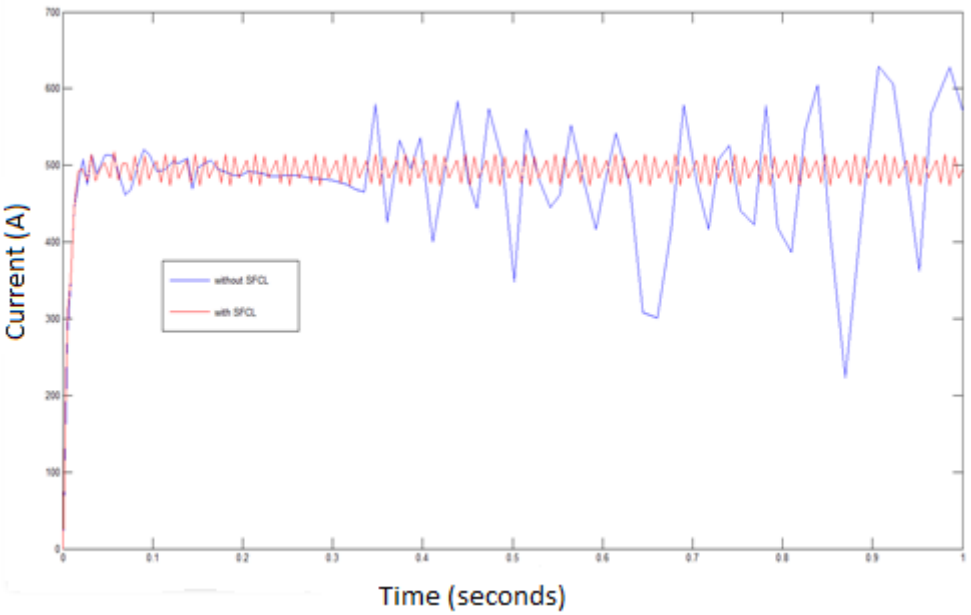

Figure 31 Single phase current waveforms in a system with and without a SFCL

A similar behaviour is expected in a three phase system. The main function of the SFCLs in a network similar to the TeDP power network will most probably

be the limitation of the fault current level interruption requirements in the minimum level possible.

3.3.4 Protection System and Converters

Generally, the zero resistance in a DC superconducting network results in a system with minimum natural damping. Thus, faults are able to be transmitted rapidly throughout the system reaching their peak fault currents in just hundreds of microseconds (Ross et al., 2014). Furthermore, the possibility of quench of the superconducting cables is another protection challenge that needs to be addressed in this type of network.

There are two design options in regards to the protection system of a superconducting network. The first one allows part of the system to quench so that the derived damping (from the line resistance) to be used for reduction of the peak of the fault currents. The second design strategy excludes the possibility of quenching in response to a fault. Clearly, in the latter option the protection system needs to react rapidly to isolate the fault before it reaches the critical current value.

Furthermore, there could be three different design paths (or a combination of two) for the protection system of such a network: to increase the fault tolerance of the several components of the network, to limit the fault currents and their effects using fault current limiting devices, and to mitigate the effects by using protection devices of really fast response.

There have been studies suggesting that some converters could be used as protection devices that can isolate the faults from the rest of the network (Baran and Mahajan, 2007). These modern voltage-source converters can be designed in such a way that can be more fault tolerant and be able to act fast as current-limiting circuit breakers. However, it is still unknown if the isolation properties of these converters will be sufficient for a superconducting network. The possibility of quenching due to the initial high fault currents might jeopardise the reliability of the FSN. It seems reasonable that even if such a protection configuration is being chosen it will need to be combined with different protection technologies.

The use of cryo-cooled power electronics in a SPN (not only as protective mechanisms) will be explored later in this research study (5.2.2).

If fast-acting design path is being chosen, then circuit breakers able to respond quickly enough to the produced fault currents could potentially be used. These circuit breakers will have to protect the converters from reverse currents incidents and the DC link against under-voltage. The prevention of system quench will also be one of the main functions of these devices. Studies have shown (Fletcher et al., 2011) that solid-state circuit breakers are capable of responding quickly enough to prevent all the fault current effects described earlier. Their response times can reach the order of some 10s of microseconds, significantly faster than any other circuit breakers technologies (i.e. hybrid, electro-mechanical etc.).

Armstrong et al. (Armstrong et al., 2012) suggested a protection system with SFCLs used in conjunction with circuit breakers. The main role of the SFCLs will be the reduction of the magnitude of the fault currents that will consequently lead to lower overcurrent requirements for the electrical system. Solid-state CBs will then be used to isolate the faulted sections. Depending on the magnitude of the derived fault currents (i.e. after the SFCLs stage) isolators could be used instead of CBs reducing the weight and the complexity of the system. Figure 32 demonstrates this proposed configuration consisted of several different zones of protection. The small white squares represent the CBs, whilst SFCL devices have been placed between the generators and the converters as well as on the DC transmission lines in order to limit the AC and DC fault currents respectively.

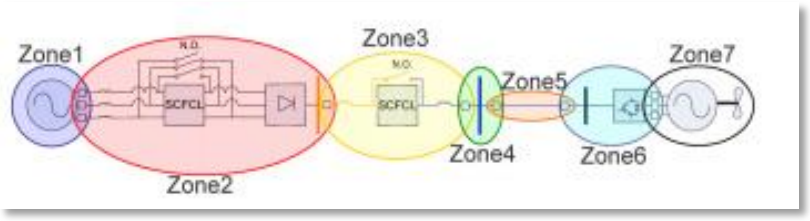

Figure 32 TeDP Protection System Proposed Architecture (Armstrong et al., 2012)

The optimal locations of the SFCLs and CBs in this proposed protection system are yet to be decided. Power flow studies should be conducted as soon as the system and component inductances are known for a SPN. An overall trade study needs to be carried out between SFCLs and CBs. The mass of the required CBs would be decreased by using SFCLs to reduce the CBs' fault current interruption ratings but deciding on the optimal number, location and ratio between these two protection devices options is a challenging task.

3.3.5 Cooling System

Furthermore, there is another caveat to the use of a superconducting network; it requires cooling to cryogenic temperatures at all times. This adds another heavy and complex subsystem to the already complicated power network. There have been studies suggesting that the required cooling system is the key technological obstacle to overcome in order the superconducting concept to become feasible. The main options of cryogenic cooling technology have already been described in the previous chapter; however a closer look at the cryo-coolers' technology will also be included in the following chapters, where also a detailed Simulink model of a Reverse-Brayton cryo-cooler (Appendix 7.2A.2) will be used for the case studies of Chapters 5 and 6.

3.4 Superconducting Electric Power Networks Design and Operation

In this section the main design priorities and issues of a SPN design will be presented with an extra focus on the TeDP aircraft application. The main differences in the design process of a conventional EPN and a superconductive one will be clearer after this section.

3.4.1 Basic Parameters Selection

As already mentioned, the first stage of the design process of a power network typically specifies the power requirements of the whole network. These requirements will then dictate the basic parameters (i.e. voltage, current, and frequency) of the power network. There are always two main design paths for satisfying the overall power requirements of a network: either to choose a High

Voltage Low Current (HVLC) power system or a Low Voltage High Current (LVHC) system.

The voltage levels in an aerospace application are typically low (less than 300V) mainly due to Paschen's Law (Figure 33). This law indicate that at higher pressures the breakdown characteristics of a gap are a function of the gas pressure and the gap length. It was found that breakdown voltage (V_B) in Volts could be described by the following equation (Lieberman and Lichtenberg, 2005):

$$V_B = \frac{\alpha pd}{\ln(pd) + b} \quad \textbf{(3-14)}$$

Where p is the pressure in atmospheres or bar, and d is the airgap distance in meters. The parameters a and b are constants that depend on the composition of the gas. For air the standard atmospheric pressure is assumed 101 kPa and the values of the constants are $a = 4.36x10^{-7}\ V/(atm * m)$ and $b = 12.8$. Figure 33 demonstrates the Paschen's Curve for air and two parallel copper electrodes separated by 1 inch. According to this diagram the minimum breakdown voltage for any product of pressure-distance is approximately 327V. However, depending on the precise conditions a voltage level in the order of 300V is typically being chosen as an upper limit. This practically means that an arc will be avoided at voltage levels less than 300V at low or high altitudes. This is the main reason why DC voltages in an aircraft are kept below this value. However, as the power demands increase in a configuration such as the TeDP, it seems necessary to increase the operational voltage levels so that the conductor weight of the cables can be reduced. By increasing the network's voltage level the system's current could then be decreased, for the same power requirements, leading to transmission lines of smaller size and weight. Nonetheless, it should be noted that possible higher voltages will require thicker insulation. A trade-off between the conductor's weight and the insulation added weight is necessary in any aircraft power network. Besides, since the electric system will be cryogenic, there is a possibility that the breakdown voltage will be

less sensitive to pressure and conductor distances than it is for room temperature applications. The revised Paschen's curve needs to be determined so that the optimal system's voltage and current to be decided.

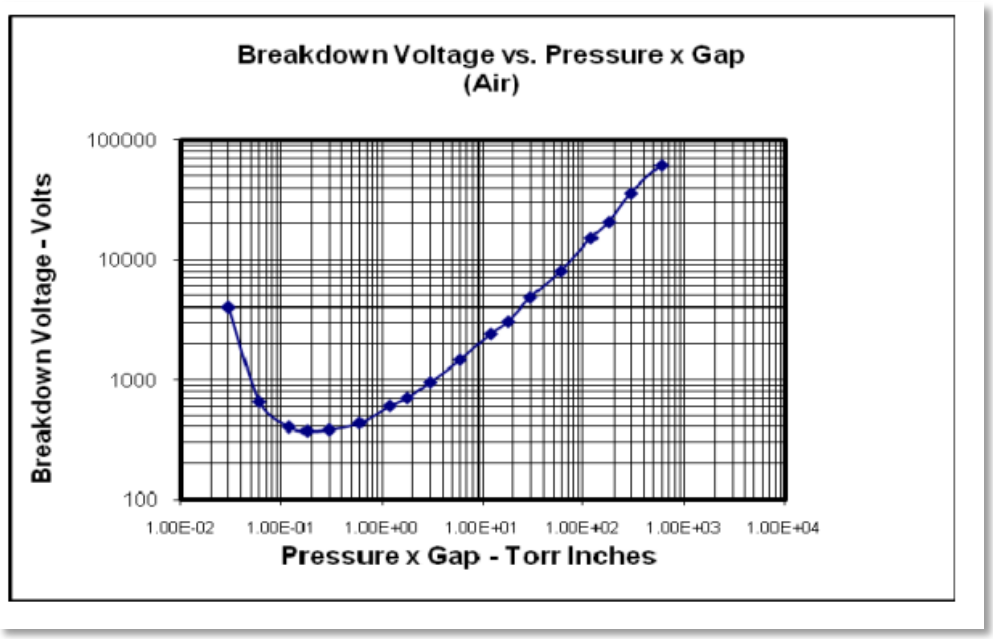

Figure 33 Illustration of Paschen's Law (Paschen, 1889)

Generally, in order to determine the optimal system voltage for the minimum weight and maximum power capability, a complete system level study is necessary. This system level study should include the power densities for each component of the electrical system. Cotton et al. (Cotton, Nelms and Husband, 2007) investigated the optimal voltage selection for aerospace electrical systems. In their study two different types of discharge were examined: discharge around insulated wires (else known as corona discharge) and discharge within the insulation of the wires (else known as void discharge). Different cable options were examined such as high current (i.e. large conductor and thin insulation), high voltage (smaller conductor, thick insulation), DC, and AC transmission cases. The study concluded that the optimal operating point for an aircraft power system does not necessarily imply the use of the highest voltage possible. Cable weight and power transfer capability trade-off studies are necessary in any proposed network architecture. Power to weight ratios of

non-floating DC systems proved to be the optimal solution in terms of frequency choice (DC or AC).

In the superconducting network of the TeDP powered aircraft the selection of a LVHC system seems inevitable, but this is actually a preferable choice for a SPN. The main superconducting materials considered for a power application have already been discussed in chapter 2.2.1, whilst some of the main characteristics of superconducting cables (including critical values of current density, temperature, and magnetic field) have been analysed in section 2.2.

Superconducting cables are characterised by their extremely high current capability. The maximum current capability of a copper or aluminium wire is limited around 1-4 A/mm^2, whilst superconductors with current capability of 25 A/mm^2 with potential to reach 50 A/mm^2 have already been experimentally used in superconducting transmission lines (Xin, Han and Liao, 2006). Even higher current densities (over 100 A/mm^2) have also been claimed (Masuda et al., 2004) which is more than 100 times better than that of a conventional copper wire. This high current capability reduces the size and cost of the transmission lines in the TeDP type of aircraft. The zero resistance of these cables also significantly decreases its transmission loss. The energy losses of a superconducting cable are derived only by the AC losses which are comparable to the magnetization loss of the superconductor itself. The transmission losses are expected to be at least halved in the case of superconducting cable as Figure 34 demonstrates.

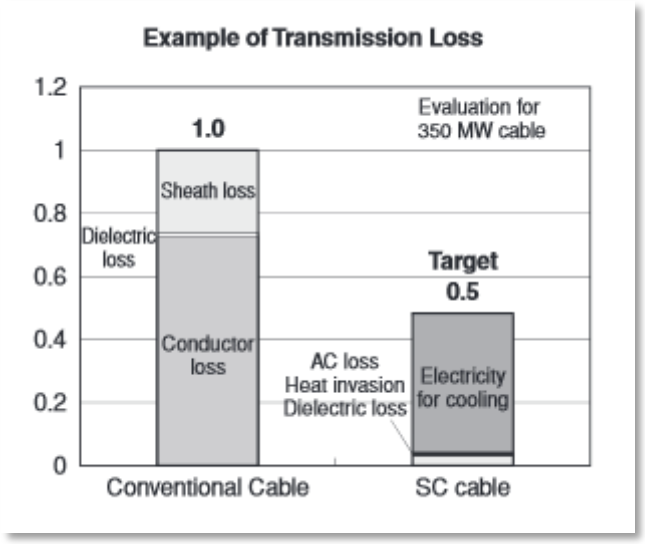

Figure 34 Comparison between the transmission losses of a conventional and a superconducting cable (Masuda et al., 2004)

The significantly increased electric power load could be satisfied using thin superconducting high current cables without having to increase the system voltages creating corona onset issues during cruise. In fact, very thin superconducting cables might create some practical issues in regards to making connections and mechanical support. Hence, it is the author's belief that in a TeDP configuration with a SPN system currents in the range of 6-30 kA will be selected (Malkin and Pagonis, 2013).

Figure 35 summarises the anticipated losses in a SPN including the superconducting electrical machines and the transmission losses. This graph is used as a comparison to Figure 28 where the typical losses of a conventional electric ship network were presented. The SPN is more than 7% more efficient than the conventional equivalent confirming one of the most attractive characteristics of SPNs. However, it should be noted that the cooling system losses have not included in the figure below. Even with these losses the overall system's efficiency is expected to be significantly higher in the superconducting case.

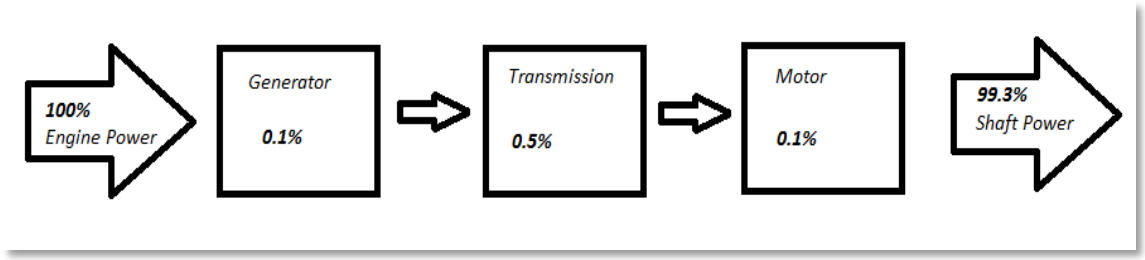

Figure 35 Typical losses diagram of a propulsion system using a superconducting network

3.4.2 Current splitting

Conventional simulation modelling tools are incapable of accurately predict the performance of a SPN. The true zero resistance of these systems results into an unknown current sharing behaviour at the circuit nodes of a superconducting network, especially in the case of a DC power network. In the case of an AC superconducting system there have been studies (Malkin, 2014) showing that the technology behind superconducting cables is a viable option for an aerospace application. In arrangements simpler than the ones described in this research study good current distribution has been obtained using multi-strand MgB2 wires (Pei et al., 2012). However, it is clear that if a network similar to the one proposed by NASA's N3-X model is to be chosen extensive work on investigating DC superconducting cables for aerospace electrical applications is necessary. A system utilising these cables will obviously benefit from the almost non-existing losses (i.e. zero resistive losses), but several issues such as parallel current sharing have to be investigated (Malkin, 2014). In any case, experimental work and validation processes are crucial in order these superconducting networks to be reliably modelled and developed.

3.4.3 Electro-magnetic Forces

The high normal currents expected in these configurations might result in stray magnetic fields and strong electro-magnetic forces. These forces exerted between conductors can be calculated using equations (3-15) and (3-16) which are derived from the Amperes Law and show that the forces per unit

length (F_{em}) are proportional to the product of the conductor currents ($I_1 * I_2$) divided by the distance of the wires (r).

$$F_{em} = 2 * k_a * \frac{I_1 * I_2}{r} \quad \textbf{(3-15)}$$

Where, $k_a = \frac{\mu_0}{4*\pi} = 10^{-7}\, N\, A^{-2}$ **(3-16)**

Hence, the system needs to be designed in such a way that it will cater for these strong forces. The interference between the several superconducting components is also unknown since there has never been an application including so many novel superconducting devices all together. The nature of this application (i.e. aerospace application) creates even more unknowns derived from the uncertainty of the superconducting components' performance in altitude.

3.5 Summary

The design process of an autonomous power network is a relatively unknown procedure since most of the current networks are extensions or modifications of already well-established networks. This uncertainty becomes even more profound in the case of a superconducting power network due to its novelty and revolutionary design aspects it presents. Particularly, in the case of a demanding power network such as the one required for the TeDP type of aircraft the existing basic parameters standards seem insufficient to address the power quality of such a complicated network. Due to the low TRL of this concept, optimised standards for the TeDP system have not been set up making the sensitivity studies of the proposed configuration a challenging task. This is also enhanced by the superconducting nature of the electrical power network.

There are undeniable benefits of using a FSN mainly derived from the improved efficiency, power density, as well as the flexibility these networks could offer. Nevertheless, there are still many aspects of these networks that have not been fully understood by the aerospace industry. The full potentials of a FSN can be obtained only if a different approach on the design process of future aircraft is followed. Several design constraints such as cable size, switching and fault current limiting capabilities are eliminated in the case of a FSN. On the other hand, several design issues of superconducting networks need extra attention since various novel components might be used concurrently for the first time in such a sensitive network

Since superconductivity appears to be as one of the main enablers of promising concepts such as the TeDP approach it is essential that further research studies and significant funding resources to be dedicated on the experimental analysis of these networks.

4 Superconducting Electrical Machines

One of the main components in a fully Superconducting Power Network (SPN) is clearly the electrical machines. There have been many studies and experimental work in regards to the construction of such machines. However, the vast majority of the superconducting machines which have been built have only their rotor superconducting while the stator remains conventional. In this chapter, initially the most important examples of tested superconducting machines will be summarised. After that, a novel method of estimating the weight of fully superconducting machines will be presented, while a sensitivity study focusing on the main parameters of these models will also be carried out. Finally, the model limitations as well as its validation references will conclude this chapter.

4.1 Status and State of the Art

The idea of building a superconducting electrical machine has been around since the discovery of the superconductivity phenomenon (1911) when many researchers started considering the possibility of constructing a Superconducting Machine (SM) predicting the possible benefits that such a configuration could offer. Until recently, it was not possible to build and test a fully superconducting machine and the majority of the tested machines compromise a “superconducting” rotor (with HTS or LTS materials) and a conventional stator. In this subchapter a brief description of the machines that have been built and tested throughout the years will be presented.

4.1.1 Superconducting Synchronous Machines

The first studies go back in the 70’s, where the development of high-field superconductors triggered the interest for using such conductors in the electrical rotating machines.

In 1974 the Westinghouse Electric Corporation got involved in the design, development and test of a 10MVA, 12000 RPM AC generator with a superconducting field winding (Blaugher, Parker and McCabria, 1977). A

predicted reduction in weight and volume of these machines was the motivation behind this work. The prototype superconducting rotor of this machine was operating in the temperature of 4.2K (LTS) while a conventional construction of stator was chosen. Although, there were some benefits using LTS in these machines it was not until the discovery of HTS that extended studies begun.

It was then almost twenty years later (1993) when American Superconductor Corporation decided to design and construct two synchronous motors using HTS field coils (Joshi et al., 1995). Both motors had a silent pole field structure excited by HTS (i.e. BSSCO) coils which remained superconducting during all the operation modes. The motors produced 1.5kW and 3.5kW power, operating at 3600 (two poles) and 1800 (four poles) RPM respectively. The potential energy savings was the main motivation behind this study since initial analysis has showed possible increase in the overall efficiency of the motors in the range of 1.3%. This research was really important because it proved the feasibility of the whole concept and it formed the basis for further studies to come.

In 1997, a research group from Tampere University (Finland) used the Bi-2223/Ag coils manufactured by American Superconductor Corp. to test a 4-pole synchronous machine in different operating temperatures (4.2K to 77K) (Eriksson et al., 1997). They ended up constructing a 1.5kW machine at 1500 RPM. A different approach in the design of the machine was chosen. More specifically, the so-called inside out concept was followed where the excitation is happening on the stator side whilst the rotor side armature operates at room temperature. This choice was proven successful mainly for moderate power levels and operating temperatures around 20K (77K was proved to be too inefficient for the wires of that era).

Around the same period the U.S. Navy started to investigate the possibility of using superconducting synchronous motors for ship propulsion (Gamble et al., 2002). The conceptual design of a 25MW motor can be seen in Figure 36. The study concluded that significant efficiency and noise benefits can be achieved with such a design. Many more studies for marine superconducting propulsion motors followed both from U.S. Navy and from other organisations. The former,

in 2000, developed a 5MW, 230 RPM HTS AC synchronous motor for electric ship propulsion (Eckels and Snitchler, 2008). The reduced size and weight of this machine allowed a more flexible design, simple installation and maintenance, while the performance both for the steady-state and the transient modes was significantly improved. This machine was the baseline for even larger machines. U.S. Navy finally tested a 36.5 MW HTS propulsion motor in 2006 operating at 120 RPM demonstrating an overall efficiency of 97.3% and concluded that the use of superconducting machines can offer architecture benefits in both existing and new ship designs (Gamble, Snitchler and MacDonald, 2011).

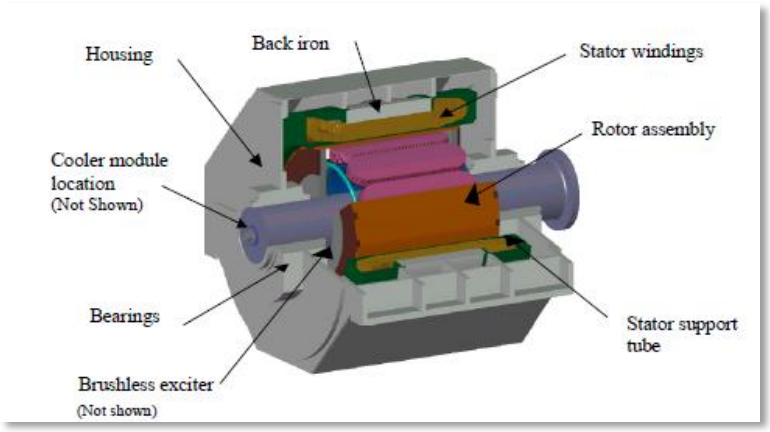

Figure 36 25MW 120 RPM superconducting synchronous motor U.S Navy conceptual design (Gamble et al., 2002)

A recent example of marine superconducting propulsion motor study comes from the University of Shahrood in 2014 where a design process of a HTS rim-driven synchronous motor for marine propulsion has been developed (Hassannia and Darabi, 2014). A 2.5MW, 220 RPM machine has been studied and ways to reduce the axial length of these machines have been proposed.

Siemens also showed some interest in the development of superconducting synchronous machines (Figure 37). In 1999, a HTS four-pole 400kW machine was built at a rated speed of 1500 RPM and performed on an overall efficiency of 96.8% (including the refrigerator) (Gieras, 2009). Two more HTS machines were tested in the following years (2002-2010), a 4MW / 3600 RPM and a 4MW

/120 RPM respectively (Wolfgang, Grundmann and Frauenhofer, 2012). Compared to a conventional generator of the same rating the former machine's efficiency raised from 96.1 to 98.4%. In general, both studies concluded that HTS technology can be the solution for a more sustainable future and especially in cases such as the marine applications a complete system re-design could capitalise the numerous benefits that superconducting machines can offer. The latter statement also stands for the TeDP concept, where a novel systems level approach, and not a simple component technology improvement, is necessary.

Figure 37 Siemens HTS Synchronous Machine Test Bed (image courtesy of Siemens)

The East Institutes showed an interest in superconducting machines both synchronous and homopolar DC (4.1.2). For the former type, Korea Electro-technology Research Institute (KERI) was the first one to develop a 100hp, 4 poles, and 1800 RPM synchronous motor with HTS (Bi-2223 tape) field coils in 2002 (Kwon et al., 2005). In 2005 Japanese Industry Academia Group built an axial gap-type brushless HTS synchronous motor using Gd-Ba-Cu-O bulk magnets for the rotor. The construction of a 3.1 kW and 720 RPM SM was feasible (Figure 38), while possible improvements using successive pulsed magnetization were claimed (Matsuzaki et al., 2005).

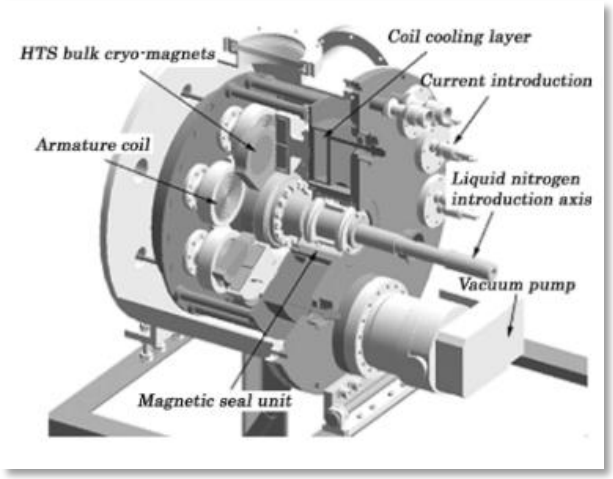

Figure 38 HTS Motor using Gd-Ba-Cu-O bulk magnets schematic illustration (Matsuzaki et al., 2005)

One year later an eight-organization joint team leading by Shikawajima-Harima Heavy Industries Co. and Sumitomo Electric Industries developed the first liquid nitrogen cooled fully superconducting motor for ship propulsion as it can be seen in Figure 39 (Takeda, Oota and Togawa, 2006). The rated output power was 12.5 kW running at the speed of 100 RPM. The study revealed some very optimistic results ending up with a machine two times lighter than the conventional equivalent, with high efficiency, and no noise or flux leakage.

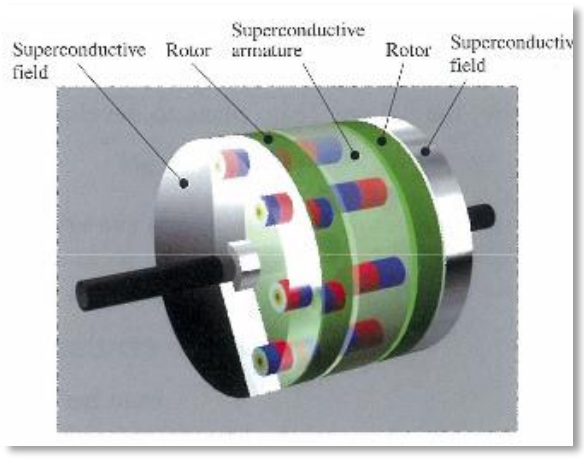

Figure 39 The first fully superconducting motor (Takeda, Oota and Togawa, 2006)

Finally, in 2007 a joint Research and Development Group funded by New Energy and Industrial Technology Development Organization developed a 15

kW, 360 RPM HTS superconducting motor (Iwakuma et al., 2007). YBCO superconducting tape was used for every field coil, whilst a copper winding with an iron core was used for the stator. The final motor was tested as ship propulsion system where a quite stable operation was verified.

YBCO bulk material was also incorporated into the rotor of a superconducting reluctance motor which was successfully built and designed by a German Institution (i.e. Oswald Elektromotoren) in 2004 (Oswald et al., 2005). A 200 kW, 3000 RPM HTS reluctance motor was finally constructed and tested (Figure 40) with results that proved the potential use of such a machine in future applications where high power density, small size and high dynamics are required. However, improvements in the bulk YBCO material should be expected and more extensive studies are anticipated.

Figure 40 200 kW HTS Reluctance Motor (Oswald et al., 2005)

Another important study that compared in terms of efficiency and size the performance of a 1000hp HTS motor with a similarly rated conventional machine was carried out by a U.S Department of Energy funded program (Dombrovski et al., 2005). Four coils wounded with a multi-filament BSCCO tape were used for the field winding, whilst the armature winding was designed for room temperature operation. The reduction of the core-end losses and the interaction between HTS motors and the power converters were some of the issues that have been pointed out as challenges for the future designs.

Finally, in UK a 100 kW HTS synchronous motor was fully constructed in 2004 in University of Southampton and a systematic test program to characterise its

performance was also developed (Wen et al., 2009). The machine operated at liquid nitrogen temperature (77K) having a superconducting winding consisting of ten Bi2223 pancake coils and a 3-phase conventional stator. The schematic layout of this machine can be found in Figure 41. It was found that the critical current of the rotor coil significantly increases as the temperature decreases. The field of the stator winding on the other hand does not affect the critical current in a similar extend.

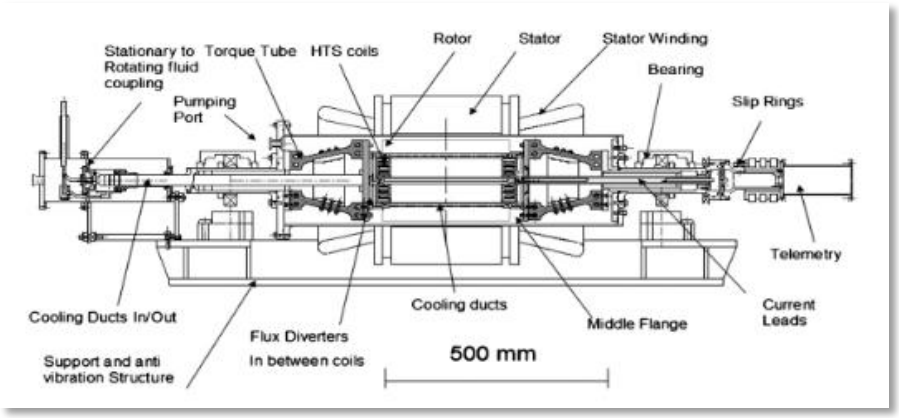

Figure 41 Layout University of Southampton's 100 kW HTS machine (Wen et al., 2009)

4.1.2 Homopolar DC Superconducting Machines

There were several companies such as General Atomics who claimed that homopolar DC SMs can be superior to the AC equivalents (Gieras, 2009). Benefits such as less noise, smaller size, better efficiency, less cost, and simpler architecture and control have been claimed. In 1995, they successfully demonstrate an electric motor (Figure 42) which uses superconducting field windings constructed with BSCCO-2223. The motor was tested for two different operating temperatures: in liquid helium temperature (i.e. 4.2 K) and in liquid neon temperature (i.e. 28 K). Eventually a 125 and a 91 kW SM were produced running at the speed of 11,700 RPM (Waltman and Superczynski, 1995).

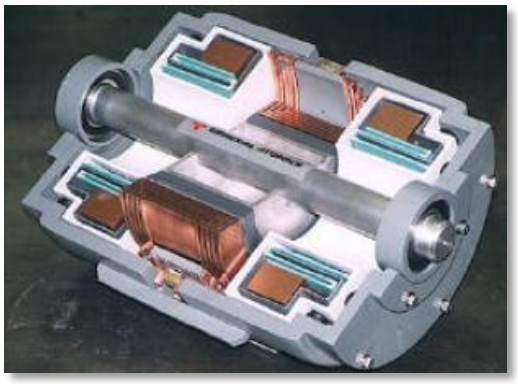

Figure 42 HTS DC Homopolar Motor (image courtesy of General Atomics).

The baseline for the aforementioned DC Homopolar SM was a 3.7 MW subscale motor at 500 RPM which utilized two NbTi superconducting coils that could be easily transitioned to HTS materials (Thome et al., 2002).

4.1.3 Superconducting Induction Machines

Significant efforts and funding from the East have been dedicated in the investigation of superconducting induction motors and generators. More specifically, a superconducting induction generator (SIG) with HTS bulk magnet has first been presented from Seoul National University in 2000 (Kim and Hahn, 2000). The machine consisted of two rotors, an outer one which was made of copper and the inner one which was constructed of HTS bulk magnets. The study concluded that the construction of a 2KVA SIG is feasible with a stable electrical and mechanical performance.

In 2003, the Ministry of Science and Technology of the Republic of Korea funded the study of a HTS induction motor (Sim et al., 2004). The motivation behind this research study was the possible efficiency benefits that an induction motor with HTS tapes as rotor bars could offer. A 0.75kW HTS induction motor was finally constructed with HTS tapes (BSSCO-2223) used as the short bars and rings and a comparison with a conventional motor of similar rating was carried out. In this configuration, the superconducting bars should quench during the starting phase to provide high current, while they recover from quench during the normal conditions in order to improve the overall efficiency. They concluded that the superconducting machine performed better than the

conventional equivalent motor with almost double starting torque and better efficiency during normal mode.

Finally, in 2006 a research group from Japan fabricated and tested a 1.5kW 3-phase HTS induction motor where both the rotor bars and the end rings were made of Bi-2223/Ag multifilament tapes (Nakamura et al., 2006). A schematic diagram of the test area is being presented in Figure 43. It was shown, both theoretically and experimentally, that the HTS induction motor requires minimum voltage for starting and could produce higher starting and accelerating torque compared to the conventional motor.

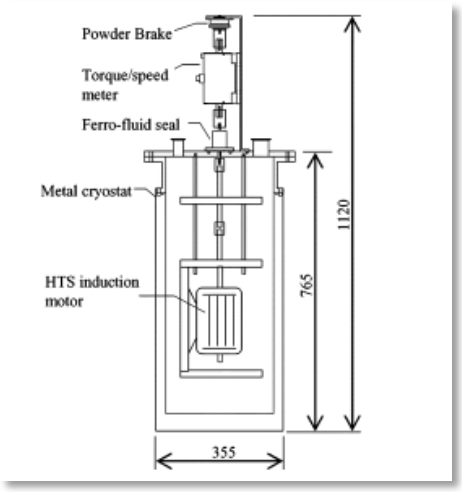

Figure 43 Schematic diagram of the test system of a fabricated HTS induction motor installed in a metal cryostat (Nakamura et al., 2006)

4.1.4 Programmable Superconducting AC Machine (PSAM) Project

PSAM project findings were used to develop a baseline machine prototype during the DEAP project. This programme was a partnership between Rolls Royce plc, Magnifye Limited, Cambridge University and EADS Innovations Group (later renamed to Airbus Group Innovations). The main objective of this technology demonstration project was initially the testing and integration of a doubly-superconducting AC machine so that the extra potential benefits over singly superconducting machines to be explored. The expected benefits in weight and efficiency of these machines could make them an attractive option for the aerospace sector. The full integration of the superconducting rotor and

stator in the same machine was not fully accomplished but the revised scope of the project which describes the outline design, some basic assumptions and some first mass estimation of these machines was successfully presented (Berg and Dodds, 2013). The machine architecture can be seen in Figure 44, where an environscreen is also included. The impact of this screen on the total weight of the machine will be calculated in one of the following subchapters (4.3.1).

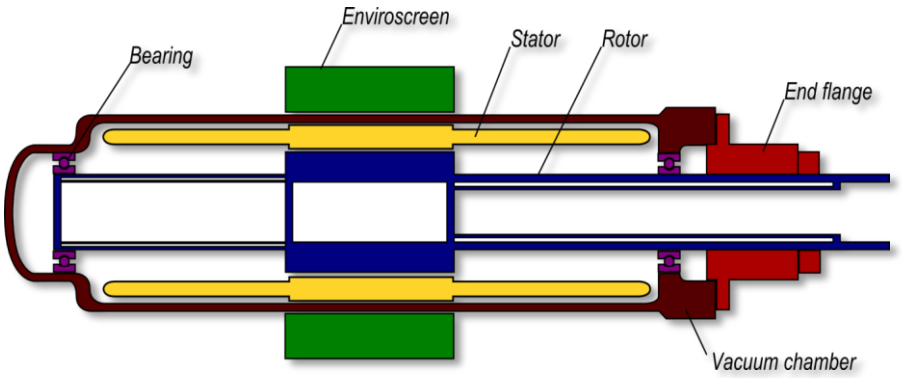

Figure 44 PSAM Machine Arrangement (Berg and Dodds, 2013)

This study is probably the only one considering the use of Magnesium Diboride (MgB2) wires for the stator of these machines. Unlike other HTS, MgB2 is a low cost superconductor available in wire form. This enables a MgB2 coil to be constructed where the wires are transposed to enable AC operation.

The project concluded that significant improvements in the power and torque densities can be achieved by using doubly-superconducting machines. However, the complexity of the whole system required (i.e. need for cryo-cooling system) in the aerospace applications dictates that the use of such machines could be more beneficial in the high power applications where the gains are major.

4.1.5 Summary

Singly superconducting HTS machines can be considered as mature technology (TRL 6) for certain applications such as the marine industry for example where a significant number of successful prototypes are already in existence. On the other hand, doubly superconducting machines are starting to

attract the interest of aircraft manufacturers since they seem ideal for innovative future concepts similar to the TeDP approach. The discovery of MgB2 superconductor is considered by some research groups the enabler to design fully superconducting machines (4.1.4). Building such a machine it is expected to bring extra benefits regarding their efficiency and their overall weight. Singly superconducting machines have already been proved more efficient with higher energy densities than the conventional equivalents. The following table summarises the already tested superconducting machines with available efficiency and overall weight data.

Table 7 List of singly superconducting electrical machines

	Type	Output Power (kW)	Rated Speed (rpm)	Efficiency (%)	Weight (kg)	Reference
1	Synchronous Motor (marine)	15	360	-	900	(Iwakuma et al., 2007)
2	Synchronous Motor (marine)	5000	230	96	23000	(Eckels and Snitchler, 2008)
3	Synchronous Motor (marine)	36500	120	97.3	75000	(Gamble et al., 2011)
4	Synchronous Generator	4000	3600	98.7	7000	(Wolfgang et al., 2012)
5	Synchronous Generator	4000	120	96.2	36000	(Wolfgang et al., 2012)
6	First High-speed Generator*	10000	12000	-	426	(Blaugher et al., 1977)
7	Homopolar DC motor (marine)	3700	500	~97	11400	(Thome et al., 2002)
8	Synchronous Motor (marine)	25000	120	97.5	70000	(Gamble et al., 2002)
9	Synchronous motor	746	1800	97.1	6000	(Dombrovski et al., 2005)

*Note that this machine has not been included in the following graph due to its oldness and its use of LTS materials

Summarising the information of Table 7 it was possible to derive some interesting results concerning the size of these machines. It is reasonable to use torque (T) as the parameter that sizes these machines. The maximum electromagnetic power at the air gap can be converted into mechanical power (P) as:

$$P = T * \omega_m \quad \textbf{(4-1)}$$

Where ω_m is the speed in rad per second (N: number of rotations):

$$\omega_m = \frac{2 * \pi}{60} * N \quad \textbf{(4-2)}$$

Figure 45 presents the results of this study. By using these eight machines, it was possible to produce an equation which links the total weight of a singly superconducting machine with its torque.

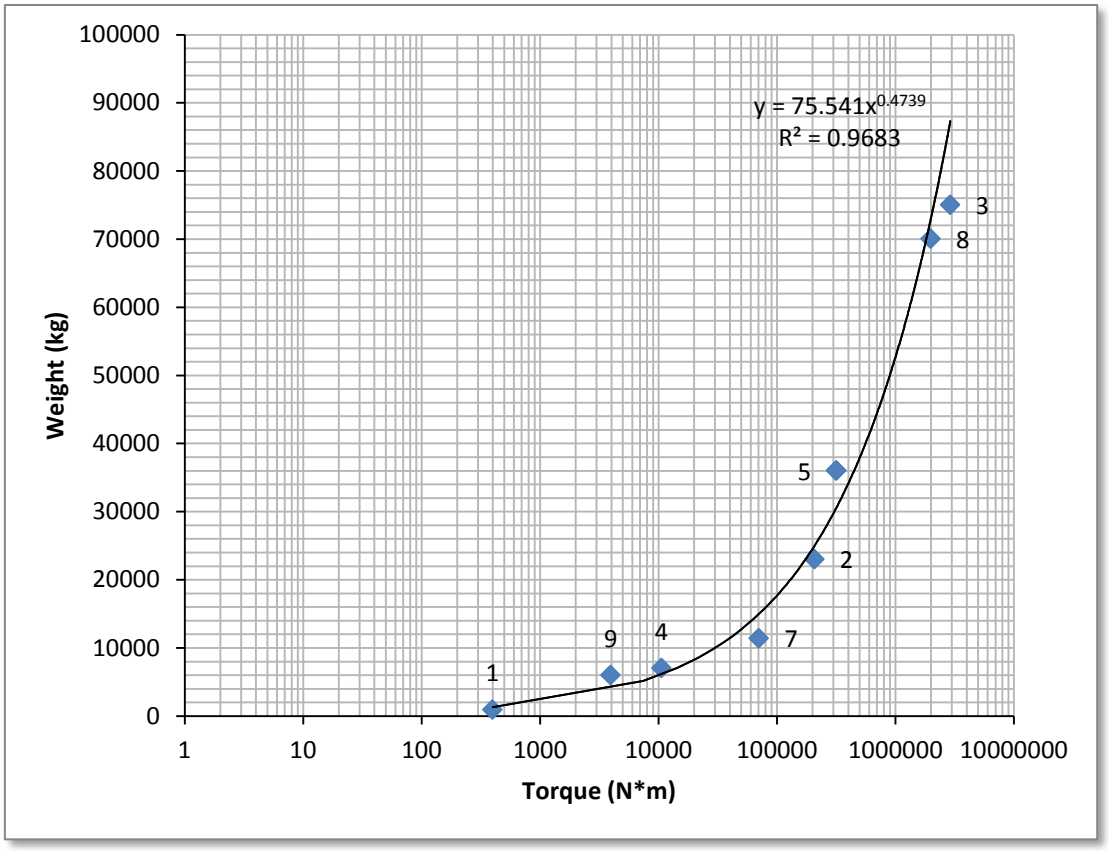

Figure 45 Weight vs Torque of singly superconducting machines

Although one might have expected a more linear relationship between the torque and the weight of these machines this apparently is not the case for the singly superconducting machines. The exact reasons for this unexpected trendline are not yet clear to the author and further research on this subject might be necessary. The derived equation (4-3) could only be used as an early stage indication for the weight of singly SMs. Its relatively low R^2 value does not

allow the use of this equation as a reference to the methods described in the following chapters (4.2).

$$Total\ Weight = 77.146 * Torque^{0.4701} \quad \textbf{(4-3)}$$

4.2 Weight Estimation of Fully Superconducting Machines

One of the most important issues of the TeDP concept is the weight of the electrical system. The fact that fully superconducting machines have only been built once or twice, and little has been published on those that have, makes the weight estimation of this system even more challenging. There has not been a study describing a reliable method of calculating the weight of these machines and in the majority of the TeDP related journal and conference papers predicted values are included without a clear description of the methodology behind them. In this chapter a novel method for calculating the weight of fully superconducting machines is described and corresponding Simulink models are presented.

4.2.1 Torque per unit of rotor volume (TRV) method

Torque per unit of rotor volume (TRV) is what generally characterises the size of electrical machines. This effectively depends on the product of the electric loading (A) and the magnetic loading (B). Both these values are limited by the properties of the materials being used as well as the temperature rise and cooling system capability (Hendershot and Miller, 2010).

Electric loading is defined as the linear current density around the airgap circumference and is given by the following equation:

$$A = \frac{total\ ampere\ conductors}{airgap\ circumference} = \frac{2mT_{ph}I}{\pi D} \quad A/m \quad \textbf{(4-4)}$$

, where m is the number of phases, T_{ph} is the number of turns in series per phase, I is the RMS phase current, and D is the diameter of the airgap. In these first calculations there is no distinction between the rotor outer diameter and the stator inner diameter assuming that the airgap is too small compared to the rotor diameter.

Magnetic loading on the other hand represents the average flux density over the rotor surface. In AC motors this is distributed sinusoidally and is derived from the following equation:

$$B = \Phi * \frac{2p}{\pi D L_{stk}} \qquad T \tag{4-5}$$

, where Φ is the fundamental flux/pole, p is the number of pole pairs and L_{stk} is the stack length. Generally, in a slotted stator of a conventional electrical machine the peak flux density is limited by the saturation losses which can be excessive for density values above 1.6T. This is not the case for the superconducting machines where this value is anticipated to be at least twice as much. Note that since it is assumed that the flux is sine-distributed, its average value will be given as:

$$B_{avg} = B_{max} * \frac{2}{\pi} \qquad T \tag{4-6}$$

Next step will be to use the standard equation that gives the generated electro-magnetic force (emf) per phase:

$$E = \frac{2\pi}{\sqrt{2}} * k_w T_{ph} \Phi f = \frac{\pi^2}{\sqrt{2}} * \frac{k_w T_{ph} B_{avg} D L_{stk} f}{p} \qquad V \tag{4-7}$$

, where f is the fundamental frequency and k_w is the fundamental harmonic winding factor.

The maximum electromagnetic power at the airgap is given by:

$$P = mEI \tag{4-8}$$

However, power could also be derived by equation (4-1) and rotational speed by equation (4-2). The rotor volume on the other hand could easily be calculated as:

$$v_r = \pi * D^2 * L_{stk}/4 \tag{4-9}$$

Combining all the above equations (4-1)-(4-9) it is possible to come up with the final equation that sizes the electrical machines:

$$TRV = \frac{T}{v_r} = \frac{\pi}{\sqrt{2}} k_{w1} AB \qquad Nm/m^3 \tag{4-10}$$

4.2.2 Relationship between rotor and stator dimensions

Generally, the torque of a load is commonly given as a requirement before designing a machine. After that, an electrical machine capable of driving this load needs to be designed. Equation (4-10) could be then used to calculate the volume of the rotor. The next step should be the estimation of the active weight of the machine. In order to do the latter a relationship between the rotor and the stator dimensions need to be found. There have been some studies (Miller, 1989) suggesting that for a rough estimation of the stator dimensions a “split ratio” (rotor diameter/stator diameter) parameter can be used. The equation normally being used is the following:

$$Stator\ volume = \frac{Rotor\ volume}{Split\ ratio^2} \tag{4-11}$$

However, the assumed value of this ratio varies with the type of the machine and the architecture (interior-rotor or exterior-rotor) being chosen. Especially for the superconducting machines further assumptions are necessary jeopardising the reliability of this method. Hence, a more reliable technique to determine the relationship between the stator and rotor dimensions was essential.

The method which has been used in this project is based on a literature survey of actual real conventional electrical machines that gave us a reliable relationship between the rotor and stator diameter. More specifically, 13 different conventional machines were included in this study (Appendix A.1), while the dimensions of three of the superconducting machines which have been presented in 4.1, as well as the PSAM conceptual baseline design (4.1.4), were added to the graph (Figure 46) in order to validate the reliability of the derived relationship for the superconducting case.

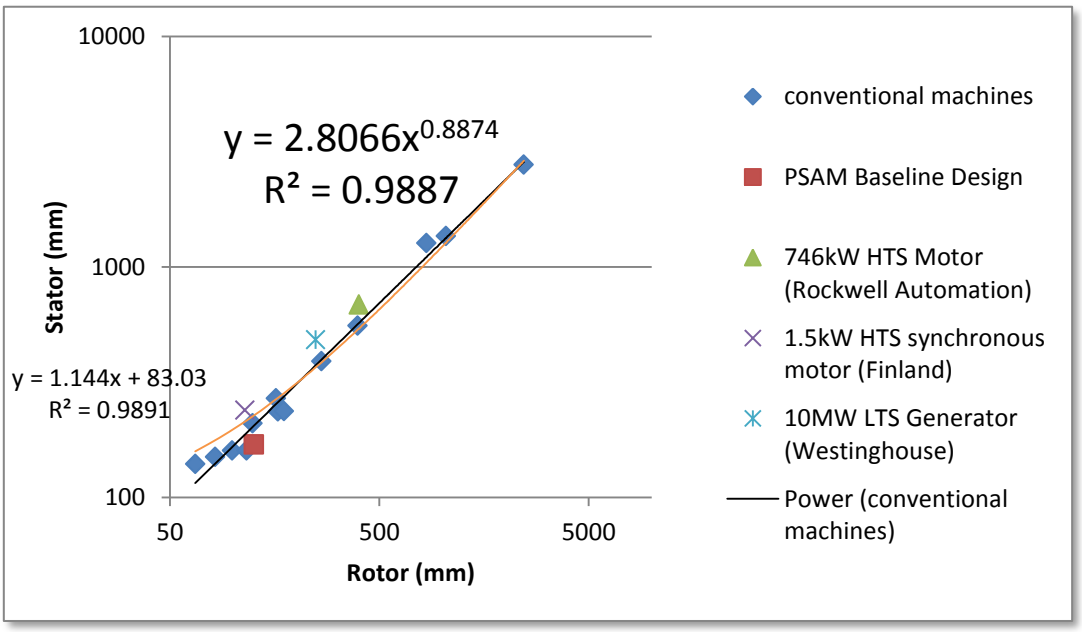

Figure 46 Rotor vs. stator dimensions relationship graph

As it can be seen, two relationships were derived from the graph above: one using the power trendline in the excel toolbox and another one using a linear relationship. These two relationships were used in the following subchapters to estimate the weight of the fully superconducting machines by two different methods. To summarize the aforementioned equations:

$$Stator\ diameter = 2.8066 * Rotor\ diameter^{0.8874} \quad \textbf{(4-12)}$$

, and

$$Stator\ diameter = (1.144 * Rotor\ diameter) + 83.03 \quad \textbf{(4-13)}$$

The superconducting machines being included in this study validate that a similar trend will most probably be followed in the design and construction of superconducting machines.

4.2.3 Basic Assumptions

In order to proceed with the weight estimation of the fully superconducting machines some basic assumptions need to be made. All the following assumptions were validated by literature studies and expert's opinions, whilst sensitivity studies will also follow, testing the impact of these assumptions on the overall weight estimation of the machines.

- Magnetic loading *B*

During the first simulations a maximum air gap flux density of 3T was assumed. This value was derived from the PSAM project outcomes and it could be considered a conservative estimate itself especially for the 2035 timeframe. Even recent experimental studies (Rada et al., 2015) have suggested magnetic field capabilities of around 4T. It is important to point out that in superconducting machines the magnetic loading has a slightly different meaning than in a conventional machine. In the latter, it indicates the working level of the flux density in the air gap measuring the flux density in the iron teeth. On the other hand, in the superconducting machines this magnetic loading is not constant across the air gap and it is just a reference of the peak value of flux at the armature conductors. For this reason equation (4-6) is being used in the calculation of the overall weight of the machines. The peak value of magnetic loading in this case does not only affect the power output of the machines but is

also an indication of the eddy currents loss in the armature conductors (Bumby, 1983).

- Electric Loading *A*

The assumed electric loading value was 400 $^{kA}/_{m}$ also derived from the PSAM experimental results. This value could also be considered as conservative especially if you compare it with higher estimates that were assumed in studies even back in the 70's (Miller and Hughes, 1977) as well as with more recent studies that claimed values even in the range of 700kA/m and more (Tixador and Daffix, 1997).

- Winding factor k_w

The fundamental harmonic winding factor k_w could be described as a reduction factor of the generated RMS voltage in 3-phase AC generator. In most conventional machines this factor varies from 0.85 to 0.95 (Skaar, Krovel and Nilssen, 2006). There is no reason to believe that this will be any different in a superconducting machine and hence a value of 0.9 was initially assumed.

- Machine design and materials assumptions

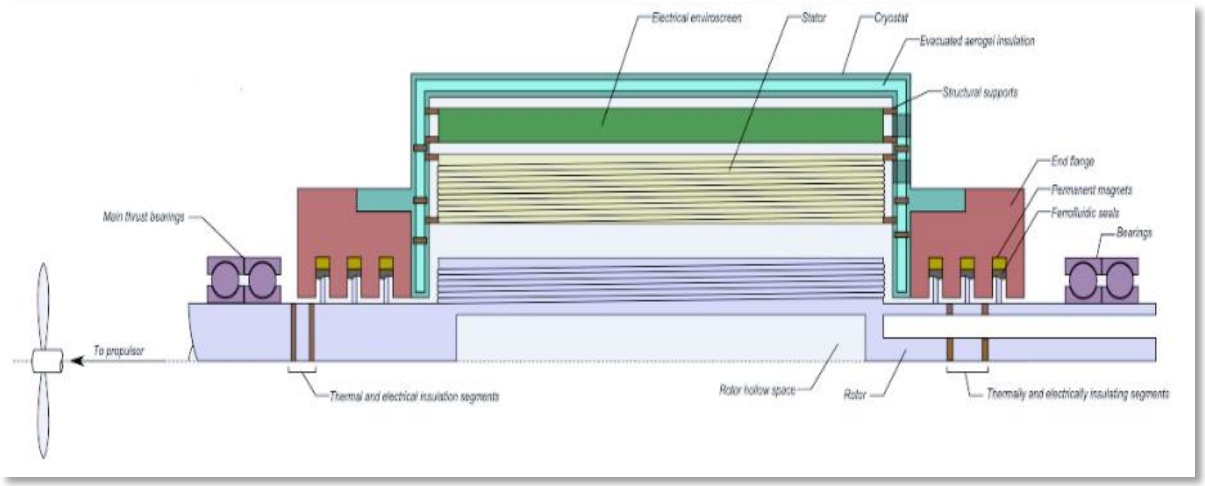

Figure 47 General view of the DEAP superconducting electrical machine (Courtesy of the DEAP project)

Figure 47 demonstrates a general overview of the machine's arrangement used in this project. It is basically a more detailed and advanced version of the one

being used in the PSAM project (Figure 44). In this design, the stator is constructed primarily of epoxy concrete with a density of 2400 kg/m^3, while the rotor is constructed primarily of steel (density of 7859 kg/m^3) with a small proportion of HTS materials. As shown in Figure 44, the active rotor also has a hollow space of the same diameter as the rotor shaft. The ball bearings are assumed to be constructed of ceramic with a density of 4700 $kg/m^3$and are 70% solid by exterior volume. Vacuum chamber and vacuum chamber end flange are assumed to be made primarily of aluminium alloy, the use of which appears feasible at cryogenic temperatures (Senkov, Bhat and Senkova, 2004). All the aforementioned material assumptions combined with the presence of the hollow space inside the rotor led to an assumed active density value of 3000 kg/m^3. By active density, we consider the overall power density of the active parts of the machine (i.e. rotor, stator and possibly environmental screen). Finally, an extended analysis about the environmental screen of this machine and its effect on the overall machine weight will follow in the sub-chapter 4.3.1.

4.2.4 Models Description

In this project two different methods estimating the weight of the superconducting machines were proposed. Both versions were based on the TRV concept, but whilst in the first approach the outcome of the TRV equation (4-10) was simply given the rotor dimensions, in the second version which shall be considered as more optimistic a further assumption was made. It is believed that for fully superconducting machines the TRV equation is linked with the mean stator winding diameter and not the outer rotor diameter (Berg and Dodds, 2013). Table 8 summarises the inputs and outputs of the two models which were developed in MATLAB Simulink to estimate the overall weight of the fully superconducting machines.

Table 8 Inputs/Outputs of the Simulink models for the weight estimation of fully superconducting machines

Inputs	Units	Outputs	Units
Output Power	W	Torque	$N\,m$
Rotational Speed	rpm	Phase Current	A
Electric Loading	$A\,m^{-1}$	Phase Voltage	V
Peak Magnetic Flux	T	Active Length	m
Winding Factor	–	Active Diameter	m
Pair of Poles	–	Active Volume	m^3
Efficiency	–	Active Weight	kg
Mean Stator Factor	–	Frequency	Hz
Number of Turns	–	Thermal Load	W
Power Factor	–	Power Density	$W\,kg^{-1}$
Active Density	$kg\,m^{-3}$	Torque Density	$N\,m\,kg^{-1}$
Cryostat Weight Factor	–	Cryostat Added Weight	kg
Length/Diameter Ratio	–	Total Weight	kg

- *First Version (TRV Original)*

In this first version, from equation (4-10) the rotor volume can be estimated. By assuming an aspect ratio of one (rotor length L=rotor diameter D) and by using equation (4-12) the stator diameter is calculated. Choosing an L/D ratio of unity is a common technique in the initial sizing estimates of electrical machines (Hendershot and Miller, 2010). The active dimensions of the machine can now be estimated and by assuming an active power density of 3000 kg/m^3 the active weight can also be calculated. The following figure presents the Simulink model which includes all the aforementioned assumptions and equations:

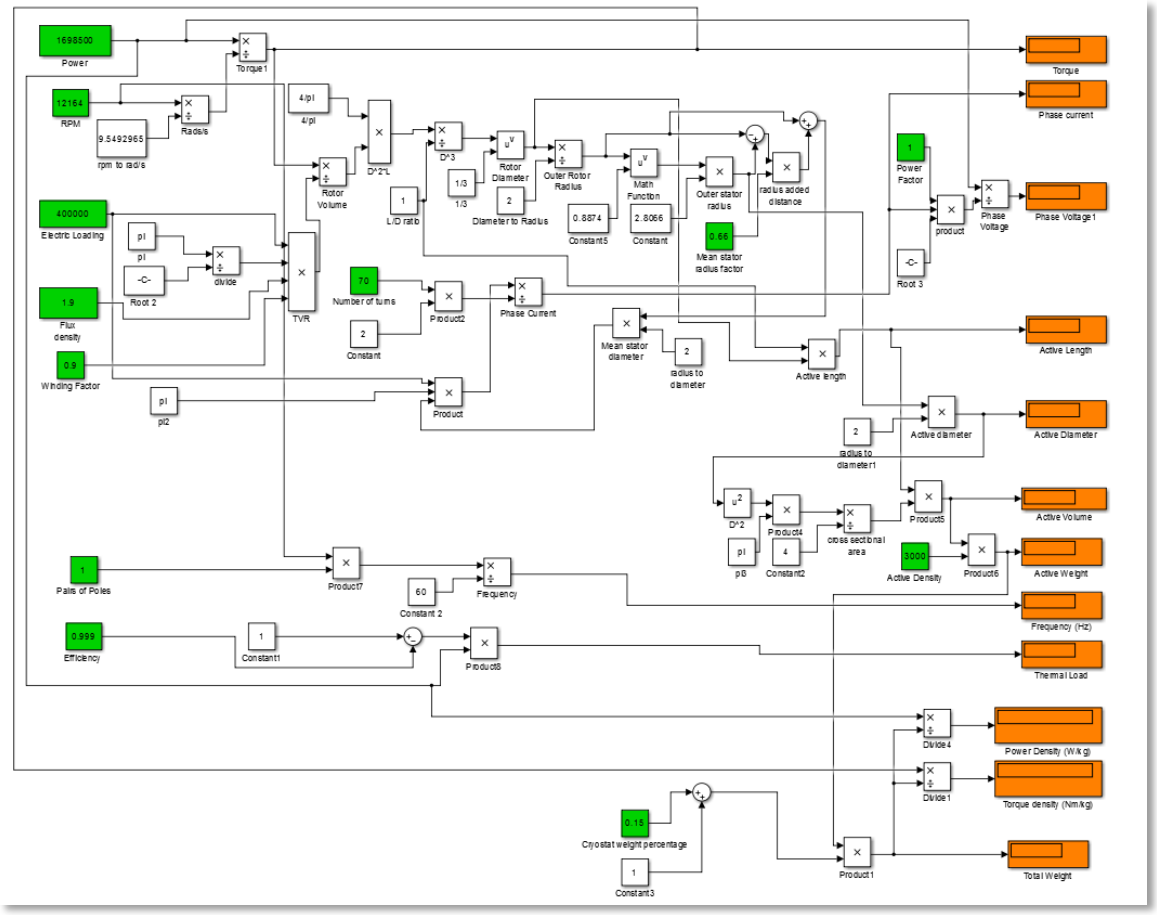

Figure 48 Simulink model (first version) for the weight estimation of fully superconducting electrical machines

In this model the power and rotational speed are used as inputs. In most applications it is common to know the power and speed requirements of the system; hence the required torque can be easily calculated (4-1). Apart from the active weight of the machines, further outputs of the model are the following: phase voltage, frequency, thermal load, power and torque density, and overall weight of the machine. The phase voltage of this machine can be found by using the well-known relationship:

$$V_{ph} = \frac{P}{\sqrt{3} * I_{ph} * \cos\varphi} \qquad \textbf{(4-14)}$$

Where I_{ph} is the RMS phase current, and $\cos\varphi$ is the internal power factor which in our case is assumed to be equal to one. The RMS phase current can be derived from equation (4-4), assuming a value for the number of turns per coil (i.e. in our models assumed as 70). The machines' frequency is being based on the number of pair poles (assumed as 1 in the first estimates), while for the thermal load calculation an efficiency of 99.9% is assumed. Although this assumed efficiency might seem relatively high, equivalent NASA studies (Brown, 2011; Felder et al., 2011a) assumed efficiencies up to 99.97%, making this project's assumptions relatively pessimistic.

Finally, to calculate the total weight of the machine an extra cryostat weight percentage is considered. The latter was chosen based on an expert's opinion (i.e. Steven Harrison-formerly of Scientific Magnetics) who suggested that a value between 10-50% of the actual machine should be added. However, since we are looking at aerospace applications a value closer to the lower limit of this range (10-20%) seems reasonable. A 15% cryostat added weight was chosen for Chapter 4 calculations, whilst a more conservative value of 30% was selected for the following chapters (i.e. Chapters 5, 6).

- *Second version (TRV optimistic)*

In this version, equation (4-10) is used to calculate the mean stator diameter instead of the outer rotor diameter. A way to calculate the outer stator diameter was then needed and this became feasible by using the linear trendline equation (4-13). An additional assumption was necessary to calculate these dimensions. More specifically, a mean stator factor was added with an initially assumed value of 0.66. This factor basically expresses the mean stator radius relative to the outer rotor and stator radius. A value close to zero means that the mean stator radius is exactly the same as the outer rotor one, something that will basically lead to similar results with the first version of the model (the TRV equation in this case will give the rotor dimensions). Values close to one will result in very optimistic estimates regarding the overall weight of the machines.

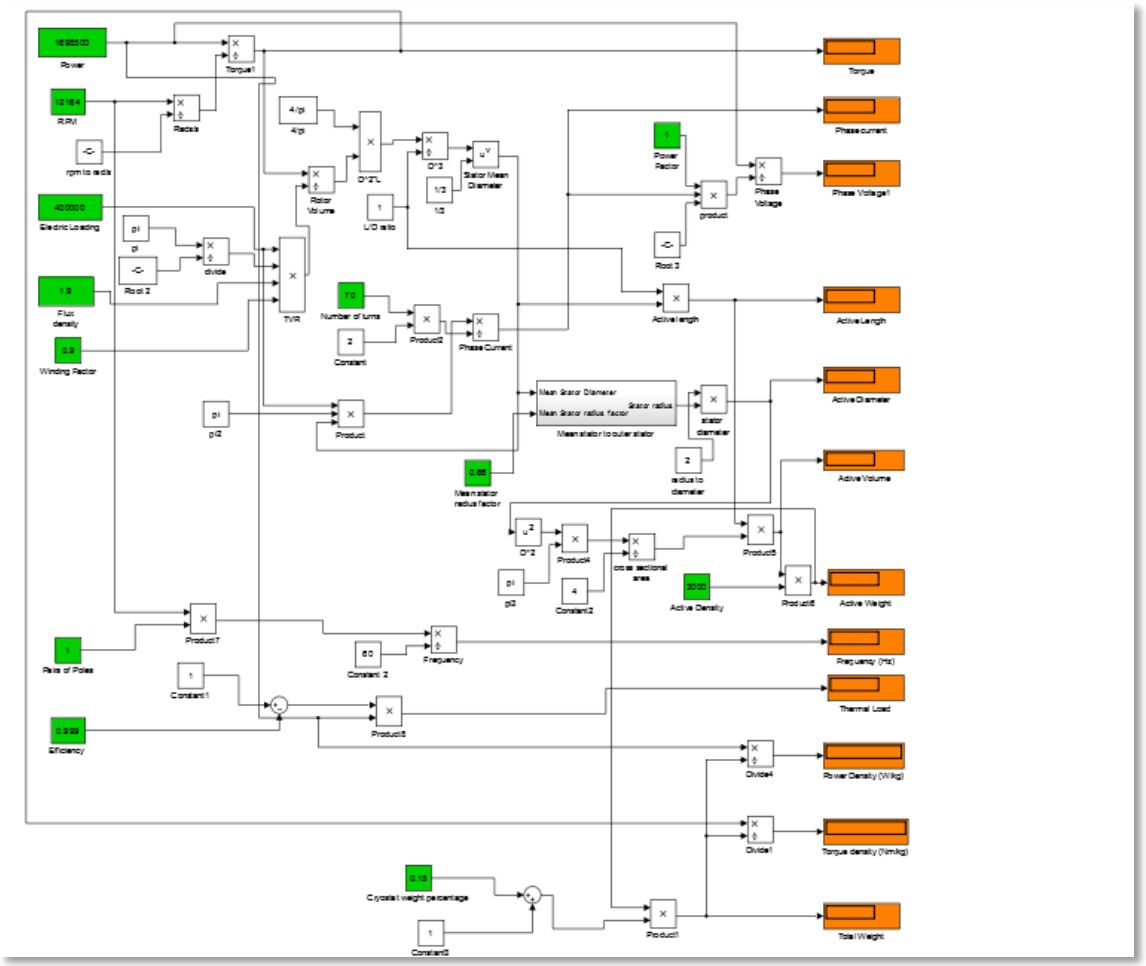

Figure 49 Simulink model (second version) for the weight estimation of fully superconducting electrical machines

The figure above shows the Simulink model of the second version, where the main difference with Figure 48 is the aforementioned way of calculating the active weight of these machines. Figure 50 demonstrates this new subsystem.

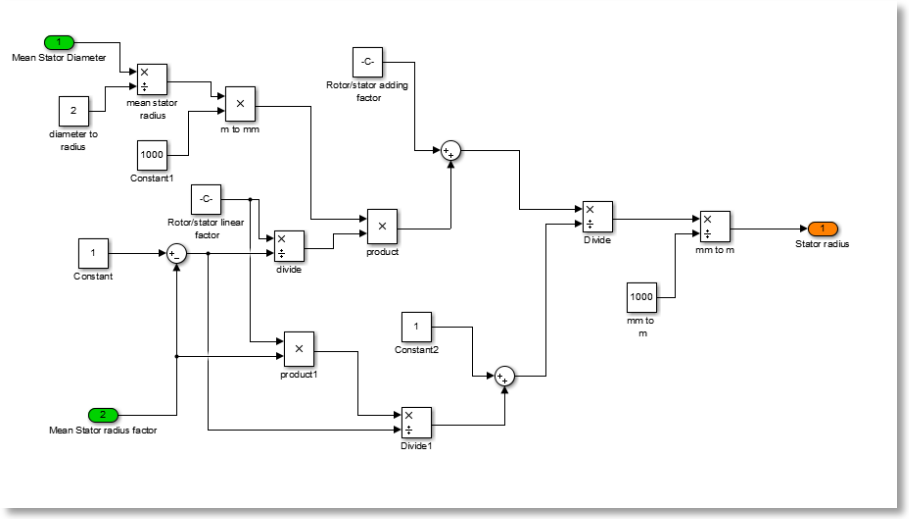

Figure 50 Mean stator to outer stator subsystem

The rest of the model, as well as all the assumptions being made in the first version of the model remain the same. A sensitivity study that will show the effect of these assumptions on the overall weight of the machine will follow on the next subchapter.

4.3 Sensitivity Study

As it is already mentioned in the previous chapters, in order to develop a model to estimate the weight of the fully superconducting machines some basic assumptions had to be made. The justification for these assumptions was described in chapter 4.2.3. In this subchapter however, the effects of the most important assumptions being made on the overall estimation of the weight will be explored for the two different versions of the model. A sensible range for every assumption will be investigated whilst the rest of the parameters will keep their initial assumed value during the progress (Table 9).

Table 9 Initial assumed values for the model's inputs

Parameter	Units	Value
Maximum Magnetic Loading	T	3
Electric Loading	$kA\ m^{-1}$	400
Power factor	–	1
Winding Factor	–	0.9
Active Power Density	$kg\ m^{-3}$	3000
Mean Stator Factor	–	0.66
Cryostat Adding Weight Factor	–	0.15
Rated Output Power	kW	1470
Rotational Speed	rpm	11100
Length/diameter (L/D)	–	1

4.3.1 The environmental screen

An environmental screen is required to contain the magnetic field within the electrical machine space in order to screen the environment from stray magnetic fields. Within a superconducting machine for a given field current the magnetic flux density at the armature depends on the type of the environscreen employed. The effect of this screen at the field winding is small since the generator/motor is practically air cored, however at the stator which is closer this effect is pronounced (Bumby, 1983). There are two main types of environscreen normally being employed: the iron environmental screen and the conducting screen.

- Iron Environmental Screen

This type of screen is typically being chosen in applications such as power station turbo-generators where the high power output per length and the low

screen losses make this type of screen an attractive option. The thickness of this screen can be calculated by the following equation:

$$t_c = \frac{1}{p}\frac{\hat{B}}{B_{max}}\left(\frac{r_s}{r_x}\right)^{p+1}\frac{2r_x}{1+\left(\frac{r_s}{r_x}\right)^{2p}} \quad m \tag{4-15}$$

The thickness of the iron screen and consequently its weight depends on the number of poles of the machine. The mass of this screen is being given by the equation:

$$W_{screen} = \gamma\pi * ({t_c}^2 + 2t_c r_x) \quad kg\ m^{-1} \tag{4-16}$$

Equations (4-15) and (4-16) are being implemented in Simulink as an additional subsystem to the previous machine models. The subsystem's inputs and outputs can be summarised in the following table:

Table 10 Inputs/Outputs of the Environmental Screen Subsystem

Inputs	**Units**	**Outputs**	**Units**
Pair of poles (p)	-	Screen Thickness (t_c)	m
Environscreen density (γ)	$kg\ m^{-3}$	Environscreen Mass (W_{screen})	kgm^{-1}
Mean stator radius (r_s)	m		
Inner screen radius (r_x)	m		

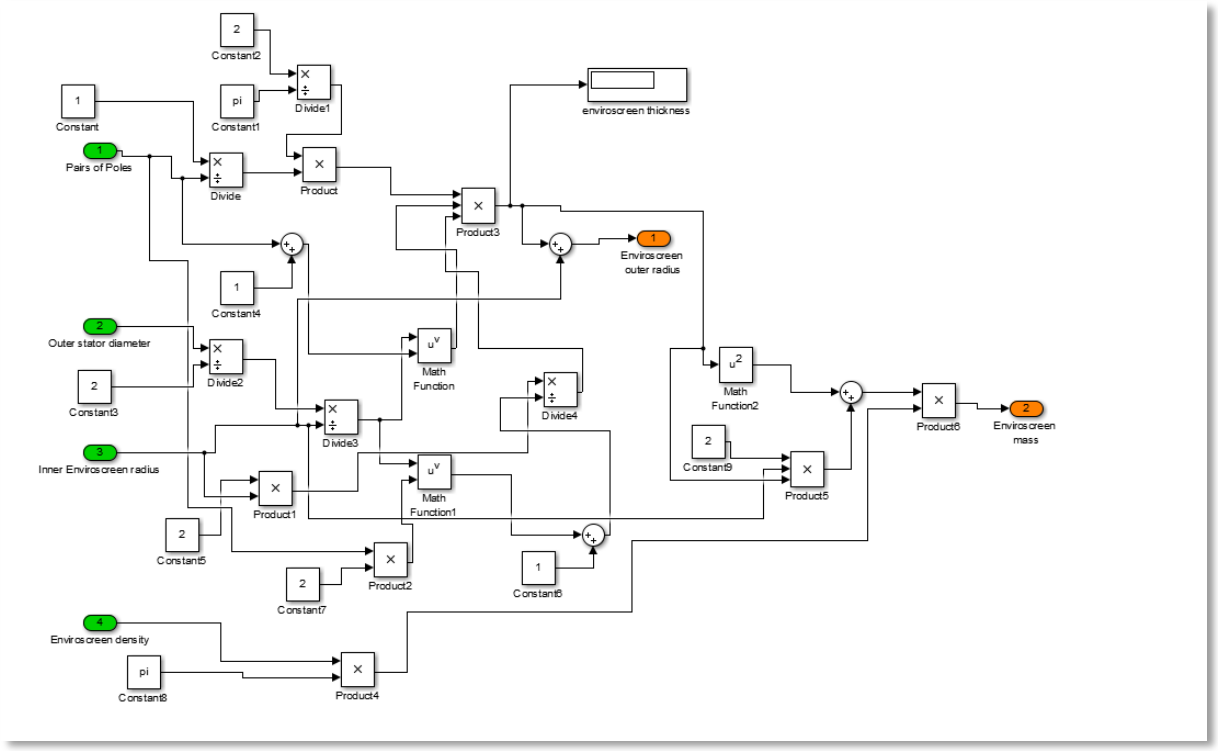

Figure 51 Environmental Screen Simulink Sub-model

Three different cases were investigated to demonstrate the extra weight that an iron environmental screen will add to these machines: (a) a case where no environmental screen is implied to the machines, (b) another case where an iron screen is being used in a 4-pole machine and finally (c) a case where an iron environscreen is added to an 8-pole superconducting machine. The last two cases will show the dependence between the pole numbers and the mass of the iron screen. A 4-pole and an 8-pole configuration were chosen as they seem the most probable options for our application where frequencies between 400 and 800 Hz will be required (this is the case for Boeing's 787 Dreamliner aircraft).

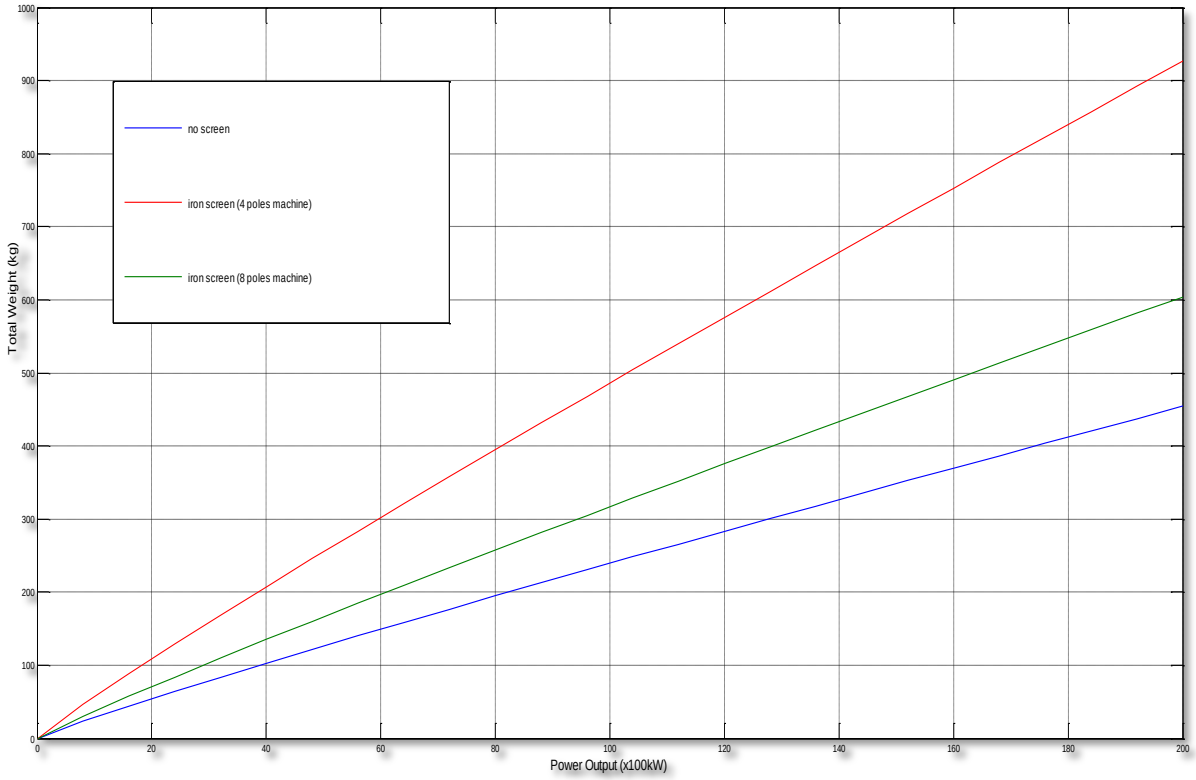

Figure 52 Overall weight of a superconducting machine (a) without environscreen, (b) with iron screen (4-poles machine) and (c) with iron screen (8-poles machine).

It is clear that as the number of poles increases the weight of the iron environmental screen drops significantly. However, even for an 8-pole machine the added weight because of the iron screen is unacceptable becoming one of the predominant machine parts on the weight estimation. Since it does not seem likely that the superconducting machines will consist of high number of poles, the additional weight of this type of screen clearly suggests that such a screen will not be used at least in the machines which will be designed for airborne applications. Particularly for high power machines (over 10MW) the weight of the screen becomes prohibitive.

- Conducting Environmental Screen

Another popular type of environmental screen is the conducting screen. Copper and aluminium are the possible material choices for this type of screen. The low density of aluminium (2700 $kg\ m^{-3}$) compared to copper (8960 $kg\ m^{-3}$) favours

aluminium screens in the machines designed for the airborne applications. Furthermore, the weight of an aluminium screen is about the one tenth that of iron screens (Bumby, 1983) and the following figure presents its effect on the overall weight of the fully superconducting machines.

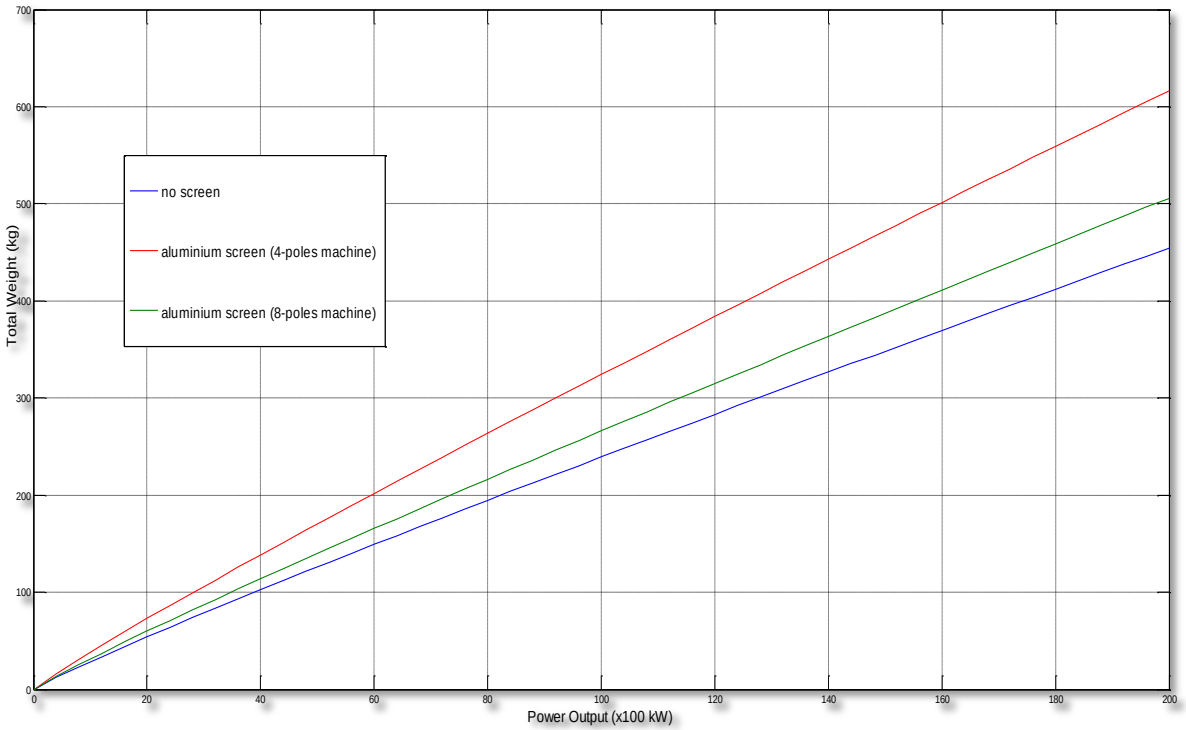

Figure 53 Overall weight of a superconducting machine (a) without environscreen, (b) with aluminium screen (4-poles machine) and (c) with aluminium screen (8-poles machine).

In this case the weight of the screen is not anymore the predominant weight factor and particularly for an 8-pole machine it seems like an obvious choice. However, this type of screen suffers from significant power losses which degrade the overall efficiency of the machine. The eddy currents in this type of screen affect the efficiency of the superconducting machines eliminating one of the main advantages of these machines. In order to achieve a similar power loss to the iron screen a substantially greater screen radius is required. Thus, a compromise between the screen dimensions and its power losses is necessary.

- Superconducting Environmental Screen

It is clear that, although for different reasons, both the iron screen and the conductive screen could be a limiting factor for the overall attractiveness of future fully superconducting machines. The weight of the former and the losses added by the latter demonstrate the need for an alternative solution. Unfortunately, there is no way of avoiding the environmental screen in this type of machines. However, there has been a suggestion by some experts from Rolls Royce that a superconducting environmental screen could be used instead (patent pending). The thickness of this screen is expected to be significantly low and so will be the added weight. The power density of the superconducting machines will be affected but its effect was considered negligible for the purposes of this study.

4.3.2 TRV Factor

In this study TRV factor is defined as the product of the magnetic and electric loading of the electrical machines as shown in equation (4-17). Usually, the designer aims to maximise the power output of a machine of given dimensions by reaching the highest possible values of these two parameters. These parameters present significantly higher operational limits in the SMs than in the conventional machines. This is the main reason why these machines demonstrate increased power density whilst the removal of Joule loss in the excitation winding also increases their efficiency.

$$TRV_{factor} = A \times B \qquad A\ m^{-1}\ T \tag{4-17}$$

Generally, *B* is limited by saturation and iron losses whilst *A* is constrained by the efficiency of stator cooling, by winding vibration, and by the space available for the conductors (Miller and Hughes, 1977). Since there are not any data available for fully SMs, their synchronous and transient reactances are unknown. In order to be able to investigate their performance relatively reliably it is reasonable to assume that the improvement rate of these two factors (i.e. magnetic and electric loading) will follow similar trends. This is why these two inputs were chosen to be studied together as a common “TRV factor” and its

effects on the total weight of the machines were investigated. The range of the factor varied from 200 to 2200 $A\ m^{-1}\ T$ based on the expected maximum values of these two parameters. There have been experimental work showing electrical machines able to trap magnetic field in the area of 4T (Rada et al., 2015) while this value could potentially reach even the maximum value of 10T. Electric loading values around 700 kA/m have also been achieved (Tixador and Daffix, 1997).

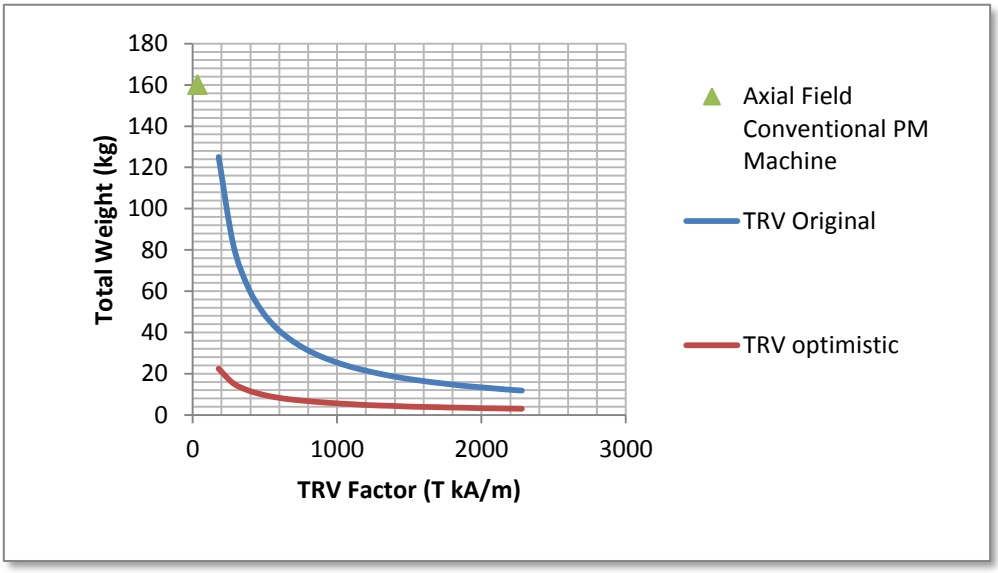

Figure 54 TRV Factor Vs. Total Weight of Fully Superconducting Machines

Quite similar trends can be seen on both versions with the first version (TRV Original) showing more clearly the effects of this factor. It is obvious that after a point the improvement of TRV factor does not reflect significant gains in the total weight estimate, a result that we should take into consideration when designing these machines. However, it is important to note that the rest of the input parameters remained constant something that in reality will be extremely difficult. Rotor and stator dimensions will have to change as well to maintain the high values of magnetic flux. Furthermore, in the upper limits of this factor, enormous electromagnetic forces should be expected and ways to control them will be necessary. In our models a value of 760 was chosen based on the PSAM results. This value seems to be the ideal based on this graph, a fact that could be used as another validation for our results. In this graph, as well as for

the rest of the sensitivity study, a comparison with the weight of a conventional axial field PM machine (Jewell, 2009) of the same torque rating is also made.

4.3.3 Active Power Density

In this study active power density is defined as the average power density of the active parts of the electric machines (i.e. stator and rotor). The effect of this assumption on the total weight of the machines is very strong and an accurate estimation of this value will be really crucial. Depending on the materials being used as well as the machine architecture being chosen it is fair to assume a range between 2000 and 8000 $kg\,m^{-3}$. A value between 3000 and 4000 $kg\,m^{-3}$seems more reasonable in the configuration under investigation in this project. For the active parts of the machine, in the initial studies as described in 4.2.3 the stator is constructed mainly of epoxy concrete with a power density of 2400 $kg\,m^{-3}$. The rotor on the other hand is constructed primarily of steel (power density of 7859 $kg\,m^{-3}$) with a small proportion of HTS material. However, a hollow space of the same diameter as the shaft is being assumed and this will significantly decrease the active power density, hence the 3000 $kg\,m^{-3}$assumed value.

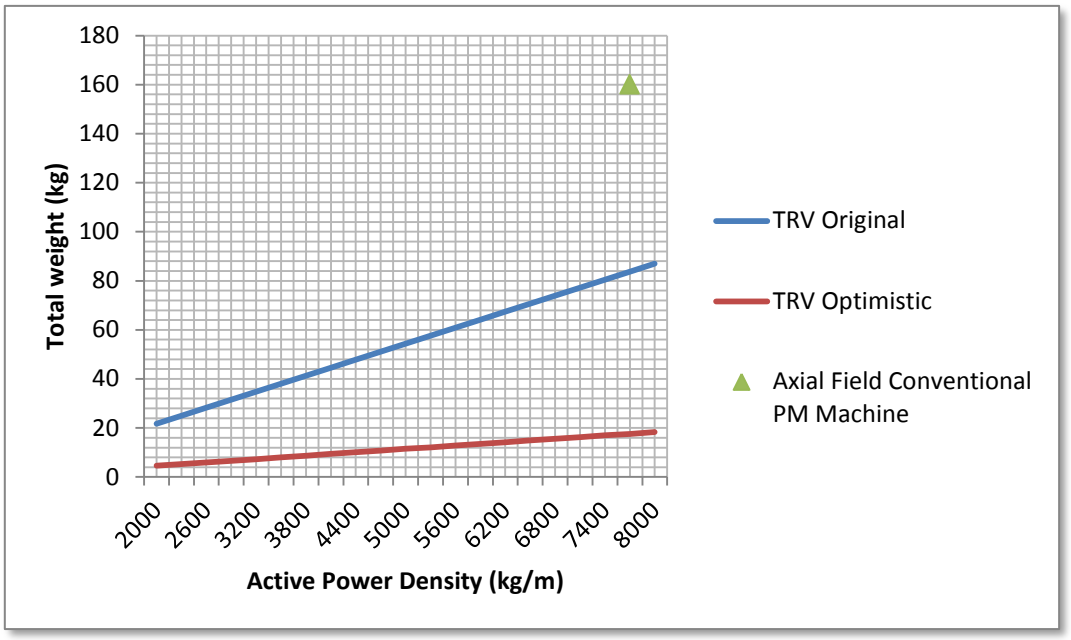

Figure 55 Active Power Density Vs. Total Weight of Fully Superconducting Machines

The effect of the active power density on the total weight of the machines can be seen in Figure 55. Although the trends of the two versions seem slightly different, the truth is that in both cases the total weight was eventually quadruplicate. However, even with the more pessimistic assumptions SMs are still a lot lighter than the reference machine.

4.3.4 Cryostat Weight

The cryostat weight is another main assumption of the model. In order to overcome this relatively unknown field, especially for the superconducting machines, an expert's opinion was asked. More specifically, Steven Harrison (founder and former director of Scientific Magnetics-Oxfordshire) suggested that a range between 10-50% of the active weight should be considered. However, his view was that since we are interested in aerospace applications it is more reasonable to look at the lower limits of this range. Thus, a sensitivity study for a range between 8-30 % was carried out for both versions of the TRV models.

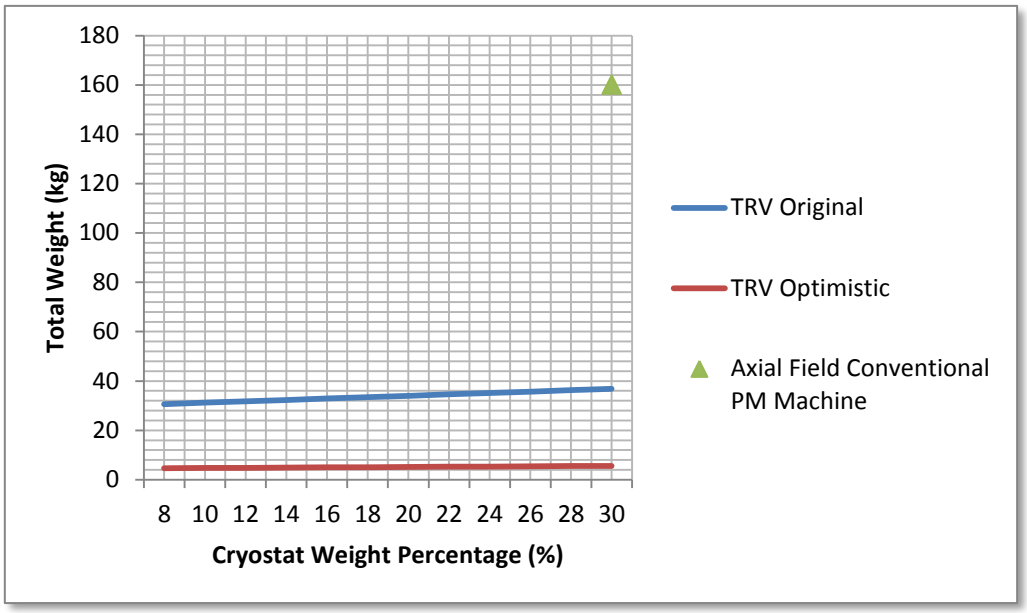

Figure 56 Cryostat Weight Factor Vs. Total Weight of Fully Superconducting Machines

The cryostat weight seems to have a stronger effect on the first version however this is not entirely truth. The heavier the machines we investigate the strongest the effect of the cryostat weight and that will be the case in both versions.

4.3.5 Winding factor

In three-phase AC electrical machines the winding factor is responsible for the decrease of the generated RMS Voltage. Most conventional machines have winding factor values between 0.85 and 0.95 (Skaar, Krovel and Nilssen, 2006). In our case a wider range between 0.80 and 0.97 was chosen and the derived results assume that the rest of the parameters remain constant. In the next graph as it was expected, it can be seen that the higher the winding factor value the lighter our machines will be:

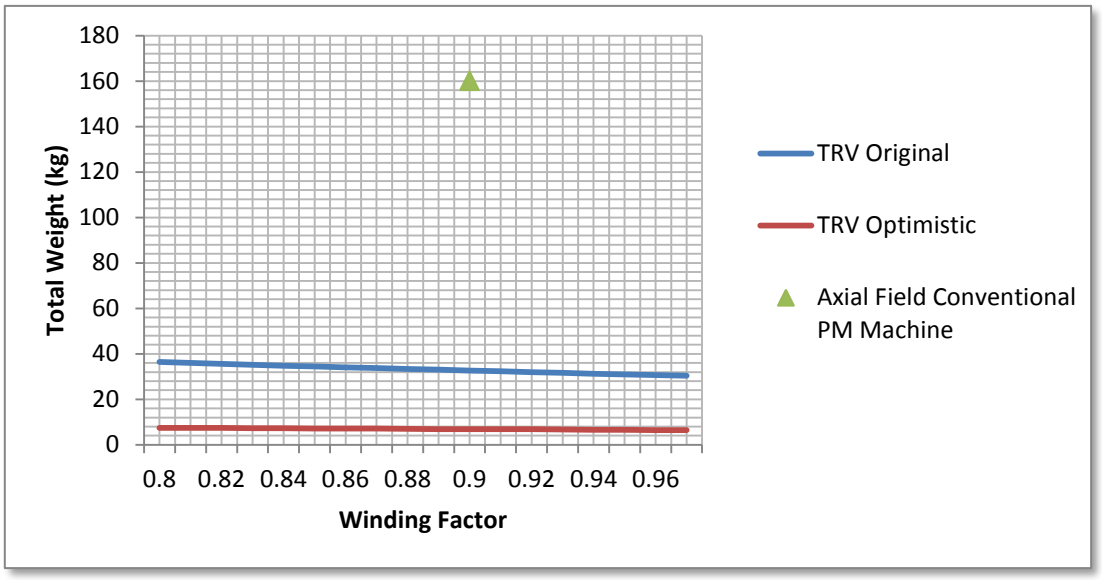

Figure 57 Winding Factor Vs. Total Weight of Fully Superconducting Machines

In PSAM Aerospace Assessment a value of 0.9 was assumed, however a winding factor around 0.95 could be a reasonable assumption for these machines. As it was expected an almost linear relationship was derived both for the first and for the second version of the model. However, it is clear that the winding factor does not play a predominant role in the overall weight of these machines.

4.4 Key Model Limitations

This model is based on the TRV concept that is normally being used as a preliminary sizing method for the design of conventional permanent magnet machines. The main characteristic of this method is that it is relied on the physical principles of the machines. Hence, some important limitations must be borne in mind when using this mass estimation method:

- **Structural limitations were neglected**: superconducting machines demonstrate high values of electric and magnetic loading compared to the conventional machines. This characteristic apart from bringing significant benefits it also creates some structural considerations because of the very high forces being anticipated. The expected flux densities dictate the use of minimum iron within the structure of the SMs

(Hughes and Miller, 1977) whilst for a machine of similar dimensions to a conventional one, larger forces must be carried. This means that especially for smaller machines the structural weight could potentially be the dominant weight factor. Since this model accounts only for the electromagnetic considerations, the calculated mass of small machines appears low and must be treated only as an optimistic preliminary sizing estimate.

- **Machine Losses not physically modelled:** as an input in this model an assumed efficiency is being used. This assumption was based on the very optimistic NASA predictions for the N+3 timeframe, where efficiency around 99.97% was predicted (Felder et al., 2011b). For the DEAP project an assumed value of 99.9% (Wright et al., 2015) was used and based on this value the thermal load of the machines was calculated. However, electrical losses being produced because of electromagnetic considerations were not calculated in the existing model. Operating temperature and speed will most probably affect the overall efficiency of these machines which are operating in cryogenic temperatures. These inefficiencies are critical on deciding the economic feasibility of this aircraft and hence higher fidelity models that take into account these losses need to be developed in the near term future. It is also expected that losses other than electrical and thermal can be kept at ambient temperature, for example by designing the bearings outside the main cryostat. The overall efficiency of the machines would suffer from some bearing and windage loss too. This has not been considered in the TRV model. Other design concerns, such as heat dissipation, may play a more dominant role when these machines become small and hence it is more likely that they will not scale linearly.
- **Overall weight estimation did not include all the parts of the machine:** in chapter 4.3.1 it has already been pointed out the lack of environmental screen weight estimate for the overall weight calculation of the SMs. This is expected to be a lightweight superconducting screen where its weight will be negligible compared to the rest of the

components. Furthermore, in the existing model there is no weight consideration for non-active machine parts such as the thrust bearings, the vacuum chamber, the end flange and other structural support. The latter might play an important role particularly in the smaller machines, but in principle all these parts have a secondary effect on the overall weight of electrical machines and at least for preliminary estimations can be neglected.

4.5 Model Validation

There is no other method in the literature that estimates the weight of the fully superconducting machines. Moreover, there are no data available for built fully SMs which could have been used as a reference. The only possible comparison could be made with the NASA TeDP concept machine weight estimations. These are considered relatively optimistic and there is no background data describing the methodology that was followed to derive these values. The following table shows the weight estimates of the superconducting machines derived from NASA N+3 predictions as well as by the two versions of this research study. In the NASA study two 53khp, 6500 rpm superconducting generators and fourteen 7.7khp, 4800 rpm superconducting electric motors were used (Brown, 2011).

Table 11 Comparison between NASA and TRV model weight estimates

Machine	**Units**	**NASA (BSSCO)**	**NASA (MgB2)**	**TRV (Original)**	**TRV (Optim.)**
Generator (w/o cooler)	kg	684	949.3	1144.9	172.16
Motor (w/o cooler)	kg	196.4	225.4	252.5	40.1

The first thing to notice in the table above is the extremely low weight estimates with the TRV optimistic version. This comparison definitely questions the reliability of the optimistic version of the TRV method. Even looking on the sensitivity study of these two methods, it was apparent that the optimistic version in most occasions has given unrealistic results, giving more than an

order of magnitude lighter machines than the original version. On the other hand, the original version seems somehow closer to the NASA predictions. In general, all NASA predictions for this concept could be considered rather optimistic and since the TRV (original) estimates are less than 20% heavier than the NASA (MgB2) values it seems like this method could be considered as a pessimistic prediction for the weight of the fully SMs. It is important to note that NASA predictions vary with the superconducting material being used (BSSCO or MgB2) and more specifically are a function of the superconductor filament diameter. Clearly, a different approach has been followed in this study and hence a reliable comparison cannot be made.

The TRV models of this research study were presented and used throughout the DEAP project. Several experts from all the partners involved (i.e. AGI, RR, CU, and Cambridge University) have validated the reliability of the TRV original method, whilst the weight estimates were used in the overall DEAP system weight estimation (Berg et al., 2015b).

5 Superconducting Electric Aircraft (SEA)

Up until this point the concepts of TeDP and SPN have been discussed. At this stage the possibility of applying these approaches to simpler aircraft electric systems will be investigated. The key example to this is the More Electric Aircraft (MEA) and therefore a study has been carried out to examine the possibility of using SPNs in such a system. The Boeing “Dreamliner” 787 and the Airbus 380 aircraft have been the first MEA in use. Both airplanes prove to be remarkably successful but there are reasons to believe that the industry is currently facing some important obstacles on scaling the aforementioned reference aircraft. Superconductivity could potentially solve most of these scaling issues, particularly if it will be combined with the TeDP concept where a superconducting network will also be present.

In this chapter a brief description of the MEA concept will follow, the electrical power network of the 787 aircraft will be described and a comparison between the use of a conventional and a superconducting network for the electrical system of such an aircraft will be made. The study will then be extended to different sized aircraft examples so that a wide range of electrical load demand could be investigated.

5.1 More Electric Aircraft (MEA) Concept

5.1.1 MEA Concept Description

The aviation industry was always driven by the demand to optimise aircraft performance, whilst reducing the operational and maintenance costs and increasing the reliability of the whole aircraft. In the last few years an extra objective to provide some more environmental friendly solutions has pushed toward a more electric approach in the design of current and future airplanes. A MEA it is typically characterised by the extended use of electrical power in the Secondary Power System (SPS).

These systems form the non-propulsive parts of the aircraft and in conventional configurations are driven electrically, mechanically, hydraulically or via

pneumatic/bleed air power (Laskaridis and Pilidis, 2004). Figure 58 (Jones, 2002) demonstrates the SPS of a traditionally powered aircraft. In such an aircraft, **pneumatic power** is obtained from the main engines' High Power Compressor (HPC) to power the Environmental Control System (ECS) and to provide hot air for the Wing Anti-Icing (WAI) System. **Mechanical power** is transmitted via gearboxes from the engines to central and local hydraulic pumps, to the main electric generator as well as to other mechanically driven subsystems. On the other hand, the actuation systems for primarily and secondary flight controls mainly use **hydraulic power**. The same goes for the landing gear and other ancillary systems. Finally, **electric power** derived from the main generator powers the avionics, the cabin power demands (lights, galley, in-flight entertainment etc.) and the aircraft lighting (Rosero et al., 2007). This combination of secondary power types has always being debated because of the additional complication and the resulted reduced efficiency of the overall system efficiency (Abdelhafez and Forsyth, 2009).

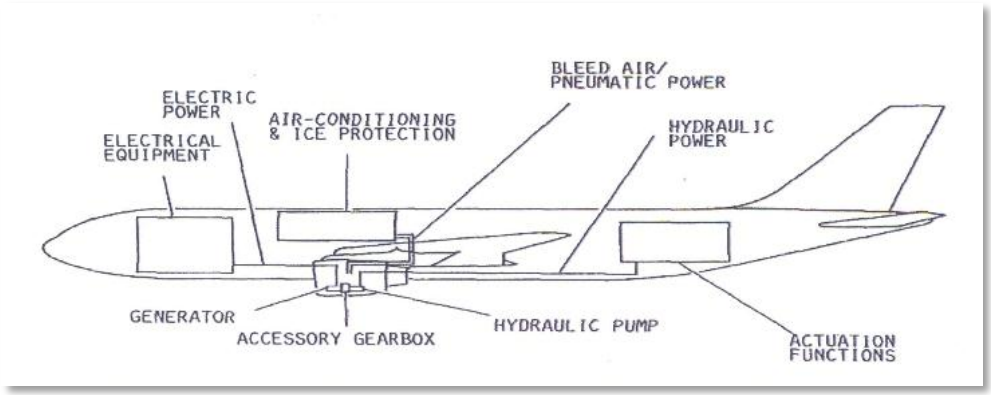

Figure 58 Conventional secondary power systems (Jones, 2002)

In the MEA concept electric power becomes the main way of distributing power to the majority of SPS. The expanded electric network now also includes the cabin pressurisation system, the ECS, the WAI, flight control actuation, landing gear, doors, fuel pumps and engine's ancillaries.

The motivation behind the more electric approach is the reduction of the operating costs, the decrease in fuel burn and last but not least the limitation of the environmental impact. In a MEA the hydraulic system is removed leading to

a reduced system weight and the simplification of the maintenance procedure. The reliability, vulnerability and redundancy of the aircraft are also improved without the presence of a complex hydraulic subsystem. Moreover, the elimination of the pneumatic power significantly improves the efficiency of the "bleedless" main engines. Much better cabin environment for both the passengers and the crew is possible in such an arrangement whilst the aircraft fuel burn is also reduced. Many heavy engine components such as bleed ducting, pre-coolers and ECS, which used to cool and pressurise engine offtake air, will no longer be needed (Provost, 2002). It is clear that a More Electric Engine (MEE) seems ideal in a configuration such as the MEA and many studies across Europe and worldwide have been focused on similar engines (Hirst et al., 2011). Figure 59 shows a comparison between a conventional and a MEA aircraft system.

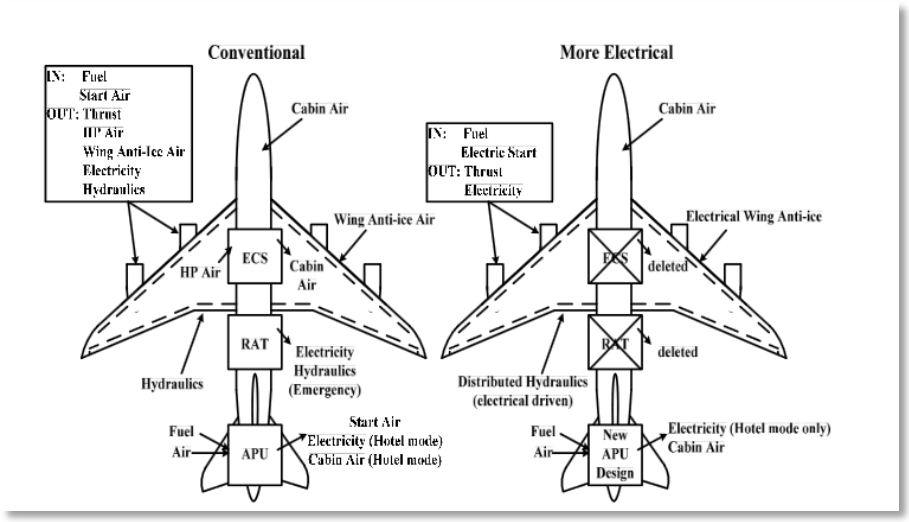

Figure 59 Comparison between conventional and MEA systems (Provost, 2002)

As indicated earlier three different individually optimised subsystems will be replaced by a common electrical system that will control the majority of SPS functions in a MEA. The main challenge is the optimisation of this electrical system, where a trade-off between AC and DC systems as well as voltage and current levels of the whole power network is necessary. In this sensitivity study the proposed superconducting concept that will later be described (5.2.2) could solve most of the issues presented in a MEA.

5.1.2 Airbus 380

The first aircraft with some more electric characteristics that entered the commercial service in 2007 was Airbus 380 (Figure 60). The main electric novelty in this aircraft can be found in the flight control architecture. Traditionally three hydraulic systems produce the required power for the flight controls. However, in the case of A380 the additional weight and complexity of the required hydraulic system due to the larger dimensions of the plane made this option particularly unattractive. Instead, hydraulic combined with electric flight control architecture was preferred. Hydraulic power is still the main power source for the flight controls, but many electrically powered actuators were used in order to save weight and reduce the complexity of the system.

Figure 60 Airbus 380 aircraft (image courtesy of Airbus)

Overall benefits such as improved maintainability and reliability as well as reduced weight and cost were considered significant innovations for the A380 aircraft. Safety margin was also increased due to the use of different power sources (Adams, 2001). .

A380 power system distribution can be seen in Figure 61. It consists of a primary 400VAC power bus (doubling the one of previous systems) with a variable frequency between 360-800 Hz. The Variable Frequency (VF) power generation enabled the reliable production of additional power with extra weight and maintenance costs benefits compared to previous systems (Adams, 2001).

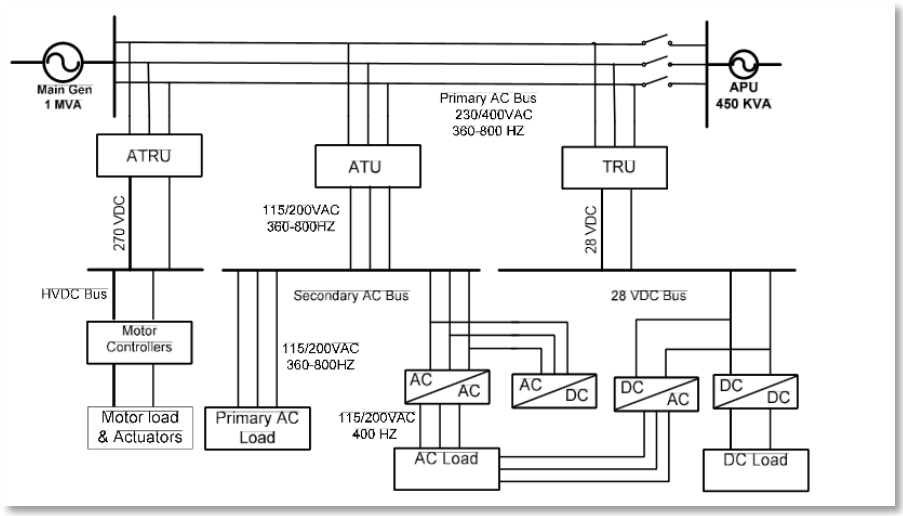

Figure 61 A380 Power distribution system (Abdel-Fadil, Eid and Abdel-Salam, 2013)

A similar power distribution system is also used to the second and most representative example of a MEA currently in service. This would be the Boeing 787 “Dreamliner” aircraft which will also be used as a reference for the upcoming proposed architectures.

5.1.3 Boeing “Dreamliner” 787

One of the most successful and popular aircraft nowadays, with more than a thousand orders already, is the Boeing Dreamliner 787 (Figure 62). This is the closest example to the MEA concept. The main difference between 787 and other more conventional models is its emphasis on electric systems, which are aiming to replace most of the existing pneumatic subsystems in the traditional architectures.

Figure 62 Boeing Dreamliner 787 Aircraft (image courtesy of Boeing)

The Boeing 787 is without any doubt on the cutting edge of airliner innovation, being considered by many experts as an “ahead of its time” aircraft (Thiétart, 2013). It was specifically designed to be 20% more fuel efficient than the 767 model, with its electrical system being the major component that made this aircraft so innovative. On the 787 the only remaining bleed system is the anti-icing system for the engine inlets. The whole system architecture is completely changed with systems such as the pneumatic engine, the APU start motors and load compressors, pre-coolers, various ducts and air control systems being just a few of the eliminated components of this novel aircraft (Hale, 2008). This transition from bleed-air to electrical power significantly reduces the complexity of the mechanical system in 787. The mechanical complexity of braking is also reduced by the use of electrical, instead of hydraulic, actuators. Leak and overheat detection systems for hydraulic fluid leaking are no longer needed, whilst failures of electric brake actuators could easily been handled without severe performance penalties. Overall, mechanical complexity has been reduced up to 50% compared to a 767. This development has reduced accordingly the maintenance costs, while the system’s reliability is increased with improved health monitoring and fault tolerance (Hale, 2008).

Figure 63 (Sinnet, 2008) presents a general overview of the electrical system in a 787 aircraft compared to a similar size conventional aircraft architecture. The Dreamliner’s architecture consists of six generators (2x 250kVA per engine and

2x225kVA for the APU) operating at 235 VAC. These generators are directly linked to the engines' gearboxes operating at a variable frequency of 360 to 800 Hz depending on the speed of the engine. The electrical system features one forward and one aft electrical/electronics (E/E) bay, as well as a number of remote power distribution units (RPDU) for supporting airplane electrical equipment. The system saves weight by reducing the size of power feeders. The system also features two forward 115 VAC external power receptacles to service the airplane on the ground without the APU and two aft 115 VAC external power receptacles for maintenance activities that require running the large-rated adjustable speed motors. All the aforementioned subsystems can be seen in Figure 63.

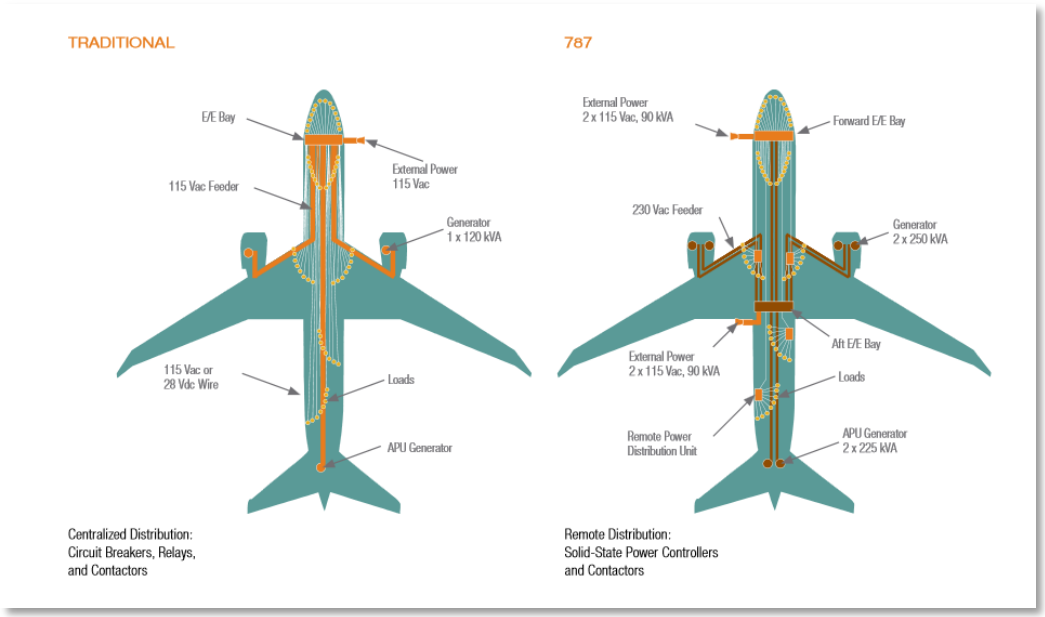

Figure 63 787's electrical system compared to traditional aircraft architecture

A more detailed description of the electric power network of this aircraft will follow in the next section since this system will be used as a reference for the proposed design architecture.

5.1.4 Going Beyond 787: Challenges and design options

The "Dreamliner" aircraft have showed some significant benefits derived from the MEA concept making it the most popular model nowadays. Ideally, this

approach would be extended to aircraft of different sizes whilst the extent of electrification will continue to grow. However, several technical reasons make the scaling of MEA approach problematic.

Electrical power systems present a number of disadvantages when applied to aircraft applications mainly due to the adding weight. Electrical machines and power electronics could be rather bulky especially for high power applications. In larger aircraft than the 787 the cables' size becomes another obstacle. In order to deal with the increased electric loads, there are two design paths: either to increase the current levels of the distribution network or to increase the system voltage levels. The former increases the weight and volume of the power cables whilst the latter suffers from the corona discharge effect. Another issue of high power networks is the efficiency of the whole network. In 787 there is an electric power load around 1MW. This number could be increased with the further electrification of future aircraft and/or with the use of MEA concept to longer range aircraft. The efficiency of a typical electrical system could be in the range of 97-98%. While this efficiency might seem high, it could give several hundreds of Watts heat losses which will create thermal management considerations. Finally the potentially higher currents of the system also increase the fault currents of the network. Further heavy protection and switching equipment will be necessary to deal with these fault arcs. The motivation behind this chapter is to address all these issues for next generation aircraft. The author believes that superconductivity could be the main enabler and problem solver for the majority of MEA challenges.

As described earlier (Chapter 4) fully superconducting machines will be significantly lighter and will occupy less space than the conventional equivalent machines. At the same time, superconducting cables' current capability is expected to eliminate the high currents constraint in a conventional power network. The derived fault currents will now be controlled by the SFCLs (Chapter 3), while no mechanical switching will be used and superconducting equipment will also be used both for switching and protection devices. Furthermore, the efficiency of the superconducting network is going to offer

further benefits. Both the machines and the cables are expected to be more than 99.9% efficient solving the thermal management problem. Regarding the power electronics, early studies have shown that operating them in cryogenic temperatures improve both the efficiency and the power density of these devices (Leong, 2011). A more detailed description of the performance of “cooled power electronics” will follow. It is clear that the use of a superconducting network will complicate the electrical system adding another important secondary system (i.e. cryogenic cooling system), but the author believes that the added complexity will be compensated by the numerous advantages that such a configuration could offer.

In the next subchapters, by using as a reference the 787 electrical system a comparison between the use of a superconducting and a conventional electrical network will be made. After that, different aircraft sizes and electric load requirements will be explored aiming on identifying the areas and limits where a superconducting solution could be proved beneficial in terms of weight.

5.2 Superconducting Electric Aircraft Approach

This chapter will start with a detailed description of the loads and components of the electrical power network of the 787 aircraft. Using as a baseline the exact same power network, a superconducting version of it will show any derived benefits and/or constraints. The conclusions of this comparison will be used for a broader sensitivity study where different electric power levels will be explored. This study will mainly focus on the weight of the secondary power network in both the conventional and the superconducting case. Four different cases will be explored based on the assumptions being made. There will be two cases for conventional networks (current and future values) and two for the superconducting versions (NASA and DEAP assumptions).

5.2.1 787 Electrical System Overview

A brief description of the secondary power system of the 787 model has already been presented. In this subchapter a more detailed representation of the electrical power network, which will include the secondary loads, the various

components (such as the electrical machines and the power electronics) and a general overview of the whole architecture will be described. The efficiency and weight of the main components will be given, whilst these values will also be used as a reference to the next subchapter where a superconducting version will be analysed.

Electric power demand in an aircraft changes depending on the flight phase. Typically, the Top of Climb (TOC) phase is the most demanding for the electrical power network but practically there are no significant differences in the total power demand during the whole flight mission (only the individual secondary loads change). More specifically, ice protection and hydraulics might require more power at lower altitudes, while ECS and cabin pressurization could be the dominant loads during cruise (Whyatt and Chick, 2012). However, the demanded electrical power drawn from the engine generators remains relatively constant throughout most of the flight mission. Figure 64 demonstrates the electrical power demand from the 787 main generators during major flight phases.

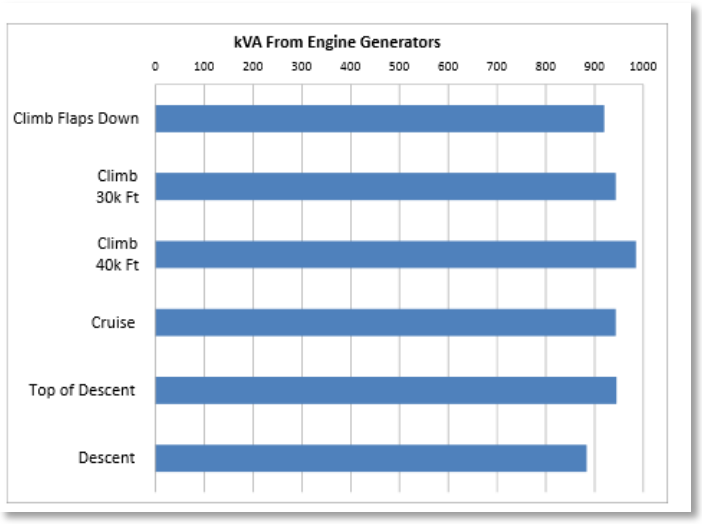

Figure 64 Total Electrical Power Demand during several flight stages of the 787 aircraft (Whyatt and Chick, 2012)

As it can be seen, the total electric load remains relatively constant at a value slightly lower than 1MW. For simplicity reasons, it has been assumed that a

constant power demand is kept during the whole flight mission and for the following analysis cruise is chosen as the design point.

Another important parameter of the upcoming analysis is the distribution of the several secondary loads. In 787's power network there are four different distribution buses: a main 235 VAC distribution line, a +/-270 VDC line which includes important loads such as the ECS, an 115 VAC 400 Hz bus for loads such as the ICS and finally a +/- 28 VDC transmission line for a smaller portion of secondary loads. It is clear that such a power network requires a significant number of power electronics. It is also a fact that the efficiencies of the electrical components in the 787 model are significantly improved compared to previous non-MEA aircraft (Whyatt and Chick, 2012). Advances in electronics and the use of Variable Frequency Starter Generators (VFSGs) are the main reason for the increased efficiency and power density of the electric components. The most important distributed loads and the efficiencies of the several components of the 787 case are summarised in the following diagram.

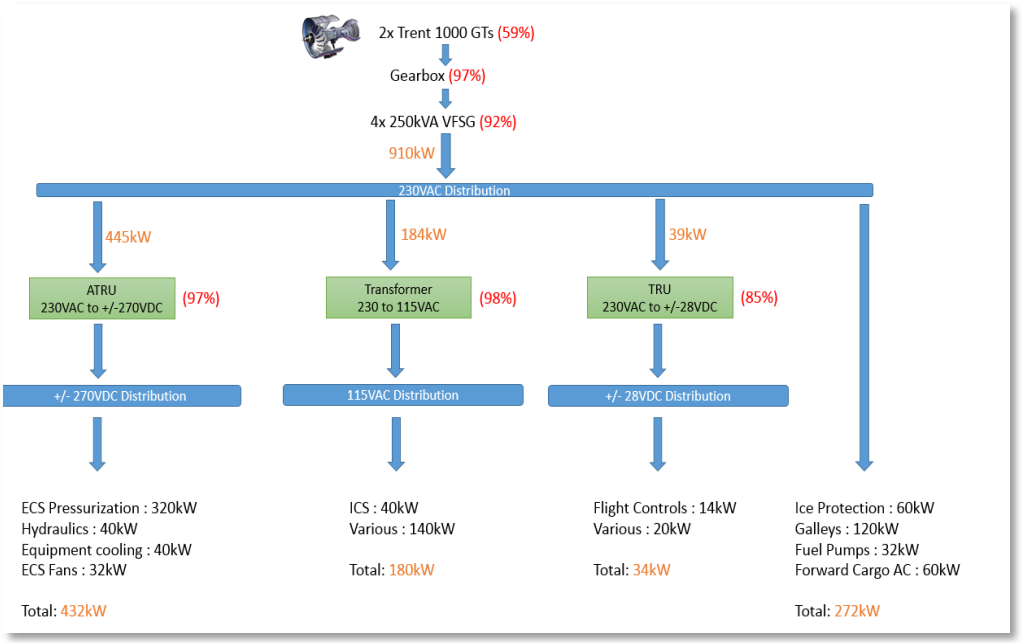

Figure 65 Electric loads and efficiencies diagram of the 787 electrical power network

The Boeing 787 aircraft is typically powered by the RR Trent 1000 engines. The Trent 1000 engine is a three shaft high bypass ratio turbofan that was specifically designed to power the 787 aircraft. It is a bleedless engine designed to fit the MEA concept requirements enabling increased levels of electric power to be transferred through the Intermediate Power (IP) spool. The engine has been up to 12% more fuel efficient than the previous model of Trent family (i.e. Trent 800) whilst there is 40% less emissions than the current legislation requirements (Ojha and Raghava, 2014). In this study a fuel efficiency of 59% is used (Whyatt and Chick, 2012).

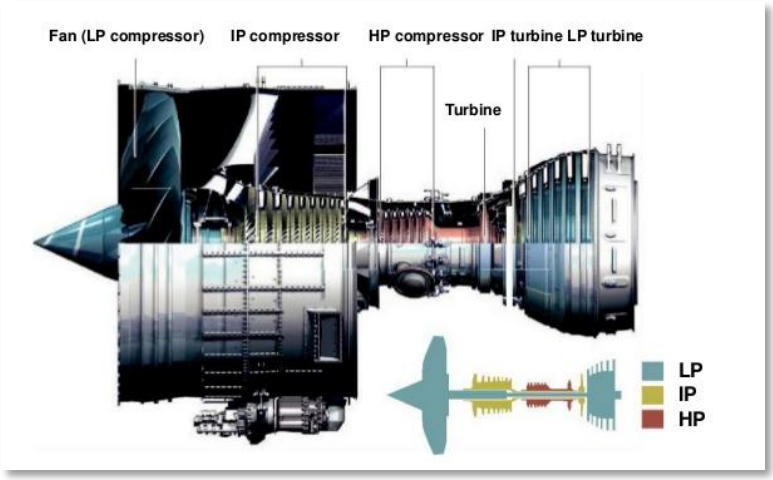

Figure 66 Trent 1000 three shaft configuration (Ojha and Raghava, 2014)

The electrical system generates the required power by extracting mechanical power from the engine accessory gearbox. In the 787 case two generator pads (2x250kVA) are provided-the term pad describes the part where a mechanical device mounts on the gearbox. Due to the higher frequency required from the VFSGs compared to the constant frequency 400 Hz AC power of the conventional integrated driver generators, the pad speed of the 787 accessory gearbox is higher (Moir and Seabridge, 2013). A typical efficiency of 97% was chosen in the sensitivity study of this chapter.

As it has already been mentioned, 787 incorporates four 250 kVA VFSGs (Figure 67) connected directly to the engine gearbox. The generated frequency of these machines depends each moment on the speed of the engine. On the

ground these machines-powered by the APU- are used to start the engine, whilst when the engines are running the VFSGs are the primary source of electric power (Boeing, 2013). This type of power generation is considered as simpler and more efficient since it does not involve the complex CVG (Constant Velocity Gearbox) or IDG (Integrated Drive Generator) subsystems (Moir and Seabridge, 2013). Hence, the reliability increases and the maintenance costs fall accordingly. The main benefit delivered by the implementation of this configuration is the elimination of the bleed system which was typically used to feed the ECS system. Heavy bleed air components are no longer present enabling significant weight savings, while the elimination of the energy losses of the bleed air system enhances the efficiency of the overall electrical power network. An overall efficiency of 92% was assumed for the purposes of this project.

Figure 67 Variable Frequency Starter Generator (VFSG) used in 787 (Clark, 2012)

One of the most important components of the network under investigation is the power electronics being used. Compared to Boeing 777 aircraft, the 787 involves the use of state-of-the-art highly efficient power converters manufactured by Thales Group (THALES, 2015a). More specifically, an Auto Transformer Rectifier Unit (ATRU) converts +/- 230 VAC to 270 VDC in an efficiency that reaches values over 97% (THALES, 2015b), while another transformer achieves 98% efficiency in converting power from +/- 230 VAC to +/- 115 VAC (THALES, 2015c). On the other hand, a less efficient Transformer Rectifier Unit (TRU) is being used to convert +/- 230 VAC to 28 VDC where

efficiency up to 85% can be reached. These high power conversion efficiencies had an important positive effect to the attractiveness of the MEA concept.

The main electrical loads of 787 are presented in Figure 65. Almost half of the required electrical power during cruise comes from the +/- 270 VDC distribution bus with the ECS load to be the most demanding load of the aircraft (~320 kW). Another relatively demanding load is the wing anti-icing system which in 787 requires in the order of 100kW of electrical power (Moir and Seabridge, 2013). Moreover, the electric motor pumps which replaced the traditional hydraulic engine driven pumps require around 400kW in total. The electrically powered air conditioning packs are located in the central sector of the aircraft, whilst the engine starter motors and the electric motor pumps are mounted in the left aft distribution panel of the plane. A more detailed representation of the 787 topology could be seen in Figure 68.

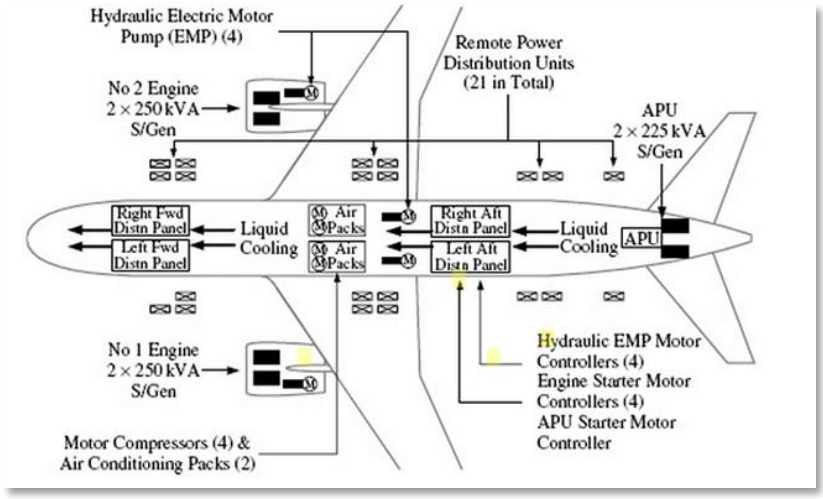

Figure 68 Electrical Power Distribution System in 787 (Moir and Seabridge, 2013)

5.2.2 Superconducting Version of 787 Electrical Power Network

In this subchapter a superconducting modification of the 787 electrical system will be investigated. This version will include fully superconducting electrical machines, cryo-cooled power electronics and a superconducting distribution system. The required weight and power for the cooling system necessary for this version will also be calculated using cryo-cooler models being developed during the DEAP project and were validated by several experts during this

project (Berg et al., 2015b). A brief description of the chosen cryo-cooler model and the main assumptions being made will be described in Appendix A.2. Two different superconducting versions will be explored: one based on the component efficiency and weight assumptions made during the DEAP program and another one based on the assumptions that NASA has used in their sensitivity studies for the TeDP concept.

- *Electrical machines*

The ‘Dreamliner’ aircraft, as it has already been described, incorporates four main VFSGs and two back-up APU generators. The benefits of the variable frequency system have been pointed out in the previous subchapter. Even with the improvements in efficiency that such a system introduced, fully superconducting machines will still be significantly more efficient.

With the current technology standards fully superconducting machines seem possible only with the use of MgB2 material for the stator of these machines. This leads to an operational temperature of 20K for the electrical machines. However, their efficiency even for the pessimistic DEAP case will reach a value of 99.9% which is more than 7% improvement than the currently used VFSGs. Their weight can be estimated using the models presented in Chapter 4.2. Note that the nominal power of these machines needs to be increased to compensate for the additional power requirements of the cooling system. Even with such an addition however both the weight and the efficiency of these machines will be enormously better.

NASA has claimed the feasibility of constructing fully superconducting machines which will be 99.97% efficient. This value has been used for the second case of this study. NASA has also investigated the possibility of using BSCCO as the main stator material for their machines. This was based on the fact that future improvements in HTS materials such as BSCCO and YBCO could allow the production of these materials in round wire form rather than in the tape form that are currently being produced. This will decrease their AC losses and will make them clear favourite candidates for the future fully superconducting machines.

For these initial stages of the study only the engine generators were assumed to be superconducting. However, a configuration where also the APU generators are fully superconducting should be considered.

- *Superconducting distributed transmission lines*

The distribution system of the 787 incorporates four different distribution buses each dedicated for a number of secondary loads. The benefits of using superconducting cables are numerous and have been pointed out in several studies (Jin, 2007). In this system, the improved efficiency and most importantly the significantly smaller conductor size is what makes their case more attractive. Scaling up the 787's electrical power network will have a direct effect on the overall electrical power load. Having cables capable of carrying high currents will both result to high losses and heavy transmission lines. Increasing the voltage level of the whole network will most probably create corona effect issues as it was pointed out earlier in this thesis. Superconducting cables can solve all these issues. Especially for the DC buses (i.e. +/-270 VDC and +/-28 VDC) superconductors show no ohmic resistance reducing the distribution loss and hence the thermal load of the network.

NASA has assumed typical losses on the order of 5 W/m of cable length (Xi et al., 2006). This assumption was also used during the DEAP program as a conservative prediction. Note that for all the superconducting cases MgB2 was chosen as the primary material being used for the transmission lines (T=20K), although there have already been applications where BSCCO transmission lines were operating efficiently (Maguire et al., 2007). However, the 20K was chosen as the most conservative case and as a way to keep the same operational temperature for the whole system. The latter will simplify the cooling system architecture and design/modelling process. For the weight predictions of this study assumptions used during DEAP project were also the baseline for this investigation. Power losses of 5 W/m and 8 W/m were assumed for DEAP and NASA cases respectively. Note that during the DEAP project even more optimistic predictions were claimed (Wright et al., 2015) but for the purposes of this study a more moderate approach was chosen.

Figure 69 Boeing 787 and Airbus A350 size (www.AviationExplorer.com, 2015)

Figure 69 demonstrates the dimensions of Boeing 787 compared to the newest Airbus model of similar range A350. In order to calculate the expected weight and losses of the distribution system, an approximation of 75m of cable for the main distribution lines was chosen based on the aircraft's length and the electrical power network architecture (Figure 68).

- Cryo-cooled Power Electronics

It is generally noted that certain semiconductor materials become increasingly efficient at cryogenic temperatures. It is true however that there have not been many published studies on the topic of using cryo-cooled power electronics in a superconducting system.

A DARPA (Defence Advanced Research Projects Agency) project focusing on a system-level theoretical study to investigate effects of using cryogenics in the power conversion components of a superconducting system was carried out between 2002 and 2005 (Hennessy, 2009). Some of the study's findings were the significant benefits with respect to energy dissipation, access to higher operating frequencies and improved reliability that many silicon-based power electronics at cryogenic temperatures presented.

Generally, exact weights for the converter, as well as for the rest of the components in such a configuration, are difficult to be estimated. Early in the design phase is really hard to find all the necessary information to reliably model the size of the various components. The simplest way to size components is by using their anticipated power to weight ratios. This is the method that was used for the weight estimation of cryo-cooled power converters. This seems appropriate for this research study since it is a common tactic especially for technologies of low TRL level, where conceptual designs are investigated.

To determine the proper power to weight ratios for the power converters, firstly the state of the art in high power low weight power electronics was examined. In the conventional case the THALES product specifications were used since they are the converters currently being used in the 787 aircraft. A power to weight ratio up to 5 kW/kg could be observed (THALES, 2015d), whilst efficiencies up to 98 % have also been achieved (Furmanczyk, 2009). Higher power density values have been achieved in non-aerospace applications. For example, manufacturers of inverters for electric cars have claimed current power to weight ratios up to 10 kW/kg with expectations of reaching values around 15 kW/kg in the near term future (Rogers, 2012). It is reasonable to expect similar values for the aerospace applications and this can be further enhanced with the additional benefits of a cryo-cooled case. Therefore, a conservative assumption of up to 20 kW/kg was used for the DEAP case. On the other hand, NASA has been relatively optimistic in terms of power density of cryo-cooled power electronics. A mass-specific power of 20 hp/lb (i.e. 32.8 kW/kg) and a 99.8% efficiency without cooling has been chosen as a target for the 2035 timeframe based on an unpublished report by MTECH Laboratories (Brown, 2011).

It is not clear yet which is the optimum cryogenic operational temperature for the various power electronic devices. The findings of a PhD thesis (Leong, 2011) focusing on the use of power devices below 100K to minimise the power losses can be summarised in the figure below. It can be seen that the optimum range of operation varies for the different semiconductor materials. It is also

clear that lower temperatures do not necessarily have a positive effect on the on-state behaviour of these materials with the example of Si n-channel and Si p-channel MOSFETs performing better in temperatures between 50 and 100K. However, for the purposes of this study an operational temperature of 20K was used for the pessimistic case, so that the worst case scenario in terms of cooling power demand to be explored. NASA has used as an operational temperature both the MgB2 case (i.e.20K) but also a more optimistic temperature of 111K without differing the power to weight ratio of these devices.

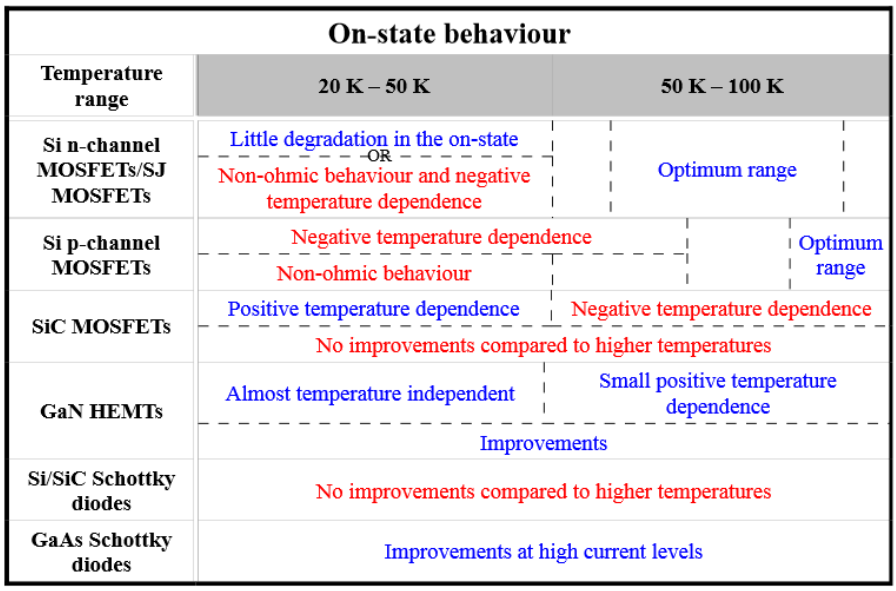

Figure 70 Tested behaviour of power electronic devices at cryogenic temperatures (Leong, 2011)

5.3 MEA and SEA Weight and Efficiency comparison studies (based on the Boeing 787 aircraft)

In this chapter a comparison between the weight and efficiency of the main components of the secondary power network of the 787 aircraft and a superconducting modification of it will be demonstrated. The components that were included in this study are the electrical machines, the power electronics, the main transmission lines and the required cooling system of these configurations.

5.3.1 Basic Assumptions

Four different cases were investigated based on the optimism of the assumptions being used. As a first case the reference aircraft (i.e. Boeing 787) was used with the minimum assumptions possible since a lot of information for the actual products was found in the literature. Moderate future predictions for the power density and efficiency of the conventional 787 secondary power system's components were the baseline for the second case under investigation. The other two cases are related to the superconducting proposed architecture. DEAP project conservative estimates were used for the first superconducting case, whilst NASA's optimistic predictions for the 2035 timeframe were used as the second superconducting case.

It is important to summarise the assumptions being made for each case separately concerning the power density, efficiency and operating temperature of the various components. The latter two are the decisive parameters for the weight estimation of the cooling system in the superconducting cases. Following the structure of the previous subchapter first of all each main component will be explored and compared separately and then a combined comparison study will conclude the first stage of this study.

- VFSGs

In this study only the weight and efficiency of the VFSGs was investigated without taking into account the APU electrical machines. For the conventional case the total weight of the four VFSGs was found to be around 363kg with 92% efficiency. For the conventional future 787 type of aircraft high speed electrical machines with power density of 10 kW/kg and an efficiency around 98% was assumed based on a study that Airbus and AGI had carried out in terms of radical aircraft concepts for a technology level beyond 2030 (Barraud et al., 2015). In the superconducting cases a different rating of these machines was necessary to counter for the extra power needed to drive the cryo-coolers of these architectures. A rating of 350 kW was chosen securing 400 kW power available to drive the cooling system. The cooling power demand was estimated to be around 220 kW for the DEAP case and around 70 kW for the NASA

estimates, but a conservative approach was chosen to secure the reliability of the results. This cooling power demand was also calculated using the double stage reverse Brayton Cryo-coolers' models developed for this study (A.2). The weight of the superconducting electrical machines was calculated using the models presented in 4.2.4 for the DEAP superconducting case, whilst for the NASA case the torque density of the MgB2 superconducting motor of the N3-X BWB aircraft (Brown, 2011) was used. Table 12 summarises all these estimations:

Table 12 VFSGs key variables values for each case

Variable	Units	787 Current	787 Future	Superconducting Case (DEAP)	Superconducting Case (NASA)
Rating	kW	250	250	350	350
Unit Weight	kg	90.75	25	19.78	9.16
Total Weight	kg	363	100	79.12	36.64
Efficiency	%	92	98	99.9	99.97
Operational Temperature	K	Ambient	Ambient	20	20

- Power Electronics

The power electronics weight estimation is a complicated procedure. All the main assumptions for the power converters of the system were mentioned in the subchapter 5.2.2. However, it should be noted that these assumptions should stand only for the ATRUs (+/- 230 VAC to 270 VDC) and the transformers (+/- 230 VAC to +/- 115 VAC) of these electrical power networks. In the conventional case, the TRU (+/- 230 VAC to 28 VDC) has a significantly lower efficiency than the other two converters (i.e. 85% instead of 98%) and a power density of only 0.65 kW/kg instead of 5 kW/kg . Hence, an efficiency of 90% was assumed for the 787 future and the DEAP superconducting cases,

whilst efficiency around 95% was used in the NASA case. Concerning the power to weight ratios of the TRUs in each case, values three times lower than the maximum expected power densities were used as an approximation.

Table 13 Power electronics key variables values for each case

Variable	Units	787 Current	787 Future	Superconducting Case (DEAP)	Superconducting Case (NASA)
Power to Weight Ratio	kW/kg	Up to 5	Up to 15	Up to 20	Up to 33
Total Weight	kg	243	48.79	36.7	21.84
Efficiency	%	Up to 98	Up to 99	Up to 99	Up to 99.8
Operational Temperature	K	Ambient	Ambient	20	20

- Cables

The weight of the main cable span of the 787 aircraft was not available in the literature. Instead the capabilities of the conventional cabling and the resulted mass were based on existing manufacturer's data; this data meets current copper cable sizing practices. The maximum current density of a copper or aluminium wire is limited to 4 A/mm^2 (Xi et al., 2006). Based on that value the required cross sectional area of the 787's main power cables was estimated to be 1086 mm^2. Data for copper cables of such a wide cross sectional area were not available. Instead, it was possible to develop a relationship that links the cross sectional area of the copper cable with its weight per meter.

$$Copper\ Cable\ Weight\ = 0.0129 * Cross\ sectional\ area^{0.9593} \quad kg/m \qquad \textbf{(5-1)}$$

This relationship (5-1) corresponds to PVC insulated stranded copper cables and is based on data available in (Keison, 2014) and are presented in Figure

71. PVC insulated cables have been approved for aircraft use by the civil aviation authority ((CAA), 2002).

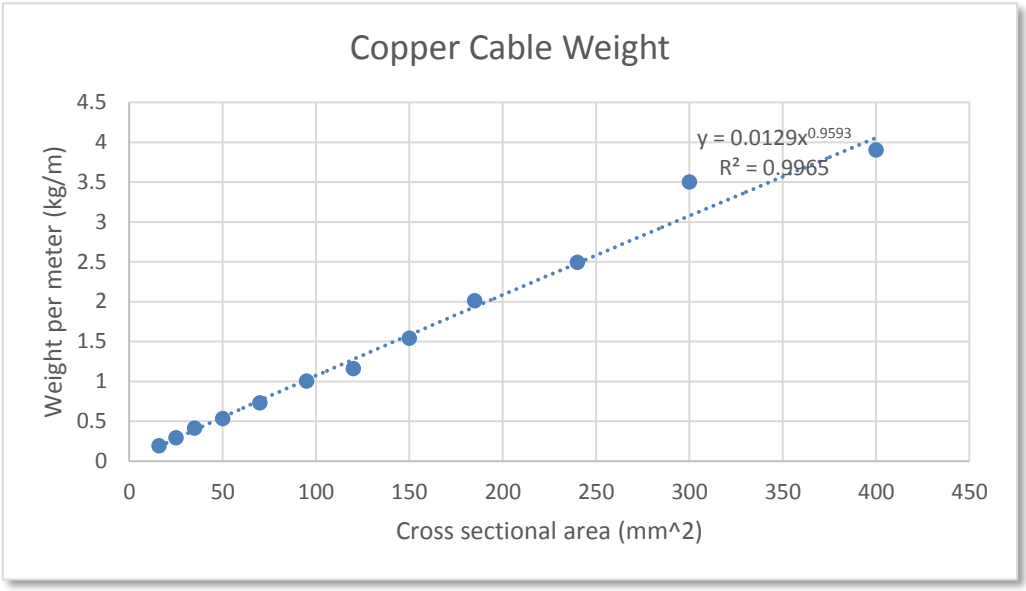

Figure 71 Weight per meter of conventional copper cable with PVC insulation

In the future technology estimations a 10% improvement was assumed. This conservative assumption was based on the fact that only improvements in insulation could be achieved in this type of cable and typically the conductor weight is what sizes the cables.

For the superconducting cases a 5 kg/m weight per unit length was assumed in the DEAP case (Wright et al., 2015) , whilst NASA based on a study by Xi (Xi et al., 2006) in their initial estimations assumed a value of 9.2 kg/m for the weight of the main transmission lines. However, a weight approximation value of 500 A/kg/m has been used in a later NASA study (Armstrong et al., 2012) and that is the value also being used in this study. It should be noted that in their initial assumptions NASA was using as a reference a High Voltage superconducting cable that requires a substantial level of insulation and this is not the case with the power system under investigation. The heat losses of a superconducting cable were assumed to be 5 W/m for both superconducting cases (Brown, 2011). In the conventional cases these losses were assumed negligible

compared to the losses of the rest of the components and hence no assumption was made.

Table 14 Main Cable line key variables values for each case

Variable	Units	787 Current	787 Future	Superconducting Case (DEAP)	Superconducting Case (NASA)
Weight per unit length	kg/m	10.55	9.5	5	8
Total Weight	kg	791.25	712.5	375	600
Losses	W/m	-	-	5	5
Total Length	m	75	75	75	75
Operational Temperature	K	Ambient	Ambient	20	20

- Cooling system

The cooling system has been characterised by many as the main drawback of having a SPN in an aircraft. Complexity, reliability, and mainly extra weight are some of the attributes that such a subsystem will add to the network. In the conventional system there is also a cooling mechanism typically consisted of a fully integrated package of pump, motor, controller, filter, and reservoir. It is not an easy task to predict the weight of this system and since no data was available in the literature for the 787 aircraft, an approximation was made; this would be that the conventional cooling system weighs 30% of the overall weight of the cooled components (Malkin and Pagonis, 2015). The same goes for both conventional cases with the 787's future case being more beneficial due to the expected reduced weight of the components.

In a SPN, different options for the cooling system have already been described (Chapter 2.3). In this study the option of cryo-coolers has been selected based on the fact that extensive cryo-cooler studies have been carried out during the

DEAP program. The models that have been developed to estimate the weight and the cooling power demand of the cooling system are described in detail in Appendix A.2. For both superconducting cases Reverse Brayton cryo-coolers were used (Palmer and Shehab, 2015). The same type of cryo-coolers was also assumed during the NASA studies (Felder et al., 2011a) . In this study double stage coolers were chosen for the configurations under investigation. Compressor polytropic efficiencies of 90% and turbine polytropic efficiencies of 92% were considered as realistic assumptions for these models. Superconducting motors were also used instead of conventional machines, whilst a 5% drop in every heat exchanger of the system was also assumed. These were the main assumptions of the models, but a full list of the parameters being used can be found in Appendix A.2.

5.3.2 Results and Comments

Based on the aforementioned assumptions a weight comparison between the different cases was carried out. These cases were considered as the most representative to determine the feasibility and attractiveness of the SEA concept. Both the DEAP program and NASA could be considered as reliable references. The former investigated in depth the aspects of having a SPN in a HEDP aircraft, whilst NASA is consistently working on the next generation aircraft where superconductivity and all its derivatives are holding a significant share on their research agenda. In regards to the conventional cases, it seemed reasonable to use the current MEA aircraft in service (i.e. Boeing 787) as the first reference since most of the system's weight could be accurately found. However, in order to make a more representative comparison it was necessary to estimate the weight units by expressing the density (in terms of power, torque, current or energy) of each component of the power network in the timeframe that this future aircraft could move into production. Hence, the second conventional case predicts the weight of the components for the 2035 timeframe. Figure 72 summarises the results of the first stage of this study:

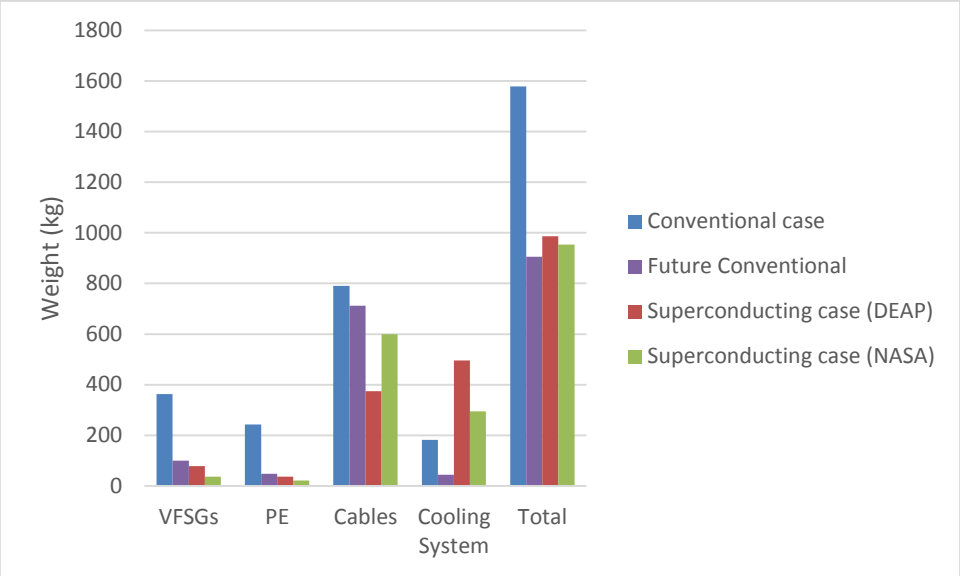

Figure 72 Weight Comparison between different 787 MEA and SEA configurations

As it was expected the superconducting electrical machines were found to weigh almost five times less-with the DEAP estimates-than the current VFSGs in use, whilst NASA estimates give more than an order of magnitude lighter machines. The 2035 estimates for conventional electrical machines however compensate somehow that gap by predicting rather competitive machines in terms of weight.

A similar trend can be noticed in the case of power electronics. The expected reduction in the size of the passive parts of the cryo-cooled power converters will give significant weight benefits compare to the state of the art products. More specifically, the power density of these components is expected to be three (DEAP prediction) to ten (NASA estimate) times better in the superconducting cases. However, once again, anticipated improvements in the current power electronics' technology could produce competitive products for the 2035 timeline.

In regards to the cables' weight in these configurations there are a lot of remarks that need to be made before commenting on the results. First of all, the presence of a SPN would most probably change the voltage and current levels of the whole system. This will have a direct effect on the weight of all the

components, while in the case of cables this effect will probably be more enhanced. In this study, for the conventional examples the main transmission lines' weight was calculated by using current aerospace manufacturer datasheets and assuming a 10% improvement for the future estimates. This improvement rate although seem moderate is only related to the insulation technology development and not the conductor's weight which is not expected to alter. Contrary to the rest of their estimates NASA has been relatively conservative on the predicted current density of superconducting cable. This is partly due to the different nature of application their reference cables are built for. The high voltage transmission line that has been used as a reference (Xi et al., 2006) will require significant amount of insulation with capability of withstanding voltages of well over 100kV, whilst in the 787 case a low voltage has been chosen and there will be no need for such a thick insulation layer. Moreover, during the DEAP project even more optimistic assumptions were made regarding the weight per unit length of MgB2 cables reaching values even close to 1kg/m (Wright et al., 2015). Nevertheless, for the purposes of this study a more conservative estimation was chosen. It is important to note that in case that these values could be reached, this will result in an important extra weight benefit. Taking all these limitations under consideration it can be seen that there is an almost 200kg (current aircraft) to almost 100kg (future conventional) benefit on the cables' weight based on the NASA predictions. On the other hand, the DEAP estimates give a more significant weight reduction over both conventional cases which could be highlighted even more if the optimistic assumptions were used.

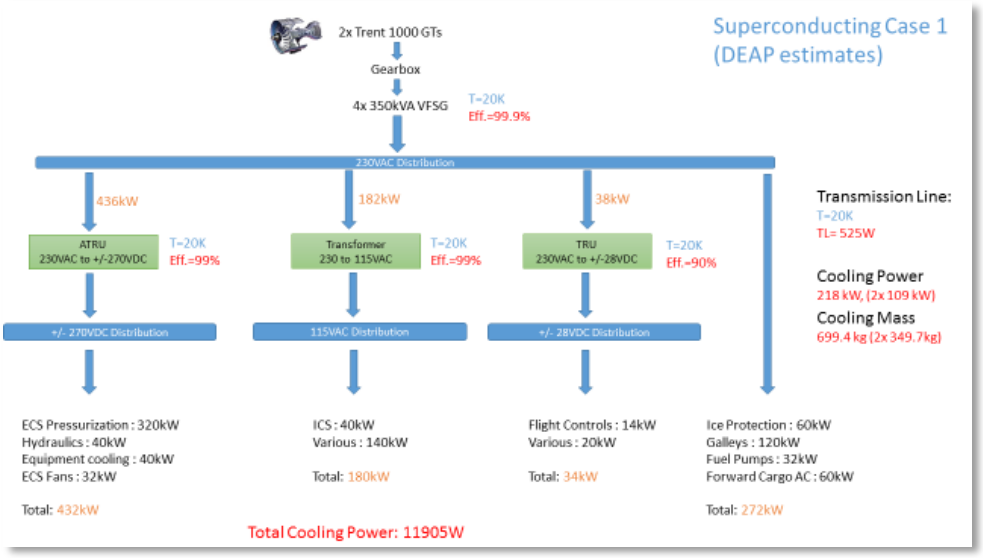

Figure 73 Electric loads and efficiencies diagram of the 787 electrical power network in SEA case (DEAP estimates)

The weight of the required cooling system has been considered as a main barrier for the superconducting cases. The results of this study however do not exactly confirm this statement. It is indeed a heavy subsystem but in the example of the existing 787 aircraft and based on the NASA efficiency figures (Figure 74), the overall weight of the required cryo-coolers will be less than two times that of the conventional cooling system. The difference becomes more significant if the DEAP efficiency estimates are considered (Figure 73) and even more enhanced when a comparison with the future conventional case is made. It should be noted however that the most conservative estimates regarding the operational temperature were chosen. An operational temperature of 20K was chosen for the whole system. This might be the case at least for the electrical machines which at this stage it seems inevitable to use MgB2 material for their stator. However, the power electronics could be operated in higher-still “cryogenic”-temperatures. In fact, as it was described in section 5.2.2, most of the power converters might operate better in temperatures close to 100K. This will significantly decrease the amount of required cooling power. Furthermore, superconducting transmission lines using BSSCO as their main material with an operating temperature around 90K might be used. With future improvements, BSSCO cables could be the ideal option for airborne applications mainly due to

their increased critical temperature. The mass of the cryo-coolers, if these higher operational temperatures for the power converters and the main cable span are chosen, will be significantly lighter. In this study, both for reasons of simplicity and conservatism, a uniform operational temperature of 20K was selected.

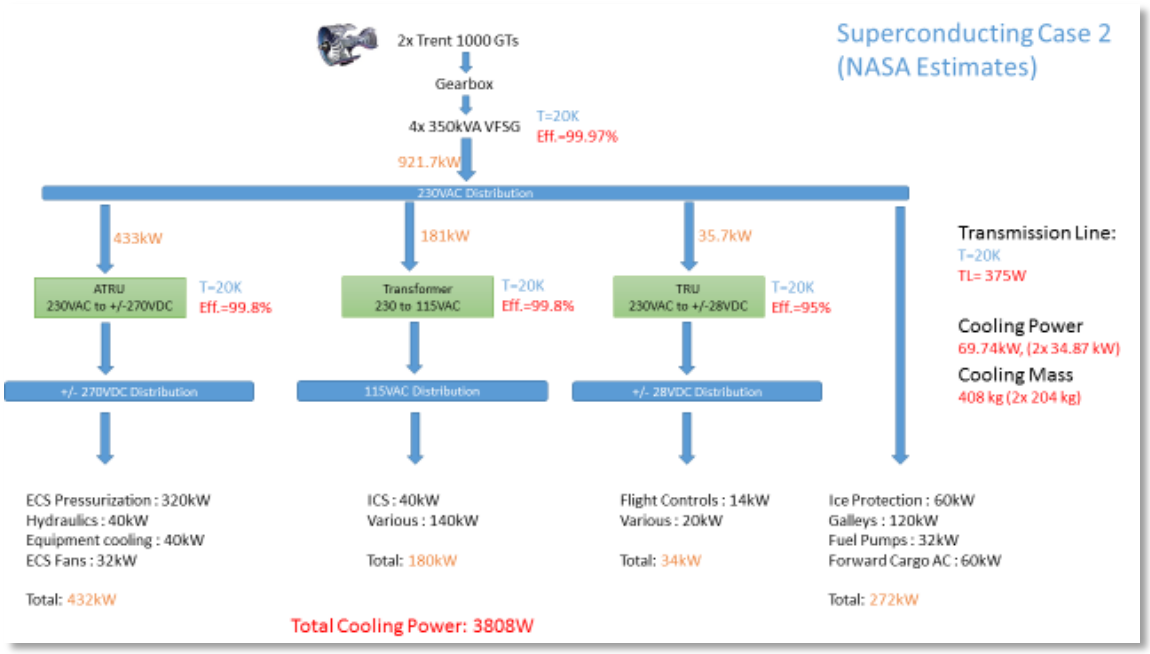

Figure 74 Electric loads and efficiencies diagram of the 787 electrical power network in SEA case (NASA estimates)

To sum up, it can be seen that SEA compared to the current MEA example of 787 aircraft would be a lighter and more efficient option both using the more conservative estimates of DEAP program but also with the optimistic NASA predictions. On the other hand, if these two superconducting versions of 787 are compared to the possible future version of a 787 type of aircraft there is no weight benefit derived from the use of superconducting components but instead around extra 50kg (NASA estimates) to 80kg (DEAP estimates) will be added to the secondary power network of this aircraft.

In efficiency terms however there is still a clear benefit of using a SPN. According to NASA efficiencies up to 99.7% can be reached in the electrical power network of such an aircraft. This number goes down to 98.9% if the

DEAP estimates are used instead. Even this efficiency however is almost 2% better than the one derived by using the optimistic future expectations for the conventional room temperature components. Although this difference might seem insignificant, it can result in excessive heat loads especially in the case that the required electric load of these aircraft increases. A 90% efficiency, which is currently assumed for the 787 aircraft in service, is a value that cannot be considered competitive with all the other design options for the 2035 timeframe.

Apart from the efficiency gains there is another important advantage of using superconducting components in the system under investigation. There are reasons to believe that the implementation of the MEA approach to aircraft of different sizes has been blocked by the fact that the scalability of the electrical components of the network is not proportional to the one of the aircraft itself. Power electronics and transmission line cables do not scale accordingly to the aircraft size and this fact complicates the design optimisation of such an aircraft. The next section (5.4) will investigate how the weight of the main components will change depending on the electric power load demand. The cases of increased electric power demand will correspond to either larger aircraft or/and to further electrified versions of future civil MEA.

5.4 SEA Sensitivity/Scalability Studies

In this section the SEA study will be extended to different aircraft sizes. State of the art aircraft will be used as references. The total required electric load for each aircraft will be decided based on a factor that will determine the electric power demand depending on the number of passengers that each aircraft can carry. More specifically, the value of this factor is derived from the 787 model where 242 passengers required 1MW of electric power. Hence, for each case the total electric power demand was estimated using the following equation:

$$Total\ Electric\ Load = PAX * Electric\ Load_{factor} \quad \textbf{(5-2)}$$

Where PAX is the number of passenger of each aircraft and $Electric\ Load_{factor}$ equals to 4.132 kW/passenger based on the 787 aircraft requirements.

This is just a simplistic method to estimate the potential electric load of different aircraft assuming that similar secondary power network architectures will be used in each case. This means that the same four different buses are assumed to be part of the secondary power network of these aircraft. Although this might not seem realistic since each aircraft design could be optimised differently it is reasonable to make such an assumption in this early stage sensitivity study.

5.4.1 Reference Aircraft Description

Five different aircraft were chosen as representative examples of different sizes/ranges commercial airplanes examples. In the near future Boeing is looking to release updated versions of their 737 and 777 models (Scott, 2014). The most recent Airbus aircraft are A350 and A380 models, whilst Bombardier in 2008 put into production their regional commercial airplane CRJ-1000. In this subsection a brief description of each reference aircraft will follow (www.airlines-inform.com, 2012) :

- Boeing 737

The Boeing 737 family is the most commercially successful family with more than 4000 units sold. The latest model of this family is the 737-900. The following table summarises its main characteristics:

Table 15 BOEING 737-900 Main characteristics

Variable	Units	Value
Range	km	5080
Passengers	-	189
Engines	lb	2*27300
Maximum speed	km/h	1000
Expected Electric Load Demand	**kW**	**780**

- Boeing 777

777 is a long range aircraft that entered production in 1995 and it flies to the largest international airports. The following table summarises the main attributes of the 777-300 which held its first flight in 1997:

Table 16 BOEING 777-300 Main characteristics

Variable	Units	Value
Range	km	11000
Passengers	-	550
Engines	lb	2*115000
Maximum speed	km/h	945
Expected Electric Load Demand	**kW**	**2275**

- Airbus A350

A350 is the newest aircraft in service, entering on 15 January 2015 with Qatar Airways. It is a long range aircraft that was developed to succeed the A330 and

A340 and compete with Boeing's 787 and 777 models. Its main characteristics can be seen in Table 17:

Table 17 A350 Main characteristics

Variable	**Units**	**Value**
Range	km	14800
Passengers	-	475
Engines	lb	2*95000
Maximum speed	km/h	945
Expected Electric Load Demand	**kW**	**1965**

- Airbus A380

A380 is the largest passengers' aircraft in the world that entered the commercial service in 2007. A more detailed description of this model has already been made (5.1.2) but the more important attributes in regards to this study can be found in the table that follows:

Table 18 A380 Main characteristics

Variable	**Units**	**Value**
Range	km	15000
Passengers	-	700
Engines	lb	4*70000
Maximum speed	km/h	1070
Expected Electric Load Demand	**kW**	**2895**

- Bombardier CRJ-1000

As a final reference a Bombardier's aircraft was chosen. CRJ-1000 is a regional airliner and it will be used as an example of minimum electric power demand in this study. Table 19 gives the main characteristics of such an aircraft:

Table 19 CRJ-1000 Main characteristics

Variable	**Units**	**Value**
Range	km	2760
Passengers	-	100
Engines	lb	2*13630
Maximum speed	km/h	880
Expected Electric Load Demand	**kW**	**415**

The difficulties of designing an all new aircraft have pushed the biggest airliners today to focus on updates on their existing products. Both Boeing and Airbus have already announced their perspective passenger jets. The former is planning to release 737Max and 777X as improved models of the already existing family, whilst Airbus is launching their Airbus 330neo as the next aircraft to be released after the recent A350 delivery to service (Shankland, 2014). Therefore, the choice of all the aforementioned reference aircraft models was based on the future trends of the top aircraft makers as well as on the fact that a wide range of aircraft sizes was necessary to be investigated.

5.4.2 MEA and SEA Simulink models overview

This sensitivity study was then extended for different aircraft sizes and electric loads with the use of Simulink models for each case separately. Figure 75 demonstrates the models being used for the conventional MEA cases. There are four main subsystems dedicated to the four components under investigation

(i.e. machines, power electronics, cables, and cooling system). The main inputs and outputs of this model can be found on the following table.

Table 20 Main inputs and outputs of MEA's power network Simulink model

Inputs	Units	Outputs	Units
Total Electric Power Load	W	Total VFSGs' weight	kg
Number of Engines	–	Total VFSGs' thermal load	W
VFSG's efficiency	%	Total P.E.s' weight	kg
VFSG's power density	kW/kg	Total P.E.s' thermal load	W
P.E.'s power factor	–	Cooling System's weight	kg
P.E.'s power density	kW/kg	Cables' weight	kg
P.E.'S efficiency	%	Total system's weight	kg
Cooling Weight Factor	–	Total system's thermal load	W
Cable Length	m		
Nominal System's Voltage	V		
Maximum Current Capability	A/mm^2		

The total electric power load and the number of engines in each aircraft can be found in 5.4.1. Depending on the number of engines, the number of VFSGs (two per engine) and consequently the power rating of each machine could be estimated. Using the assumed values of VFSGs' power densities and efficiencies the weight and total thermal load of the machines could be estimated. In this study, the total electric power demand was distributed to the several buses in accordance to the current conventional 787 case. Hence, 48.9% of the total load was delivered in the +/- 270VDC line, 20.22% is transmitted to the 115VAC bus bar, only 4.28% is used to satisfy the +/- 28VDC loads, whilst the rest 26.6% of the total electric power available is used to power the remaining 230VAC secondary loads. These power factors were used as inputs to the power electronics subsystem in order the required power rating of

each converter to be predicted. As it was stated in previous sections, a cooling weight factor of 0.3 was assumed in order to estimate the conventional cooling system's weight. Furthermore, the main transmission line's total length for each aircraft (5.4.1) combined with the system's nominal voltage (230VAC), and the maximum current capability of copper wires (4 A/mm^2) were the transmission lines subsystem inputs. Finally, combining the outputs of each subsystem, the MEA's power system total weight and thermal load could be estimated for both conventional cases (current and future technology).

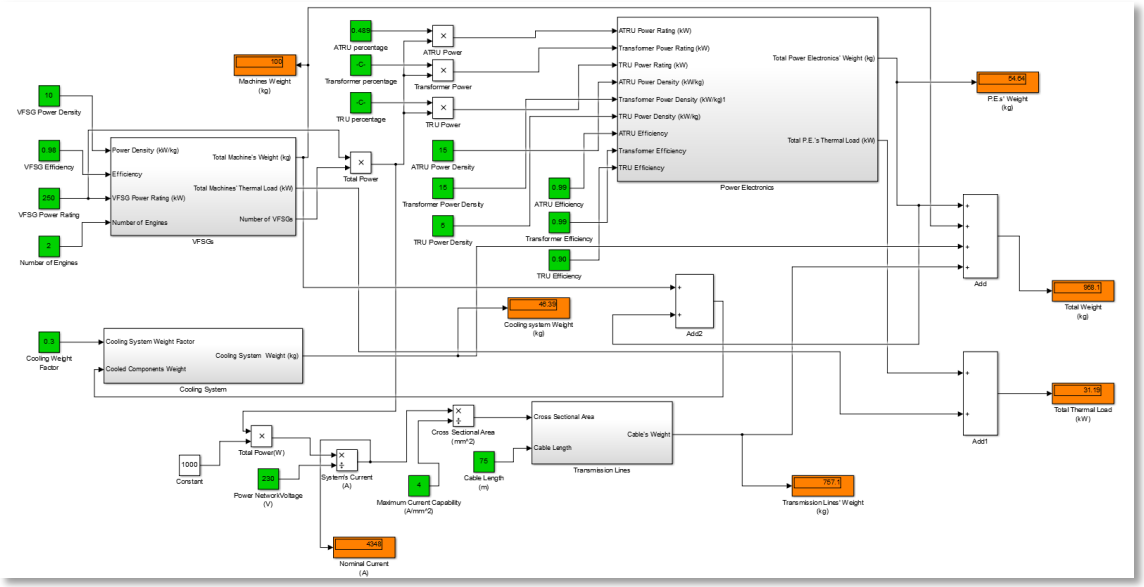

Figure 75 MEA's Electric Power Network Simulink Model

For the superconducting cases a more complicated power network model has been developed (Figure 76). The superconducting electrical machine and the cryo-cooler models have been extensively analysed in 4.2 and Appendix A.2 respectively. The power electronics' subsystem is the same as in the conventional cases, whilst the main transmission lines' weight and total thermal load is being calculated by using simple weight and losses per unit length values (presented in 5.3.1). The only difference between the models of the superconducting cases is in the way the machines' weight is calculated. In the NASA cases a simple torque density value is being used to estimate the machine's weight instead of the complicated fully superconducting machine models used in the DEAP case. The majority of inputs and outputs of SEA

power network model are the same as the ones in Table 20. However, there are a significant number of additional inputs due to the complex superconducting VFSGs and Cryo-cooler models. The inputs of these subsystems can be found in the respective chapters where they were presented (i.e. 4.2.4 and Appendix A.2).

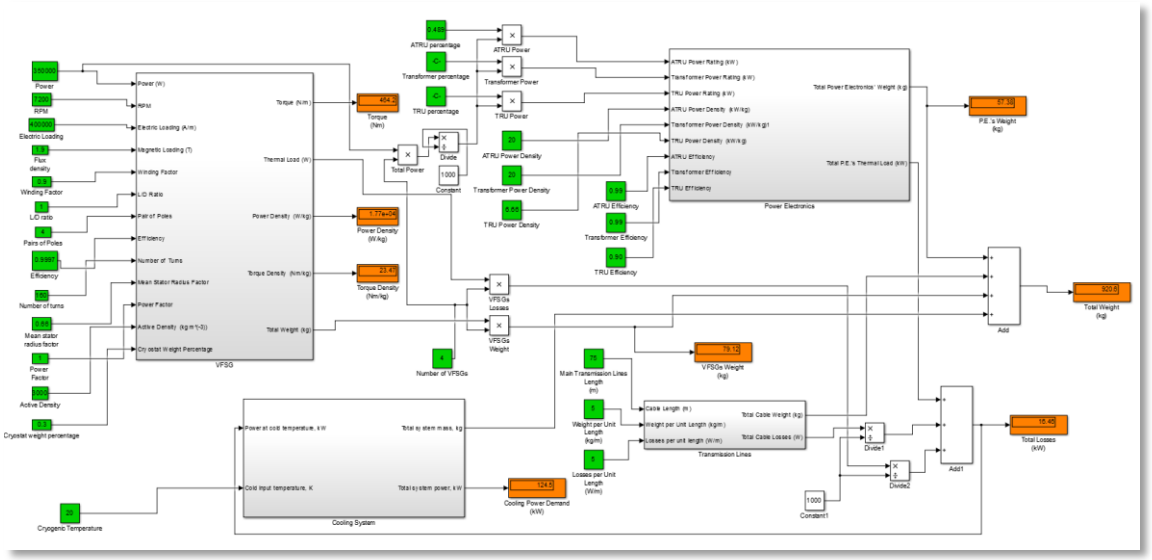

Figure 76 SEA's Electric Power Network Simulink Model (Superconducting DEAP case)

5.4.3 Weight Trends in reference aircraft

The next step for this study will be the comparison of the weight of the various components for each reference aircraft using the same four different versions of secondary power networks used in 5.3 and the Simulink models presented in the previous section. The various components will be investigated separately, whilst a total system's weight comparison will follow.

- Electrical machines

The weight of the VFSGs in each case was calculated by using the majority of the assumptions presented in section 5.3.1. Depending on the electric power requirements of each aircraft the nominal power rating of the machines in each case was calculated. In the superconducting cases the machines were adequately oversized in order to deal with the cryo-coolers power demand.

Moreover, two generators per engine were assumed in every reference aircraft. In the current technology case a torque density of 3.65 N*m/kg was assumed based on the VFSGs that are used in the 787 aircraft. In order to simplify this study all the generators were assumed to have the same variable frequency as the initial reference aircraft (i.e. 360-800 Hz). The following figure presents the total weight of the electrical machines for each reference aircraft in all four different versions.

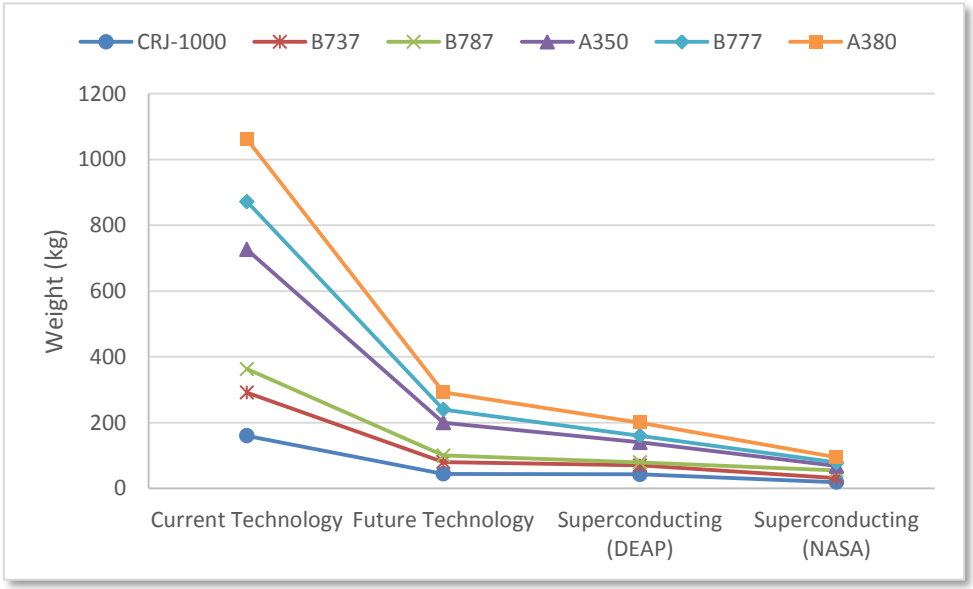

Figure 77 VFSGs' weight for each reference aircraft in all four different versions

As it was expected the total weight of the electrical machines increases as the electrical power demand rises. The benefit of using superconducting machines is particularly highlighted for larger aircraft-such as the A380, B777, and A350-where the machines in the superconducting versions are anticipated to be over an order of magnitude lighter (with NASA estimates) than the ones currently used in 787. Three times lighter machines (NASA values) are expected in comparison to the optimistic estimates for the future technology in the long range type of aircraft. The moderate estimates of the DEAP program slightly decrease the weight benefit compared to the current technology figures; however there is still an important difference in these two versions. On the other hand, there is hardly any benefit compared to the future trends especially for the short range aircraft (i.e. CRJ-1000 and B737).

To sum up, the advantage of using superconducting machines in terms of weight savings in undeniable compared to the current technology being used in such an advanced aircraft as “The Dreamliner” example. However, if the relatively optimistic predictions for future technology of the electrical machines will be verified then the resulted benefit will be significantly limited. It is important to note that for the future technology a power density factor is used due to available data in the literature. However, this is not a common method for calculating the weight of the electrical machines, since the torque is what typically sizes these machines. In this study the frequency-and hence the rotational speed-of the machines was held constant in each case so that the torque and power density will change accordingly.

- Power Electronics

The same assumptions as the ones summarised in Table 13 were used for the weight calculation of the main power converters necessary in each reference aircraft. As it was previously stated the same architecture was assumed for each aircraft although this does not correspond to reality at the moment. However, it seems reasonable that if a more electric approach will be followed in all the aircraft under investigation a similar electrical power network to the existing one of 787 will be most probably used. In any case, the majority of the electric load produced by the VFSGs will have to be converted to different voltage levels to be useable for the secondary loads of the aircraft. Figure 78 demonstrates the Simulink subsystem for the weight and thermal load calculation of the power electronics in the MEA and SEA concepts. The inputs of this subsystem can be found in the overview Simulink models previously presented in 5.4.2 and differ based on the total electric load of the aircraft, as well as its nature (conventional or superconducting).

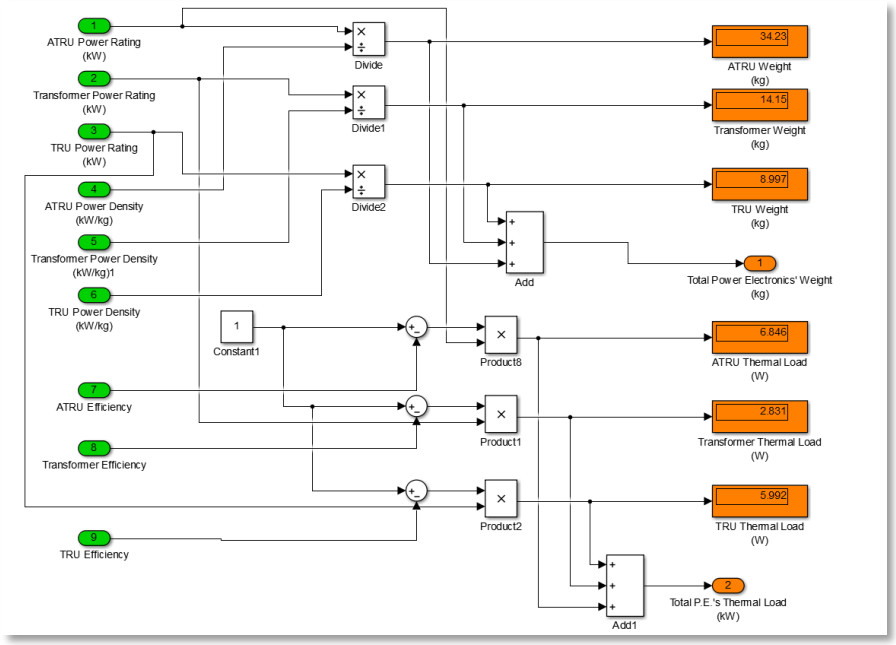

Figure 78 Power Electronics' Simulink Model

The results of the power electronics' weight study are presented in the following figure:

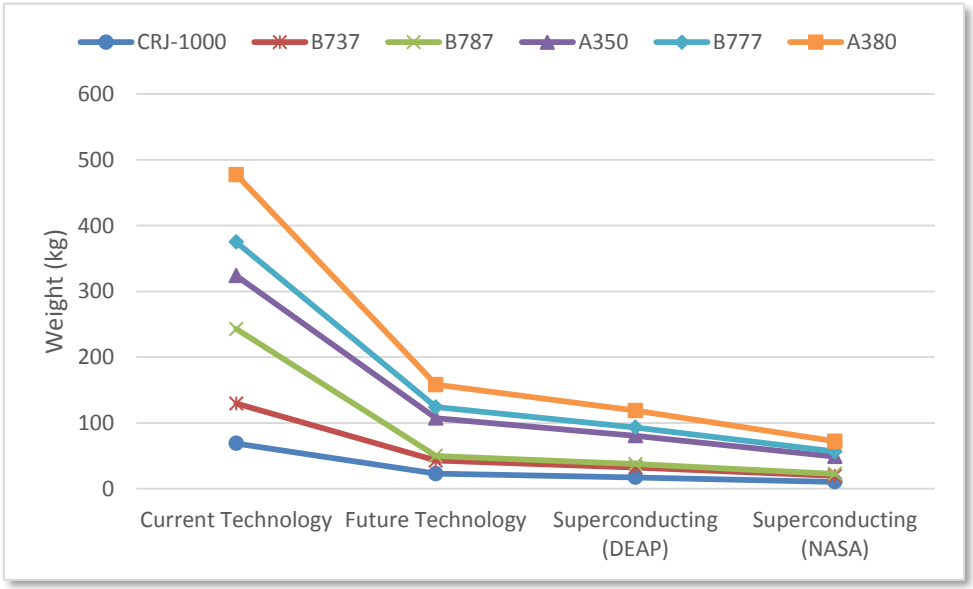

Figure 79 Power Electronics' weight for each reference aircraft in all four different versions

The outcomes of this study resulted in similar trends as the electrical machines' study. There is a clear benefit of using cryo-cooled power electronics in

comparison to the current technology that results in almost seven times lighter converters. Since this study was practically a power density examination it is easy to make similar conclusions for each case. The DEAP estimates and the conventional future technology expectations differ only by 5kW/kg per converter, a difference that could prove to be significant only in high power applications. Over two times lighter equipment is expected with NASA estimates compare to the future technology predictions.

To conclude, power electronics weight seems able to block the feasibility of MEA approach particularly in long range aircraft where they could add close to half a tonne in the system (A380 case). However, if the future expectations for the conventionally cooled power electronics could be met then the superconducting cases will not result in significantly lighter equipment.

- Cables

First of all, the length of the main transmission lines needs to be estimated in each reference aircraft. In the case of Boeing 787 a length of 75 m for the main transmission lines was chosen based on the aircraft's length and the location of the engines on the wing. Since there is not a clear idea of the exact electrical architecture in each aircraft this method just gives an approximation of the required length. Following a similar strategy for each reference airplane the required length of cables was calculated in each case. Equation (5-1) was then used to calculate the weight per meter of the conventional copper cables (with a 10% improvement for the future technology). In the superconducting versions the weight per meter of the power cables is assumed constant in all cases. The required thermal insulation in this type of transmission line is expected to be the main weight factor in the low power applications, whilst the increased current density capabilities of superconducting wires will allow them to keep the size of their superconductor relatively constant to any power changes. When the normal currents are relatively low (i.e. CRJ-1000, B737 cases) using thin superconducting wires will make the connections and mechanical support a challenging task (Malkin and Pagonis, 2013). Table 21 summarises the weight

density of the main span cables in each reference aircraft for all the different versions under investigation.

Table 21 Weight per meter (kg/m) of the main transmission lines for each reference aircraft in all four different versions

Aircraft	Length (m)	787 Current	787 Future	Superconducting Case (DEAP)	Superconducting Case (NASA)
CRJ-1000	65	4.8	4.3	5	8
B737	70	8.5	7.7	5	8
B787	75	10.5	9.5	5	8
A350	80	20.5	18.5	5	8
B777	90	24.4	21.9	5	8
A380	120	29.4	26.5	5	8

The total weight of these cables can be seen in Figure 80 where it shows that the benefit of having superconducting cables can be capitalised for aircraft larger than the Boeing 737 model. This weight benefit is extremely highlighted in examples such as the Boeing 777 and Airbus A380 where both the aircraft length and the aircraft electric power demand have a detrimental effect on the weight of conventional copper power cables. This weight benefit can reach values over a tonne in the case of A380.

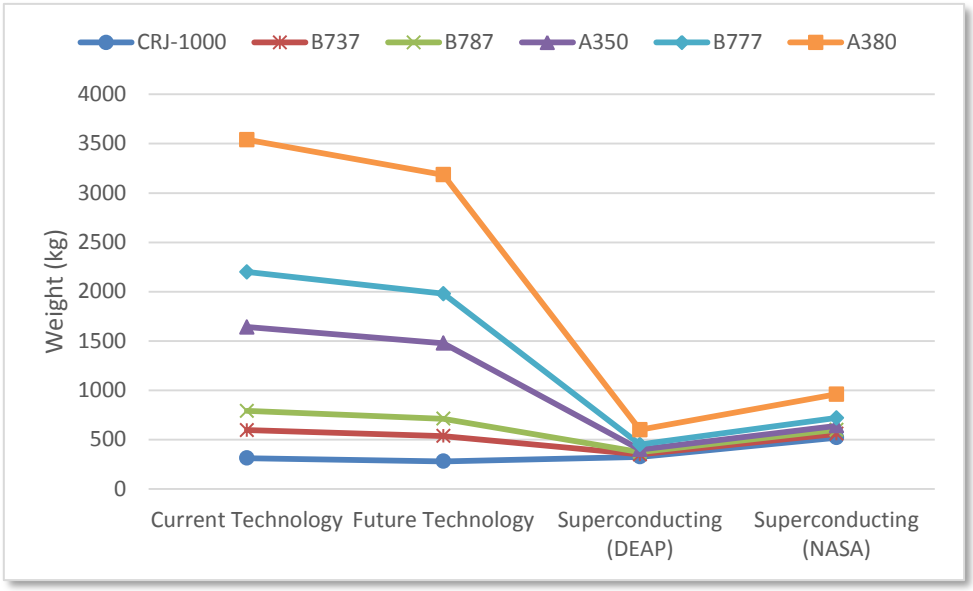

Figure 80 Cables' weight for each reference aircraft in all four different versions

Finally, it is important to note that in both superconducting versions losses in the order of 5 W/m of cable length were assumed (Brown, 2011). This parameter is important for the calculation of the thermal load that the superconducting configurations produce. The latter will be the predominant factor on the weight estimation of the required cooling system.

- Cooling system

In this section the weight of the cooling system in each case will be estimated. In the conventional configurations, where room temperature equipment is used, the cooling system was assumed to weigh 30% of the overall weight of the cooled components. This approximation was used since no relative information was found in the literature and it is based on an expert's opinion (i.e. Stephen Harrison). In regards to the superconducting versions of each reference aircraft the two-stage reverse Brayton cryo-coolers-presented in 5.3.1 and fully described in A.2- were used. NASA has made some approximations regarding the expected cryo-cooler weight assuming a power density around 5 lb/input-hp. However, the cryo-cooler models developed during the DEAP project can be considered as more reliable than a simple power density assumption. Hence, these models were used for both superconducting cases giving a more constant

representation of the cooling system in these cases. Aircraft estimations based on the NASA assumptions will nonetheless benefit from the increased components' efficiency which will result in lower thermal loads.

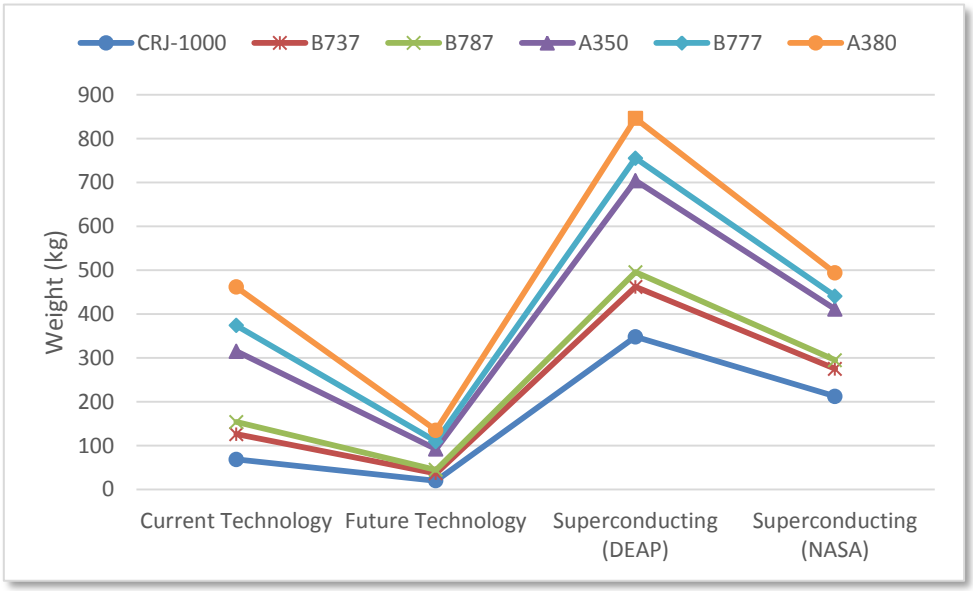

Figure 81 Cooling system's weight for each reference aircraft in all four different versions

As it was expected in the superconducting versions the weight of the cooling system is significantly higher in most of the cases. However, it should be noted that as the electric load increases the difference between conventional and superconducting cooling system is dramatically decreasing. For example, in the A380 type of aircraft the cryo-coolers' weight based on the DEAP efficiency assumption will weigh less than two times the conventional cooling system weight, whilst if the NASA efficiency figures are used there is only a 30 kg penalty in the superconducting modification of the aircraft. Clearly, this changes if the future technology predictions are used as a comparison to the superconducting models. In that case, the cryo-coolers' weight can be up to ten times heavier if the NASA estimates are used or even up to 17 times heavier by using the DEAP efficiency predictions (CRJ-1000 model).

It is becoming clear that the weight of the required cryo-coolers does not increase linearly to the overall electric load of the aircraft. In the contrary, the

longest the range of the aircraft the less effect on the overall weight of the system the cryo-coolers weight will have. This result was somehow anticipated but the extent of this effect was highlighted via this study.

5.4.4 Final Remarks

Figure 82 summarises the overall estimated weight of the secondary power network of each reference aircraft based on current and future technology component density estimations as well as superconducting component weight predictions made both by the DEAP project team and NASA.

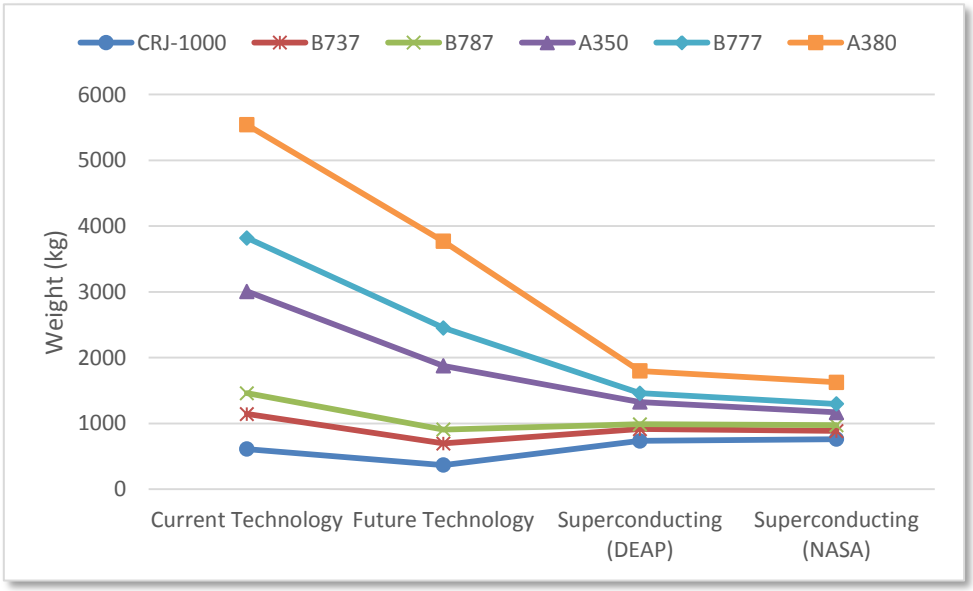

Figure 82 Electrical Power Network total weight for each reference aircraft in all four different versions

The first thing to notice is the different scalability ratios between conventional and superconducting versions. Although in the short/medium range aircraft models (i.e. CRJ-1000, B737, and B787) the overall weight of the conventional electric power network is comparable or even lighter than the superconducting equivalent, in the longer range aircraft examples (i.e. A350, B777, and A380) the SEA concept becomes a very attractive option in terms of the overall system's weight and efficiency even if the aggressive density targets for the conventional equipment could be reached. If instead of specific aircraft models the electric load requirement was used as a reference, it seems like the 1.5 MW

is the limit where the superconducting case gives an overall weight benefit compared to the future conventional technology case (Figure 83). Hence, as the electrification of future aircraft is expecting to rise, even shorter range aircraft could benefit by the use of superconducting components. Figure 83 demonstrates the weight trendline compared to the electric load requirements of an aircraft for all four cases. It is clear that as the electric load demand rises the superconducting cases become more attractive options in terms of weight.

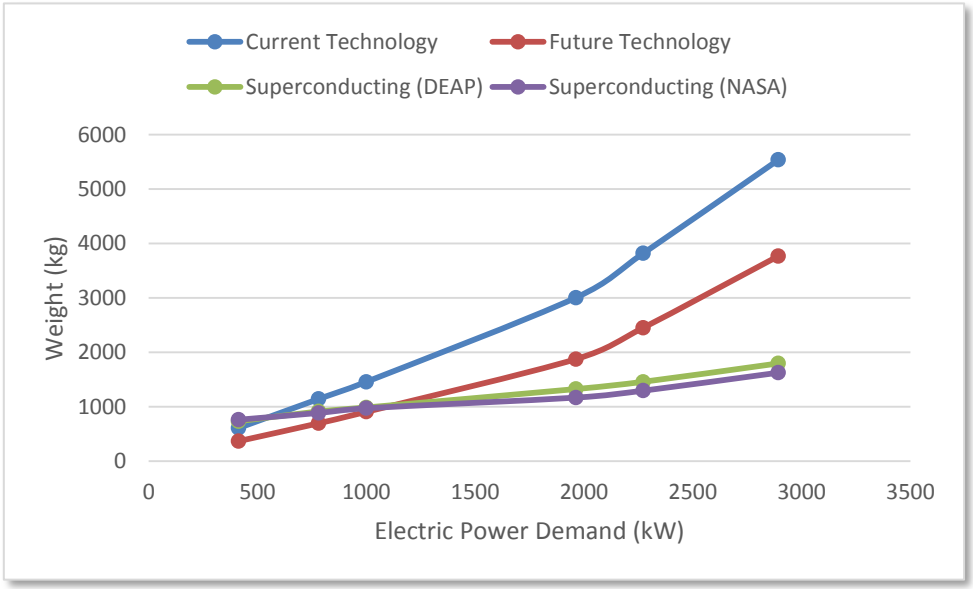

Figure 83 Electrical Power Network total weight for different electric load requirements

This weight benefit derives from the non-linear way in which cryo-cooler weight is increasing with the cooling power demand. Another thing to note is that if higher operational temperatures were chosen for components such as the power electronics and the main transmission cables the cooling power demand and consequently the cryo-cooler weight would have been significantly lower. Furthermore, the main transmission lines start to take advantage of the attractive characteristics of superconducting wires mainly as the nominal current of the system significantly increases. As it was described in Chapter 3 the way superconducting networks are designed is relatively different than the procedure in conventional power networks. High normal currents are actually preferred in these cases due to the incredibly high current capability of

superconductors. The acceptable range in voltage levels in an airborne application is not wide enough to allow lower normal currents in the conventional configurations and this fact has a detrimental effect on the weight and size of the cables in long range aircraft where a MEA approach is followed.

Finally, whilst in a MEA the use of a SPN could be considered as optional at least for shorter range aircraft, in the TeDP or HEDP concepts their use seems inevitable. There is at least an order of magnitude difference in the electric power requirements between the two approaches and the potential weight and efficiency gains of a SPN make their use necessary in the case of HEDP. Hence, if SPNs were adopted by MEA this will make the eventual transfer to hybrid/electric more progressive (Malkin and Pagonis, 2015a).

5.5 Key Study Limitations

This study could be considered as a preliminary feasibility study of the SEA approach in existing and future aircraft. The SEA concept includes a number of components that have not been built yet and hence a number of assumptions were necessary. Therefore, there are a number of factors that limit the accuracy of this investigation and are presented in this subchapter.

- The majority of the **superconducting components** are still in the early stages of development **with low technology readiness levels** (TRL) of 0-2. The same goes for the future technology estimates where aggressive power density values were assumed. Although these assumptions are adequate for preliminary weight studies, a lot of work needs to be done so that the technology could be considered mature enough to be implemented in an aerospace application. In regards to the superconducting electrical machines and cryo-coolers models the key limitations have been described in chapter 4.4 and A.2 respectively.
- An **operational temperature of 20K** for the whole system in the superconducting cases was assumed. This temperature was chosen for two main reasons: a) to explore the worst case scenario in terms of cooling demand and b) to simplify the architecture of the cooling system. Having different component operational temperatures will have resulted

in separate branches of cryo-coolers adding complexity and possibly weight in the electrical power network. However, it is fair to assume that higher operational temperatures will be achievable both for the power electronics and for the main transmission lines resulting in a significant drop on the cooling power demand. The fully superconducting machines on the other hand might need to operate on the 20-25 K range due to the AC losses of the stator that can be acceptable only in the case of MgB2 material.

- A final remark about the cooling system is the **possibility of using a liquid cryogenic fluid** and a heat sink instead of the bulky cryo-coolers being investigated in this study. The main benefit of such a cooling method could be the use of a coolant fluid from which the boil-off gas can be also used as a low emissions fuel (Malkin and Pagonis, 2015a). Especially, if an operating temperature of 111K was chosen for the power electronics, LNG could be used reducing the overall costs significantly. However, the investigation of the optimal cooling system was not in the scope of this research study. The optimisation of this system could enhance even more the feasibility of the SEA concept.
- **The main transmission line's weight** -especially for the superconducting cases- **was based on generic assumptions** of low fidelity. In the superconducting versions, a constant weight per meter value was chosen, neglecting any effect the different power, voltage and current levels might have. Notwithstanding these remarks, it should be noted that the reference superconducting cables were characterised either by their high voltage (Xi et al., 2006) or their high power (Wright et al., 2015) levels; hence, they could be considered as moderate assumptions.
- There are also **other components** of the aircraft's secondary power network **that have not been included in this weight sensitivity study**. Switching and protection devices for example could add significant weight in the whole system both in the conventional and in the superconducting cases. Equipment devices such as circuit breakers,

SFCLs, and solid-state switches will be necessary in these configurations and an extended study of the ideal protection system could modify the optimal electrical system architecture for different aircraft. It is not clear yet if there will be a significant weight and efficiency difference between the conventional and the superconducting configurations.

- Last but not least, the **electrical system architecture of each aircraft could be optimised differently**. The Boeing 787's electrical power network was used as a baseline since it was the only existing architecture implementing the MEA concept. Nevertheless, as the electric load demand increases alternative design routes might be followed. In regards to voltage levels as it was stated in Chapter 3, Paschen Law's limits the maximum voltage level acceptable for an airborne application to approximately 327 V (Armstrong et al., 2012). MEA and SEA will most probably follow different design approaches but the most favourable one in each case will be decided after extensive sensitivities studies.

6 Novel Flight Cycles for Hybrid/Electric Aircraft Using Energy Storage

Hybrid/electric approaches have attracted the interest of many industries (i.e. marine, automotive etc.) mainly due to the benefits derived from the flexibility they offer in the operating cycles. Here in aerospace field the motivation towards HEDP approach is forced by the improvements in propulsive efficiency and aerodynamics. In this chapter we will look at aircraft operational cycles to investigate if any additional improvements can also be attained.

The previous chapters had already shown some of the potential benefits that a TeDP configuration could offer. However, it was apparent that extra benefits could be obtained if an overall novel optimised system's approach is followed. The hybrid/electric nature of the proposed configuration could free the propulsion system of this type of aircraft from the restrictions that conventional configurations are facing. The main approach is based on the fact that each propulsive unit could be optimised for a specific function (propulsive or not) increasing its efficiency throughout the flight cycle. The optimisation of an electric power network increases the flexibility of the whole system and this is one of the main advantages of these configurations that up until now have not been fully explored.

Energy storage could play an important role on these novel designs adding even more flexibility to the whole network. These devices could be used either as a short term power unit, as a boost power source or as a main prime mover depending on the range and power requirements of the aircraft. Batteries, supercapacitors and Superconducting Magnetic Energy Storage (SMES) are some of the energy storage options for the flexible integrated power system under investigation.

Several architecture proposals and novel flight cycles will be explored in this chapter. The DEAP aircraft will be used as a reference aircraft and the weight estimation of the main components of these novel configuration proposals will be calculated so that the feasibility of these designs to be determined. After

that, the study will be extended to different aircraft sizes from short to long range cases.

6.1 Energy Storage

Energy storage mechanisms are currently been used in numerous applications including the main transportation industries (i.e. aerospace, automotive, marine etc.). More electric or all electric vehicles are continuously attracting the interest of these industries that are eager to create more efficient and environmentally friendly vehicles. Energy storage devices are present in all these more electric configurations with different requirements each time depending on the application. Batteries is clearly the most mature and well-established technology of energy storage. However, other storage mechanisms such as the supercapacitors seem to improve rapidly creating competitive to battery products especially for specific applications where quick and short term power demands are necessary. SMES could also play an important role in a concept such as the TeDP, since they can be integrated in the already existing superconducting network increasing remarkably their actual power and energy densities.

6.1.1 Batteries

- State of the art

A study about battery technology is highly dependent on the application. Batteries can be divided into two main types depending on their charging capability: primary and secondary (or else rechargeable). In this study only the latter type will be investigated. In this category, at present, there are four main types that have been broadly used in the industry:

- Lead-acid
- Nickel-Cadmium
- Ni-Metal Hydride
- Lithium-Ion

Since the study is made for airborne applications the energy density of the battery becomes the crucial feature. In addition, safety, life cycle, and reliability

are also important factors. Figure 84 presents the theoretical and the current practical specific energy values of the four aforementioned types of battery.

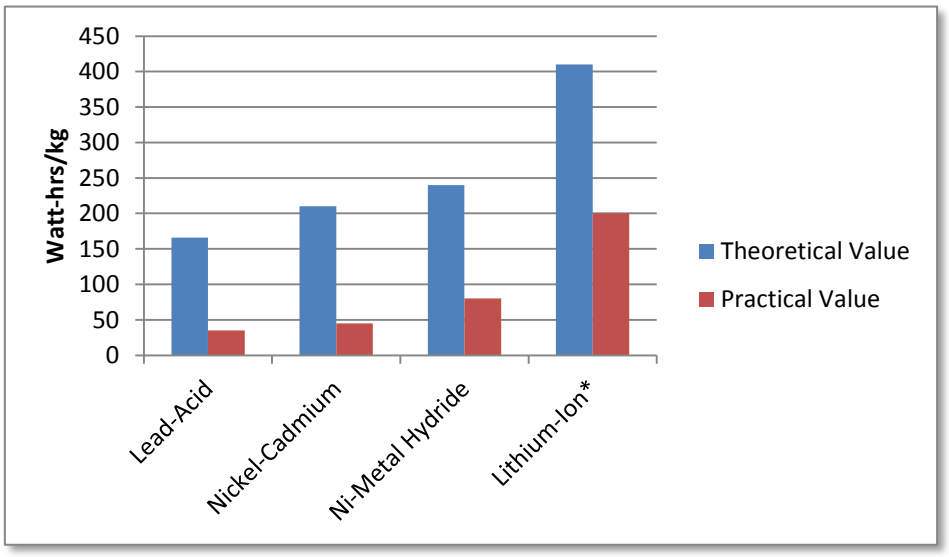

Figure 84 Current Specific Energy values of different battery types

*Note that multiple Li-ion technologies are currently commercially used and the values given in the figure are just an average of the best cases

A more detailed table which includes several important factors for a vast variety of battery types can be found next:

Table 22 Comparison of different types of battery currently in use (www.batteryspace.com, 2015)

Chemistry	Voltage	Energy Density	Working Temp.	Cycle Life	Safety	Environmental	Cost based on cycle life x wh of SLA
$LiFePO_4$	3.2V	>120 wh/kg	-0-60 °C	>2000(0.2C rate, IEC Standard)	Safe	Good	0.15-0.25 lower than SLA
Lead acid	2.0V	> 35wh/kg	-20 - 40°C	>200	Safe	Not good	1
NiCd	1.2V	> 40wh/kg	-20 - 50 °C	>1000	Safe	Bad	0.7
NiMH	1.2V	>80 wh/kg	-20 - 50 °C	>500	Safe	Good	1.2-1.4
$LiMn_xNi_yCo_zO_2$	3.7V	>160 wh/kg	-20 - 40 °C	>500	better than LiCo	OK	1.5-2.0
$LiCoO_2$	3.7V	>200 wh/kg	-20 - 60 °C	> 500	Unsafe w/o PCM	OK	1.5-2.0

The table above is useful for making some important conclusions. Looking exclusively at the energy density values lithium cobalt oxide ($LiCoO_2$) seems the most attractive option. However, this type of battery is characterised by its high cost and most importantly as being unsafe for high power applications such as the aerospace. It is normally used in portable applications, being the most common option in mobiles, laptops and cameras. A far safer option and with the extra benefit of long cycle life and extremely low cost is the lithium iron phosphate ($LiFePO_4$) battery. However, its energy density is limited to around 120 Wh/kg lower that other lithium-ion types.

Focusing on similar to aerospace applications could be more useful to understand the current technology trends for batteries. Electric vehicles seem the closest application to aircraft propulsion with similar priorities in the choice of energy storage. Toyota Prius 04 uses a prismatic NiMH battery with specific energy density of 46 Wh/kg (www.eaa-phev.org, 2015). The Chevy Volt on the other hand uses a Li-ion battery pack with specific energy of 53 Wh/kg (Murphy, 2012). Finally, Nissan Leaf uses a laminated lithium ion pack with energy density around 140 Wh/kg (wikipedia.com, 2015) which seems to be the most reliable state of the art example of battery that could also be used in an aerospace application. New Li-ion cells for automotive applications are under development with the examples of Saft VL45E and VL41M (with energy densities of 160 and 146 Wh/kg respectively) to present the most attractive characteristics (Rosenkranz, Kohler and Liska, 2007).

In conclusion, the decision about which battery technology to use in a TeDP configuration is more complex that might have been believed. Although lower weight, and as a consequence higher energy density, is the number one priority other factors such as safety, life expectancy, cost and power delivery cannot be neglected. The author believes that the most appropriate method of estimating current energy densities of batteries is by comparing the battery types being used in similar applications. Thus, electrical vehicles which have similar priorities -such as high energy density, safety, life, and high power density-were chosen as a reference. As a result, a specific energy around 200 Wh/kg and a

specific power performance up to 4000 W/kg can be considered as the state of the art values for batteries (Jow et al., 2014). These two values will later been used as the state of the art Li-ion parameters for the novel flight cycle study. Figure 85 summarises the specific energy values of the different battery technologies currently been used in the industry. Lithium Nickel Cobalt Aluminium Oxide battery is the clear winner in regards to energy density storing more capacity than any other technology (close to 260 Wh/kg), however it suffers in terms of power density and thermal stability. Hence, the values being used in this study as the state of the art density limits are closer to the ones presented in Nickel-manganece-cobalt (NMC) and Lithium Cobalt technologies.

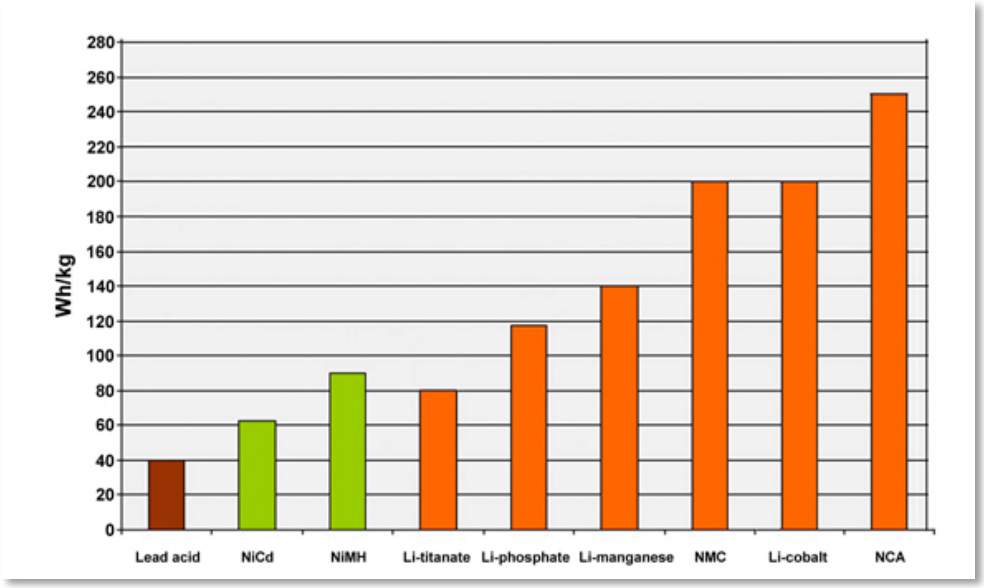

Figure 85 Typical specific energy values for different battery technologies (batteryuniversity.com, 2015)

- Future trends

Lithium-ion batteries have not yet reached their optimum performance and their technology is continuously improving. Since the anode in lithium-ion type of battery has been optimised, then batteries are cathode limited devices and further developments in the cathode materials could lead to better battery performance. However, there is a practical limit of lithium-ion battery capability which even if it is attained it would still not provide the required energy density

for aerospace applications. There have been research groups aiming on providing rechargeable Li-ion batteries with energy densities around 400 Wh/kg and power densities up to 16000 W/kg (Jow et al., 2014).

Another type of battery which has gathered a lot of interest lately and it is believed by many researchers to be the future of battery technology is the so called *lithium-air* battery. The main difference between a lithium-ion and a lithium-air battery is that the cathode is replaced by air making the latter type significantly more lightweight and with greater energy capabilities (Ayre, 2014). Lithium air batteries have a theoretical limit of around 12 kWh/kg without the oxygen mass, a value comparable to the one of gasoline (~13 kWh/kg) (Imanishi and Yamamoto, 2014). Li/Air technology is nearing commercialization and has already achieved specific energies in excess of 700 Wh/kg (PolyPlus, 2009). However, there are still many problems that need to be addressed such as the low discharge rate, poor life cycles, and low efficiency (Shen et al., 2013). Power density of this type of batteries is also relatively low. Depending on the degree of hybridization a target for a 140 to 1400 W/kg power density in battery level has been set (Christensen et al., 2012).

Finally, one of the most promising high specific energy battery types is the lithium-sulphur (Li-S). Li-S batteries present a theoretical specific energy five times greater than the Li-ion technology (i.e. 2500 Wh/kg) (Shuli and Zhan, 2015). They hold the record in the highest specific energy density being achieved to date by rechargeable batteries in an actual application (350 Wh/kg for the Qinetiq's Zephur UAV) (Millikin, 2010). Their relatively low cost makes them even more attractive for potential extensive use. One of the main drawbacks however is their low cyclability. Many studies and researchers have been focused on increasing the life cycles of this type of batteries and many labs have claimed that a 500 Wh/kg commercialised Li-S battery will soon be available (Van Noorden, 2014), (Dodson, 2013). Extremely high power densities in the range of 11000 W/kg after 100 cycles have been claimed for an all solid state Li-S battery (Nagata and Chikusa, 2014). The benefits and drawbacks of this technology can be seen in Figure 86. Specific power and energy are

extremely high, whilst the cycle life of these batteries is the field that urgently needs improvement.

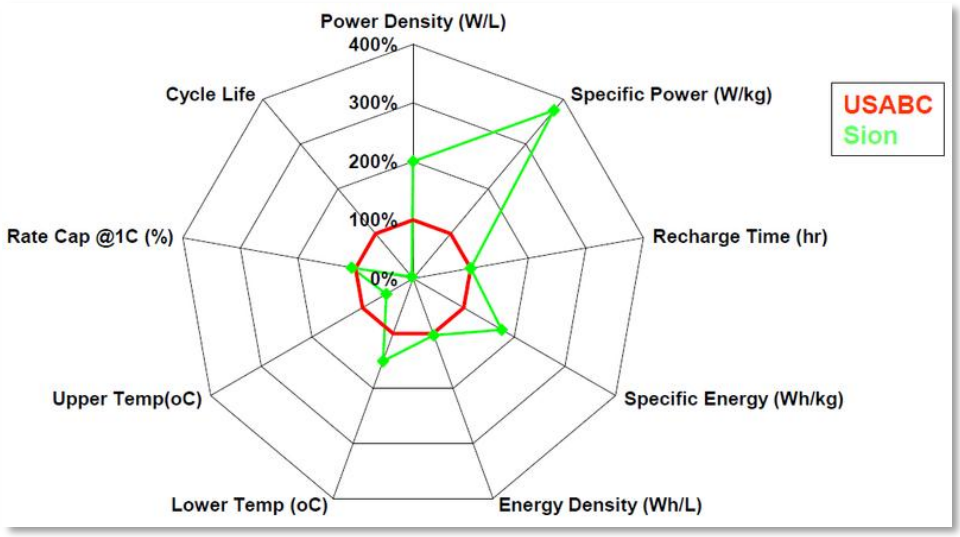

Figure 86 Status of Li-S batteries compared to the United States Advanced Battery Consortium (USABC) baseline standards (Mikhaylik et al., 2015)

Battery technology keeps improving throughout the years bringing the future of all or more electric applications closer to reality. In this section the most promising technologies have been briefly described. Table 23 gives a summary of the specific energy and power of these promising technologies. These values will later be used in the sizing models developed in Simulink which will assess the feasibility for novel flight cycles approach for the future hybrid/electric aircraft. The table also includes an approximation of the expected cyclability of the technologies under investigation. The Li-ion values mainly depend on the specific technology being chosen; hence the wide range. In any case, the life cycles expectance of Li-ion batteries is significantly higher than the other two technologies. There is a general interest in improving Li-air cyclability figures (Roveglia, 2015), whilst Li-sulphur cycle life is as Figure 86 shows the main drawback of this technology.

Table 23 Battery technology summary and sizing parameters

Type	Specific Energy (Wh/kg)	Specific Power (W/kg)	Life Cycles
Li-ion (current)	200	4000	400-1200
Li-ion (future)	400	8000	400-1200
Li-air	750	700	50-150
Li-sulphur	500	10000	~100

6.1.2 Supercapacitors

Another mean of energy storage that is starting to attract more interest in the industry is the capacitors; and more specifically the supercapacitors (also known as ultracapacitors). Unlike batteries, who store energy in chemical reactions, capacitors store energy in an electric field which is created between two oppositely charged particles when they are separated by a dielectric. Supercapacitors use a different storage mechanism to traditional electrostatic capacitors, but behave in a similar way due to the way they store the energy. In the vast majority of supercapacitor applications today (almost 95%) Electric Double Layer Capacitors (EDLCs) are used with carbon as the active electrode material (Simon and Gogotsi, 2010). In order to increase the energy stored in these devices it is essential to increase the surface area. This surface storage mechanism is partially one of the reasons for the relatively low energy density of supercapacitors (typically around 5Wh/kg) (Simon and Gogotsi, 2008). Other reasons are the limited operating voltage range, the required thickness of the separator, as well as some practical limits such as packaging and internal losses (Edwards, 2011).

The main attractive attribute of supercapacitors is their ability to deliver all their stored energy in a really short time (around 5 sec). Moreover, they are capable

of withstanding thousands of cycles; even in the range of 500.000 cycles with less than 20% capacitance decrease (Mouser Electronics, 2015).

In airborne applications supercapacitors have been used in Airbus 380 for the emergency door opening. On the other hand, in automotive world the general trend is the hybrid/electric vehicles with a combination of EDLCs and batteries for fast acceleration and breaking energy recovery which leads to an increase of the battery life expectance. This might also be the future in airborne applications, where a hybrid system with batteries and supercapacitors could become the most beneficial configuration.

Li-based hybrid systems with nanostructured Li4Ti5Oi2/AC formation (introduced by (Amatucci, Badway and DuPasquier, 2000)) were the first ultracapacitors which reached energy densities of 10 Wh/kg and high power densities. Since then, several companies and institutions have been studied the lithium based capacitors option. JM energy Corp. started the mass production of Lithium-ion capacitors in 2009 with gravimetric densities of 12-14 Wh/kg (Millikin, 2009). ACT (Advanced Capacitors Technology) also claimed to have built LIC (Lithium-ion Capacitors) such as the so-called Premlis which uses for the cathode a nanoporous carbon material and for the anode graphitic carbon material doped with lithium ions. This capacitor device doubles the energy density of the company's existing products (Hampton, 2013). Premlis 5000 was initially developed in Bhutan for LED light applications that were used in areas without electrical supply in the city. The energy storage per unit volume of this LIC was 25 Wh/kg (Montgomery, 2012). This type of capacitors combines the relatively high energy of Li-ion batteries and the high power of EDLCs. Next figure partially presents the aforementioned conclusions:

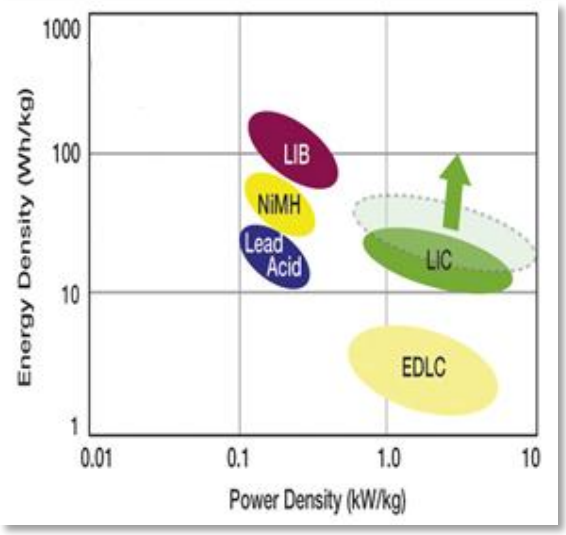

Figure 87 Energy and power density of different energy storage options (Hampton, 2013)

Another type of supercapacitors that have attracted a lot of interest recently is the EDLCs that use carbon nanotubes (CNTs). Several studies have been carried out to explore the potentials of the CNTs with extended efforts to improve the specific surface area and/or the operational voltage range. For the former a controlled oxidation of single walled CNTs had led to a high energy density of 24.7 Wh/kg, while an operational voltage of up to 4V has been achieved in supercapacitors with high purity CNTs in conventional organic solvents leading to an energy density of around 94 Wh/kg (Kim, Chung and Kim, 2012). However, it must be pointed out that the last results were calculated possibly without taking into account the 'dead components' of the final device. But even if we assume a 50% decrease due to internal losses and packaging a supercapacitor of deliverable stored energy around 50 Wh/kg can be feasible in the short term. In the aforementioned CNTs, there is also enough room for improvement for their power densities which are relatively low for ultracapacitors' standards.

To sum up, it is really difficult to predict the future improvements in supercapacitors technology. There are several research studies focusing on different materials that have shown promising results. Electrode materials such as activated carbon, carbon fibres, carbon aerogel, CNTs, and graphene are all

being currently explored and showing potentials of reaching competitive specific energy values. However, it seems unlikely that they will ever approach energy densities similar to the ones expected from the future battery technologies. On the other hand, the impact of the future improvements is less predictable than in the batteries case; hence supercapacitors should not be ruled out. Especially due to their extremely high power densities they could be the ideal candidates for several applications where high power is required for a short period of time. In this study, a specific energy of 50 Wh/kg and a specific power of 15 kW/kg were considered as realistic estimates for the 2035 timeframe.

6.1.3 Superconducting Magnetic Energy Storage (SMES)

The superconducting nature of the networks under investigation in this research study makes the use of SMES a viable option for an aerospace application. This system stores energy in the magnetic field created by the flow of direct current in a superconducting coil (Sutanto and Cheng, 2009). SMES does not include any energy conversion (pure electrical conversion only) resulting in fast response times. Their efficiencies are relatively high and their capability of unlimited discharges and recharges give them an extra advantage over batteries. Moreover, they present a good balance between power and energy density which could be important for an aerospace application. The main advantage however, seems to be the capability of discharging large amounts of power for a small period of time and unlimited times (Yuan et al., 2010).

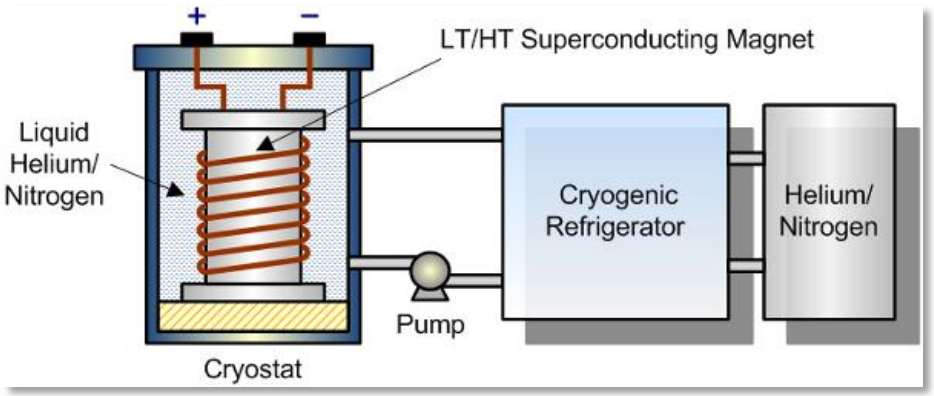

Figure 88 Schematic of a SMES device (Molina, 2010)

The main disadvantage of these devices is their cost, as the materials being used are normally too expensive to be considered in large applications. Furthermore, the refrigeration system also normally poses an obstacle in most applications. However, in a TeDP configuration a cooling system will already be present; hence, the cooling power requirements of a SMES are not expected to affect the feasibility of this type of storage. Finally, their mechanical instability and their high self-discharge ratio for long periods are also significant concerns (Yuan, 2011).

SMES systems are typically used to improve the network's stability and power quality. In our network, SMES could work as a supplementary source of energy storage. More specifically, in a power failure their fast response allows them to provide electrical power in the very few first seconds while other types of energy storage could supply power later on.

6.2 Novel Hybrid Configurations and Flight Cycles

One of the major benefits of the Turbo-electric Distributed Propulsion (TeDP) concept is the flexibility that offers to the whole system design. There are many design options regarding the complete flight cycle of this new aircraft that have not been investigated yet. Energy storage could play an important role on future aircraft designs, especially if the technologies described earlier reach their full potential. In a hybrid/electric configuration significant electrical power is being used in the distributed propulsion system. Typically, this required power is produced by the gas-turbine alternators which produce electrical power to satisfy the demands of the whole network at all times. An aircraft mission profile consists of five main flight phases: taxi, take-off, cruise, descent, and landing. By looking on the power demand during these phases someone will notice a significant peak during the take-off phase. Obviously, this fact puts constraints on the engines' design which are rated to satisfy this peak power whilst for most of the mission are working at the half of their potential or less. The possibility of using alternative power sources such as energy storage either to reduce the power peaks of the engines or to optimise all the prime movers involved for specific flight phases will be the main target of this chapter.

6.2.1 Baseline Aircraft and Mission Profile

For the purposes of this study and for reasons of consistency the “DEAP aircraft” was used as a reference. This is a short/medium range aircraft with capacity of around 100 passengers. A brief description of the DEAP project’s aircraft has been presented in 1.3 and in 2.1.5, whilst its main characteristics are summarised in Table 24. Note that the thrust requirements differ depending on the configuration being chosen but this value is used to give an approximation for the power requirements of this aircraft.

Table 24 Main characteristics of DEAP Aircraft

Characteristic	Value	Units
Mach Number	0.75	-
PAX	100	passengers
Range	2000	Nm
TOC	34000	Ft
Thrust Requirements	~25	kN

The mission profile of the DEAP aircraft can be seen in Figure 89. The red circles indicate the three main sensitive areas of the mission which need optimisation during the design process of the GTs in conventional configurations. The most crucial targets of the GTs are:

- To satisfy the peak power demand of the mission (i.e. EOR-one engine out safety case).
- To satisfy the highest corrected flow at inlet to the compression system (i.e. TOC).
- To be as efficient as possible during the longest phase of the mission (i.e. the cruise).

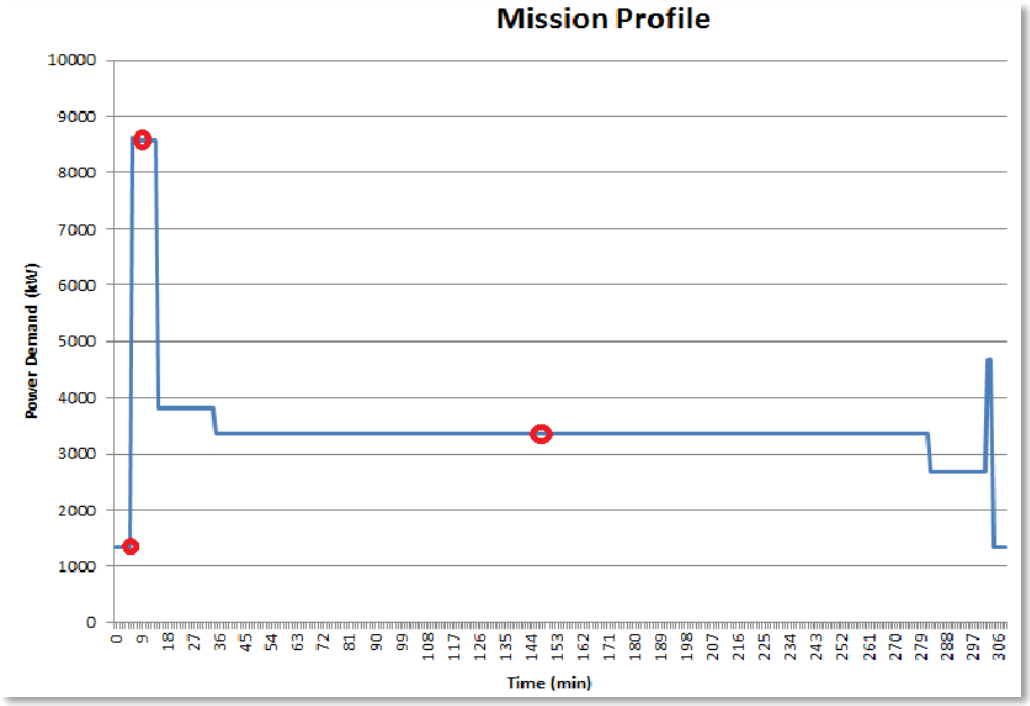

Figure 89 Mission profile of the DEAP aircraft

The former of the above three crucial design “hot spots” is an important criterion as it effectively sizes the power system of the aircraft. In the proposed configurations the system could be designed in the EOR-one engine out safety case to land safely powered by one or two GTs combined with the use of E.S subsystems. This eventually could reduce the size of the GTs allowing more optimal GT design points that would probably increase the efficiency of the engines (effect on the rest of “hot spots”). To cope with several design challenges that may occur, the electrical system should be designed in a way that a fully symmetrical thrust can be produced during the one engine out safety case. Furthermore, the overrating of electrical machines could give significant design benefits. More specifically, the electrical machines could withstand excessive power demands for short periods of time, such as the safety case or even during the landing phase. This will ease the design of such a system, while following a similar strategy with the E.S. devices (i.e. higher power discharge during the short climb phase) could potentially reduce the size and weight of these components.

6.2.2 Overview of the Modelling Approach

This thesis' section aims to investigate the feasibility in terms of weight of using energy storage mechanisms throughout the flight cycle of a HEDP type of aircraft. Other benefits and challenges will also be explored but a number of Simulink models were developed to estimate the weight of the main components of a hybrid configuration. The weight of components such as the GTs, electrical machines, cryo-coolers, and energy storage devices will be estimated for a number of different proposed configurations. Most of the models were developed during the DEAP project, although a wider feasibility study in terms of energy storage use has been investigated in this research study.

Although the DEAP project assumed geared turbofans as the main engines for their proposed architectures, in this study the GTs are assumed to be turboshaft, an assumption that was also used during the NASA N3-X studies. It seems reasonable that since the main role of the gas turbines in a hybrid/electric configuration will be the production of power-and not thrust-turboshaft engines will be the preferred option. An easy way to predict the weight of these engines based only on their power rating was necessary to be found. Since no such method was available in the literature, an equation was derived based on civil turboshaft/turboprop specifications available online (Meier, 2005). A significant number of engines used in airborne applications have been included in this study to derive the required equation. Figure 90 presents the weight and shaft power of the machines included in this study, whilst the manufacturer and the model being used at are summarised in Appendix A.3.

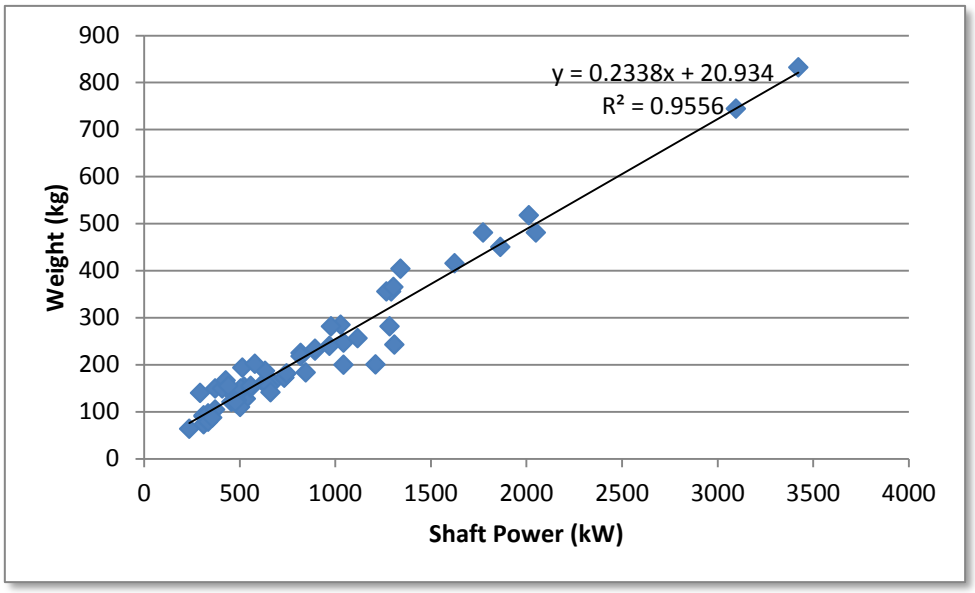

Figure 90 Weight vs. Shaft Power of Turboshaft/turboprop engines

Equation (6-1) was used in the Simulink models later being described. It should be noted that only engines of rating less than 4MW were included in this study both for reasons of specifications' availability and also because this will be the upper limit of rating for the DEAP engines.

$$Engine's\ weight = (0.2338 * Shaft\ Power) + 20.934 \quad \textbf{(6-1)}$$

In all the proposed configurations of HEDP, superconducting machines were assumed. Their weight was calculated based on the models being described in 4.2 and were also used during Chapter 5 calculations. Apart from the output power, the RPM was also used as an input for these models. Values for the speed of these machines were based on the DEAP project cases where speeds around 12300 and 11100 RPM were assumed for the superconducting motors and generators respectively (Wright et al., 2015). The weight of the cryo-coolers required for these superconducting machines was estimated based on the models described in the previous chapter and presented in Appendix A.2. This method could give some misleading results since these machines most likely will not have dedicated cryo-coolers but this weight estimation is used more as

an indication on the relative weight of the cryo-cooler between the several cases rather than an absolute number in each case.

Finally, the weight of the energy storage mechanisms will also be calculated using Matlab/Simulink models. These models will take into account both the energy and the power density of the candidate energy storage solutions. Table 23 summarises the battery technologies investigated in this study, whilst a single 2035 prediction for the supercapacitors case was used. SMES was not included in the models because of the uncertainty of the actual power and energy density that they will present in the overall system. Using the values available in the literature was considered as an “unfair” representation of their case which might become attractive mainly due to the superconducting nature of the whole network.

6.2.3 HEDP proposed configurations

A number of different architectures will be proposed and a weight sensitivity study will be carried out for each case. The ideal energy storage system in terms of weight will also be decided in each configuration.

Case 1: Use of energy storage during take-off

The first case is based on the E-thrust concept investigated by EADS and Rolls Royce in the recent years. This concept was considered as a hybrid electric propulsion system aiming to reduce fuel consumption and emissions of the next generation aircraft. E-thrust implemented the Distributed Propulsion approach consisted of six electrically driven fans powered either by an advanced battery system or by a gas power unit depending on the phase of the flight (Singh, 2013). In the present study a superconducting version of this concept will be explored. The energy storage will be used mainly during take-off reducing the power requirements of the gas turbine. The latter will be designed to perform in a constant power rating which will correspond to the power requirements during cruise. The advanced battery system will assumed to be fully charged in the beginning of each flight and it will be used as a boost for the take-off phase. It will later been recharged during cruise (power derived from the GT) so that it

will be fully charged again for the next flight. The Simulink model developed to estimate the weight of the energy storage system can be seen in Figure 91.

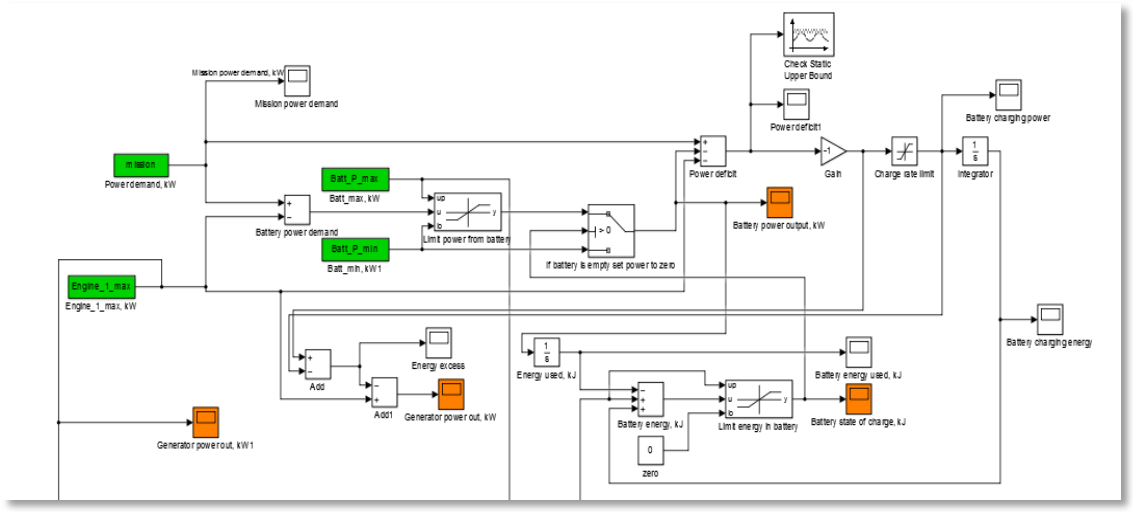

Figure 91 HEDP case 1 energy storage sizing Simulink model

The mission power demand as seen in Figure 89 is being used as the main input. A code developed in MATLAB -being presented in Appendix A.4- gives the required power at each moment of the fight. This mission profile is based on the requirements of the baseline aircraft investigated during the DEAP project. The maximum power of the turbo-generator (i.e. GTA) is also given as an input combined with maximum and minimum power that the energy system could produce. In order to size the latter, the battery energy capacity and its charge rate limit were also used as inputs to the model. The overall target of the model is to ensure that the mission power demand is being satisfied at all times by the engine and the battery pack. A check of static upper bound block is being used to ensure that there is never a power deficit in the system. The energy capacity and power of the energy storage system is manually varied aiming on keeping the minimum possible required weight for the whole network whilst the mission demand is always satisfied. Figure 92 demonstrates the power output of the GTA (red line) and the Energy Storage Device (blue line) during the whole flight mission. The sum of these two lines corresponds to the DEAP aircraft mission power demand earlier presented (Figure 89).

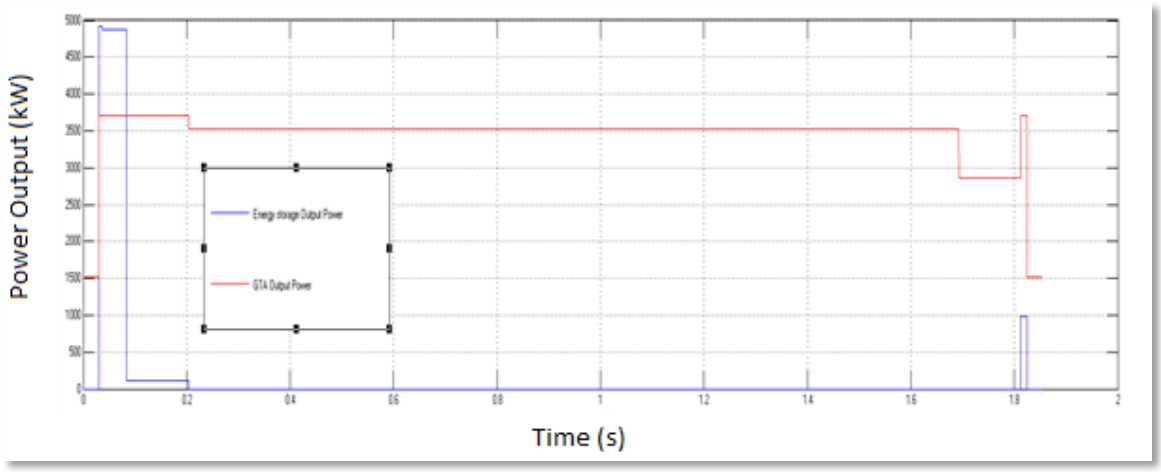

Figure 92 Case 1 GTA (red line) and Energy Storage (blue line) power output with time

The main concept developed in this first case is to use the energy storage during take-off in order to reduce the power requirements of the GTA. Moreover, the GT can be optimised to run at an almost constant power throughout the whole mission. The engine is slightly oversized in order to deal with the additional power demand of the required cryo-coolers. The State of Charge (SoC) of the energy storage mechanism in the first case examined in this chapter is shown in Figure 93. As it was described earlier the battery sharply discharges during take-off and it is recharged during cruise so that it will be fully charged and ready to be used again for the next flight.

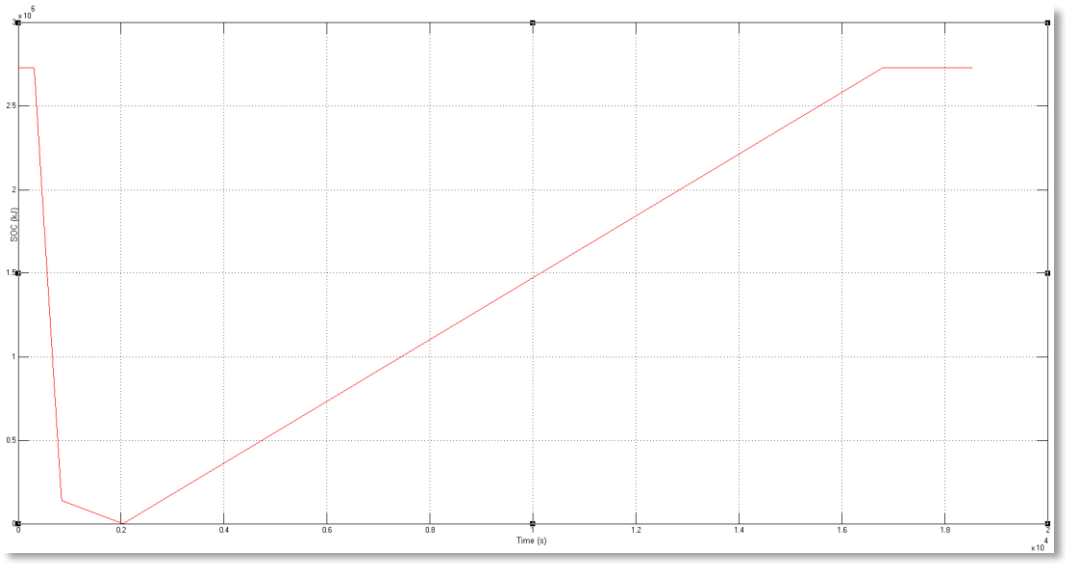

Figure 93 Case 1 Energy Storage State of Charge (SoC) in kJ with time (s)

Especially for this first case the sizing values for the engine and the battery required for the baseline aircraft can be found in the following table:

Table 25 Case 1 GTA and Energy Storage sizing factors

Variable	Value	Units
GTA Power Output (1 engine)	3700	kW
Energy Storage Power Output	5000	kW
Energy Storage Maximum Energy	2.73	GJ
Energy Storage Charging Power	185	kW

The weight of the several energy storage options was calculated based on their energy and power density capabilities via the Simulink subsystem demonstrated in Figure 94. The four different battery technologies described in 6.1.1 and the supercapacitor option were the technologies investigated.

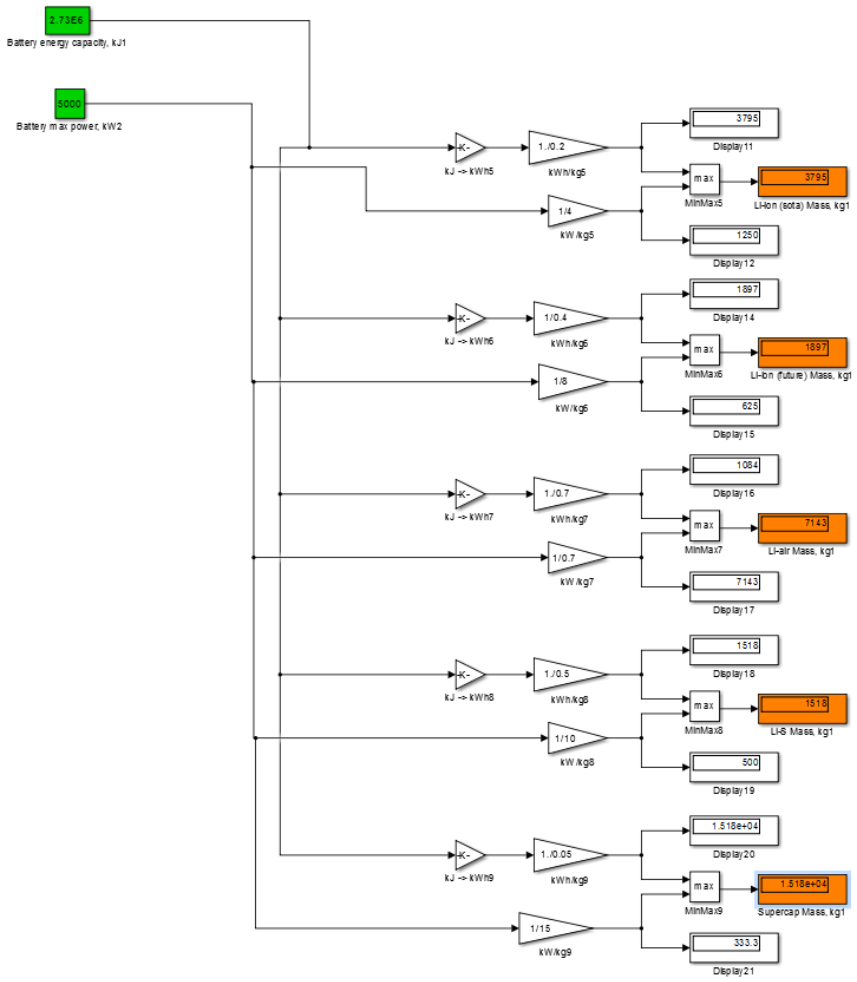

Figure 94 Energy storage weight estimation Simulink model

The following table summarises the results of the Simulink model. Li-sulphur technology seems to be the most attractive option in terms of weight for the Case 1 configuration. For every technology apart from the Li-air battery type, specific energy is the sizing restricted factor. It also becomes clear that the use of a supercapacitor in such a configuration will be prohibitive.

Table 26 Case 1 Energy storage technology sizing values

Technology	Sizing Restriction	Mass (kg)
Li-ion (SOTA)	Energy	3795
Li-ion (future)	Energy	1897
Li-air	Power	7143
Li-sulphur	Energy	1518
Supercapacitor (future)	Energy	15180

Energy storage was not the only component that adds significant weight in this first proposed conceptual aircraft architecture. Using equation (6-1) the anticipated weight of the turboshaft engine was estimated. The superconducting machine models were used to estimate the weight of the generator driven by the main engine, whilst the required cryo-cooler weight was also calculated by assuming 99.9% efficiency for the machines and an operational temperature of 20K. The weight of the superconducting motors was not included in this study because it is not expected to differ between the various configurations. The required propulsive power will be relatively constant in all three cases and thus the weight of the propulsors (superconducting motor driven fans) is expected to remain the same. Figure 95 presents the overview of the Simulink model used for the first case, whilst Table 27 summarises the weight of each main component of this configuration. All the subsystems have been described earlier in the research study and will not be analysed any further.

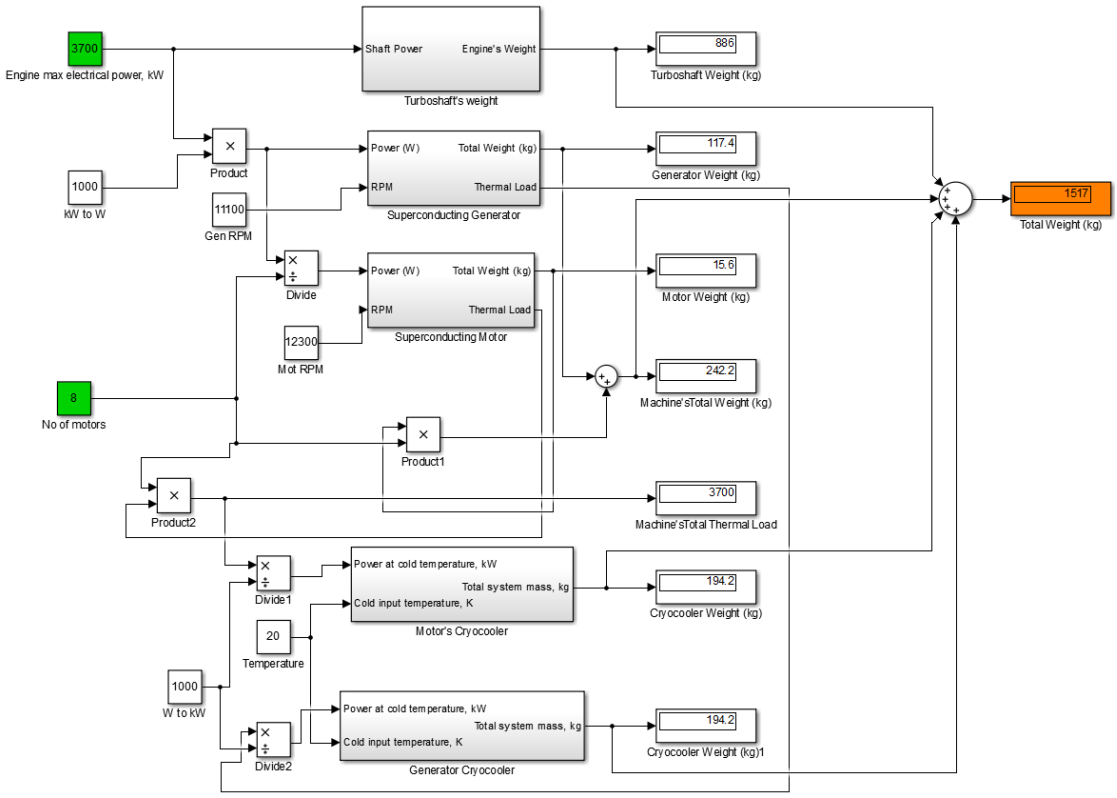

Figure 95 Case 1 Electric Components sizing Simulink model

The following table will be used as a comparison with the rest of the cases being studied in this section.

Table 27 Summary of Case 1 components' weight

Component	Unit Mass (kg)	Qty.	Total Mass (kg)
Turboshaft Engines	886	1	886
Generators	117.4	1	117.4
Cryo-cooler	194.2	1	194.2
Energy Storage	1518	1	1518
Total System's Weight			**2715.6**

Case 2: Use of Energy storage during cruise

Battery powered aircraft are growing in interest mainly due to the important fuel and emission benefits that could potentially offer. However, their specific energy is significantly lower than the one of kerosene and depending on the range of the aircraft could lead to enormously heavy battery packs. Besides, the case of supercapacitors is not even considered in such an application due to their low specific energy. There have been many studies investigating concepts similar to the one of Case 2. The Boeing's Sugar Volt aircraft (1.2.2) for example is using batteries to enable portions of flight with low emissions. More specifically, twin engines are jet fuel powered during take-off, whilst at altitude the hybrid/electric system takes over (Owano, 2012). The all electric transport concept was also investigated by EADS (later renamed to AGI) with the Voltair conceptual design investigating the feasibility of such an aircraft (Stuckl, Van Toor and Lobentanzer, 2012). Finally, Bauhaus Luftfahrt also examined the so-called Universally-Electric Systems architecture where advanced Li-ion batteries constituted the only electric power source (Isikveren et al., 2012).

In this second case, the advanced battery system is being used exclusively during cruise. Since the cruise phase is the lengthiest one, significant fuel burn and emissions benefits are expected by using only battery-powered propulsion. These benefits will not be quantified during this study, where only a weight feasibility study will be carried out for an aircraft of the range similar to the DEAP baseline example. The Simulink model being used for this case is shown in Figure 96, where the main difference is the use of a second twin engine during take-off and landing phases instead of the energy storage devices which in this case take over during the cruise at altitude.

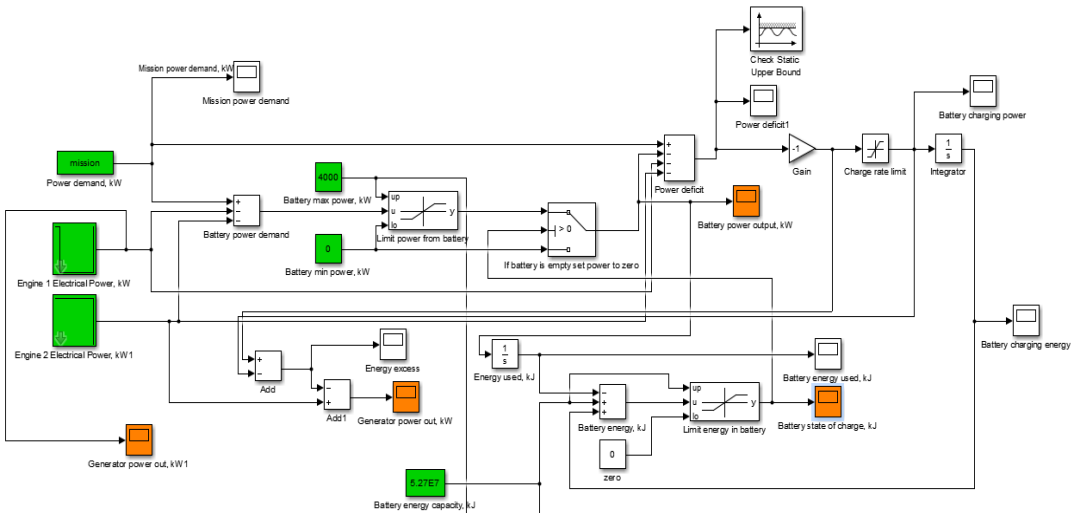

Figure 96 HEDP case 2 energy storage sizing Simulink model

A similar sizing strategy to the one presented in Case 1 is also used for Case 2. However, this time the energy storage is being sized so that it can produce the required power during the cruise phase, whilst the twin engines are used for the demanding take-off, climb, and landing phases. Table 28 summarises these sizing factors for the engines and the energy storage devices. It is clear that the required maximum energy of the energy storage system will have an enormous effect on the size of these devices.

Table 28 Case 2 GTA and Energy Storage sizing factors

Variable	Value	Units
GTAs Power Output (2 engines)	4300	kW
Energy Storage Power Output	3350	kW
Energy Storage Maximum Energy	52.4	GJ
Energy Storage Charging Power	185	kW

The power output values mentioned in the table above can also be seen in Figure 97. The red line represents the output power of the two GTAs who are being used in full power during the take-off and almost half power during the descent, landing and taxi phases.

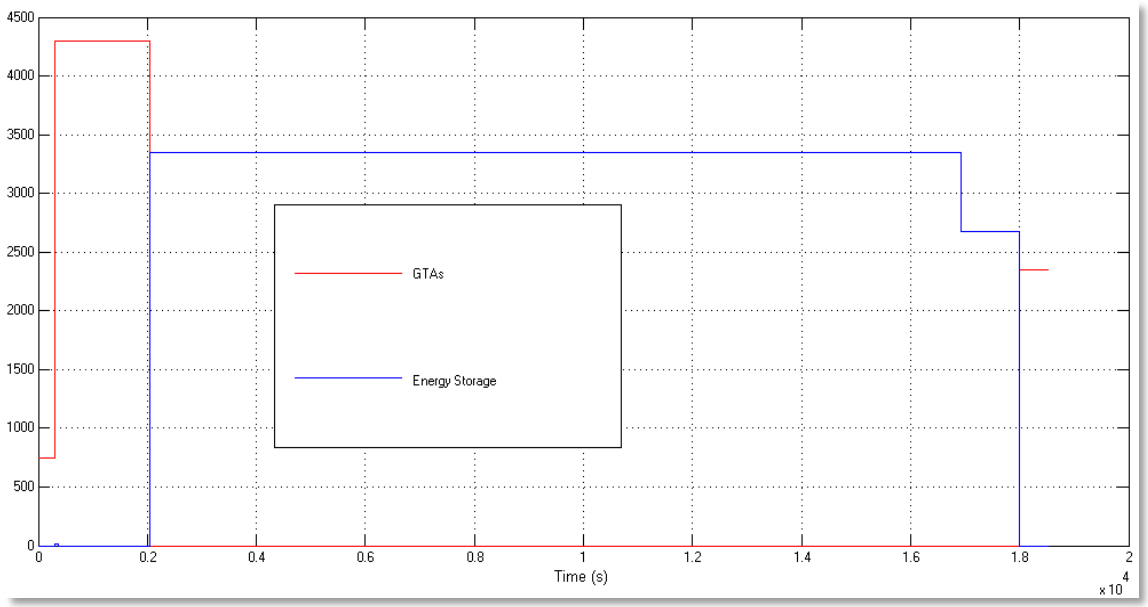

Figure 97 Case 2 GTAs (red line) and Energy Storage (blue line) power output (kW) with time (s)

In case 2 the energy storage system is assumed to be fully charged in the beginning of the flight, whilst it is fully discharged when the aircraft will be landing. This tactic creates several issues; firstly, the batteries will have to be recharged again before the next flight. This could take several minutes or hours making this choice as impractical. Depending on the cost another option will be the complete replacement of the batteries with new fully charged ones. Another issue will be the Depth of Discharge (DoD) of these batteries. Typically, batteries' life expectancy highly depends on their DoD levels. 100% DoD (battery completely empty) is really harmful for their life expectancy. Lower values of DoD could increase their lifetime but also increase the weight of these devices. The following figure shows the SoC of the energy storage system in Case 2:

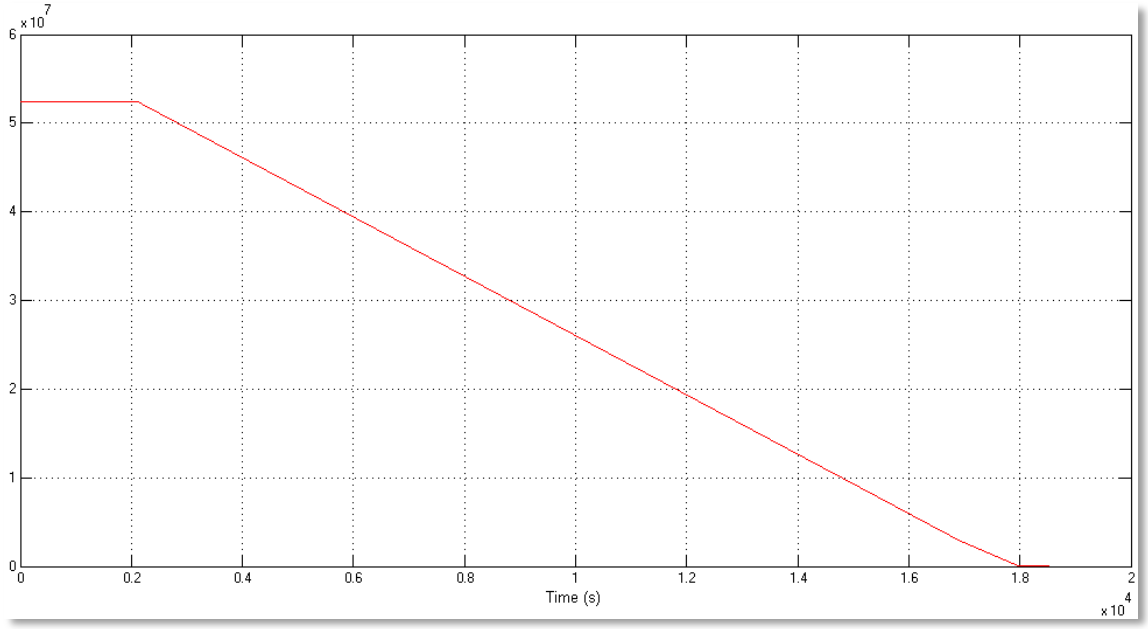

Figure 98 Case 2 Energy Storage State of Charge (SoC) in kJ with time (s)

Table 29 indicates the weight of several energy storage technologies in a configuration similar to the universally all electric aircraft investigated in Case 2. Li-air technology seems the preferable choice in terms of weight this time. Nonetheless, the energy storage system will still weigh almost 20 tonnes even in the best case scenario. This added weight is unacceptable for an aerospace application.

Table 29 Case 2 Energy storage technology sizing values

Technology	Sizing Restriction	Mass (kg)
Li-ion (SOTA)	Energy	72840
Li-ion (future)	Energy	36420
Li-air	Energy	19420
Li-sulphur	Energy	29130
Supercapacitor (future)	Energy	291300

Such a configuration does not seem feasible at least with the assumptions being made in this research study. Table 30 proves the infeasibility of this concept where a total weight of around 22 tonnes is estimated for such a configuration. Case 2 does not bring any weight benefits for the weight of the electrical components involved, however, it offers some benefits that are difficult to be quantified at this stage. Apart from the obvious fuel burn benefits during cruise, the optimisation of the engines for the take-off phase would increase the efficiency of these GTs and consequently reduce the fuel burn even further. Noise and emissions reductions will also be significant gains of such architecture.

Table 30 Summary of Case 2 components' weight

Component	Unit Mass (kg)	Qty.	Total Mass (kg)
Turboshaft Engines	1026	2	2052
Generators	134.9	2	269.8
Cryo-cooler	294.8	1	294.8
Energy Storage	19420	1	19420
Total System's Weight			**22036.6**

In this study a maximum specific energy value of 750 Wh/kg has been assumed for the battery technologies under investigation. However, in similar studies more optimistic energy density values up to 2000 Wh/kg have been assumed by several companies and institutions (Isikveren et al., 2012). Figure 99 demonstrates the effect that specific energy assumptions have to the weight of the battery packs in a configuration similar to the one described in Case 2. The optimistic assumption of 2000 Wh/kg could save up to 12.095 tonnes to the overall weight of the architecture under consideration.

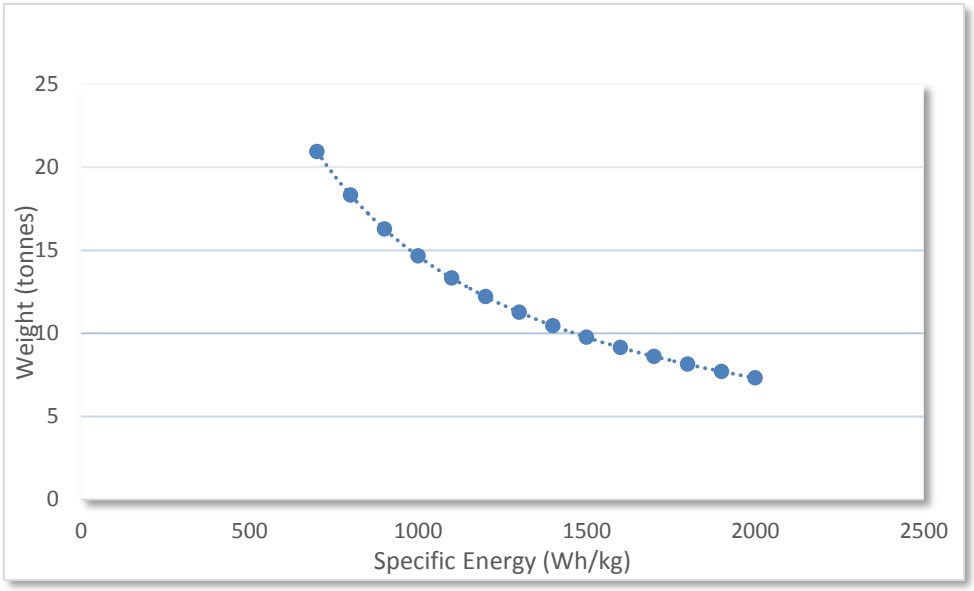

Figure 99 Weight of the battery system vs. specific energy assumptions for Case 2 configuration

Generally, it can be seen that the relationship between specific energy and overall weight of the battery system is not linear as one might think. A more exponential trendline can be noticed, where improvements of specific energy values higher than 1300 Wh/kg do not affect the overall weight of the system to the same extend as they do in the range of 700-1300 Wh/kg.

It is becoming clear that fully electric (battery-powered) configurations for aircraft of similar range to the DEAP one are too heavy to be realised. Possibly, in aircraft of smaller range and minimum power requirements this concept could become feasible. Especially, if the optimistic targets of future advanced battery systems of energy density higher than 1300 Wh/kg could be met.

Case 3: Use of Energy storage as a supplementary power unit source

In this third choice energy storage would play a more secondary but still important role. The idea behind this case is again to design engines of a "specific purpose". The GTs will be optimised for the cruise phase, whilst the deficit in required power demand during the take-off and climb phases will be covered by the energy storage subsystem. This case is a modification of SUGAR Volt conceptual design developed by Boeing and presented in the

Introduction Chapter (1.2.2). In this conceptual configuration one of the two engines could be switched off during cruise increasing the fuel, emissions, and maintenance cost benefits. The switched-off engine could also be altered from flight to flight increasing their life expectancy and reducing their maintenance costs.

Table 31 summarises the required power ratings for the GTAs and the energy storage mechanisms in Case 3. The twin engines are specifically sized so that one of them would be enough to deal with the cruise power requirements. The energy storage is sized to provide the additional required power during take-off and climb or any other dynamic requirement of the whole mission (i.e. landing, emergency cases).

Table 31 Case 3 GTA and Energy Storage sizing factors

Variable	Value	Units
GTAs Power Output (2 engines)	3820	kW
Energy Storage Power Output	1000	kW
Energy Storage Maximum Energy	0.464	GJ
Energy Storage Charging Power	185	kW

The Simulink model of this case is similar to the one presented in Case 2. The main difference is the power outputs of the several components throughout the whole mission. These can be seen in Figure 100 where one of GTAs is being used for the whole mission, whilst the second GTA is switched off during cruise, descent, and landing flight phases. On the other hand, energy storage is sized so that it can provide the extra required power during take-off and landing phases. Both the engines and the energy storage devices are slightly oversized to deal with the requirements of the cooling system.

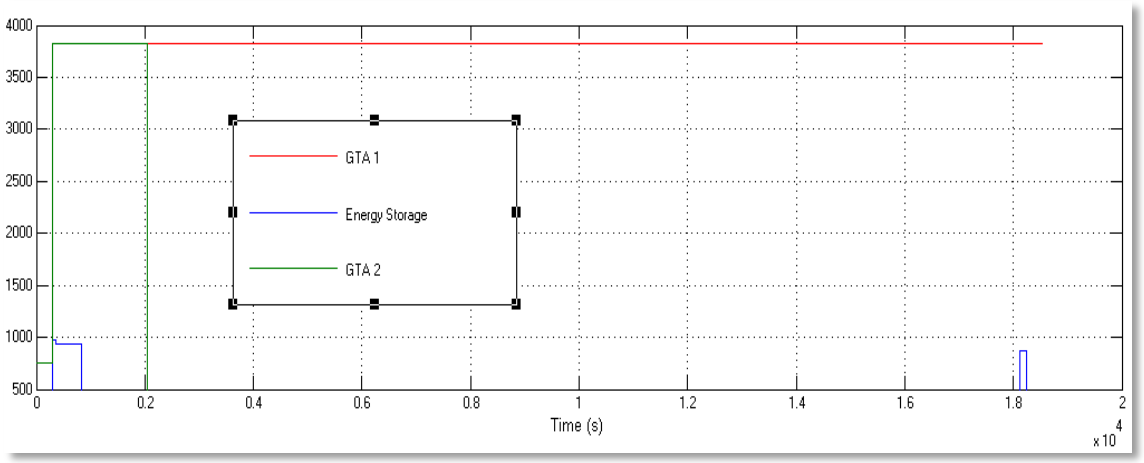

Figure 100 Case 3 GTA 1 (red line), GTA 2 (green line) and Energy Storage (blue line) power output (kW) with time (s)

The energy storage is assumed to be fully charged in the beginning of the flight. During cruise the GTA is providing enough energy to recharge the batteries, while the landing power requirements are lasting for a short period of time that do not practically affect the SoC of the energy storage subsystem. By the end of the whole mission, batteries are again fully charged and ready for the next flight. The following figure demonstrates the SoC of the energy storage system in Joules for the Case 3 of this section.

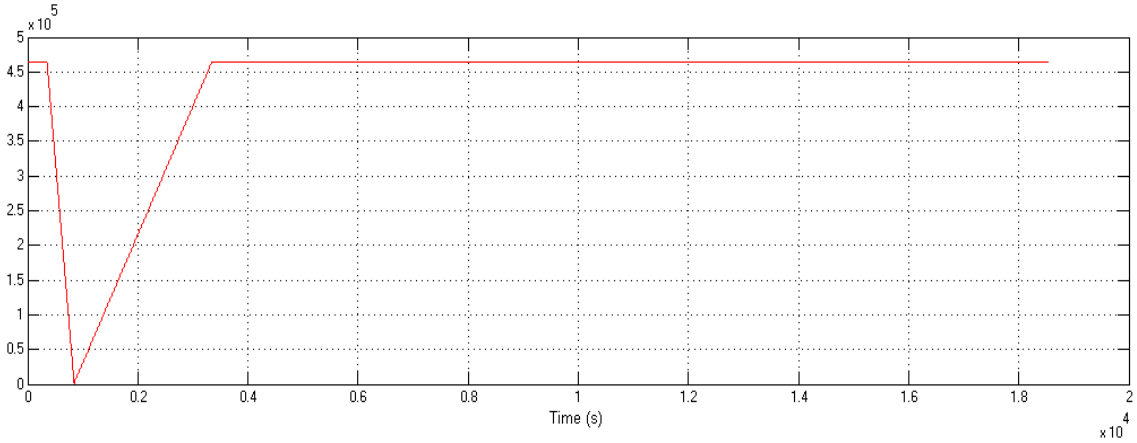

Figure 101 Case 3 Energy Storage State of Charge (SoC) in kJ with time (s)

The preferable energy storage technology in terms of weight is again estimated via the Simulink submodel presented in Figure 94. In the Case 3 study, Li-sulphur battery technology is proved to be the most lightweight choice adding to

the system only 258 kg. On the other hand, Li-air technology that seemed to be the ideal option for Case 2 weighs significantly more (~1430kg) mainly because of its anticipated specific power. This technology is the only one that specific power is the decisive sizing factor instead of specific energy which dictates the weight of the rest of energy storage technologies. This proves that an exclusive look on the energy density values of future energy storage trends could lead to misleading results. Table 32 sums up the mass of the energy storage technologies under investigation for Case 3.

Table 32 Case 3 Energy storage technology sizing values

Technology	Sizing Restriction	Mass (kg)
Li-ion (SOTA)	Energy	645
Li-ion (future)	Energy	322.5
Li-air	Power	1429
Li-sulphur	Energy	258
Supercapacitor (future)	Energy	2580

In Case 3 the estimated weight of energy storage does not seem to affect the feasibility of the conceptual design. On the contrary, it is one of the most lightweight components of the whole electric system. Table 33 summarises the weight of all the components involved in this study. The overall system's weight is less than 3 tonnes and even lighter than Case 1 configuration. Besides, this configuration has a comparable weight to a more conventional architecture (no energy storage involved) because the added weight of energy storage system is compensated by the expected weight reduction of the GTAs and the cooling system. More specifically, a configuration for the DEAP aircraft with two GTAs and no energy storage involved will weight 2623.5kg, almost 100kg less than Case 1, but 20 kg heavier than Case 3 configuration.

Table 33 Summary of Case 3 components' weight

Component	Unit Mass (kg)	Qty.	Total Mass (kg)
Turboshaft Engines	914	2	1828
Generators	120.9	2	241.8
Cryo-cooler	277.9	1	277.9
Energy Storage	258	1	258
Total System's Weight			**2605.7**

Case 3 combines the concepts of distributed propulsion, superconductivity, and novel flight cycles in the most efficient way in terms of weight. Furthermore, the fact that GTAs are sized for a specific phase of the mission (i.e. cruise) frees the design approach of the engines from take-off power requirements, possibly making their optimisation a simpler procedure. Hence, efficiency benefits are expected to add up to the already estimated weight profits.

6.2.4 Final Remarks

In the previous section three different cases of HEDP configurations with energy storage were explored in terms of weight. The first case investigated the use of energy storage as the main power source during take-off, whilst the whole network also included a single GTA as the main prime mover during the rest of the flight mission. Case 2 was based on the idea of a battery-powered aircraft where battery packs are used as the main propulsion power source during cruise. Finally, a more conservative use of energy storage (as a "boost power unit") was investigated in Case 3 where energy storage systems are mainly used to secure the constant function of the GTAs during the whole mission. Case 1 and 3 proved to be competitive configurations compared to similar HEDP architecture where no use of energy storage will be made. Figure 102 demonstrates a weight comparison between the various components of the network for Cases 1, 3, and a hybrid DP configuration without any energy storage in use. Case 2 was not included in this comparison since the weight of

energy storage and consequently of the whole network is around 20 tonnes heavier, thus no useful comparison could be made at this stage.

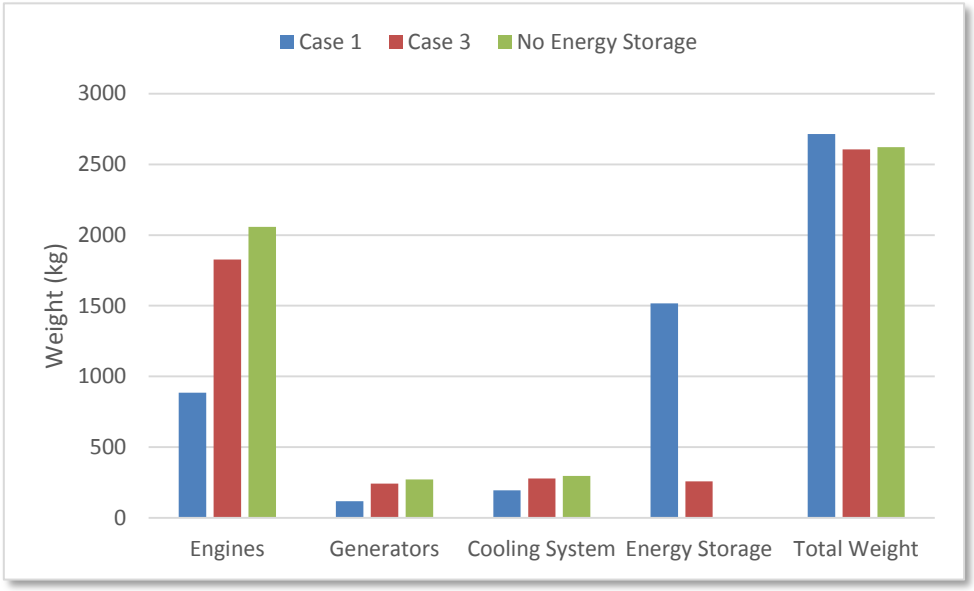

Figure 102 Overall Weight comparison for the different cases

6.3 Sensitivity Study for Hybrid Configurations for aircraft of different sizes

The extension on different aircraft sizes was problematic due to the uncertainty of the mission profile of different aircraft implementing the HEDP concept. It is really challenging to accurately compare and contrast the thrust rating of a jet engine with the power rating of the turboshaft engines potentially used in a HEDP configuration. Such a comparison could lead to misleading results as these two quantities are not equivalent. In the distributed propulsion concept the engines will be rated by how much power they will need to deliver to the propellers (i.e. motor-driven fans). In a conventional "jet engine configuration", the propulsive power of the engine is decided using the following equation:

$$P = F\frac{d}{t} \tag{6-2}$$

Power (P) is the force (F) needed to drive an item over a distance (d) divided by the time (t). In a jet aircraft this force is equal to the thrust produced by the engines, hence:

$$P = T * v \quad \textbf{(6-3)}$$

However, in the HEDP cases turboshaft engines will be used instead of turbojets. In order to decide the required mission power of each reference aircraft a similar strategy to the one being used in Chapter 5 will be followed. A value of power demand per passenger will determine the required power of the most important flight phases (i.e. SLS, EoR, Climb, and Cruise). Landing, descent, and taxi phases are typically being determined as a percentage of the cruise power demand (140, 80, and 40 % respectively). In regards to the time length of the flight mission of each aircraft this will be estimated based on the maximum range and speed of each reference aircraft. Only Cases 1 and 3 will be investigated in this section. Case 2 has already been proven significantly heavy for an aircraft of the size of DEAP baseline (short to medium range). As the range and power requirements increase, the required weight for the battery packs will be expected to increase even further enhancing the infeasibility of the whole “Case 2” concept.

6.3.1 Reference Aircraft Mission Profiles

The previous subchapter has shown some of the potential benefits that a hybrid configuration could offer in a short to medium range aircraft. It seems reasonable to extend this study to a vast variety of aircraft with different power requirements and ranges. The same reference aircraft used in Chapter 5.4.1 will also be the reference aircraft models for this chapter, with the exception of Bombardier CRJ-1000 which was substituted with a smaller model of the same company (i.e. CRJ-100) and without the B777 example. This choice of aircraft was based on the idea of exploring a wide range of mission profiles in terms of power required and length. Furthermore, the consistency of the whole study and the investigation of the state of the art and most popular aircraft models were other reasons for this choice. Table 34 summarises the main characteristics of these reference models:

Table 34 Reference Aircraft Main Characteristics

Model	PAX	Range (km)	Speed (km/h)	Cruise Power (kW)	Cruise time (min)
CRJ-100	50	1800	860	1673	126
DEAP	100	3704	918	3346	242
B737	189	5080	1000	6324	304
B787	242	14500	950	8098	915
A350	475	14800	945	15894	940
A380	700	15000	945	23422	952

The PAX, Range, and Speed columns were filled based on data found in the literature (www.airlines-inform.com, 2012). The cruise time was calculated using the following equation:

$$Cruise\ time\ (\min) = \left(\frac{Range}{Speed}\right) * 60 \quad \textbf{(6-4)}$$

The duration of the rest of the flight cycles was assumed to be the same as the DEAP baseline aircraft. Slight changes on the duration of each flight phase might occur but for reasons of simplicity these have been ignored. Table 34 only includes the cruise power requirements of each aircraft. However, for every phase of the reference aircraft the following set of equations has been used:

$$SLS\ Power\ (kW) = 86.18 * PAX \quad \textbf{(6-5)}$$

$$EOR\ Power\ (kW) = 85.78 * PAX \quad \textbf{(6-6)}$$

$$Climb\ Power\ (kW) = 38.16 * PAX \quad \textbf{(6-7)}$$

$$Cruise\ Power\ (kW) = 33.46 * PAX \quad \textbf{(6-8)}$$

The constants in the equations above have been estimated using the DEAP aircraft power requirements per phase and per passenger. This might seem as a simplistic method to calculate the power requirements of each aircraft but even in the conventional configurations the thrust requirements of the main engines change linearly with the number of passengers as can be seen in Figure 103. There is no reason to believe that this would be any different for a HEDP configuration.

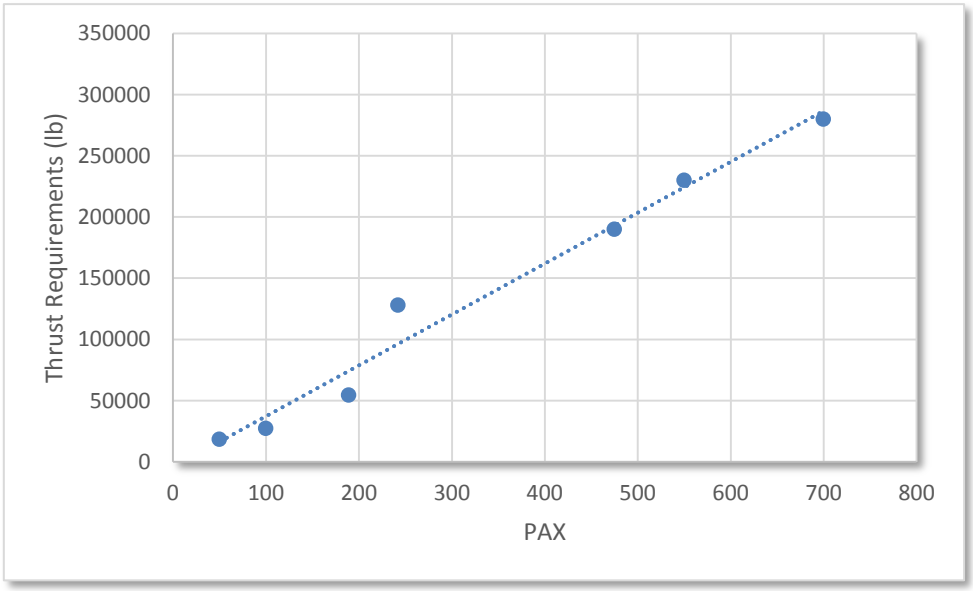

Figure 103 Main engines' thrust ratings vs number of passengers in the reference aircraft

For the remaining parts of the flight the required power was estimated based on the cruise power requirements and by using the following equations:

$$Descent\ Power\ (kW) = 0.8 * Cruise\ Power \quad \textbf{(6-9)}$$

$$Landing\ Power\ (kW) = 1.4 * Cruise\ Power \quad \textbf{(6-10)}$$

$$Taxiing\ Power\ (kW) = 0.4 * Cruise\ Power \quad \textbf{(6-11)}$$

Using all the aforementioned information the mission profile of each aircraft was estimated. Figure 104 combines the mission profiles of all five reference aircraft in one graph. From the really short range example of CRJ-100 to the biggest aircraft currently in service (A380) a weight assessment of hybrid configurations will be presented in the following section.

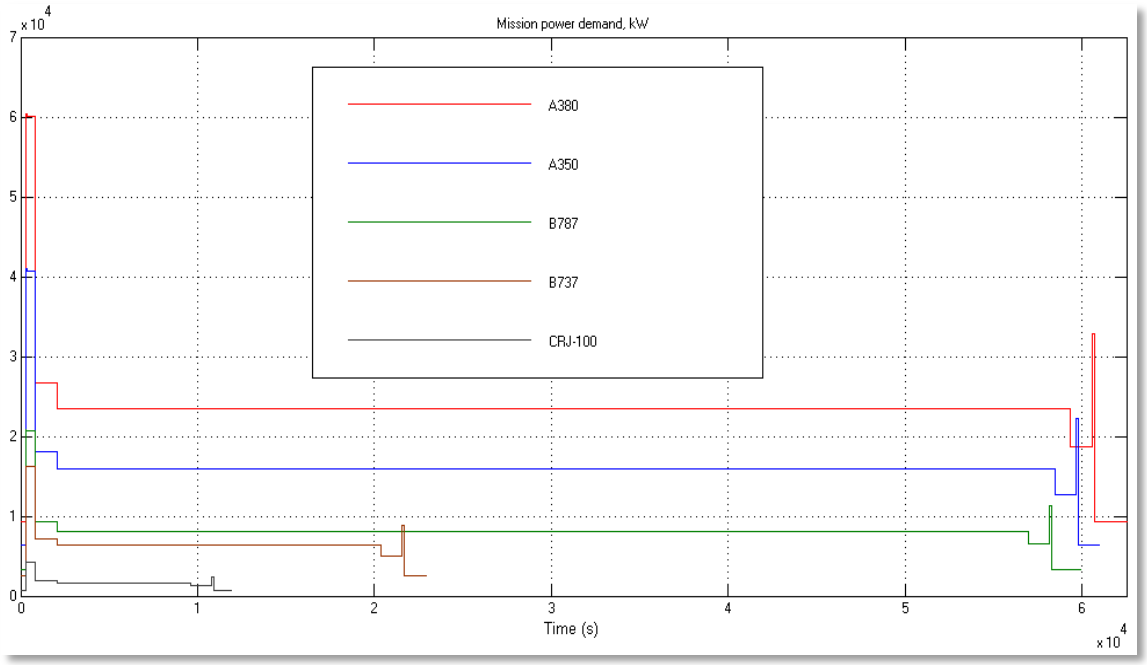

Figure 104 Mission Profiles of the reference aircraft

6.3.2 Results and comments

As it was mentioned before only Cases 1 and 3 of 6.2.3 will be included in this sensitivity study since Case 2 (i.e. use of energy storage during cruise) has already been proven infeasible even for a short range aircraft such as the DEAP aircraft. A weight comparison between configurations with and without energy storage will be carried out for each aircraft separately, whilst an overall comparison will conclude this section.

- *Bombardier CRJ-1OO*

The present aircraft was selected as an example of a really short range aircraft that could benefit by the use of energy storage to implement novel flight cycles which could increase the efficiency and reduce the costs (fuel, maintenance etc.) of future hybrid architectures. Table 35 sums up the mass of different energy storage technologies used in an aircraft similar to CRJ-100 for the hybrid/electric configurations of Cases 1 and 3. Note that for both cases the engines' power output was assumed to be 1700 kW (single engine for Case 1 and two identical engines 1700 kW each for Case 3).

Table 35 CRJ-100's Energy storage technology sizing values

Technology	Sizing Restriction (Case 1)	Mass (kg) (Case 1)	Sizing Restriction (Case 3)	Mass (kg) (Case 3)
Li-ion (SOTA)	Energy	2224	Energy	756.2
Li-ion (future)	Energy	1112	Energy	378.1
Li-air	Power	3857	Power	1314
Li-sulphur	Energy	889.6	Energy	302.5
Supercapacitor (future)	Energy	8896	Energy	3025

The table above shows that Li-sulphur seems to be the ideal option in terms of weight. However, future improvements in Li-ion technology could create competitive products that might be preferable due to the maturity and better understanding of this technology. Notwithstanding other criteria, Li-sulphur sizing values will be used in the following sizing study of CRJ-100 example. Furthermore it should be stated that the power requirements for the energy storage mechanisms was 2700 and 920 kW for Case 1 and 3 respectively. Finally, the maximum energy capacity was 1.60 GJ for the Case 1 configuration and 0.544 GJ for Case 3.

Table 36 Summary of CRJ-100 components' weight

Component	Mass (kg) (case 1)	Mass (kg) (case 3)	Mass (kg) (No E.S.)
Turboshaft Engines	418.4	836.8	1049
Generators	57.17	114.34	142.34
Cryo-coolers	133	186.3	209.3
Energy Storage	889.6	302.5	-
Total System's Weight	**1498.17**	**1439.94**	**1400.64**

The above table shows that the hybrid/electric configurations are actually weight neutral in the case of CRJ-100 aircraft size. However, it should be noted that the novel hybrid flight cycles of Case 1 and 3 could offer extra benefits that cannot be easily quantified in these preliminary studies. Fuel consumption, noise levels, emissions, and maintenance costs will all decrease in the case of hybrid architectures. The option of hybrid/electric aircraft in case of a short range aircraft such as CRJ-100 and DEAP aircraft seems to be an attractive and viable option for the next aircraft generations at least based on the current assumptions for future energy and power densities of energy storage mechanisms.

- *Boeing 737*

Although the feasibility of these novel flight cycles with energy storage use seems a rather beneficial alternative for the short range aircraft, it is interesting to investigate their viability for medium range aircraft. In this category Boeing's 737 is a representative example. For B737 Case 1 a 6.6 MW GT has been used, whilst two 6.8 MW engines were assumed for Case 3 example. This led to energy storage power requirements of 9.7 and 2.75 MW respectively in order the power demands to be satisfied at all flight phases of the mission in both Cases. The following table presents the anticipated mass of the energy storage mechanisms under investigation:

Table 37 B737's Energy storage technology sizing values

Technology	Sizing Restriction (Case 1)	Mass (kg) (Case 1)	Sizing Restriction (Case 3)	Mass (kg) (Case 3)
Li-ion (SOTA)	Energy	8201	Energy	1946
Li-ion (future)	Energy	4101	Energy	973
Li-air	Power	13860	Power	3929
Li-sulphur	Energy	3280	Energy	778.4
Supercapacitor (future)	Energy	32800	Energy	7784

It should be noted that maximum energy capacities of 5.9 and 1.4 GJ were required for Case 1 and Case 3 battery options. Once again Li-sulphur was found to be the lightest option. For Case 3 future Li-ion technology could also be used without a severe weight penalty.

Table 38 summarises the components' weight for the hybrid and more conventional configurations of B737 type of aircraft. This time Case 1 weighs almost half a tonne more than the other two versions. The use of energy storage as a supplementary power unit during take-off and landing phases (Case 3) gives a slight weight penalty of 40kg for the medium range example of B737 type of aircraft. This however will be counteracted by the anticipated fuel and emission benefits described earlier in this study.

Table 38 Summary of B737 components' weight

Component	Mass (kg) (case 1)	Mass (kg) (case 3)	Mass (kg) (No E.S.)
Turboshaft Engines	1564	3222	3850
Generators	200.05	412.2	487
Cryo-coolers	258.3	371.2	406.8
Energy Storage	3280	778.4	-
Total System's Weight	**5302.35**	**4783.8**	**4743.8**

It is becoming clear that if the distributed propulsion will indeed be chosen as the way forward in the next generation aircraft, energy storage could play an important role further enhancing the benefits of such a configuration at least for the short to medium range aircraft models. The remaining reference aircraft will investigate the viability of the concept for the longer range aircraft that are currently dominating the air traffic (i.e. B787, A350, and A380).

- *Boeing 787*

Boeing's 787 aircraft has already been presented in detail during the previous sections of this research study as being the most representative example of MEA. The electric network of this aircraft consists of state of the art electrical components. Further electrification of this type of aircraft is anticipated and the proposed configurations would be an important step towards this direction.

In order the mission profile of such an aircraft to be satisfied at all times, a 8.4 MW GTA was chosen for the Case 1 configuration and two GTAs with power rating of 8.5 MW each were used for the Case 3 B787 design. Table 39 presents the estimated mass for the energy storage mechanisms in an aircraft similar to the "Dreamliner" example. Battery packs of 12.5 and 4 MW were required for Case 1 and 3 respectively. The energy capacities of these two energy storage subsystems were 7.7 and 2.04 GJ and were the sizing

restriction factor for all the cases but the Li-air battery which was sized based on the power requirements.

Table 39 B787‘s Energy storage technology sizing values

Technology	Sizing Restriction (Case 1)	Mass (kg) (Case 1)	Sizing Restriction (Case 3)	Mass (kg) (Case 3)
Li-ion (SOTA)	Energy	10700	Energy	2836
Li-ion (future)	Energy	5352	Energy	1418
Li-air	Power	17860	Power	5714
Li-sulphur	Energy	4281	Energy	1134
Supercapacitor (future)	Energy	42810	Energy	11340

Li-sulphur technology is again the most lightweight option and especially for the Case 1 configuration seems to be the ideal technology in terms of weight. It is important to note that if energy density was the only factor under investigation, then Li-air battery would have been almost two times lighter than the Li-sulphur equivalent. Hence, if these batteries could be designed in a more efficient way in terms of power density (probably at a slight expense of energy density limits) a more competitive Li-air product could be designed.

The list of the components’ weight in the 787 type of aircraft can be seen in Table 40. The difference in overall weight between Case 1 concept and the other two designs starts to grow. Although Case 1 involves fewer components the scalability of the energy storage subsystem creates a heavier overall network. On the other hand, Case 3‘s configuration remains competitive in terms of weight with a distributed propulsion design with no energy storage in place.

Table 40 Summary of B787 components' weight

Component	Mass (kg) (case 1)	Mass (kg) (case 3)	Mass (kg) (No E.S.)
Turboshaft Engines	1985	4016	4918
Generators	250.6	506.6	612.2
Cryo-coolers	291.3	415.8	461.7
Energy Storage	4281	1134	-
Total System's Weight	**6807.9**	**6072.4**	**5991.9**

- *Airbus A350*

The last two reference aircraft are the most demanding in terms of power and range. The latest model being launched by Airbus is the A350 aircraft which according to equations (6-5) and (6-8) will require around 40 and 16 MW of power during the take-off and cruise phase respectively. Thus, the engines power rating was accordingly set to 16 and 16.2 MW for the two cases leading to energy storage power demand of 25 (Case 1) and 8.6 (Case 3) MW. Table 41 highlights the derived weight of the various energy storage alternatives.

Table 41 A350's Energy storage technology sizing values

Technology	Sizing Restriction (Case 1)	Mass (kg) (Case 1)	Sizing Restriction (Case 3)	Mass (kg) (Case 3)
Li-ion (SOTA)	Energy	22240	Energy	6297
Li-ion (future)	Energy	11120	Energy	3148
Li-air	Power	35710	Power	12290
Li-sulphur	Energy	8896	Energy	2519
Supercapacitor (future)	Energy	88960	Energy	25190

It is no surprise that Li-sulphur is again the lightest energy storage option for both configurations. However, the almost 9 tonnes added in Case 1 study might prove to be a prohibitive number. It is also interesting to point out that if current technology was to be used for these novel designs then more than 22 tonnes of Li-ion battery would be needed in Case 1. This shows how essential the technology improvements are for the feasibility of these concepts.

The following table compares the weight of the components for aircraft sizes similar to A350 for the two novel configurations using energy storage (Cases 1 and 3) as well as for a superconducting distributed propulsion version (no energy storage) of such an aircraft.

Table 42 Summary of A350 components' weight

Component	Mass (kg) (case 1)	Mass (kg) (case 3)	Mass (kg) (No E.S.)
Turboshaft Engines	3762	7616	9612
Generators	454.8	920	1142.2
Cryo-coolers	403.1	580.2	656.1
Energy Storage	8896	2519	-
Total System's Weight	**13515.9**	**11635.2**	**11410.3**

In this case the version with no energy storage is again the lighter configuration, with more than 200 kg difference to the third case design option. On the other hand, the use of energy storage during take-off in a one engine configuration (Case 1) is almost two tonnes heavier, a number that cannot be neglected. As the range and size of the aircraft increases, the weight difference between Case 1 and the other two options rises accordingly.

- *Airbus A380*

The last reference aircraft is also the largest aircraft currently in service. Its power demand reaches the 60 MW range during take-off and the 23.5 MW during cruise. Following the same strategy as in the previous examples the energy storage required power was found to be 36.6 MW for the Case 1 model and 12.4 MW for the Case 3 design option. Hence, the required power output in Case 1 is almost three times higher than in Case 1, a trend that was observed in almost every reference aircraft being investigated in this section. An energy storage mass summary of the different technologies for both cases can be found in the following table.

Table 43 A380's Energy storage technology sizing values

Technology	Sizing Restriction (Case 1)	Mass (kg) (Case 1)	Sizing Restriction (Case 3)	Mass (kg) (Case 3)
Li-ion (SOTA)	Energy	32250	Energy	9091
Li-ion (future)	Energy	16120	Energy	4545
Li-air	Power	52290	Power	17710
Li-sulphur	Energy	12900	Energy	3636
Supercapacitor (future)	Energy	129000	Energy	36360

Almost 13 tonnes of energy storage mechanism will be required in a Case 1 configuration even in the best case scenario. This is a value that at first glance seems prohibitive for an aerospace application. Li-sulphur battery, as in the rest examples, is the most promising technology for a long range aircraft such as A380. Just less than one tonne heavier is the Li-ion technology based on the optimistic future predictions for the Case 3 conceptual design.

Table 44 Summary of A380 components' weight

Component	Mass (kg) (case 1)	Mass (kg) (case 3)	Mass (kg) (No E.S.)
Turboshaft Engines	5585	11264	14148
Generators	656.6	1323.4	1635
Cryo-coolers	494.2	713.9	806.9
Energy Storage	12900	3636	-
Total System's Weight	**19635.8**	**16937.3**	**16589.9**

The table above sums up the components' weight for the last reference aircraft. Case 1 is this time more than three tonnes heavier than a configuration with no

energy storage in use. The latter is also 400 kg lighter than the Case 3 design option which however can still be considered as a competitive alternative option in terms of weight.

6.3.3 Final Remarks

In this section the feasibility in terms of weight of novel hybrid configurations using energy storage was investigated. The study had two main targets: firstly to decide which energy storage technology is the most promising in terms of weight for hybrid configurations such as the ones described in 6.2 and secondly to explore if the use of energy storage either as the main power unit during take-off (Case 1) or as a supplementary power unit in a two engines configuration (Case 3) are feasible design concepts for a wide range of aircraft.

In regards to the first target, Li-sulphur was the clear winner compared to the rest of energy storage options. This technology was estimated to be the most lightweight option in every single aircraft (short or long range) for both cases. Only future Li-ion batteries could potentially be competitive products for short to medium range aircraft especially if their technology maturity is taken into consideration. Furthermore, the cyclability of Li-ion batteries is significantly higher than the Li-sulphur case, a fact that makes their option a lot more attractive at least in regards to the cost. Unless future Li-S life cycles do not improve significantly then Li-ion technology might be the preferable choice especially in Case 3 configurations where the weight difference was not that profound. Li-air technology, which by many has been considered as one of the most promising battery technologies of the future, suffers from a low specific power that restricts its size in most of the cases instead of the specific energy factor. However, if higher values of specific power than the ones assumed in this study could be obtained then this technology could become the ideal candidate for these hybrid configurations. Nonetheless, Li-air technology life expectancy is also a barrier in using this type of batteries in an aerospace application.

An overall weight comparison of the system for each reference aircraft implementing the three different novel configurations is demonstrated in Figure

105. For short to medium range aircraft (i.e. CRJ-100, DEAP, B737) all three design options present comparable systems in terms of weight and further sensitivity studies concentrating on different factors need to be carried out. On the other hand, as the take-off power demand increases (i.e. B787, A350, and A380) Case 1 starts to weigh significantly more than the other two versions. Any other benefits that such a configuration could offer will most probably be met by the Case 3 design option.

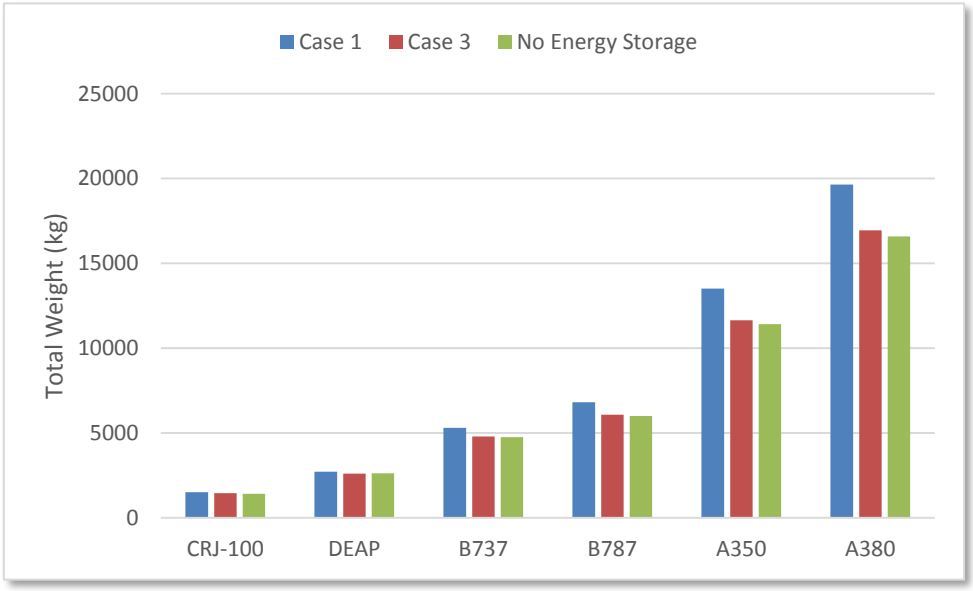

Figure 105 Weight Comparison between Case 1, Case 3, and a configuration without energy storage for all the reference aircraft

It is also important to observe how the weight of the energy storage differs with the power demand of each aircraft. Figure 106 demonstrates how the weight of Li-sulphur batteries increases with the SLS power demand as we go from smaller to larger aircraft (i.e. CRJ-100 to Airbus A380). In both cases an almost linear relationship can be observed. However, in Case 1 the angle of this linear trendline is a lot sharper revealing the main reason why Case 1 is less competitive in terms of weight in the longer range aircraft. Similar trends could be seen in every other energy storage technology, but Li-sulphur was chosen as the most promising one of all.

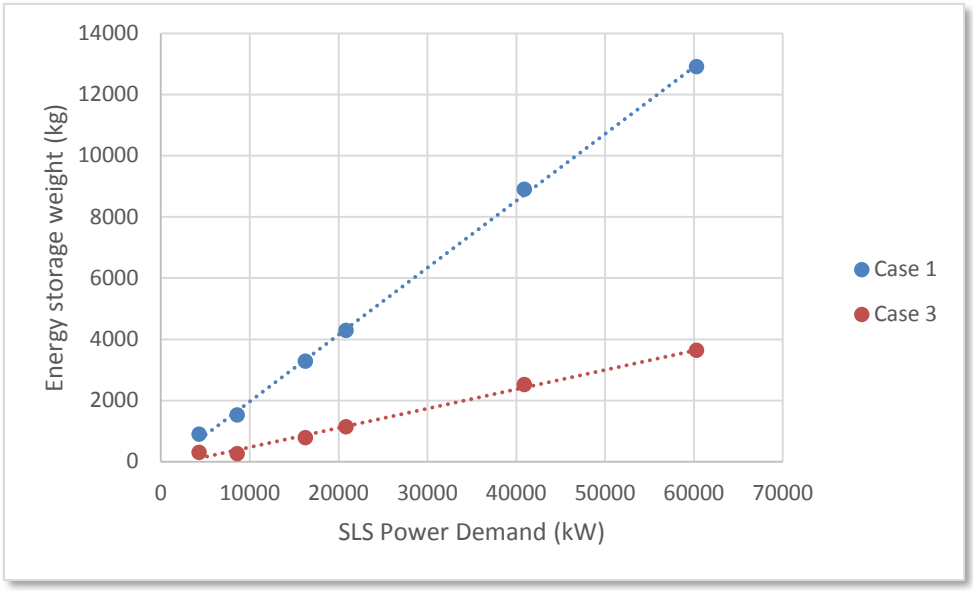

Figure 106 Li-sulphur weight vs. reference aircraft SLS power requirements

To sum up, this study showed that a hybrid configuration implementing the superconducting distributed propulsion concept with extensive use of energy storage could be feasible in the medium term future (i.e. 2035 timeframe). Li-sulphur has proven to be the most promising technology in terms of weight for almost all the proposed configurations and aircraft. Supercapacitors on the other hand seem to be too heavy to be considered as a main power unit in these designs. Furthermore, the concept of an all-electric aircraft which will be using batteries as the main power source during cruise, at this point and with the relatively conservative assumptions been made for the 2035 timeframe, has been found significantly heavier than the rest of the conceptual designs. Finally, although in the medium to long rage aircraft the use of energy storage as a main power source during take-off is clearly not the preferred option in terms of weight, this is not the case in shorter range aircraft similar to the DEAP baseline aircraft. Hence, other factors such as fuel savings, emissions and noise reductions, maintenance costs etc. need to be explored in more depth so that the ideal architecture for each aircraft to be decided. This should be combined with a more detailed sensitivity study for the energy storage options which will include factors such as DoD, life cycles, and safety.

This chapter proved the feasibility of hybrid configurations in terms of weight for the majority of the cases. These proposed propulsion systems are attractive for several additional reasons. First of all, the safety of these designs is enhanced mainly due to the various power sources which will be available in the aircraft. Both the GTs and the energy storage should be sized in such a way that they will be able to deal with any possible safety case. The increase in critical components also improves the reliability and redundancy of the whole system. Finally, the flexibility of the whole network is enhanced. The concept behind these proposed designs is the optimisation of each prime mover for a specific function. This will have a direct positive effect on the efficiency of each component and consequently in the emissions (i.e. noise, NOx, fuel consumption) of the whole aircraft.

6.4 Key study Limitations

It is important to emphasise that this study could be used only as a preliminary high TRL investigation of the feasibility in terms of weight for some novel hybrid configurations. Thus, there are important limitations due to some uncertainty of the assumptions been made but mainly because of the fact that only some aspects of these configurations were investigated. More specifically:

- The **energy storage options review was exclusively focused on the weight** of these components. Other factors that could prove to be equally important in the selection of the ideal energy storage mechanism were not part of this study. Particularly, the cyclability and safety issues of each type of battery could determine the final decision being made. Volume is also an important attribute especially in the case of an aerospace application. In large aircraft where the required power is extremely high, the volume of the batteries could be the main barrier of the whole concept. Also, an aerospace propulsion system is far more sensitive in reliability issues than any other ground based application. The recent examples of Boeing 787 battery issues confirm the need of a highly reliable and safe energy storage mechanism particularly in the cases when the latter is being used as the main power source during

take-off. Nonetheless, weight is still considered as the decisive factor in the feasibility of the whole concept and that is the reason this study is dedicated exclusively on it.

- This study has been based on the fact that future aircraft propulsion systems will adopt the distributed propulsion concept using a fully superconducting network and cryo-coolers as their cooling system. **A weight comparison with a more conventional configuration** similar to the one being used from the majority of the reference aircraft **could have given some useful results**. However, the whole purpose of this chapter was to further explore the possibilities of TeDP configurations and decide on the possible role that energy storage mechanisms could play on these architectures.
- **The additional benefits of using energy storage in these hybrid configurations were not explored.** These include fuel consumption, fuel weight benefits, noise levels, emissions reduction, and maintenance costs. Although important, all these advantages are difficult to be quantified in such an early stage. Nonetheless, it is reasonable to believe that if the weight factor does not block the feasibility of these conceptual designs then most probably these added benefits will enhance the attractiveness of the whole concept.
- **The efficiency deficit of the GTs in the altitude and the EOR safety case** were not clearly taken into consideration. The difference in the air density in altitude somehow offsets the presented asymmetry of the cycle in regards to the GTs power rating. However, the mission profile of each aircraft included the extra power demands in the case of one engine out EOR safety case, whilst both the GTs and the energy storage were slightly oversized in every proposed propulsion system.
- The **limitations of the Simulink models** of the machines (i.e. superconducting generators and cryo-cooler) have already been mentioned. To these we should add the limitations of the battery sizing model itself. The model inputs are varied manually to ensure the battery power and energy capacity can reduce the power requirements by the

generators, reducing their size and cooling requirements. A more robust way of varying these inputs is necessary in the future models. This could facilitate the generation of results in a more time efficient way. Furthermore, other outputs such as volume and life cycles should be included in higher TRL studies.

6.5 Roadmap for Novel Flight Cycles Investigation

In the previous sections several novel hybrid configurations using energy storage were investigated. The majority of hybrid/electric approach proposals in aviation industry are based on conventional configurations at least regarding the propulsion system design. However, it is fair to claim that Turbo-electric Distributed Propulsion (TeDP) concept represents a disruptive technology that requires the synergy of several subsystems and a more integrated approach between the airframe and the propulsion system design procedures. Thus, the aircraft design must be adapted to best capitalise on the potential benefits of this new propulsion system. A simple modification of an existing aircraft design with a novel propulsion system will most probably lead to pessimistic results since no optimisation will be made.

The first step towards the full hybridisation of future aircraft should be the optimisation of the main power sources. The GTs will no longer provide thrust and their new role will be the production of electric power. Hence, new optimised GT architectures need to be designed and in the case of novel cycles their role could be even more specific. The concept behind these hybrid configurations is to optimise each component for a specific function and/or phase of the flight (Malkin and Pagonis, 2015b).

Apart from the traditional GTs option, other power units could be also investigated in these configurations. In Figure 107 an example of a novel HEDP architecture is being presented. The power system is illustrated by a main power bus bar that is supplied by several prime movers such as gas-turbine alternators (GTAs), a Secondary Power Unit (SPU) and energy storage. The role of the SPU will vary depending on the range, power requirements and the

overall architecture being chosen. Different SPU options could be explored such as:

- Reciprocating engines
- Hydrogen Fuel Cells
- Tailored optimised GTs

The GTAs might be either of different sizes or identical and the merits of both options need to be explored. A full performance assessment of all the SPU options could affirm the ideal candidate for each aircraft.

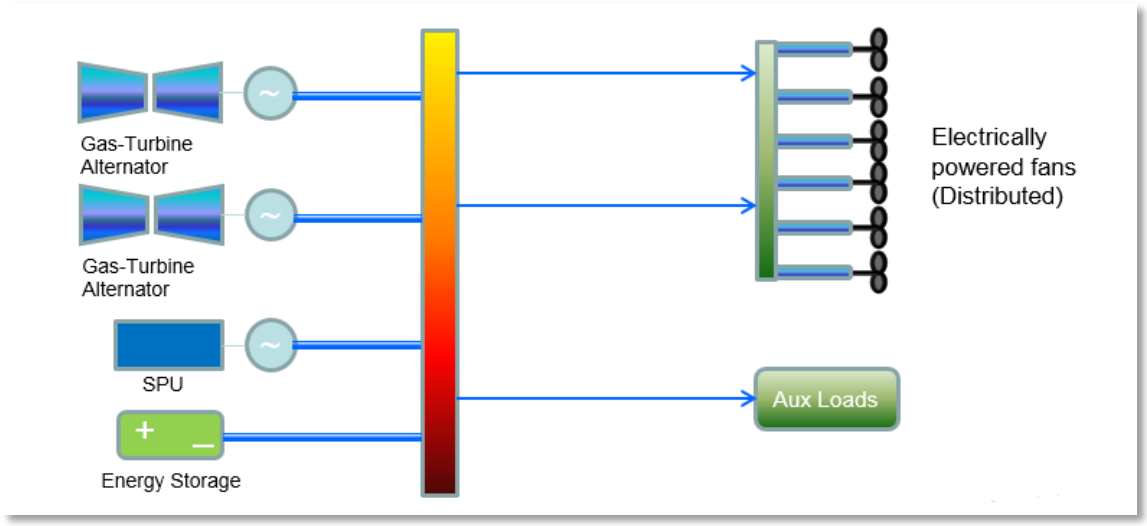

Figure 107 HEDP Architecture Proposal

A full analysis of the flight envelope of each aircraft could identify the potential dynamic requirements of their whole flight cycle. These dynamic requirements could be handled by the energy storage mechanisms in order the rest of the power units to perform more efficiently in a constant power rating. This was basically investigated in the previous sections (6.2-6.3) and its feasibility in terms of weight was confirmed in most of the cases. However, as it was already pointed out a more extensive study of the energy storage mechanisms is necessary since their design procedure is a complicated task that differs depending on the application.

The dynamic analysis of the power requirements of the aircraft power network should be one of the last stages of the novel flight cycles research study. In this

stage different rates of climb and descent could be investigated. Cruising altitude and speed could also be altered to match the propulsion system maximum efficiency. Note that power does not lapse with altitude in the case of electrical machines and hence new criteria need to be met in case of the hybrid aircraft. Finally, the already more electric approach will enhance the use of electric power for phases such as taxiing and for secondary systems such as the ECS, anti-icing, landing gear etc. The benefits of such an electric approach should be clearly pointed out, quantified and combined with the propulsion system hybridisation benefits.

In conclusion future studies of hybrid configurations should focus on the following issues:

- reduce peak power demands of the main prime movers

-efficient management of dynamic requirements of the flight mission

-use of energy recovery at various stages

-varying operating cycles' factors such as cruising altitude, speed, climb and descent rate to further optimise each hybrid configuration

-possibility of electric taxiing without any extra equipment

-increase safety for certain failure modes

7 Conclusions and Future Work

The aerospace industry has been pressured to develop more environmental friendly aircraft designs for the next generation commercial aircraft. Aggressive targets in regards to emissions (i.e. noise, NOx, and fuel consumption) have been set by both American and European institutions. Conventional configurations seem unable to satisfy these optimistic goals; hence there is a general interest in technologies which can be considered disruptive.

Distributed Propulsion (DP) technology is one of the most promising concepts which could make a positive impact on environment in the following years. There are several DP modifications which have been explored throughout the years, but the most beneficial seems to be the Hybrid Electric Distributed Propulsion (HEDP). This HEDP concept is nonetheless associated with various supporting technologies, many of which are still in an early stage of development.

Superconducting technology is considered the main enabler for the whole concept due to the weight and efficiency improvements that could become feasible by the implementation of a fully Superconducting Power Network (SPN) in the propulsion system of such an aircraft. This network will include many novel elements, some of which are still in an embryonic state. The concurrent use of these elements in the same network creates several unknowns in the system design which will require additional and extended experimental work to be fully understood. Moreover, a SPN requires constant cooling to cryogenic temperatures in order to perform according to its full potentials. Several studies have been focused on the optimisation of the cooling system in a HEDP configuration.

7.1 Concluding Remarks

In this project, several aspects of future HEDP configurations have been investigated. First of all, the role of SPNs has been explored looking at the constraints and the potential benefits that such a network could bring in a DP design. The reduced weight of superconducting components is one of the

already well-established characteristics of these networks. In this study, a method of estimating the weight of fully superconducting machines was established and corresponding models were developed and used during the DEAP project. These models were also used in the novel concept of Superconducting Electric Aircraft (SEA) that was investigated in Chapter 5. SEA is a modification of the More Electric Aircraft (MEA) which was proposed as an enabling technology for the extension of MEA concept to aircraft of different sizes. Finally, different HEDP conceptual configurations with enhanced use of energy storage mechanisms were explored in the final chapter of this research study focusing on their feasibility in terms of weight for future aircraft designs. The following concluding remarks were derived from this study:

7.1.1 Superconducting Power Networks (SPNs)

It became clear in the early stages of this research study that it is impossible to model and simulate the performance of a SPN by using conventional modelling strategies and without any further experimental work. The true zero resistance of superconducting DC networks complicates the modelling process, whilst the current sharing in the transmission system of such a network cannot be predicted. The design procedure of an autonomous power network is a complicated task which has not be fully analysed in the recent literature. The hybrid/electric ship is the most recent example of power network designed in a similar way to the HEDP aircraft design. However, even this example does not fully cover the particularities that a SPN brings in the design process. Starting from the basic parameters selection a SPN follows completely different criteria and priorities compared to a more conventional network. Different, novel components for power generation, transmission, protection, and switching will also be present in a superconducting configuration. The concurrent presence of so many novel devices might complicate the performance prediction of such a network but also adds flexibility in the design procedure. This flexibility has been proven both in the SEA and in the HEDP concepts analysed in this research study.

7.1.2 Superconducting Electrical Machines

The vast majority of superconducting machines currently being commercially available have only their rotor primarily made by superconducting materials, whilst a more conventional stator is normally used. However, in a HEDP configuration fully superconducting machines will be required in order to fully capitalise the weight and efficiency benefits of such a type of machines. A Simulink model that can estimate the weight of these machines has been developed for the purposes of this research study as well as for the purposes of the DEAP project. Two different versions of this method have been designed and compared with the NASA weight figures for superconducting machines. The more conservative method could be considered as a pessimistic prediction method for the weight estimation of these machines but its reliability has been verified by the use of these models in the DEAP project weight calculations. Furthermore, conventional environmental screens (i.e. iron and conducting) proved to be either too heavy or too inefficient especially for high power machines. On the other hand, novel superconducting screens might be the solution for these fully superconducting machines.

7.1.3 Superconducting Electric Aircraft (SEA)

A novel concept aiming on further enhancing the already successful More Electric Aircraft (MEA) concept was also proposed in this project. The feasibility in terms of weight of using a superconducting network for the secondary power systems of aircraft of different sizes was explored. Results show that SEA aircraft becomes weight beneficial for electric power requirements over 1.5 MW, whilst it is still weight neutral for electric loads around 1MW (Boeing 787 case). The anticipated further electrification of future aircraft might enhance the attractiveness of SEA concept even further. Besides, SEA designs will also be more efficient, easily scalable, and more fault tolerant than the conventional equivalent versions. Finally, whilst in a MEA approach the use of a SPN might be considered as optional, in a HEDP type of aircraft its use appears to be necessary. The latter is dictated by the over an order of magnitude higher electric power requirements in the case of a HEDP system.

7.1.4 Novel Flight Cycles with Energy Storage

The flexibility of several HEDP configurations using energy storage mechanisms was also investigated in this research study. The use of energy storage as a main prime mover during take-off, as the main power source during cruise, and as a boost supplementary power unit during take-off and climb were considered for a number of different aircraft cases including the DEAP baseline aircraft. Different battery and supercapacitor technologies were considered as potential candidates for such configurations. The study showed that using a battery pack as a boost unit during the demanding phases of take-off and climb seems as the most promising configuration in terms of weight for most of the aircraft sizes. On the other hand, using energy storage during cruise showed some very pessimistic results in regards to the weight feasibility of such a system. Lithium sulphur batteries proved to be the most weight efficient energy storage option in almost all cases explored. Their low cyclability however might give the advantage to future Lithium ion technologies especially for shorter range aircraft cases. Similar to the SEA case, using energy storage in an aircraft propulsion system could bring extra benefits in terms of efficiency, redundancy, and flexibility of the whole aircraft power network.

7.1.5 Key Findings Summary

The key findings of this research study could be summarised as follows:

- Lack of appropriate simulation tool for the steady-state models of a SPN due to the uncertainty of the current splitting in these networks
- Different basic parameters selection in the case of a SPN (higher normal currents which will be easier to handle)
- More than 7% increased overall network efficiency with a superconducting transmission system
- Novel Simulink models to estimate the weight of fully superconducting machines based on the TRV method were developed
- Requirement for a novel type of environmental screen for SMs has been identified since the conventional types (i.e. iron and conducting) are too heavy and/or inefficient

- A superconducting version of a MEA Boeing 787 type of aircraft can be almost two times lighter based on the current technology being used or weight neutral if future technology of conventional equipment is used
- In larger aircraft (i.e. A380 size) the SEA could be more than two times lighter even compared to future technology predictions
- SEA concept becomes weight beneficial when the aircraft electric load demand is around 1.5 MW or higher
- Lithium sulphur technology is the most promising technology in terms of weight for the HEDP configurations investigated here
- An all-electric aircraft proved to be significantly heavier than the rest of the hybrid configurations at least based on the assumptions being made in this study
- The use of batteries as a supplementary power unit during demanding flight phases showed the most promising results in terms of weight for hybrid configurations
- Batteries could also be used as the main power source during take-off in short range aircraft without any weight penalty

7.2 Recommendations for future work

This project investigated several technologies that are still in an early stage of development; hence there is a wide range of activities that can be recommended as future work in this field. In the concluding remarks of each chapter the technology gaps have been identified and suggestions for future work have been pointed out. Some of the areas that seem more essential to be explored will be prioritised in this sub-section.

- **Extensive laboratory work in regards to the superconducting power networks.** It has been pointed out numerous times that superconductivity is the main enabler of the disruptive concepts presented in this research study and form the most promising concepts for future aviation. However, there are several issues related to the use

of these networks. First of all, the uncertainty of their steady-state and dynamic performance. Superconducting DC networks are characterised by their zero resistance which might seem as an ideal case but at least for these preliminary studies it also creates certain unknowns. The current sharing on these networks cannot be predicted and experimental work on this field is urgent. The resistive divider effect that typically splits the current into the several nodes of the network is not present in a SPN. Although early experimental studies (Pei et al., 2012) reported normal current distribution for multi-strand MgB2 wires in an AC system, a superconducting DC network load flow still remains a mystery. Furthermore, superconducting equipment such as SFCLs should be optimised for airborne applications. Also, the protection coordination of these networks is a field that needs extra attention.

- **Cooling system further studies are essential.** The two cooling system options which were presented in the literature section need to be optimised for aerospace applications. Especially the cryo-coolers currently used in the industry have not be designed in the most weight efficient way. Furthermore, the models used for the cryo-coolers' weight estimation for the DEAP project are approaching the limit of their capability. New models are required which will take into account the difference in components efficiency as well as they will predict the mass based on component-level estimations and not overall system considerations (Palmer, Pagonis and Malkin, 2015). Concerning the cryogenic fluid solution a whole different systems' approach is necessary. Issues such as location and volume of the tank, liquid hydrogen production and storage in the airports, and advanced fuel system development are just a few examples of the fields which need additional extensive studies. The first two recommended future studies are strongly related since the feasibility of SPNs highly depends on the existence of an efficient and lightweight cooling system.
- **Components' performance in cryogenic temperatures needs to be fully understood.** Elements such as cryogenic power converters, fully

superconducting machines, and superconducting switching devices need to be widely produced and used in less fault sensitive applications before the 2035 timeframe which has been set as a goal for the next generation aircraft. Furthermore, the interaction between all these novel components needs to be observed in a real network situation.

- **Energy storage more application-specific study is necessary.** The design of a battery system is a complicated task which is more application specific than most people believe. The majority of preliminary studies (including the current one) looking at energy storage devices simply assume a power or energy density value to estimate their weight without taking into account any other characteristics of these systems. Especially when a future technology is being used for these studies, overoptimistic predictions are typically being made and parameters such as safety, life cycles and environmental impact are simply ignored.

REFERENCES

(CAA), C.A.A. (2002) *AIRWORTHINESS INFORMATION LEAFLET* CAA,

Abdel-Fadil, R., Eid, A. and Abdel-Salam, M. (2013) 'Electrical Distribution Power Systems of Modern Civil Aircrafts', *2nd International Conference on Energy Systems and Technologies*, , pp. 201–210.

Abdelhafez, A.A. and Forsyth, A.J. (2009) 'A review of More Electric Aircraft', *13rd International Conference on Aerospace Sciences &Aviation Technology*. Cairo, Egypt.

Adams, C. (2001) A380: 'More Electric Aircraft' *Avionics Today*.

Akimitsu, J. (2001) 'Discovery of MgB2 Superconducting Material (unpublished)', *Symposium on Transition Metal Oxides*.

Alderman, J. (2014) *DEAP QMM3- Airbus Group Work Package 1 Summary*.

Amatucci, G.G., Badway, F. and DuPasquier, A. (2000) 'Novel Asymmetric Hybrid Cells and the Use of Pseudo-reference Electrodes in Three Electrode Cell Characterization', in Nazri, G. A., Thackeray, M. M. and Ohzuku, T. (eds.) *Intercalation Compounds for Battery Materials*. , p. 344.

Ameyogo, G. (2007) *Distributed Propulsion and Future Aerospace Technologies*. Cranfield University.

Ameyogo, G. and Singh, R. (2007) 'Advanced Cycles for Distributed Propulsion', ISABE (ed.)*18th International Symposium on Airbreathing Engines*. Beijing.

Amy, J. (2005) 'Modem, high-converter-populations argue for changing how to design naval electric power systems', *IEEE Electric Ship Technologies Symposium*. Philadelphia, PA: IEEE.

Andersson, G. (2006) *Modelling and Analysis of Electric Power Systems*. Zurich.

Armstrong, M.J., Christine, A.H.R., Blackwelder, M.J. and Rajashekara, K. (2012) 'Propulsion System Component Considerations for NASA N3-X Turboelectric Distributed Propulsion System', *SAE International J. Aerospace*, 5(2), p. 344.

Ashcraft W., S., Padron S., A., Pascioni A., K., Stout W., G. and Huff L., D. (2011) 'Review of Propulsion Technologies for N+3 Subsonic Vehicle Concepts', *NASA technical memorandum*, 2011-21723

AVO (2015) *Transient Motor Starting Analysis*.

Ayre, J. (2014) Lithium-Air Batteries Take Step Forward *EVObsession*.

Baran, M. and Mahajan, N. (2007) 'Overcurrent Protection on Voltage-Source-Converter- Based Multiterminal DC Distribution Systems', *IEEE Transactions on Power Delivery*, 22(1), p. 406.

Barnes, P.N., Sumption, M.D. and Rhoads, G.L. (2005) 'Review of high power density superconducting generators- Present state and prospects for incorporating YBCO windings', *Cryogenics*, 45(10-11), pp. 670–686.

Barraud, G., Thomas, M., Charr, N., Nespoulous, S. and Smaoui, H. (2015) 'Study of Hybrid Electric Propulsion for a Radical Aircraft Concept', *MEA 2015- More Electric Aircraft*. Toulouse, France.

batteryuniversity.com (2015) *BU-205: Types of Lithium Ion*.

Bellis, M. (2015) *History of Superconductors*., *about.com*

Berg, F. and Dodds, G. (2013) *PSAM Aerospace Applications Report*. PSAM Project.

Berg, F., Palmer, J., Miller, P., Husband, M. and Dodds, G. (2015a) 'HTS Electrical System for a Distributed Propulsion Aircraft', *IEEE Transactions on Applied Superconductivity*, 25(3)

Berg, F., Palmer, J., Pagonis, M. and Malkin, D. (2015b) *DEAP D2-2c Superconducting System Model*. Unpublished: Airbus Group.

Biswas, A., Khan, M.E. and Sarker, U. (2013) 'Transient Stability Improvement of a Conventional Power System by Superconducting Fault Current Limiter', *Global Journals of Researches in Engineering*, 13(5), pp. 25–30.

Blaugher, R.D., Parker, J.H. and McCabria, J.L. (1977) 'HIGH SPEED SUPERCONDUCTING GENERATOR', *IEEE Transactions on Magnetics*, 13(1), p. 755.

Boeing (2013) *787 Dreamliner Electrical System*.

Bollman, A.M., Armstrong, M.J., Jones, C.E., Norman, P.J. and Galloway, S.J. (2015) 'Development of Voltage Standards for Turbo-electric Distributed Propulsion Aircraft Power Systems', *Electrical Systems for Aircraft, Railway, Ship Propulsion and Road Vehicles (ESARS), 2015 International Conference*. Aachen: IEEE, p. 1.

Brown, G. V (2011) 'Weights and Efficiencies of Electric Components of a Turboelectric Aircraft Propulsion System', *49th AIAA/ASME/SAE/ASEE Joint Propulsion Conference*. Orlando, Florida: AIAA.

Bumby, J.R. (1983) *Superconducting rotating electrical machines (Monographs in Electrical and Electronic Engineering)*. Clarendon Press.

Buquet, M. (2007) *Distributed Propulsion: An Overview of Possible Transmission Technologies*. Cranfield University.

Chambon, T. (2012) *Impact of the boundary layer ingestion on the noise generated by distributed propulsion concept*. Cranfield University.

Chengyuan, L., Doulgeris, G., Laskaridis, P. and Singh, R. (2012) 'Turboelectric Distributed Propulsion System Modelling for Hybrid-Wing-Body Aircraft', *48th AIAA/ASME/SAE/ASEE Joint Propulsion Conference*. Atlanta, Georgia: AIAA.

Christensen, K., Albertus, P., Sanchez-Carrera, R.S., Lohmann, T., Kozinsky, B., Liedtke, R., Ahmed, J. and Kojic, A. (2012) 'A Critical Review of Li/Air Batteries', *Journal of Electrochemical Society*, 159(2), p. 1.

Clark, S.F. (2012) 787 Propulsion System *Boeing Aeromagazine*.

Costi, F. (2012) *Investigation on boundary layer ingestion effects on a ducted axial fan for a distributed propulsion system*. Cranfield University.

Cotton, I., Nelms, A. and Husband, M. (2007) 'Defining Safe Operating Voltages for Aerospace Electrical Systems', *Electrical Insulation Conference and Electrical Manufacturing Expo, 2007*. Nashville, TN: IEEE, p. 67.

Dodson, B. (2013) *New Lithium/sulphur battery doubles energy density of lithium-ion*.

Doerry, N.H. and Fireman, H. (2006) 'Designing All Electric Ships', *Proceedings of the Ninth International Marine Design Conference*. Ann Arbor, MI, p. 475.

Dombrovski, V., Driscoll, D., Shoykhet, B.A., Umans, S.D. and Zevchek, J.K. (2005) 'Design and Testing of a 1000-hp High-Temperature Superconducting Motor', *IEEE Transactions on Energy Conversion*, 20(3), p. 638.

Doulgeris, G., Lelias, G., Laskaridis, P., Pilidis, P. and Singh, R. (2012) 'Dynamic Response and High Cycle Fatigue Analysis of Fan Blades under Inlet Distortion', *48th AIAA/ASME/SAE/ASEE Joint Propulsion Conference*. Atlanta, Georgia.

Ebner, A. (2007) 'Transient Transformer Inrush Currents due to Closing Time- and Residual Flux Measurement- Deviations if Controlled Switching is used', *Proceedings of European EMTP-ATP Conference*. Leon, Spain.

Eckels, P.W. and Snitchler, G. (2008) ‘5 MW High Temperature Superconductor Ship Propulsion Motor Design and Test Results’, *Electric Machines Technology Symposium*, 117(4) Naval Engineers Journal, p. 31.

Edwards, H. (2011) *Extract from DNS171343, Sugar volt (hybrid electric aircraft) assessment - The future of energy storage (20 year time frame)*. SRC, Derby, UK: Rolls Royce Private Data.

Eggenspieler, F. (2006) *Distributed Propulsion Aircraft Wing Structure and Systems Design*. Cranfield University.

Electronics, M. (2015) *Maxwell 16V Ultracapacitor Modules* .

Eriksson, J.T., Mikkonen, R., Paasi, J., Perala, R. and Soderlund, L. (1997) ‘A HTS Synchronous Motor at Different Operating Temperatures’, *IEEE Transactions on Applied Superconductivity*, 7(2), p. 523.

Felder, J.L., Brown, G. V, Kim, H.D. and Chu, J. (2011a) ‘Turboelectric Distributed Propulsion in a Hybrid Wing Body Aircraft’, *20th International Society for Airbreathing Engines (ISABE 2011)*. Gothenburg, Sweden.

Felder, J.L., Kim, H.D. and Brown, G. V (2009) ‘Turboelectric Distributed Propulsion Engine Cycle Analysis for Hybrid-Wing-Body Aircraft’, *47TH AIAA Aerospace Sciences Meeting Including the New Horizons Forum and Aerospace Exposition*. Orlando, Florida: AIAA.

Felder, J.L., Kim, H.D., Brown, G. V and Chu, J. (2011b) ‘An Examination of the Effect of Boundary Layer Ingestion on Turboelectric Distributed Propulsion Systems’, *49th AIAA/ASME/SAE/ASEE Joint Propulsion Conference*. Orlando,Florida: AIAA.

Felder, J.L., Tong, M.T. and Chu, J. (2012) ‘Sensitivity of Mission Energy Consumption to Turboelectric Distributed Propulsion Design Assumptions on the N3-X Hybrid Wing Body Aircraft’, *48th AIAA/ASME/SAE/ASEE Joint Propulsion Conference*. Atlanta, Georgia: AIAA.

Fletcher, S.D.A., Norman, P.J., Galloway, S.J. and Burt, G.M. (2011) ‘Determination of Protection System Requirements for DC UAV Electrical Power Networks for Enhanced Capability and Survivability’, *IET Electrical Systems in Transportation Journal*, 1(4), p. 137.

Furmanczyk, K. (2009) ‘Power Conversion Technologies for Improved System Performance’, *2009 Join Service Power Expo*. New Orleans, Louisiana: Crane Aerospace and Electronics.

Gamble, B., Kalsi, S., Snitchler, G. and Madura, D. (2002) ‘The Status of HTS Motors’, IEEE (ed.)*Power Engineering Society Summer Meeting*. Chicago, IL, USA, Vol.1, p. 270.

Gamble, B., Snitchler, G. and MacDonald, T. (2011) 'Full Power Test of a 36.5 MW HTS Propulsion Motor', *IEEE Transactions on Applied Superconductivity*, 21(3), p. 1083.

Gibson, A.R., Hall, D.W., Schiltgen, B.T., Foster, T.J., Keith, J. and Masson, P. (2010) 'The Potential and Challenge of TurboElectric Propulsion for Subsonic Transport Aircraft', *47TH AIAA Aerospace Sciences Meeting Including the New Horizons Forum and Aerospace Exposition*. Orlando, Florida.

Gieras, J.F. (2009) 'Superconducting Electrical Machines State of the Art', *Przeglad Elektrotechniczny*, 85(12), pp. 1–19.

Glover, J.D., Sarma, M.S. and Overbye, T.J. (2010) *Power System Analysis and Design*.Fifth. Global Engineering: Christopher M. Shortt.

Gohardani, A.S., Doulgeris, G. and Singh, R. (2011) 'Challenges of future aircraft propulsion: a review of distributed propulsion technology and its potential application for the all electric commercial aircraft', *Progress in Aerospace Sciences*, 47(5), pp. 369–391.

Golovashkin, A.I., Ivanenko, O.M., Kudasov, Y.B., Mitsen, K. V., Pavlovsky, A.I., Platonov, V. V. and Tatsenko, O.M. (1991) 'LOW TEMPERATURE DIRECT MEASUREMENTS OF Hcz IN HTSC USING MEGAGAUSS MAGNETIC FIELDS', *Physica C: Superconductivity*, 185-189, pp. 1859–1860.

Graham R., W., Hall A., C. and Morales V., M. (2014) 'The potential of future aircraft technology for noise and pollutant emissions reduction', *Transport Policy Special Issue Aviation and the Environment*, 34, pp. 36–51.

Green, M.W., Schiltgen, B.T. and Gibson, A.R. (2012) 'Analysis of a Distributed Hybrid Propulsion System with Conventional Electric Machines', *48th AIAA/ASME/SAE/ASEE Joint Propulsion Conference*. Atlanta, Georgia.

Griffith, A.A. (1954) *Improvements relating to aircraft and aircraft engine installations*.

Guynn D., M., Berton J., J., Hendricks S., E., Tong T., M., Haller J., W. and Thurman R., D. (2011) 'Initial Assessment of Open Rotor Propulsion Applied to an Advanced Single-Aisle Aircraft', *11th AIAA Aviation Technology, Integration, and Operations (ATIO) Conference*. Virginia Beach, VA.

Guzik, M.C. and Tomsik, T.M. (2011) 'An Active Broad Area Cooling Model of a Cryogenic Propellant Tank with a Single Stage Reverse Turbo- Brayton Cycle Cryocooler', *Thermal and Fluids Analysis Workshop*., pp. 1–15.

Hale, J. (2008) Boeing 787: From the Ground Up *Boeing Aeromagazine*.

Hampton, K. (2013) Small but mighty *Energy Storage Journal*.

Harada, H. (2003) ‘High Temperature Materials for Gas Turbines: The Present and Future’, *Proceedings of the International Gas Turbine Congress*. Tokyo.

Harrop, P. (2013) *Global marine electric vehicle market to reach $6.3bn in 2023* . IDTechEx Research report.

Hassannia, A. and Darabi, A. (2014) ‘Design and Performance Analysis of Superconducting Rim-Driven Synchronous Motors for Marine Propulsion’, *IEEE Transactions on Applied Superconductivity*, 24(1)

Hendershot, J.R. and Miller, T.J.E. (2010) *Design of Brushless Permanent-Magnet Machines*. Venice, Florida: Motor Design Books LLC.

Hennessy, M. (2009) *Lightweight, Efficient Power Converters for Advanced Turboelctric Aircraft Power Systems* MTECH Laboratories, LLC,

Hirst, M., McLoughlin, A., Norman, P.J. and Galloway, S.J. (2011) ‘Demonstrating the More Electric Engine: a step towards the power optimised aircraft’, *IET Electrical Power Applications*, 5(1), p. 3.

Hughes, A. and Miller, T.J.E. (1977) ‘Analysis of fields and inductances in air-cored and iron-cored machines’, *Proceedings of the Institution of Electrical Engineers*, 124(2), p. 121.

Imanishi, N. and Yamamoto, O. (2014) ‘Rechargeable lithium-air batteries: characteristics and prospects’, *Materials Today*, 17(1), p. 24.

Isikveren, A.T., Seitz, A., Vratny, P.C., Pornet, C., Plotner, K.O. and Hornung, M. (2012) ‘Conceptual Studies of Universally-Electric Systems Architectures Suitable for Transport Aircraft ’, *61. Deutscher Luft- und Raumfahrtkongress 2012* . Berlin, Germany.

Iwakuma, M., Tomioka, A., Konno, M., Hase, Y., Satou, T., Iijima, Y., Saitoh, T., Yamada, Y., Izumi, T. and Shiohara, Y. (2007) ‘Development of a 15 kW Motor With a Fixed YBCO Superconducting Field Winding’, *IEEE Transactions on Applied Superconductivity*, 17(2), p. 1607.

Jin, J.X. (2007) ‘High Efficiency DC Power Transmission Using High-Temperature Superconductors’, *Physica C: Superconductivity*, 460-462, p. 1443.

Jin, J.X., Xin, Y., Wang, Q.L., He, Y.S., Cai, C.B., Wang, Y.S., Wang, Z.M., Fault, A.H.T.S. and Limiters, C. (2014) ‘*Enabling High-Temperature Superconducting Technologies Toward Practical Applications*’, 24(5)

Jones, R.J. (2002) ‘The More Electric Aircraft - Assessing the Benefits’, *Proceedings of the Institution of Mechanical Engineers*, 216(G), p. 259.

Joshi, C.H., Prum, C.B., Schiferl, R.F. and Driscoll, D.I. (1995) 'Demonstration of Two Synchronous Motors Using High Temperature Superconducting Field Coils', *IEEE Transactions on Applied Superconductivity*, 5(2), p. 968.

Jow, T.R., Xu, K., Allen, J., Borodin, O., Cresce, A., Behl, W., Marx, M. and Allen, J. (2014) *High Energy and High Power Li-ion Batteries*.

Keison (2014) *Keyson Products*.

Kim, B., Chung, H. and Kim, W. (2012) 'High-Performance Supercapacitors based on vertically aligned carbon nanotubes and nonaqueous electrolytes', *IOP Publishing Nanotechnology*, 23, p. 1.

Kim, H., Felder, J., Tong, M. and Armstrong, M. (2013) 'Revolutionary Aeropropulsion Concept for Sustainable Aviation: Turboelectric Distributed Propulsion', *ISABE Conference*, , pp. 1–12.

Kim, H.D. (2010) 'Distributed Propulsion Vehicles', *27th International Congress of the Aeronautical Sciences*. Nice, France: ICAS.

Kim, H.R., Sim, J. and Hyun, O.B. (2006) 'Temperature distribution in SFCLs based on Au/YBCO films during quenches', *Cryogenics*, 46(4), pp. 305–311.

Kim, S.-H. and Hahn, S.-Y. (2000) 'Analysis and Design of a Induction Generator with a Superconducting Bulk Magnet Rotor', *IEEE Transactions on Applied Superconductivity*, 10(1), p. 931.

Ko, A., Leifsson, L.T., Schetz, J. a, Mason, W.H. and Grossman, B. (2003) 'MDO of a Blended-Wing-Body Transport Aircraft with Distributed Propulsion', *AIAA ' s 3rd Annual Aviation Technology , Integration , and Operations (ATIO) Technical Forum*. Denver , CO.

Kongsberg (2015) *Marine switchboards*., *http://www.km.kongsberg.com/ks/web/nokbg0240.nsf/AllWeb/6591A4733274161DC125766400373AAF?OpenDocument*

Kwon, Y.K., Sohn, M.H., Baik, S.K., Lee, E.Y., Kim, J.M., Monn, T.S., Park, H.J., Kim, Y.C. and Ryu, K.S. (2005) 'Development of a 100 hp Synchronous Motor With HTS Field Coils', *IEEE Transactions on Applied Superconductivity*, 15(2), p. 2194.

Larbalestier, D., Gurevich, a, Feldmann, D.M. and Polyanskii, a (2001) 'High-Tc superconducting materials for electric power applications.', *Nature*, 414(6861), pp. 368–377.

Laskaridis, P. and Pilidis, P. (2004) *Performance investigations and systems architectures for the more-electric aircraft*. Cranfield University.

Laskaridis, P., Valencia, E., Kirner, R. and Wei, T.J. (2015) 'Assessment of Distributed Propulsion Systems Used with Different Aircraft Configurations', *51st AIAA/SAE/ASEE Joint Propulsion Conference*. Orlando, Florida.

Leong, K.K. (2011) *Utilising Power Devices Below 100 K to Achieve Ultra-low Power Losses*. http://wrap.warwick.ac.uk/46807/: University of Warwick.

Li, G.Z., Sumption, M.D., Susnrer, M.A., Yang, Y., Reddy, K.M. and Rindfleisch, M.A. (2012) 'The Critical Current Density of Advanced Internal-Mg-Diffusion-Processed MgB2 Wire', *IOP Publishing*, (Superconductor Science and Technology)

Lieberman, M.A. and Lichtenberg, A.J. (2005) *Principles of plasma discharges and materials processing*.Second (ed.) Hoboken, N.J.: Wiley-Interscience.

Liu, C. (2013) *Turboelectric Distributed Propulsion System Modelling*. Cranfield University.

Luongo, C.A., Masson, P.J., Nam, T., Mavris, D., Kim, H.D., Brown, G. V, Waters, M. and Hall, D.W. (2009) 'Next Generation More-Electric-Aircraft: A Potential Application for HTS Superconductors', *Applied Superconductivity*, 19(3), pp. 1055–1068.

Maeda, H., Tanaka, Y., Fukutomi, M. and Asano, T. (1988) 'A new high-T (c) oxide superconductor without a rare earth element', *Japanese Journal of Applied Physics*, 27(2), p. 209.

Maguire, J.F., Schmidt, F., Bratt, S., Welsh, T.E., Yuan, J., Allais, A. and Hamber, F. (2007) 'Development and Demonstration of a HTS Power Cable to Operate in the Long Island Power Authority Transmission Grid', *Applied Superconductivity*, 17(2), pp. 2034–2037.

Malkin, D. (2014) *Superconducting Cables for Aerospace Electrical Systems*. University of Manchester: Faculty of Engineering and Physical Sciences.

Malkin, P. and Pagonis, M. (2013) 'The Design of Fully Superconducting Power Networks for Future Aircraft Propulsion', *49th AIAA/ASME/SAE/ASEE Joint Propulsion Conference*. San Jose, CA.

Malkin, P. and Pagonis, M. (2014) 'Superconducting Electric Power Systems for Hybrid Electric Aircraft', *Aircraft Engineering and Aerospace Technology: An International Journal*, 86(6), p. 515.

Malkin, P. and Pagonis, M. (2015a) 'Future Energy Solutions For Hybrid-Electric Powered Aircraft', *The 22nd International Symposium on Air Breathing Engines*. Phoenix, AZ USA, Vol.to be publ.

Malkin, P. and Pagonis, M. (2015b) ‘Propulsion System Optimisation Approach for Hybrid / Electric Aircraft’, *More Electric Aircraft (MEA) Conference*. Toulouse, France.

Manzel, C. (1924) *Propelling mechanism for airships and the like*.

marine.man.eu (2015) *Diesel-electric Propulsion Plants*.

Masson, P.J., Brown, G. V, Soban, D.S. and Luongo, C.A. (2007) ‘HTS machines as enabling technology for all-electric airborne vehicles’, *Superconductor Science and Technology*, 20(8)

Masuda, T., Yumura, H., Watanabe, M., Takigawa, H., Ashibe, Y., Suzawa, C., Kato, T., Okura, K., Yamada, Y., Hirose, M., Yatsuka, K., Sato, K. and Isojima, S. (2004) *High-temperature Superconducting Cable Technology and Development Trends*. SEI Technical Review.

Matsuzaki, H., Kimura, Y., Ohtani, I., Izumi, M., Ida, T., Akita, Y., Sugimoto, H., Miki, M. and Kitano, M. (2005) ‘An Axial Gap-Type HTS Bulk Synchronous Motor Excited by Pulsed-Field Magnetization With Vortex-Type Armature Copper Windings’, *IEEE Transactions on Applied Superconductivity*, 15(2), p. 2222.

McConnell, B.W., Walker, M.S. and Mehta, S.P. (2000) ‘HTS Transformers’, *IEEE Power Eng. Rev.*, 20, pp. 7–11.

Meier, N. (2005) *Civil Turboshaft/Turboprop Specifications*.

Mikhaylik, Y., Kovalev, I., Schock, R., Kumaresan, K., Xu, J. and Affinito, J. (2015) *High Energy Rechargeable Li-S Cells for EV Application. Status, Challenges and Solutions*., *Sion Power Corporation*

Miller, T.J.E. (1989) *Brushless Permanent Magnet and Reluctance Motor Drives*. United States: Oxford University Press.

Miller, T.J.E. and Hughes, A. (1977) ‘Comparative design and performance analysis of air-cored and iron-cored synchronous machines’, *Electrical Engineers, Proceedings of the Institution of Electrical Engineers*, 124(2), p. 127.

Millikin, M. (2010) *QinetiQ Zelphyr Used Sion Li-S Batteries in Record Unmanned Flight* greencarcongress.com,

Millikin, M. (2009) *FDK To Begin Mass Production of High-Capacity Li-Ion Capacitors; Automotive and Renewable Energy Applications*

Moir, I. and Seabridge, A. (2013) *Design and Development of Aircraft Systems*. John Wiley & Sons Ltd.

Molina, M.G. (2010) 'Dynamic Modelling and Control Design of Advanced Energy Storage for Power System Applications ', in Brito, A. (ed.) *Dynamic Modelling*.

Montgomery, S. (2012) *ElectroniCast- Solar PV Outdoor LED Lighting Using LIC*

Murphy, T. (2012) The battery performance deficit disorder *GIGAOM Research*.

Nagata, H. and Chikusa, Y. (2014) 'A lithium sulphur battery with high power density', *Journal of Power Sources*, 264, p. 206.

Nakamura, T., Miyake, H., Ogama, Y., Motita, G., Muta, I. and Hoshino, T. (2006) 'Fabrication and Characteristics of HTS Induction Motor by the Use of Bi-2223/Ag Squirrel-Cage Rotor', *IEEE Transactions on Applied Superconductivity*, 16(2), p. 1469.

Van Noorden, R. (2014) 'The rechargeable revolution: A better battery', *NATURE*, 507(7490), p. 26.

Ojha, P. and Raghava, K. (2014) TRENT 1000: Aircraft Engine *www.slideshare.com*.

Oswald, B., Best, K.-J., Setzer, M., Soll, M., Gawalek, W., Gutt, A., Kovalev, L., Krabbes, G., Fisher, L. and Freyhardt, H.C. (2005) 'Reluctance Motors with Bulk HTS Materials', *Superconducting Science and Technology*, 18, p. 24.

Owano, N. (2012) Sugar Volt: Boeing puts vision to work in hybrid electric aircraft *Phys.org*.

Palmer, J., Pagonis, M. and Malkin, P. (2015) 'Configuration Options for High-Power, Low Weight Aerospace Superconducting Distributed Propulsion Cryocoolers', *ISABE 2015 (to be published)*.

Palmer, J. and Shehab, E. (2015) 'Modelling of Cryogenic Cooling System Design Concepts for Superconducting Aircraft Propulsion', *IET Electrical Systems in Transportation Journal*, Pending pu

Palmer, J., Shehab, E., Fan, I.S. and Husband, M. (2013) 'Quality Function Deployment and Sensitivity Analysis of Requirements for Future Aircraft Propulsion Cryogenic Cooling Systems', *Proceedings of the 11th International Conference on Manufacturing Research*.

Paschen, F. (1889) *Breakdown Voltage vs. Pressure Paschen's Law and the 'Paschen Curve'.*

Pei, X., Smith, A.C., Husband, M. and Rindfleisch, M. (2012) ‘Experimental tests on a superconducting fault current limiter using three-strand MgB2 wire’, *IEEE Transactions on Applied Superconductivity*, 22(3)

Pei, X., Zeng, X., Smith, A.C. and Malkin, D. (2015) ‘Resistive Superconducting Fault Current Limiter Coil Design Using Multistrand MgB 2 Wire’, *IEEE Transactions on Applied Superconductivity*, 25(3)

Pilidis, P. (2012) *Gas Turbine Theory and Performance*

PolyPlus, B.C. (2009) *Advanced Lithium Battery Technology*.

Provost, M.J. (2002) ‘The More Electric Aero-Engine: A General Overview from an Engine Manufacturer’, Plc., R.-R. (ed.)*Conference on Power Electronics, Machines and Drives*. Derby: IET, p. 246.

Rada, A., Lubin, T., Lévêque, J., Berger, K., Douine, B., Rezzoug, A., Mezani, S., Didier, G., Hinaje, M. and Netter, D. (2015) ‘Study of a superconducting motor with high specific torque’, *MEA 2015 More Electric Aircraft*. Toulouse, France, p. 346.

Radebaugh, R. (2012) ‘Cryocoolers for aircraft superconducting generators and motors’, *AIP Conf. Proc. ADVANCES IN CRYOGENIC ENGINEERING: Transactions of the Cryogenic Engineering Conference*. Washington, USAs: AIP.

Ranade, S.J. and Xu, W. (1998) ‘Tutorial on Harmonics Modeling and Simulation (Chapter 1)’, *Proc. IEEE Power Eng. Society*, , pp. 1–7.

Rogers, S. (2012) Electric Drive Status and Challenges *Energy Efficiency & Renewable Energy*. U.S. Department of Energy,

Rosenkranz, C.A., Kohler, U. and Liska, J.L. (2007) ‘Modern Battery Systems for Plug-In Hybrid Electric Vehicles’, *23rd International Battery and Fuel Cell Electric Vehicle Symposium and Exposition (EVS 23)*. Anaheim, CA, USA.

Rosero, J.A., Ortega, J.A., Aldabas, E. and Romeral, L. (2007) ‘Moving towards a More Electric Aircraft’, *IEEE Aerospace and Electronic Systems Magazine*, 22(3), p. 3.

Ross, C., Armstrong, M., Blackwelder, M., Jones, C., Norman, P. and Fletcher, S. (2014) ‘Turboelectric Distributed Propulsion Protection System Design Trades’, *SAE International*, 2014-01-21

Roveglia, C. (2015) *STABLE (STable high-capacity lithium-Air Batteries with Long cycle life for Electric cars*.

Scanlan, R.M., Malozemoff, A.P. and Larbalestier, D.C. (2004) 'Superconducting materials for large scale applications', *Proceedings of the IEEE*, 92(10), pp. 1639–1654.

Schaub, U., Vlasic, E. and Moustapha, S. (1993) 'Effect of Tip Clearance on the Performance of a Highly Loaded Turbine Stage', *Proceedings of AGARD PEP 82nd Symposium*.

Schiltgen, B., Green, M.W., Gibson, A.R., Hall, D.W., Cummings, D.B. and Hange, C. (2012) 'Benefits and Concerns of Hybrid Electric Distributed Propulsion with Conventional Electric Machines', *48th AIAA/ASME/SAE/ASEE Joint Propulsion Conference*. Atlanta, Georgia: AIAA.

Schiltgen, B.T., Green, M.W., Gibson, A.R., Foster, T.J. and Waters, M. (2011) 'Split-Wing Propulsor Design and Analysis for Electric Distributed Propulsion', *49th AIAA/ASME/SAE/ASEE Joint Propulsion Conference*. Orlando, Florida: AIAA.

Scocco, D. (2006) *S-Curves*., *Innovation Theory*

Scott, A. (2014) New Boeing Jets hold key to more than half of future sales, *Reuters*, Aerospace May.

Senkov, O.N., Bhat, R.B. and Senkova, S. V (2004) 'High Strength Aluminium Alloys For Cryogenic Applications', *Metallic Materials with High Structural Efficiency*, , p. 151.

Shankland, S. (2014) *Want major new aircraft designs? Wait until 2030*., *Cnet*

Shcherbakov, A.V. (2011) *Magnesium diboride superconductor : thermal stabilization and doping*. University of Wollongong.

Shen, Y., Sun, D., Yu, L., Zhang, W., Shang, Y., Tang, H., Wu, J., Cao, A. and Huang, Y. (2013) 'A high-capacity lithium-air battery with Pd modified carbon nanotube sponge cathode working in regular air', *Carbon*, 62, p. 288.

Shi, J., Tang, Y., Zhou, Y., Chen, J., Xu, D., Wang, H., Lu, Y., Ren, L., Wei, B., Li, J. and Cheng, S. (2007) 'Development of a conduction-cooled HTS SMES', *IEEE Transactions on Applied Superconductivity*, 17(3), pp. 3846–3851.

Shuli, L. and Zhan, L. (2015) 'Lithium-Sulphur Batteries', in *Rechargeable Batteries*. Springer, p. 587.

Sim, J., Lee, K., Cha, G. and Lee, J.-K. (2004) 'Development of a HTS Squirrel Cage Induction Motor With HTS Rotor Bars', *IEEE Transactions on Applied Superconductivity*, 14(2), p. 916.

Simon, P. and Gogotsi, Y. (2010) 'Charge storage mechanism in nanoporous carbons and its consequence for electrical double layer capacitors', *Philosophical Transactions of the Royal Society*, 368, p. 3457.

Simon, P. and Gogotsi, Y. (2008) 'Materials for electrochemical capacitors', *NATURE Materials*, 7, p. 845.

Singh, T. (2013) EADS E-Thrust Electric Airliner Could Transform Air Travel by 2050 *Inhabitat*.

Sinnet, M. (2008) 787 No-Bleed Systems: Saving Fuel and Enhancing Operational Efficiencies *Boeing Aeromagazine*.

Skaar, S.E., Krovel, O. and Nilssen, R. (2006) Distribution, coil-span and winding factors for PM machines with concentrated windings *NTNU Website*.

Solovyov, V.F. and Li, Q. (2013) 'Fast high-temperature superconductor switch for high current applications', *Applied Physics Letters*, 103(3), p. 032603.

Sözeri, H., Özkan, H. and Ghazanfari, N. (2007) 'Properties of YBCO superconductors prepared by ammonium nitrate melt and solid-state reaction methods', *Journal of Alloys and Compounds*, 428(1-2), pp. 1–7.

Stephenson, D. (2010) *Envisioning tomorrow's aircraft* www.boeing.com,

Stuckl, S., Van Toor, J. and Lobentanzer, H. (2012) 'Voltair - The All Electric Propulsion Concept Platform - A Vision for Atmospheric Friendly Flight', *28th Congress of the International Council of the Aeronautical Sciences* . Brisbane, Australia.

Sutanto, D. and Cheng, K.W.E. (2009) 'Superconductic Magnetic Energy Storage Systems for Power System Applications', *Proceedings of 2009 IEEE International Conference on Applied Superconductivity and Electromagnetic Devices*. Chengdu, China, p. 377.

Takeda, T., Oota, T. and Togawa, H. (2006) 'Development of Liquid Nitrogen-cooled Full Superconducting Motor', *Journal of Interactive Media In Education*, 41(6)

THALES (2015a) *Electrical Systems: Power Thinking*.

THALES (2015b) *Electrical Power Conversion Solutions- HVDC*.

THALES (2015c) *Electrical Power Conversion Solutions- AC to AC*.

THALES (2015d) *Advanced Electrical Power Conversion Solutions- Active Solutions*.

Thiétart, R.A. (2013) The Boeing 787. The Dreamliner wakes up to reality *ESSEC Business School Webpage*.

Thome, R.J., Creedon, W., Reed, M., Bowles, E. and Schaubel, K. (2002) 'Homopolar Motor Technology Development', IEEE (ed.)*Power Engineering Society Summer Meeting*. Chicago, IL, USA, Vol.1, p. 260.

Tixador, P. and Daffix, H. (1997) 'Conceptual design of an electrical machine with both low and high Tc superconductors', *IEEE Transactions on Applied Superconductivity*, 7(4), p. 3858.

Torenbeek, E. (1992) *Development and application of a comprehensive, design-sensitive weight prediction method for wing structures of transport category aircraft*. Delft University of Technology.

Valencia, E. and Nalianda, D. (2015) 'Methodology to assess the performance of an aircraft concept with distributed propulsion and boundary layer ingestion using a parametric approach', *Proceedings of the IMechE*, 229(May), pp. 682–693.

Waltman, D.J. and Superczynski, M.J. (1995) 'High-Temperature Superconducting Magnet Motor Demonstration', *IEEE Transactions on Applied Superconductivity*, 5(4)

Warwick, G. (2013) *eConcept - EADS's Hybrid-Electric Airliner*., *Aviation Week Network (Things with Wings)*

Wen, H., Bailey, W., Goddard, K., Al-Mosawi, M., Beduz, C. and Yang, Y. (2009) 'Performance Test of a 100 kW HTS Generator Operating at 67 K–77 K', *IEEE Transactions on Applied Superconductivity*, 19(3), p. 1652.

Whitlow B., J. and Sievers K., G. (1988) 'NASA Advanced Turboprop Research and Concept Validation Program', *Conference and Exposition on Future Transportation Technology sponsored by the Society of Automotive Engineers*. San Francisco, California: NASA Technical Memorandum 100891.

Whyatt, G.A. and Chick, L.A. (2012) *Electrical Generation for More-Electric Aircraft using Solid Oxide Fuel Cells*. Pacific Northwest National Laboratory Richland, Washington 99352: U.S. Department of Energy.

wikipedia.com (2015) *Nissan Leaf*.

Williams, M., Muley, A., Bolla, J. and Strumpf, H. (2008) '*Advanced Heat Exchanger Technology for Aerospace Applications*', Seattle, Washington, United States.

Wolfgang, N., Grundmann, J. and Frauenhofer, J. (2012) 'Test results from Siemens low-speed, high-torque HTS machine and description of further steps towards commercialisation of HTS machines', *Physica C*, 482, p. 105.

Wright, J., Alderman, J., Berg, F., Raffaelli, L., Miller, P., Malkin, P. and Pagone, E. (2015) *DEAP Final Technical Report*

www.airlines-inform.com (2012) *Commercial Aircraft of the World*.

www.AviationExplorer.com (2015) *Airbus A350 XWB Aircraft Airliner History Pictures and Facts*.

www.batteryspace.com (2015) *Category: LiFePO4 Batteries*.

www.eaa-phev.org (2015) *Toyota Prius Battery Specs*.

www.what-when-how.com (2015) *Electrical Conduction in Metals and Alloys (Electrical Properties of Materials) Part 2*.

Xi, H.X., Gong, W.Z., Zhang, Y., Bi, Y.F., Ding, H.K., Wen Hou, B., H. and Xin, Y. (2006) 'China's 33.5m, 35kV/2 kA HTS ac power cable's operation in power grid', *Physica C: Superconductivity*, 445-448, p. 1054.

Xin, Y., Han, Z. and Liao, Z. (2006) 'Experimental 35 kV/21 MVA Superconducting Cable System Installed at PUJI Substation in China Southern Power Grid', *IEEE Trans. on Electrical and Electronic Engineering*, 1(1), p. 8.

Yuan, W. (2011) *Second-Generation High -Temperature Superconducting Coils and Their Applications for Energy Storage*. Cambridge University.

Yuan, W., Xian, W., Ainslie, M., Hong, Z., Yan, Y., Pei, R., Jiang, Y. and Coombs, T.A. (2010) 'Design and Test of a Superconducting Magnetic Energy Storage (SMES) Coil', *IEEE Transactions on Applied Superconductivity*, 20(3), pp. 1379–1382.

Zhang, Y., Lehner, T., Fukushima, T., Sakamoto, H. and Hazelton, D. (2014) 'Progress in production and performance of second generation (2G) HTS wire for practical applications', *2013 IEEE International Conference on Applied Superconductivity and Electromagnetic Devices*, 24(5), pp. 557–558.

APPENDICES

A.1 Conventional Electrical Machines Rotor and Stator Dimensions

The following table includes the conventional machines that have been used in 4.2.2 in order to find a reliable relationship between the stator and rotor diameter of electrical machines. The table consists of the required dimensions, the type of the machines as well as their development stage at the moment when these parameters were acquired. A further analysis of these machines is not in the scope of this research study. All these data were collected by a Rolls Royce internal study and the summary datasheet was available during the DEAP project.

Table_A-1 Conventional Electrical machines dimensions

Machine type	Development stage	Rotor Diameter (mm)	Stator Diameter (mm)
PM BLAC	Prototype manufactured	66	144
PM BLAC	Prototype manufactured	394	556
PM BLAC	Prototype manufactured	265	390
SR	Prototype manufactured	164	236
PM/VR Hybrid	Prototype manufactured	99	160
PM BLAC	Prototype manufactured	124	210
IM	High level concept study	82.1	150
PM BLAC	In production (Toyota Prius traction motor)	160.4	269.24
PM BLAC	Detailed Concept Design	2450	2780
WF Synchronous	In production (Trent	170	237

	1000)		
PM BLAC	Detailed Concept Study	1040	1000
IM	Prototype Manufactured	840	1267
PM BLAC	Prototype Manufactured	116	160

A.2 Reverse Brayton Cryo-coolers (RBC) Simulink Model

A.2.1 Introduction and Simulink model overview

For project DEAP two different cryo-cooler models were developed by Joseph Palmer (PhD student of Cranfield University, funded by RR), a single stage and a double stage reverse-Brayton cryo-cooler. For the purposes of this study the double stage version was used. Both systems are similar to operation with the key difference that in the double stage case the heat rejection from the first stage is removed by the second stage. Hence, the temperature difference between the hot and cold parts is reduced enhancing the efficiency of the whole system. There is an offset between the adding weight of the second stage and the efficiency and potential reduction in input power of this type of cryo-coolers. However, this version was preferred both because of the conservative weight prediction and also due to its attractiveness in terms of efficiency. The following figure illustrates a schematic diagram of a double stage Reverse-Brayton cryo-cooler opposed to the actual overview of the Simulink model being developed.

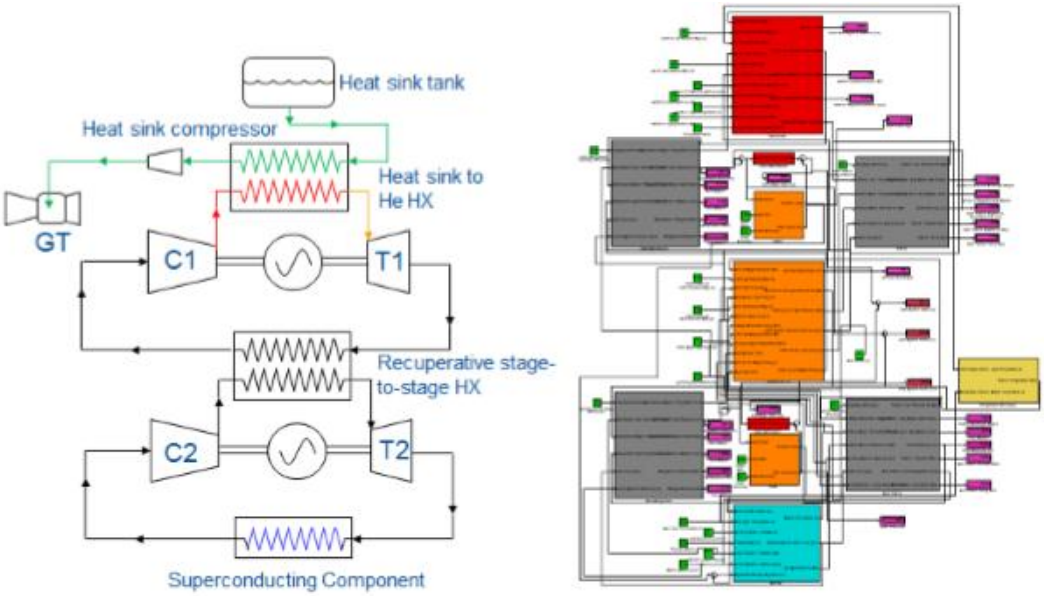

Figure_A-1 Schematic diagram showing RBC next to the Simulink model

The main inputs and outputs of this model can be found in the following table. The models are relatively complex based on numerous equations which are not in the scope of this research study to be analysed. However, these models were verified during the DEAP project by several experts and they were used for the sensitivity studies carried out throughout the project; hence they could be considered as reliable.

The cryo-cooler mass is calculated using equation (2-2), whilst for the two-stage cryo-coolers of this study, this equation is used for each stage and the individual mass values were added together. The compressor and turbine polytropic efficiencies were assumed to be 0.90 and 0.92 respectively, assumptions relatively conservative for the 2035 timeframe. The cold operating temperature and the heat exchanger temperature delta could be varied depending on the superconducting material and the coolant being used in each case. A pressure drop of 5% was assumed for every heat exchanger of this model, whilst a heat sink latent heat of 510 kJ/kg was considered.

Table_A-2 Main inputs/outputs of Cryo-cooler Simulink models

Inputs	Units	Outputs	Units
Cold thermal load	kW	Heat sink required mass flow rate	kg/s
Cold operating temperature	K	Required input power	kW
Heat Exchanger pressure drop	-	Cryo-cooler mass	kg
Heat exchange latent heat	kJ/kg		
Heat Exchanger Temperature delta	K		
Compressor polytropic efficiency	–		
Turbine polytropic efficiency	–		

A.2.2 Main Assumptions and model limitations

There were a number of assumptions necessary to be made to reduce the complexity and the number of variables of these models. These can be summarised as follows:

- There is no external heat transfer to the system (i.e. close system)
- Transport losses were ignored (i.e. perfect transfer between components was assumed)
- Constant specific heat capacity values
- Superconducting motors were used (models presented in Chapter 4.2)
- Numerical assumptions taken based on current aerospace examples available
- The intermediate heat exchanger is defined by firstly taking the overall temperature delta between the cold desired temperature and the heat sink helium output temperature. This ratio is then square rooted. This

effectively implies the temperature ratio is equally shared among both stages, allowing each system to be optimally efficient.

There are two main model limitations which need to be pointed out. First of all, this is a steady-state model where no transient effects are taken into consideration. Secondly, there are several technology uncertainties which needed a number of assumptions to be made (i.e. heat exchanger performance, components efficiency etc.). These values have not yet been verified neither by experimental work nor by numerical methods and hence the uncertainty in the estimation of the cryo-cooler mass remains high.

A.3 Turboshaft/Turboprop engines datasheet

In order to estimate the weight of the turboshaft engines for the Chapter 6 sensitivity study the specifications of several civil turboshaft/turboprop engines were used. The following table summarises some of the engines which were included in this study. Overall, 61 engines were included in the survey, but only the most representative examples of each manufacturer were included in the table that follows. The table also includes the application in which these engines were used, the rated power and the overall dry weight in kg for each case. Note that some of the reference engines were used in more than one application but for reasons of space economy only one application per engine is mentioned.

Table_A-3 List of turboshaft/turboprop engines

Manufacturer	Application	Power (kW)	Weight (kg)
Allison	Cesna 402/414	313.19	89.8
Allison (Rolls-Royce)	MD600N	484.7	124.2
Avco Lycoming	Cessna/Riley 421	458.6	142.88
Baranov (OMSK)	An-38-200	1029	284.86
Garrett	Commander 840/900	733.7	172.4
Garrett (Allied-Signal)	Jetstream 4101	1284.8	281.2
General Electric	Bell 214ST	1211.8	200.5
Isotov (Klimov)	Mi-2/-2B/-2R	293.8	139.3
LHTEC	Ayres LM200	2013.4	517.1
Mitsubishi	MH-2000	653.2	154.2
Pratt Whitney Canada	Starship 2000	894.8	229.5
Pratt Whitney Canada	King Air F90	559.3	154.2
PZL Rzeszów	W-3 Sokol	662.2	140.6
Rolls Royce	Westland 30 Series 100	846.4	183.2
Saturn	An-38	970.9	239.9
Turbomeca	SA365C	477.9	120.2
Walter	Ae-270	580.1	201.8

A.4 Aircraft Mission Profile in MATLAB

For the sensitivity study of Chapter 6 a MATLAB function has been developed to produce the mission profile of each aircraft under investigation. This code was based on work being produced during the DEAP project by the AGI but it

has been modified accordingly to match the requirements of the different aircraft of the current study. The maximum power of the engines and the battery/supercapacitor system was given as inputs combined with the maximum energy storage energy available in each case. After that, the exact time duration and power requirements of each phase are estimated and are given as outputs from this MATLAB function and used as an input in the Simulink models presented in Chapter 6.3. The following code was used for the Boeing 787 case and it is showed just as a representative example of a mission profile MATLAB function.

```
function [ ] = missionmaker( )

%787 MISSIONMAKER Primes the workspace for the Chapter 6 study

Engine_1_max = 4200; %kW

Engine_2_max = 4200; %kW

Batt_P_max = 12500; %kW

Batt_P_min = 0; %kW

Batt_E_max = 111000; %kJ


assignin('base','Engine_1_max', Engine_1_max);

assignin('base','Engine_2_max', Engine_2_max);

assignin('base','Batt_P_max', Batt_P_max);

assignin('base','Batt_P_min', Batt_P_min);

assignin('base','Batt_E_max', Batt_E_max);

assignin('base','Batt_Chg', Batt_Chg);

%   Power in kW, time in minutes

SLS_power = 10428.*2;

SLS_time = 1;

EoR_power = 10379.*2;
```

```
EoR_time = 8;

Climb_power = 4617.*2;

Climb_time = 20;

Cruise_power = 4049.*2;

Cruise_time = 915;

Descent_power = Cruise_power .* 0.8;

Descent_time = 20;

Landing_power = Cruise_power .* 1.4;

Landing_time = 2;

Taxi_power = Cruise_power .* 0.4;

Taxi_time = 5; %each end


mission = zeros(16,2);

mission(1,1) = 0;

mission(1,2) = Taxi_power;

mission(2,1) = Taxi_time .* 60;

mission(2,2) = Taxi_power;

mission(3,1) = mission(2,1) + 1;

mission(3,2) = SLS_power;

mission(4,1) = mission(3,1) + (SLS_time .* 60);

mission(4,2) = SLS_power;

mission(5,1) = mission(4,1) + 1;

mission(5,2) = EoR_power;

mission(6,1) = mission(5,1) + (EoR_time .* 60);

mission(6,2) = EoR_power;
```

```
mission(7,1) = mission(6,1) + 1;

mission(7,2) = Climb_power;

mission(8,1) = mission(7,1) + (Climb_time .* 60);

mission(8,2) = Climb_power;

mission(9,1) = mission(8,1) + 1;

mission(9,2) = Cruise_power;

mission(10,1) = mission(9,1) + (Cruise_time .* 60);

mission(10,2) = Cruise_power;

mission(11,1) = mission(10,1) + 1;

mission(11,2) = Descent_power;

mission(12,1) = mission(11,1) + (Descent_time .* 60);

mission(12,2) = Descent_power;

mission(13,1) = mission(12,1) + 1;

mission(13,2) = Landing_power;

mission(14,1) = mission(13,1) + (Landing_time .* 60);

mission(14,2) = Landing_power;

mission(15,1) = mission(14,1) + 1;

mission(15,2) = Taxi_power;

mission(16,1) = mission(15,1) + (Taxi_time .* 60);

mission(16,2) = Taxi_power;

%done = mission;

assignin('base','mission', mission);

end
```